Optical fibre sensors with applications in gas and biological sensing

Edward Davies

Doctor of Philosophy

Aston University
May 2011

Abstract

Optical fibre sensors with applications in gas and biological sensing

Edward Davies

Doctor of philosophy

May 2011

Aston University

This thesis describes the study of various grating based optical fibre sensors for applications in refractive index sensing. The sensitivity of these sensors has been studied and in some cases enhanced using novel techniques. The major areas of development are as follows.

The sensitivity of long period gratings (LPGs) to surrounding medium refractive index (SRI) for various periods was investigated. The most sensitive period of LPG was found to be around 160 μm and this was due to the core mode coupling to a single cladding mode but phase matching at two wavelength locations, creating two attenuation peaks, close to the waveguide dispersion turning point.

Large angle tilted fibre gratings (TFGs) have similar behaviour to LPGs, in that they couple to the co-propagating cladding modes. The tilted structure of the index modulation within the core of the fibre gives rise to a polarisation dependency, differing the large angle TFG from a LPG. Since the large angle TFG couple to the cladding mode they are SRI sensitive, the sensitivity to SRI can be further increased through cladding etching using HF acid. The thinning of the cladding layer caused a reordering of the cladding modes and shifted to more SRI sensitive cladding modes as the investigation discovered. In a SRI range of 1.36 to 1.40 a sensitivity of 506.9 nm/URI was achieved for the etched large angle TFG, which is greater than the dual resonance LPG.

UV inscribed LPGs were coated with sol-gel materials with high RIs. The high RI of the coating caused an increase in cladding mode effective index which in turn caused an increase in the LPG sensitivity to SRI. LPGs of various periods of LPG were coated with sol-gel TiO_2 and the optimal thickness was found to vary for each period. By coating of the already highly SRI sensitive 160μm period LPG (which is a dual resonance) with a sol-gel TiO_2, the SRI sensitivity was further increased with a peak value of 1458 nm/URI, which was an almost 3 fold increase compared to the uncoated LPG.

LPGs were also inscribed using a femtosecond laser which produced a highly focused index change which was no uniform throughout the core of the optical fibre. The inscription technique gave rise to a large polarisation sensitivity and the ability to couple to multiple azimuthal cladding mode sets, not seen with uniform UV inscribed gratings. Through coupling of the core mode to multiple sets of cladding modes, attenuation peaks with opposite wavelength shifts for increasing SRI was observed. Through combining this opposite wavelength shifts, a SRI sensitivity was achieved greater than any single observed attenuations peak. The maximum SRI achieved was 1680 nm/URI for a femtosecond inscribed LPG of period 400 μm.

Three different types of surface plasmon resonance (SPR) sensors with a multilayer metal top coating were investigated in D shape optical fibre. The sensors could be separated into two types, utilized a pre UV inscribed tilted Bragg grating and the other employed a post UV exposure to generate surface relief grating structure. This surface perturbation aided the out coupling of light from the core but also changed the sensing mechanism from SPR to localised surface plasmon resonance (LSPR). This greatly increased the SRI sensitivity, compared to the SPR sensors; with the gold coated top layer surface relief sensor producing the largest SRI sensitivity of 2111.5nm/URI was achieved. While, the platinum and silver coated top layer surface relief sensors also gave high SRI sensitivities but also the ability to produce resonances in air (not previously seen with the SPR sensors).

These properties were employed in two applications. The silver and platinum surface relief devices were used as gas sensors and were shown to be capable of detecting the minute RI change of different gases. The calculated maximum sensitivities produced were 1882.1dB/URI and 1493.5nm/URI for silver and platinum, respectively. Using a DFB laser and power meter a cheap alternative approach was investigated which showed the ability of the sensors to distinguish between different gases and flow rates of those gases. The gold surface relief sensor was coated in a with a bio compound called an aptamer and it was able to detect various concentrations of a biological compound called Thrombin, ranging from 1mM to as low as 10fM. A solution of 2M NaCl was found to give the best stripping results for Thrombin from the aptamer and showed the reusability of the sensor. The association and disassociation constants were calculated to be $1.0638\times10^{6}Ms^{-1}$ and $0.2482s^{-1}$, respectively, showing the high affinity of the Aptamer to thrombin. This supports existing working stating that aptamers could be alternative to enzymes for chemical detection and also helps to explain the low detection limit of the gold surface relief sensor.

Keywords: Fibre optic, UV and Femtosecond gratings, Surface plasmon Resonance, gas/biological sensing

Acknowledgements

I would like to thank Prof. Lin Zhang for firstly giving me the opportunity for my study at Aston University without which I wouldn't be where I am today. I would also like to thank her for the courage and support she gave me throughout my PhD with her always being willing to help and discuss experimental results. I would also like to say thank you for having the patience to read through my thesis and give me guidance.

I would like to thanks Dr. Tom Allsop for introducing me to the relatively new and growing field of surface plasmon resonance. Not only did he present to me an interesting scientific field but also gave me considerable work making my thesis more novel and interesting than would have been thought possible before.

I would like to thank Prof Kyriacos Kalli for the experimental work carried out concerning femtosecond laser inscription which was interesting, challenging and useful. Perhaps more importantly were the discussions we had, through him constantly challenging ideas and thoughts he made me think more deeply about the work and science in general and without which this thesis would not be what it is.

I would like to thank: Herbert Biggs for his technical support in the laboratory, which was invaluable; Ian Johnson, whose discussion and sometimes distraction were invaluable when trying to understand my work; Chengbo Mou for always being helpful in both developing new ideas and the understanding of equipment and finally Dave Negal and Reeta Huhtinen whose collaboration made this thesis possible.

List of contents

List of figures

List of tables

List of symbols				
Λ	Optical fibre Grating period		n_{m}	Refractive index. Where m is the core or cladding mode
Λ_p	Phase mask grating period		ω	Angular frequency
$E(x,y,z)$	Electric field		A_m	Amplitude of electric field, where m is the core or cladding
β_m	Propagation constant of the optical fibre, where m is the core/cladding of an optical fibre or a dielectric or a surface plasmon mode		μ	Permeability of free space
$\Delta\varepsilon$	Perturbation of the dielectric		K	Coupling coefficient of the overlap of two electric fields
$\overline{\Delta n}$	DC change in refractive index		f	Fringe visibility
$\Delta n(z)$	Varying induced refractive index change in the optical fibre		λ_{res}	Central wavelength of the Bragg or long period grating
Λ_g	Period of the a tilted grating		ε	Dielectric constant of a material
c	Speed of light		κ_0	Wave vector of a wave in a vacuum
ε_0	Dielectric constant		$H(x,y,z)$	Magnetic field
k	Wave vector		Φ	Electric potential
r_{cl}	Cladding radius of an optical fibre, with the superscript denoting etched		r_{co}	Core radius of an optical fibre

	or un-etched			
n_{co}^{eff}	Effective core mode index		n_s	Refractive index of a surrounding material
$n_{cl,m}^{eff}$	Effective cladding mode index		$\emptyset$	Azimuthal angle of the cladding
M	Low frequency modulation of a sampled Bragg grating		T_m	The transmission minimum for a LPG resonance
L	Length of the inscribed grating		$\Delta\lambda_b$	Bragg wavelength shift
ΔT	Change in temperature		α_p	Thermal expansion coefficient of the optical fibre
α_n	Thermooptic coefficient of the optical fibre		$d\emptyset$	Change in azimuthal angle
δ_{l1}	Dirac delta function		λ_ω	Wavelength of UV inscription laser
$\partial\theta_{int}$	Internal angle of tilt deviation for an inscribed grating		θ_{ext}	External angle of the phase/amplitude mask

1 Introduction

1.1 Thesis overview

The thesis is concerned with the development of optical fibre sensors, mainly those with surrounding medium refractive index (SRI) sensitivities. Fibre optic sensors have been long established in the scientific community with most utilizing grating structures with an index modulation within the core of a single mode optical fibre. These techniques, though well utilized, often have inherent limitations. A typical example of this is the high sensitivity of long period gratings (LPGs) to high SRIs, around 1.45, while a low sensitivity at low SRI, around 1.36. To overcome inbuilt drawbacks various sensitivity enhancements or alternative sensing methods have been investigated in this thesis and the various methods can be separated into distinct section.

The background chapter gives the reader the relevant theory so that they can understand the key results of this thesis; explaining coupled mode theory, surface plasmon resonance (SPR) theory and localised surface plasmon resonance theory (LSPR). This chapter also gives an experimental overview to follow the various inscription techniques implemented.

The first experimental chapter concerns itself with UV induced grating structures in hydrogenated single mode optical fibre and the sensitivity enhancement of such devices. The behaviour of LPGs with various periods and large angle tilted fibre gratings (TFGs) to changing SRI was investigated and the most sensitive period of LPG was found. This was then followed by study of two methods for increasing the gratings sensitivity to SRI. The first method involves a porous sol-gel coating applied to LPGs of various periods and followed by a systematic investigation concerning LPG period, coating thickness and coating refractive index (RI). The second method concerns the claddings layer of a series

of large angle TFGs being partially removed. The large angle TFGs were immersed in the HF for various times which resulted in multiple cladding etching depths. The behaviour between cladding modes and cladding thickness was then established along with the reasoning behind the associated sensitivity increase.

The second experimental chapter investigates the novel use of infrared femtosecond laser inscription of grating structures in non-hydrogenated single mode optical fibres. Femtosecond LPGs were inscribed with multiple periods; this allowed the examination of many cladding modes including those with azimuthal orders no equal to one. Femtosecond sampled fibre Bragg gratings (SFBGs) were also inscribed in single mode optical fibre. The transmission and reflection spectra were investigated for two different low frequency modulation periods which were related to theoretically predicted values. The temperature response of these devices was also investigated and the sensitivity reported. A final femtosecond device was produced which was a hybrid of both LPG and SFBG. The behaviour of the hybrid device to both SRI and temperature was examined and its feasibility of a multi-parameter sensor reported.

The third experimental chapter is concerned with the initial work of SPR and LSPR optical fibre sensors which were made in optical fibres lapped to a D shape. There were three different types of sensors investigated: pre UV inscribed tilted Bragg gratings sensors with a single metal layer coating, tilted Bragg grating sensors with a multilayer metal and insulator coating and multilayer coated sensors with a post UV exposure which created a surface perturbation. This work characterised the different sensors sensitivities to SRI and their polarisation responses. For the surface relief sensors, three metals of platinum, gold and silver were used since each metal has a different dielectric property and sensitivity. From the experimental results and current literature, each devices mechanism for both out coupling of light and sensing (SPR or LSPR) were discussed and the most likely conclusions established.

The final experimental chapter describes the uses of the most sensitive sensors from the previous chapter (the surface relief devices) and applied them to real sensing applications. The silver and platinum surface relief sensors were implemented as gas sensors, characterising the both the wavelength and amplitude shift in resonance for changing SRI associated with four different gases. The ability of the devices to operate as cheap sensor the resonances of the sensors were also studied, using a DFB laser and power meter, for various flow rates of a gas. To remove any doubt about the results the temperature sensitivity of one of the devices was ascertained and compared to the shift due to increasing SRI. The second experiment for bio-detection discussed in this chapter is to use the most sensitive sensor, the gold surface relief device, as a biological compound sensor, specifically thrombin. This was achieved through coating of the sensing area with a species specific detecting compound called an aptamer, which is an alternative to enzymes. Various light sources were used for the experiment so that the maximum number of resonances could be investigated. Various concentrations of thrombin solution were applied to the sensor ranging from 10mM to 10fM and the ability of the sensor to detect these concentrations investigated. From these values the binding association and disassociation constants are calculated, giving an idea the quality and strength of both the aptamer and sensor.

2 Background

2.1 Photosensitivity and Hydrogenation

2.1.1 UV induced photosensitivity

Optical fibre is made of a high index core and a lower index cladding glass to confine light into the cladding. The difference in the refractive indices (RI) is achieved through doping the core glass with germanium, which increases the core RI. The exact reason behind the photosensitivity of germanium doped optical fibre is still unclear, however what is clear is that the germanium oxygen defect in the glass, and its concentration, play a major role in fibre photosensitivity[1]. In the optical fibre germanium can form multiple defects depending on the number of surrounding Ge/Si molecules[2, 3]. The GeO defect has a bond with an absorption peak at 240nm and this is common within germanium doped SiO_2 glass fibres. Thus, on exposure to ultra-violet (UV) illumination, the bond breaks down forming a GeE' centre molecules with the free electron free to be trapped at another germanium defect. The release of the electron is believed to change the shape of the molecule, and hence through the Kramers-Kronig relationship the refractive index[4]. Along with this there also may be a densification of the glass as another possible mechanism for an associated refractive index change[5]. The photosensitivity of optical fibre is directly related to the concentration of GeO defects within the core of the fibre[6]. By increasing the germanium concentration, generally, the concentration of defects also increases, thus providing a way of increasing photosensitivity.

When dealing with standard telecommunications fibre it is not possible to increase the germanium concentration. This is because, increasing the RI of the core too much results in an increase in numerical aperture. However, it is desirable to get a large refractive index

change in standard fibre for low cost in-fibre devices. One of the easiest methods for doing this is through hydrogenation of the fibre, which was first reported by Lemaire et al[7]. Hydrogen is forced into the fibre using high pressures, ranging from 20-750 Atmospheres, with a temperature from 20-70^{o}C, however room temperature is commonly used for its ease. The H_2 infusion doesn't increase the absorption at 240nm, but is believed to perform a UV initiated reaction with both silicon and germanium, forming SiOH and GeOH molecules respectively. These two molecules both contribute to the induced refractive index change. It is also believed that now all the germanium molecules are free to react and the index change is no longer reliant on the concentration of defects. After the exposure, any unreacted hydrogen molecules will slowly diffuse out of the fibre causing stability issues when making gratings, especially for long period gratings. This process can take up to 450 hours[8] because the hydrogen has to diffuse out of the core through the cladding and into the surrounding atmosphere. Increasing the temperature, and hence the kinetic energy of hydrogen molecules, increases the out diffusion rate of hydrogen from the optical fibre core. The heating, or annealing, is usually at 100^{o}C for a minimum of 24 hours and a more detailed explanation is found in Chapter 2.6.1.

2.1.2 Femtosecond laser inscription induced photosensitivity

The photosensitivity of femtosecond laser inscription, unlike UV inscription, does not require germanium doping and hydrogenation of the optical fibre. UV laser inscription uses a single photon linear process that directly changes the structure of the germanium defect within the glass core through an excitation of an electron from the valence band to the conduction band. It should be noted that the exact understanding of femtosecond RI changes is still being investigated but this has been reviewed on its current state by Rafael R. Gattas et al[9]. Femtosecond lasers transfer the optical energy of the laser beam to the material through the excitation of electrons in the valence band to the conduction band. In

transparent materials, like silica, the electrons absorption of light must be non-linear because the electron transitions require a greater energy than is available in a single photon[10, 11]. With no doping or impurities present, this is achieved through a multiphoton absorption process. This is when multiple photons arrive at the electrons rapidly enough to impart enough energy to overcome the band gap and this is drawn schematically in Figure 2-1.

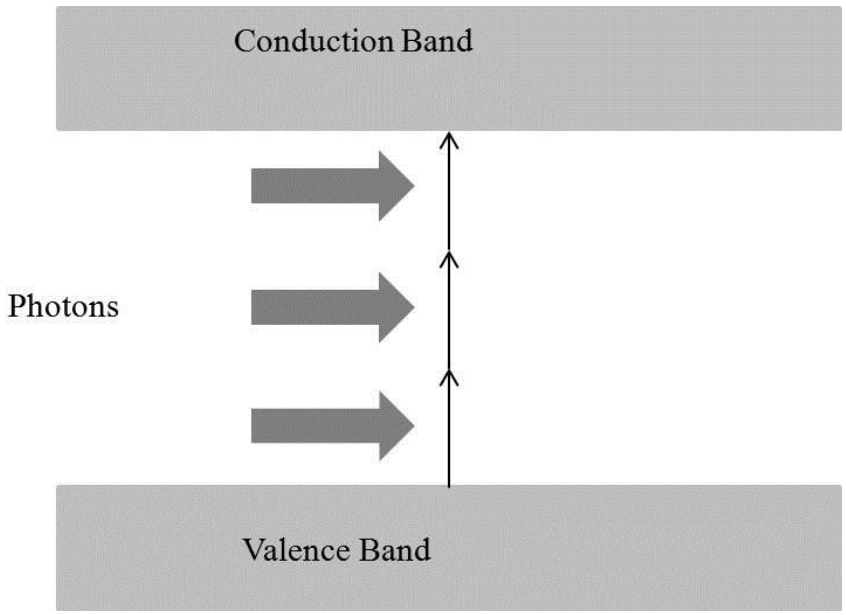

Figure 2-1 showing a schematic of the multi-photon absorption process

This frees the electrons in the material and when the density of free electrons reaches approximately $10^{29}m^{-3}$, the electrons begin to behave like a plasma. Depending on the amount of energy transferred to the material, several things can occur including cracking, void formation and localised melting. This structural change is caused by part of the excited electrons energy being transferred to the s lattice, which causes an expansion into the material away from the hot dense focal volume[12, 13]. When the energy is sufficiently high enough, the process causes a melting or non-thermal ionic motion creating a permanent change in the material[14]. There is a minimum amount of energy that needs to be transferred into the material for change in material to take place, this is commonly referred to as the threshold criterion[15]. Keeping the energy at about threshold causes a

refractive index change which can be due to multiple effects including; stress induced, densification and colour centre changes and the exact contribution of each parameter is still under investigation. If the energy is increased and taken above threshold the size of the exposed area and the average plasma energy increases. This results in a decrease in ionic shielding and a coulomb repulsion between ions, which in turn can lead to a void formation[16] and produce both a negative and refractive index change in the material.

2.2 Fibre grating fabrication techniques

2.2.1 Point by Point Inscription

One of the simplest methods for grating fabrication is that of point by point inscription[17]. The setup of the apparatus is shown in Figure 2-2.

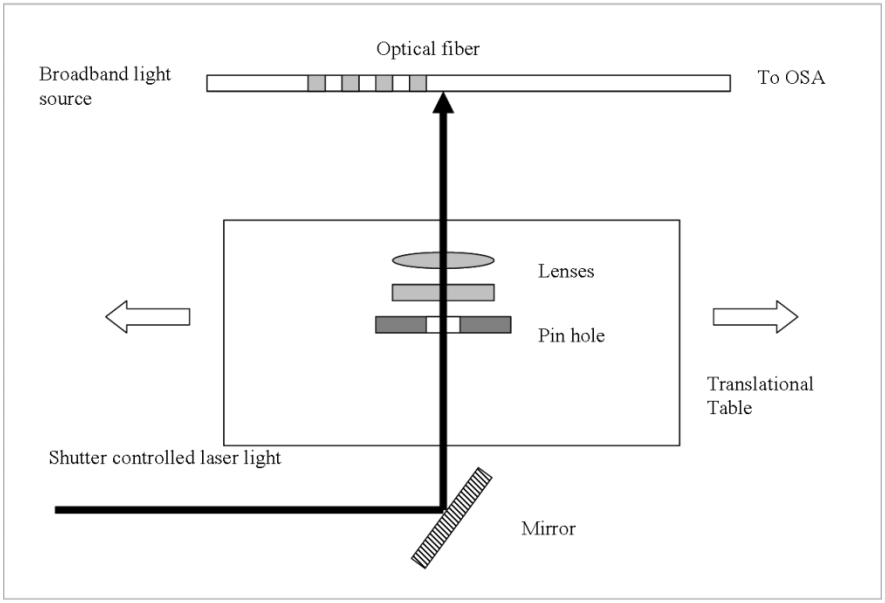

Figure 2-2 showing the system setup used for point by point inscription

The light source used is a frequency double CW argon laser with a wavelength of 244nm. The pinhole removes unwanted effects due to the laser source before the light is focused onto the optical fibre using two half cylindrical lenses. To ensure the beam is focused onto the core, the diffraction pattern created is examined and symmetry is assured through

movement of the fibre up and down relative to the beam. A Labview program is used to control both the translation stage and shutter. The beam is scanned at a constant speed and for a fixed length across the optical fibre, using the motion of the translation stage. As it does so the shutter is programmed to open and close at a specific rate. The rate is determined by the desired period of the LPG. This creates the periodic index perturbation within the core of the optical fibre. The power density at the optical fibre is between 1.3 kWm^{-2}-2.7 kWm^{-2} (depending on the grating period and type of fibre used). The advantage of this technique is its controllability, through changing the translation stage's speed and the rate at which the shutter operates there is complete control over grating period, pitch, length of grating and exposure time.

2.2.2 Phase Mask Technique

The phase mask technique is a commonly used method for grating inscription [18, 19]. A phase mask, usually made from fused silica, has a one dimensional surface relief with a pattern period of Λ_p. A UV beam is focused onto its surface where diffraction into multiple orders, namely $m = 0, \pm 1, \pm 2, ...$ where 0 is the transmitted beam. This is shown schematically in Figure 2-3. The incident and diffracted beams are governed by the established diffraction equation, Equation 2-1.

$$\Lambda_p = m \frac{\lambda_\omega}{sin(\theta_m) - sin(\theta_i)}$$

Equation 2-1

Where θ_i is the incident angle, $\theta_m$is the diffraction angle of the mth order and λ_ω is the wavelength of the UV beam. The special case where the incident beam is perpendicular to the phase mask results in the diffracted beams, both negative and positive order, having equal angles. The resultant fringe pattern can be used to inscribe Bragg grating but with

some modification. Any order can be used, usually ±1, but this order has to be maximised by suppressing all other orders and equalizing the power split between them.

The resultant interference pattern of the two beams creates a power modulation. By placing photosensitive optical fibre near the phase mask, with a cylindrical lens to focus the power on the core, a grating structure will be induced with a period half that of the phase mask, i.e. $\frac{\Lambda_p}{2} = \Lambda$. Using a translation stage the beam can be scanned across the fibre creating gratings with variable length, limited only by the length of the phase mask.

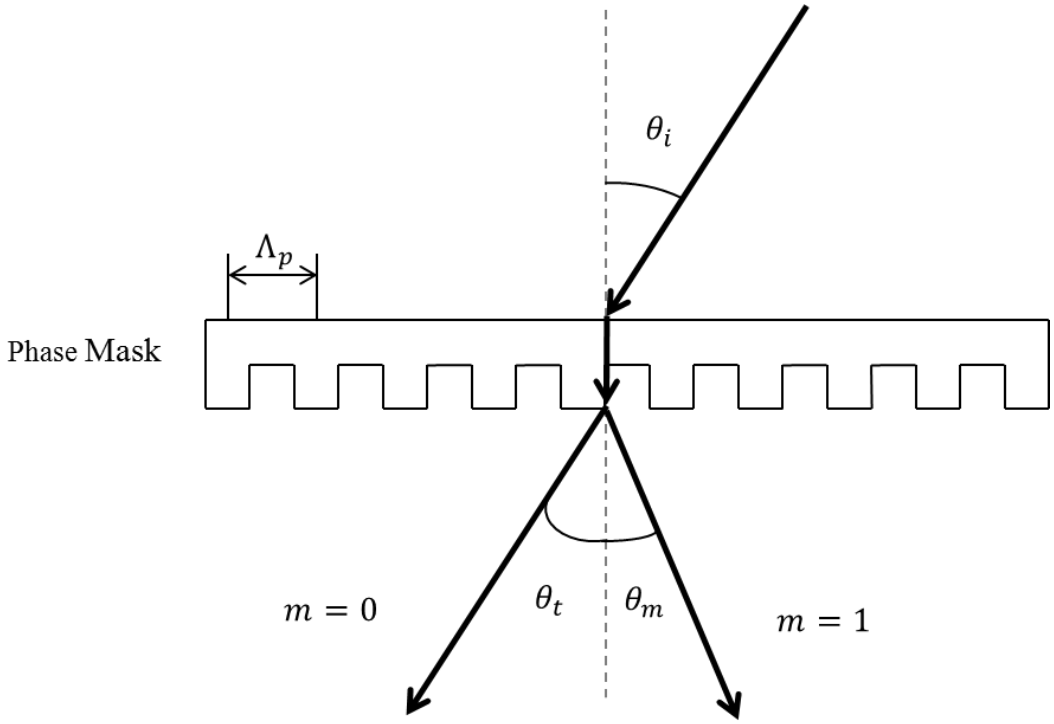

Figure 2-3 a diagram showing the phase mask technique with incident beam being split into a diffracted (m=1) and transmitted (m=0) beam

A phase mask can also be used to produce a fibre grating that has a tilt with respect to the fibre axis[20]. The mask is held in place with a holder whose angle is a variable. The phase mask is aligned to the fibre axis using the diffraction pattern from the fibre core as a reference. The phase mask holder is then angled the required amount for the desired grating tilt. However, due to the refractive index of the optical fibre the tilt of the inscribed

gratings is not that of the external angle of the phase mask. To explain this, the optical fibre can be considered a cylindrical lens. If a straight line is at angle θ_{ext} with respect to the cylinder rod axis the image is rotated by $\partial\theta_{int}$. The angle can be found by calculating it a zero distance from the object using a paraxial approximation[21]. This results in Equation 2-2 and is found to be only dependant on the refractive index and external angle of the optical fibre and not the optical fibre geometry[22].

$$\partial\theta_{int} = \tan^{-1}\left(\frac{n}{(2-n)}\tan\theta_{ext}\right) - \theta_{ext}$$

Equation 2-2

2.2.3 Amplitude Mask

The amplitude mask is formed by a consistent series of opaque lines of periods ranging from 5 to 120μm on a fused silica substrate. For the work carried out in this thesis the period of the mask was 6.6 μm. This increase in period means the beam of incident light is not diffracted and hence does not cause an interference pattern. What does occur is the blocking of the incident beam, created a transmitted beam that has a periodic modulation matching that of the mask, as shown in Figure 2-4. The laser light is focused onto the fibre using a cylindrical lens, and using the diffraction pattern from the fibre to ensure alignment. By using a translation stage, the beam can be scanned across the surface of the mask producing any grating length, up to that of the amplitude mask.

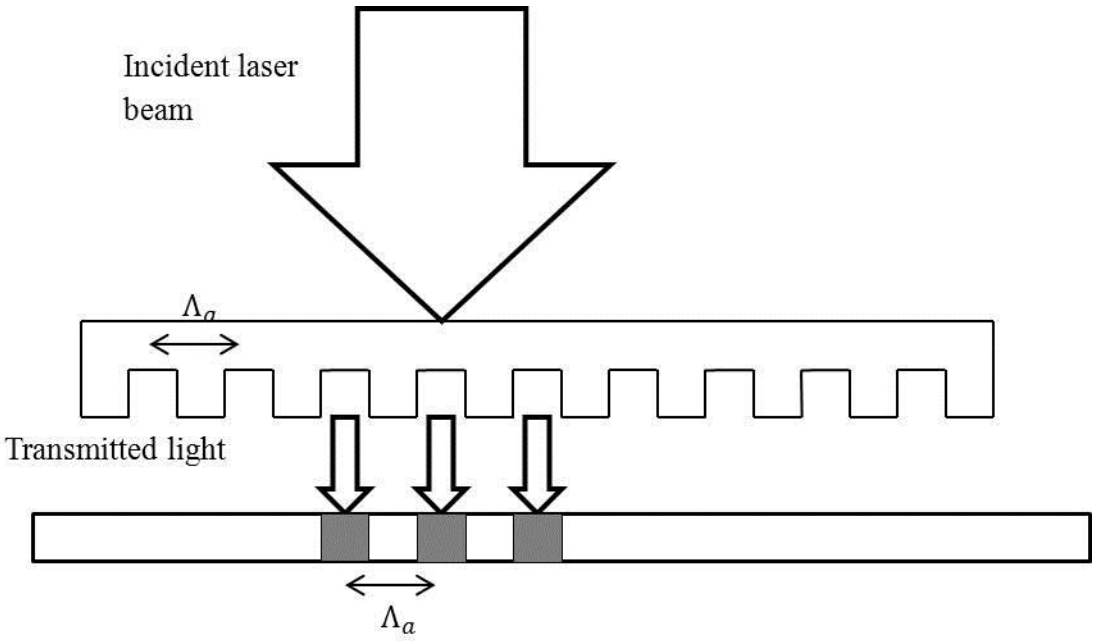

Figure 2-4 showing the periodic transmitted light caused by the amplitude mask

2.3 Coupled Mode Theory

Coupled mode theory is derived, from various texts[23], using Maxwell's wave equations with suitable approximations, which will be discussed at the relevant points. Firstly, it is assumed that the solutions of the electromagnetic waves propagating in an unperturbed medium in the z direction can be written in the form of Equation 2-3. The first term on the right deals with the discrete bound modes while the second is the representation of the continuous radiation modes. Since the concern here is only with bound core/ cladding modes the radiation modes will be neglected from here on.

$$E(x,y,z) = \sum_{m} A_m E_m\,(x,y) e^{-j(\omega t - \beta_m z)} + \iiint_{m} A_m\, E_m(x,y) e^{-j(\omega t - \beta_m z)} dxdydz$$

Equation 2-3

Dropping the time dependency, the perturbed form of Maxwell's wave equation is

$$\nabla^2 E + \omega^2 \mu \{\varepsilon(x,y) + \Delta\varepsilon(x,y,z)\} E = 0$$

Equation 2-4

To obtain an approximate solution to Equation 2-4 Equation 2-3 is applied, remembering that the unperturbed wave equation is equal to zero and this gives Equation 2-5. However since there is now a z dependency of the dielectric function the amplitude coefficients are no longer constants and hence $A_m \rightarrow A_m(z)$

$$\sum_m \left(\frac{d^2}{dz^2} A_m(z) - 2j\beta_m \frac{d}{dz} A_m(z) \right) E_m e^{j(\omega t - \beta_m z)} = -\omega^2 \mu \sum_m \Delta\varepsilon(x,y,z) E_m e^{j(\omega t - \beta_m z)}$$

Equation 2-5

To solve the Equation 2-5, a few steps have to be taken, to make finding the solutions easier. The dielectric perturbation is assumed to be "weak", meaning that the mode amplitude varies slowly i.e.

$$\frac{d^2}{dz^2} A_m(z) \ll \beta_m \frac{d}{dz} A_m(z)$$

Equation 2-6

Thus producing

$$2j \sum \beta_m \frac{dA_m}{dz} E_m(x,y) e^{-j\beta_m z} = \omega^2 \mu \sum \Delta\varepsilon(x,y,z) A_m E_m(x,y) e^{-j\beta_m z}$$

Equation 2-7

To solve the equation requires both sides to be multiplied by E_n^* and integrated over all x and y, then using the normalised orthogonality relationship, which gives Equation 2-8. Giving Equation 2-9, which is the basis of the coupled mode equations.

$$\iint E_n^*(x,y).E_m(x,y)dxdy = \frac{2\omega\mu}{|\beta_m|}\delta_{nm}$$

Equation 2-8

$$\frac{dA_n}{dz} = -j\sum_n K\,A_m(z)e^{j(\beta_n-\beta_m)z}$$

Equation 2-9

where:

$$K = \frac{\langle m|\Delta\varepsilon|n\rangle}{\beta_m\langle n|n\rangle} = \pm\frac{\omega}{4}\iint E_m^*\Delta\varepsilon\,E_n dxdy$$

Equation 2-10

is known as the coupling coefficient and the ± arises from the $\frac{|\beta_m|}{\beta_m}$ and determines the direction of propagation. Where K is the measure of the overlap of the core mode and the cladding mode and as a result represents the efficiency of the core mode coupling to a cladding mode. Although there is coupling for both the longitudinal and transverse electric fields, the longitudinal is very much smaller and hence can be neglected from the calculations. Theoretically, an infinite number of modes can be coupled to as Equation 2-10 shows, however only those whose transverse electric field overlap will couple strongly. So in the case of single mode fibre, it will be the overlap between the forwards and backwards propagating core modes for a FBG, or the forward propagating core to cladding modes for the LPG. The index induced perturbation is assumed to take the form:

$$\Delta n(z) = \overline{\Delta n}\left(1 + f\cos\left(\frac{2\pi z}{\Lambda}\right)\right)$$

Equation 2-11

Where $\overline{\Delta n}$ is the DC refractive index change, f is the fringe visibility and Λ is the period of the grating. Applying Equation 2-11 to Equation 2-10 means along with the electric field distribution the coupling coefficients for each mode can be calculated[24, 25]. For mode

coupling between the core mode in a single mode fibre to any cladding mode the coupled mode equations become,

$$K_t = k_t\left(1 + f cos\left(\frac{2\pi z}{\Lambda}\right)\right)$$

Equation 2-12

$$k_t = \frac{\omega \varepsilon_o n}{4}\iint \overline{\Delta n}\, E_m E_n dx dy$$

Equation 2-13

$$\frac{dA_{co}}{dz} = -jf\frac{k_{cl/co}}{2}A_{cl/co}(z)e^{j\delta z}$$

Equation 2-14

$$\frac{dA_{cl/co}}{dz} = \pm jf\frac{k_{cl/co}}{2}A_{co}(z)e^{-j\delta z}$$

Equation 2-15

Where $\delta = \left(\beta_{co} \pm \beta_m - \frac{2\pi}{\Lambda}\right)$, cl signifies a cladding mode coupling and co signifies a core mode coupling. When light passes through the fibre grating well defined attenuation bands are formed because coupling only occurs to discrete single modes. For all types of grating this relationship is defined by the phase matching condition, in other words strong coupling only takes place when $\delta = \left(\beta_{co} \pm \beta_m - \frac{2\pi}{\Lambda}\right) = 0$. Putting this in another form and equating it to the types of gratings gives Equation 2-16[26].

$$\lambda_{res} = (n_{co} \pm n_m)\Lambda = \begin{cases} (n_{co} - n_{cl})\Lambda & Long\ period\ \ bragg\ gratings \\ 2n_{co}\Lambda & bragg\ gratings \\ (n_{co} + n_{cl})\Lambda & bragg\ gratings \end{cases}$$

Equation 2-16

This analysis assumes that the perturbation is perpendicular to the z axis, however there is the special case where the index perturbation is offset from the axis of the fibre by an angle. This type of grating is known as blazed or tilted and has been examined in several texts[27, 28]. To allow for this the index perturbation is now assumed to take the form:

$$\Delta n(z) = \overline{\Delta n}\left(1 + f\cos\left(\frac{2\pi}{\Lambda_g}z'\right)\right)$$

Equation 2-17

Where $z' = xsin(\theta) + zcos(\theta)$ and $\Lambda_g = \Lambda\cos(\theta)$, however since the index perturbation is slowly varying a good approximation is $z' \approx zcos(\theta)$. Also, the introduction of tilt has the adverse effect of reducing fringe visibility[29]. Applying Equation 2-17 into the coupling coefficient the phase matching condition is modified to Equation 2-18[29, 30]:

$$\lambda_{res} = (n_{co} \pm n_m)\frac{\Lambda}{cos(\theta)}$$

Equation 2-18

The introduction of tilt further increases the complications of the calculations by introducing polarisation dependence[27]. The polarisation dependency means the coupling coefficient differs depending upon the polarisation of light. The negative or plus sign denotes whether the coupling is to the forward or backward cladding modes, respectively. Whether the coupling occurs to forward, backward or radiation modes is determined by the phase matching condition

2.4 Surface Plasmon Resonance

2.4.1 Surface Plasmon Resonance Theory

To describe the behaviour of a Surface Plasmon Resonance (SPR)[31, 32], the standard starting point is to use Maxwell's equations and rearrange. Using standard identities and assuming the dielectric ε = ε(x,y,z) does not vary compared to an optical wavelength this gives rise to:

$$\nabla^2 E - \frac{\varepsilon}{c^2}\frac{\partial^2 E}{\partial t^2} = 0$$

Equation 2-19

where c is the speed of light, t is time and E is the electric field. To solve Equation 2-19 each region of ε is used as a boundary and for each area a general solution is calculated with arbitrary constants. Since the electric field has to be continuous at the boundary a full solution can then be formulated. As always an electric field of form below is assumed to be a solution:

$$E(x, y, z, t) = E(x, y, z)e^{-j\omega t}$$

Equation 2-20

Where ω is the angular frequency. Thus inserting Equation 2-20 into Equation 2-19 yields:

$$\nabla^2 E + \kappa_0^2 \varepsilon E = 0$$

Equation 2-21

Where $\kappa_0 = \omega/c$ is the wave vector of the propagating wave in a vacuum. The solution proposed so far is for a general case, by defining the geometric structure, Figure 2-5, and redefining the electric field a more specific example can be achieve. In Figure 2-5 $z = 0$ is

where the two interfaces meet and the dielectric variation occurs only in z axis, hence $\varepsilon = \varepsilon(z)$.

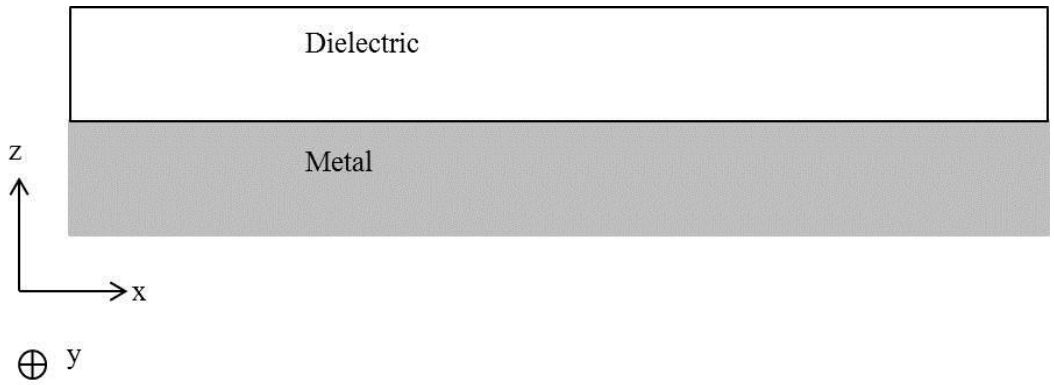

Figure 2-5 showing the axis and structure for the surface plasmon resonance.

Applying this, the electric field can now be defined $E = E(z)e^{j\beta x}$ and putting this into Equation 2-21 gives Equation 2-22. A similar equation exists for the magnetic field:

$$\frac{\partial^2 E}{\partial z^2} + (k_0^2 - \beta^2)E = 0$$

Equation 2-22

This alone does not describe surface plasmon resonance behaviour. To do this, the electric and magnetic field in each axis needs to be determined using two of Maxwell's equations:

$$\nabla \times E = -\mu_0 \mu \frac{\partial H}{\partial t}$$
$$\nabla \times H = J + \varepsilon_0 \varepsilon \frac{\partial E}{\partial t}$$

Equation 2-23

Assuming harmonic time dependence produces a set of equations that can be further simplified by assuming that propagation occurs only in the x direction and continuity has to occur in the y direction, $\frac{\partial}{\partial y} = 0$, the equations are simplified. It can be shown that this allows for two sets of solutions; the first is the transverse magnetic waves (TM/p modes)

where only the E_x, E_y and H_y components are non-zero; the second is the transverse electric waves (TE/s modes) where only the E_y, H_x and H_z components are non-zero.

It is best to take a look at each set of modes individually, the reasons for which will become clear afterwards. Looking first at TM modes, the aim is to find a wave which travels across the metal surface and is confined at the interface. Keeping this in mind and defining the metal dielectric interface of that in Figure 2-5 the TM mode equations are for $z > 0$(the dielectric):

$$H_y(z) = A_2 e^{j\beta x} e^{-k_2 z}$$

Equation 2-24

$$E_x(z) = jA_2 \frac{1}{\omega \varepsilon_0 \varepsilon_2} k_2 e^{j\beta x} e^{-k_2 z}$$

Equation 2-25

$$E_z(z) = -A_2 \frac{\beta}{\omega \varepsilon_0 \varepsilon_2} e^{j\beta x} e^{-k_2 z}$$

Equation 2-26

and for $z < 0$ (the metal):

$$H_y(z) = A_1 e^{j\beta x} e^{-k_1 z}$$

Equation 2-27

$$E_x(z) = jA_1 \frac{1}{\omega \varepsilon_0 \varepsilon_1} k_1 e^{j\beta x} e^{-k_1 z}$$

Equation 2-28

$$E_z(z) = -A_1 \frac{\beta}{\omega \varepsilon_0 \varepsilon_1} e^{j\beta x} e^{-k_1 z}$$

Equation 2-29

Where the subset 2 relates to the dielectric layer and the subset 1 relates to the metal layer. Through this math some important factors start to drop out. The propagation constant, k_z, represents the electric field perpendicular to the interfaces with $\hat{Z} = \frac{1}{|k_z|}$ evanescent decay into the dielectric, i.e. the skin depth and wave confinement. Since there must be continuity of H_y and $\varepsilon_i E_z$ between the two interfaces the two amplitudes must equal each other, hence:

$$\frac{k_2}{k_1} = -\frac{\varepsilon_2}{\varepsilon_1}$$

Equation 2-30

An important result arising from Equation 2-30 is the negative sign. This means for the wave to be confined at the interface, the real part of their dielectric permittivity needs to be of opposite sign, this obviously is case between a metal and a conductor. Since the expression for H_y has to satisfy the magnetic wave equation this is analogous to Equation 2-22 resulting in:

$$k_1^2 = \beta^2 - k_0^2 \varepsilon_1$$
$$k_2^2 = \beta^2 - k_0^2 \varepsilon_2$$

Equation 2-31

Using Equation 2-31 and combining it with Equation 2-30 results in the main focus for this derivation, the dispersion relationship of a surface plasmon wave.

$$\beta = k_0 \sqrt{\frac{\varepsilon_1 . \varepsilon_2}{\varepsilon_1 + \varepsilon_2}}$$

Equation 2-32

Looking at the TE modes gives rise to a similar set of equations than for those of the TM modes. Again there must be continuity between the interfaces of H_x and E_y giving the condition:

$$A_1(k_1 + k_2) = 0$$

Equation 2-33

Since the real part of the propagation constants must be positive, $A_1 = A_2 = 0$, is the only solution. This is a non-physical result and means surface plasmons surface modes only exist for TE polarisation. Thus it proves that no TE modes can exist, giving rise to strong polarisation sensitivity to the SPR. More behaviour can be established by looking at the phase matching condition, Equation 2-32. To excite an SPR, the propagation constant of the exciting light wave and the surface plasmon must be equal. However, typically the dispersion curves cross and as such special phase matching techniques must be implemented, as will be discussed in section 2.4.2 Prism Coupling: the Kretschmann method. The dispersion relationship is strongly dependent upon the conductor's dielectric permittivity, as such any small change in surrounding refractive index will result in a large change to any SPR propagation constant, making it an ideal refractive index sensor.

2.4.2 Prism Coupling: the Kretschmann method

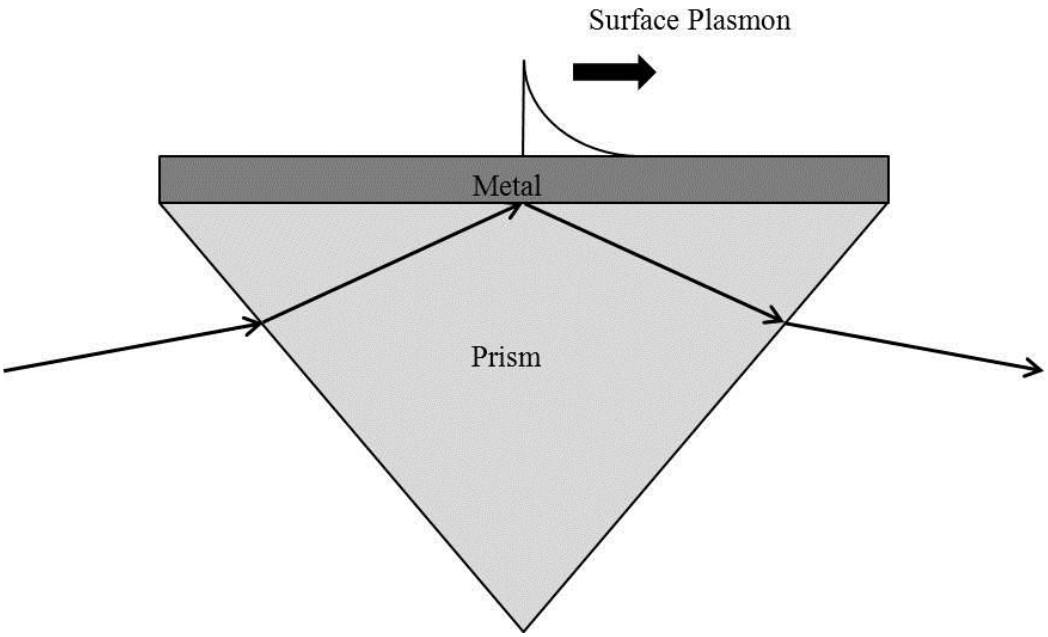

Figure 2-6 showing the Kretschmann configuration and its principle of operation.

Typically surface plasmons cannot be excited by light directly since $\beta > k$, thus the x component of the light wave is always going to be smaller than the propagation constant. A way around this is to use a prism to couple light into the SPR. One of the most common setups used and one that is analogous to polished optical fibre is the Kretschmann configuration, as shown in Figure 2-6. Since the light wave is now travelling through a prism its' x-plane propagation constant is $k_x = k\sqrt{\varepsilon}sin(\theta)$. This means it is capable of producing surface plasmon at the metal/air surface, as such requires tunnelling of the light through the metal to the metal/air surface. The modes created using this technique are inherently leaky, propagating back into the prism. However, through proper design of the metal coating thickness, the leaky radiation can be destructively cancelled out using the reflected excitation beam[32, 33]. The optimisation calculation can be carried out using Fresnel's equations and is derived in "Surface plasmons on rough and smooth surface and on gratings" by Heinz Raether[32].

2.5 Localised Surface Plasmon Theory

As previously described, surface plasmon are a propagating electromagnetic wave coupled to the electron plasma of a metal and confined to the metal dielectric interface, however localised surface plasmon resonances (LSPRs) differ. An external electric field excites the conducting electrons of a metallic nanostructure, which are non-propagating. The shape of the particle can cause a restoring force upon the driven electrons which can lead to a resonance. This effect can lead to an amplification of the electric field both inside and the near field zone outside of the particle structure. The advantage of this mechanism is that direct light can be used to stimulate LSPR, comparing to the phase matching technique that need to be employed for SPR.

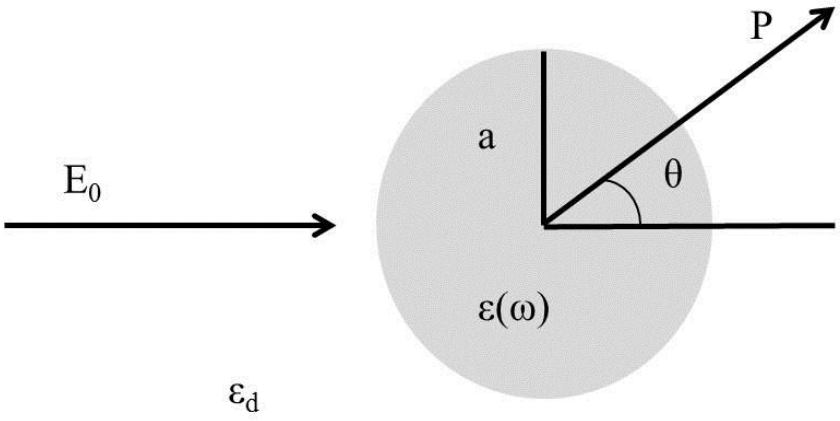

Figure 2-7 showing the LSPR structure of a metal sphere surrounded by a dielectric with an implied electric field.

The size and shape of the particle will have a great effect on the properties of the LSPR, however to get an understanding of the operating principle of a LSPR it is best to take the simplest case of a metal spherical particle surrounded by a dielectric, as shown in Figure 2-7. Taking the electro static approach, the electric field is defined as being uniform and in the z direction with the field lines parallel in the z direction and larger than the sphere. The dielectric response is $\varepsilon(\omega)$ and is considered to be a simple complex number and the surrounding dielectric medium is ε_d.

Starting with Laplace's equation for:

$$\nabla^2\Phi = 0$$

Equation 2-34

The electric field can be found since:

$$E = -\nabla\Phi$$

Equation 2-35

Since the particle has azimuthal symmetry the general form of the solution can be found in Jackson[34] and is:

$$\Phi(\mathrm{r},\theta) = \sum_{l=0}^{\infty}(A_l r^l + B_l r^{-(l+1)})P_l(\cos\theta)$$

Equation 2-36

Where P_l are the Legendre polynomials of order l and the angle θ is defined as being between the vector r at point a P and the z axis. Since the potentials, and hence electric field, must remain finite at the origin the potentials inside and outside of the sphere are given by:

$$\Phi_{in}(\mathrm{r},\theta) = \sum_{l=0}^{\infty}(A_l r^l P_l(\cos\theta)$$

Equation 2-37

$$\Phi_{out}(\mathrm{r},\theta) = \sum_{l=0}^{\infty}(B_l r^l + C_l r^{-(l+1)})P_l(\cos\theta)$$

Equation 2-38

The electric potential must be $-E_0 z$ as $r \to \infty$ and the tangential components must be equal. This gives the boundary conditions required to solve the equations and find the coefficients, yielding the solved equations.

$$\Phi_{in}(\mathrm{r},\theta) = \frac{3\varepsilon_d}{\epsilon(\omega) - 2\varepsilon_d} E_0 \mathrm{r}\cos\theta$$

Equation 2-39

$$\Phi_{out}(\mathrm{r},\theta) = -E_0 \mathrm{r}\cos\theta + \frac{P.r}{4\pi\varepsilon_0\varepsilon_d r^3}$$

Equation 2-40

Where P is the dipole moment inside the sphere and is proportional to the electric field. To arrive at the physical meaning of this and the main result the polarisability of P is defined as $P = \varepsilon_0\varepsilon_d\alpha E_0$, where.

$$\alpha = 4\pi a^3 \frac{\varepsilon - \varepsilon_d}{\varepsilon + 2\varepsilon_d}$$

Equation 2-41

From the Equation 2-41, when the denominator approaches zero a resonance and enhancement occurs, when $Re[\varepsilon] = -2\varepsilon_d$. This resonance is dependent on the dielectric of the surrounding medium and as such makes LSPR particles ideal refractive index sensors. This approach is only valid for sufficiently small particles, below 100nm, since it relies upon the quasi-static approximation (provided the size of the particle is smaller than the wavelength of light)[31]. Also the resonance condition is dependent on shape, size and material of the particles meaning all these must be optimized depending on the sensing application. For larger particles Mie, where the approximation is no longer valid, theory[35] can be applied but is beyond the scope of the work here, since it is intended only to explain the basic properties and refractive index sensitivity of LSPRs.

2.6 Optical fibre gratings sensors to date

2.6.1 UV inscribed Long period grating

Long period gratings (LPGs), typically, have a period ranging from 100μm to 1mm. The LPG couples light from the core mode to the co-propagating cladding modes. The co-propagating modes of the cladding have a high attenuation. This creates a series of losses at specific wavelengths in the transmission spectrum. The location of the attenuation peaks, in the transmission spectrum, is dependent upon the local environment. As such, they have been used to sense temperature[36], strain[37-39], bending[40, 41] and (because the cladding modes evanescent fields extends in to the surrounding) refractive index[42-44].

As discussed in section 2.3, the spectral location of the attenuation peaks of an LPG is governed by the phase matching condition. The strength of the attenuation peak is governed by[45].

$$T_m = 1 - \sin(K_m L)$$

Equation 2-42

In standard SMF the cladding radius is a lot larger than that of the core and as a result can support many modes. The modes that can be effectively coupled to is governed by the coupling coefficient. Only cladding modes that have a large overlap with the core mode will efficiently couple. This is the case when the cladding modes are circularly symmetric and of odd order. This is because, even modes have very little electric field within the core, whereas the odd modes have a large proportion of electric field within the core[24]. To model the central wavelengths of a LPG the effective index of the core and cladding modes have to be calculated. This is normally carried out using a three layer system of, core, cladding and air and the using the weakly guided field approximation. The

approximation states, the difference between the effective core mode and effective cladding modes are small[46]. Further to this, instead of HE and EH modes, linearly polarised can be used to further simplify the calculations. For lower order modes this is valid since the difference in effective indices is small[47]. This results in an eigenvalue equation[24, 47, 48] that when solved calculates the effective indices of low-order cladding modes[26]. Once the effective index of each cladding mode has been calculated a dispersion relationship can be calculated. This has been done by several authors[45] and an example of which is taken from Xuewen Shu et al and shown in Figure 2-8[49]. From Figure 2-8 two periods have been selected, shown by the straight lines, to demonstrate why different periods of an LPG have different attenuation resonances in the transmission spectrum. Longer periods LPGs couple to the lower order cladding modes, of which there are more, in the wavelength range 1250-1700nm. While, shorter period LPGs couple to higher order cladding modes, of which there are fewer. This means that a LPG with a period of approximately 500μm will have five attenuation resonances while a LPG with a period of approximately 164μm will have two attenuation resonances. Also, for certain higher order cladding modes it is possible for a LPG to couple to the same cladding mode at two different wavelengths and is commonly referred to as a dual resonance.

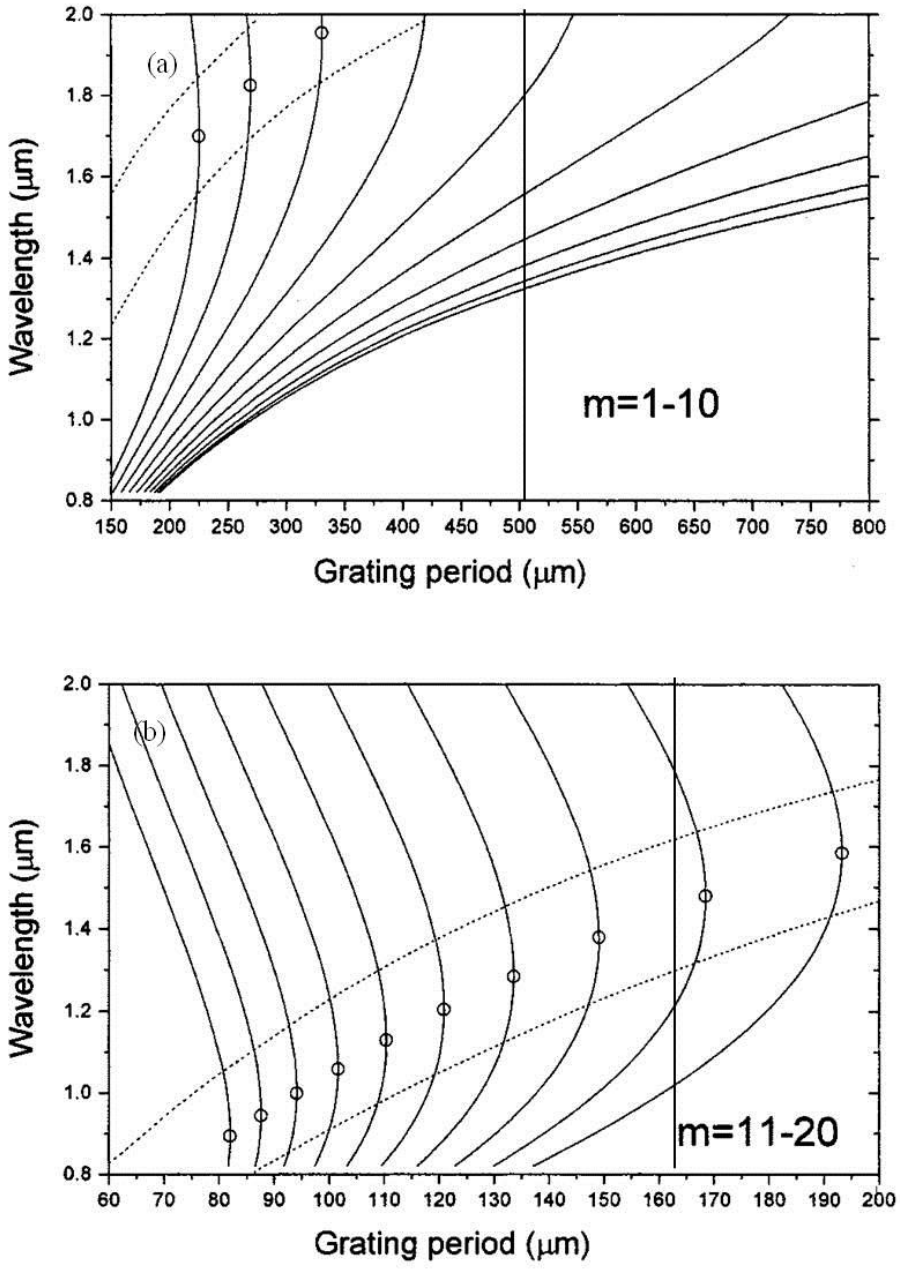

Figure 2-8 Showing the calculated dispersion relationship by Xuewen Shu et al

Different cladding modes have different dispersion relationship and as a result different sensitivities to external environmental changes. Shu et al called this the general sensitivity factor and calculated it for the first 30 cladding modes, this is taken from his paper and shown in Figure 2-9[49]. The most sensitive cladding mode of SMF optical fibre was found to be m~12, i.e. around the 12^{th} cladding mode, and is due to a dual resonance.

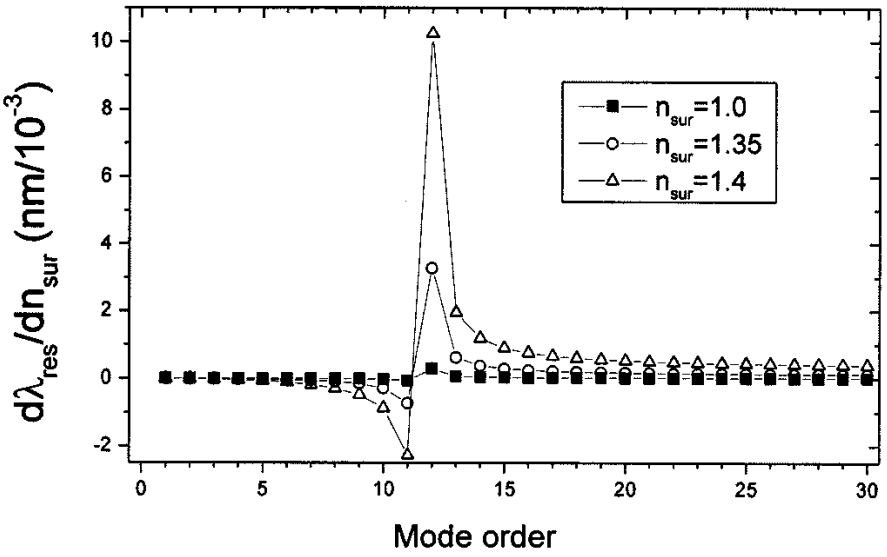

Figure 2-9 Showing the sensitivities of the first 30 cladding modes to changes in SRI

The RI sensitivity of the LPG arises from the cladding modes effective index being dependent upon the SRI. Thus, a wavelength shift occurs in the transmission spectrum with any change in SRI, which is governed by the phase matching condition. The highest sensitivity occurs when the SRI approaches that of the cladding[42]. This is a limiting factor in using LPGs as refractive index sensors, with their sensitivity limited to relatively high RIs. When the SRI is equal to that of the cladding RI the electric field sees the cladding as infinite. As a result, discrete cladding modes are no longer supported and the attenuation resonances disappear. Increasing the SRI beyond the RI of the cladding results in a large decrease in sensitivity[42, 50] as shown in Figure 2-10, which is taken from Kaliq et al 2001 paper[51]. This is because the cladding is no longer acting as a waveguide and the modes are now attenuated cladding modes due to Fresnel reflections rather than total internal reflections from the cladding air interface[52].

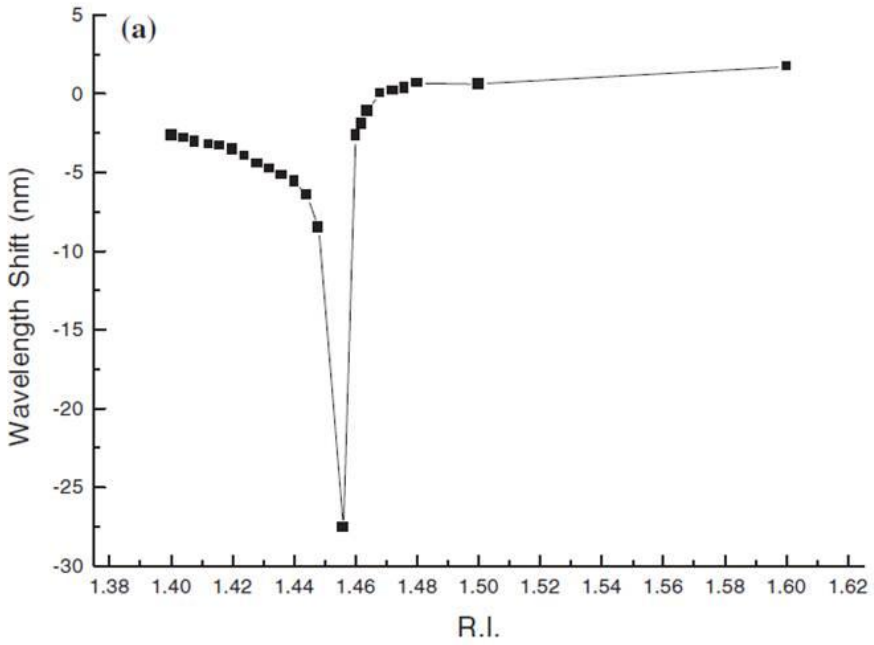

Figure 2-10 Showing the typical response of a LPG over the RI range 1.39 to 1.62 and taken from S. Khaliq et al paper

Both the phase matching condition and the Equation 2-42 are functions of the refractive index change of the optical fibre. Since the UV induced RI change in the fibre is unstable, over time, there is a change in coupling strength and wavelength of the attenuation bands[53]. This instability can be removed through high temperature annealing but means, when designing a LPG the annealing effect needs to be taken in to account. Hydrogenating the optical fibre, for increased photosensitivity, induces further complications for precise design of a LPGs transmission characteristic. Demonstrating this, Gaun Bou et al observed a 40nm wavelength shift and a14dB growth in attenuations bands in the first 20 hours after UV exposure. After 450 hours there was a decrease in central wavelength of 50nm and a slow reduction in attenuation band strength[8]. This is explained by two steps. First, hydrogen diffuses into the expose region, which has been depleted due to UV exposure. This causes an increase in RI change in the exposed regions and a decrease in the non-exposed regions, leading to the observed change in attenuation band characteristics. Secondly, this is followed by a slow out diffusion of the hydrogen from the core of the fibre. This has the effect of reducing DC RI of the core and causing the change in attenuation bands central wavelength and strength[45].

LPGs have been reported to have refractive index sensitivities as high as ~680nm/URI, when considering a dual resonance peak[49], though for single mode coupling attenuation peaks the sensitivity is typically ~113nm/URI[43]. As such, LPGs have found various uses as RI sensors being implemented as chemical concentration sensors[54, 55], liquid level sensors[56, 57] and quality control in industry measuring various concentrations of solutions[58].

2.6.2 Femtosecond long period gratings

LPGs have also been inscribed into optical fibres using femtosecond lasers [59-61]. Femtosecond inscribed gratings have a far greater focus than UV inscribed gratings and only induce an index change in a small section of the fibre core. Much like small and large angle tilted gratings; there is now angular and polarisation dependence on femtosecond gratings. Mathematically, Turan Erdogan showed that the coupling efficiency between two modes (shown in Equation 2-10) has an extra term when coupling between all azimuthal modes becomes possible[24].

$$\int_0^{2\pi} e^{j(l-1)\emptyset} d\emptyset = 2\pi\delta_{l1}$$

Equation 2-43

As a result, the small focus of femtosecond inscribed grating and the localised RI change associated with it has two different properties compared to the uniform RI change throughout the core of UV inscribed gratings. Firstly, a polarisation dependency arises since different polarisations of light will see the RI perturbation differently. Secondly, the azimuthal dependence now means that the cladding mode coupling is not limited to LP_{1l} but can now couple to multiple sets of cladding modes LP_{ml}, unlike the UV LPG which can only couple to cladding modes of azimuthal order 1[24]

Further to this, though the linearly polarised light approximation is adequate for the uniform index perturbation of UV inscribed gratings and to explain why a femtosecond LPG can couple to azimuthal modes it is not sufficient to explain the full mode coupling behaviour. To achieve a more accurate modelling the linearly polarised approximation must be avoided, especially for higher order modes[24]. In fact, to fully explain the polarisation properties of femtosecond inscribed gratings a full vectoral approach is necessary, since it accounts for the splitting of the resonance peaks[62]. The task is further made more difficult by the dependence of the core-cladding coupling efficient on the size, shape and location of the void within the optical fibre[63]. These variables mean the modelling of the femtosecond LPG is a more difficult task than that of a UV inscribed grating. Due to the femtosecond LPG ability to couple to multiple sets of cladding mode orders it has the possibility of coupling to cladding modes with higher sensitivities to external stimuli in the wavelength range of 1250-1700 nm than a standard UV LPG. To date, most of the literature on femtosecond LPGs has been investigating their inscription characteristics. However, they have been used to sense bending[64] and temperature (producing sensitivities ~0.12 nm/^{o}C)[59, 65, 66].

2.6.3 Tilted optical fibre gratings

A further type of optical fibre index perturbation is that of the tilted gratings. A tilt, or blaze, can be introduced into the inscription process. The first tilted grating structure investigated was that of a Bragg grating with a small tilt angle(TFBG)[27]. T Erdogan et al showed that through inscribing a Bragg grating with a tilt the grating was now capable of stronger coupling to both the low order cladding modes and radiation modes. Through varying the angle of the grating tilt, the degree to either cladding mode or radiation mode coupling could be controlled. The index perturbation within the core of a TFBG has a X, Y and Z axis dependence, this allows the TFBG to couple to both the LP_{0m} and LP_{1n}

cladding modes, unlike the LPG which can only couple to LP_{0m} cladding modes[28, 67]. Since the TFBG couples to the cladding modes it has been used by various authors as SRI sensors[30, 68]. However, the TFBG couples to the lower order cladding modes and is less sensitive to changes in SRI producing typical sensitivities of ~8.5 nm/URI[68], which is smaller than an LPG .

If the tilt of the TFBG is increased beyond around 5^o the coupling efficiency to both the reflective core mode and cladding modes decreases overall[67]. This is because the phase matching condition favours radiation mode coupling for intermediate angles. At an angle of 45^o all the light coupled out of the fibre is into the radiation modes and also has a very high polarisation dependence[69]. As a result this has found a direct use as an in line optical fibre polariser[70]. Though most of the current theoretical work has been limited to angles below 60^o there has been some experimental work carried out on large angle tilted grating structures. K. Zhou et al[71] investigated a grating with a tilt larger than 80^o. Though the amplitude mask used had a period of 6.6 μm, with the tilt angle being so large the actual period of the grating in the fibre could be considered closer to around 67 μm. This period is closer to that of a LPG than an FBG and this combined with the forward tilt of the structure results in strong coupling to the cladding modes. The modes that are coupled to are higher order cladding modes, supported by the fact that the resonances disappear when the SRI is around 1.41. Also, the attenuation peaks consist of doublets which the author contributed to the coupling of light to two orthogonal polarisation states. A similar transmission spectrum, with the splitting of the cladding peaks, was observed by Jens Thomas et al[63]. As already stated, for lower order cladding modes the LP approximation can be used. However, for higher order modes this approximation breaks down because the difference between the EH and HE effective index's is sufficiently large to be observed in the transmission spectrum. When this is accounted for, the splitting of the attenuation peaks corresponds well to theory. K. Zhou et al reported a SRI sensitivity of

around 320 nm/URI[71] which is higher than most LPGs, except those with dual resonances. Also, lower temperature sensitivity of 3-7 pm/^{o}C was reported, which is lower than both a LPG, 3-10 nm/^{o}C[72], and FBG, 10 pm/^{o}C[73]. This is probably due to the grating period being smaller than a typical LPG and being less effected by thermal expansion and effective index changes associated with temperature variations.

2.6.4 Nanoscale coated long period gratings

Although LPGs have proven themselves to be very good RI sensors they still have limitations on their effective RI sensing range, as discussed previously. Due to this, techniques have been investigated to improve the overall sensitivity of LPGs. One of these ways is through the coating of LPGs with higher RI materials. The increase in sensitivity of coating LPGs with high RI materials will be discussed first followed by the various nanoscale coating techniques people have implemented.

When an optical fibre is coated with a high RI material the material itself can act as a waveguide, if its RI is higher than the cladding[74]. The higher RI increases the effective index of the cladding mode[75] and also, with sufficient thickness, reorganises the cladding modes[76, 77]. Ignacio Del Villar et al theoretically calculated this occurrence and their results showing this are displayed in Figure 2-11[75]. With increasing coating thickness there is a small increase in cladding mode effective index until there is sufficient overlay to sustain a mode where upon a reorganisation of cladding modes occurs. When this happens cladding mode m has an effective index matching cladding mode m+1, before the coating[77]. This is associated with a steep transitional change in effective cladding index compared to overlay thickness. This occurs several times in Figure 2-11 occurring each time the cladding overlay increases enough to support another mode in the coating. If the overlay thickness it selected carefully the effective index of a cladding mode is found in the transitional stage and as a result has an increased sensitivity to SRI changes. The

maximum sensitivity is achieved when the coated cladding modes index is half way between its original uncoated effective index and the effective index of the next uncoated cladding mode. This means there is an optimum for the coating thickness that is dependent upon both the coatings RI and thickness. Different modes still have their individual sensitivities, thus the sensitivity increase is different for each cladding mode. C. S. Cheung et al. investigated the behaviour of nanoscale coatings on cladding modes near the dispersion turning point who exhibit dual resonances[78]. For this special case, they found the optimum coating thickness theoretically and observed the wavelength shift with increasing coating thickness experimentally.

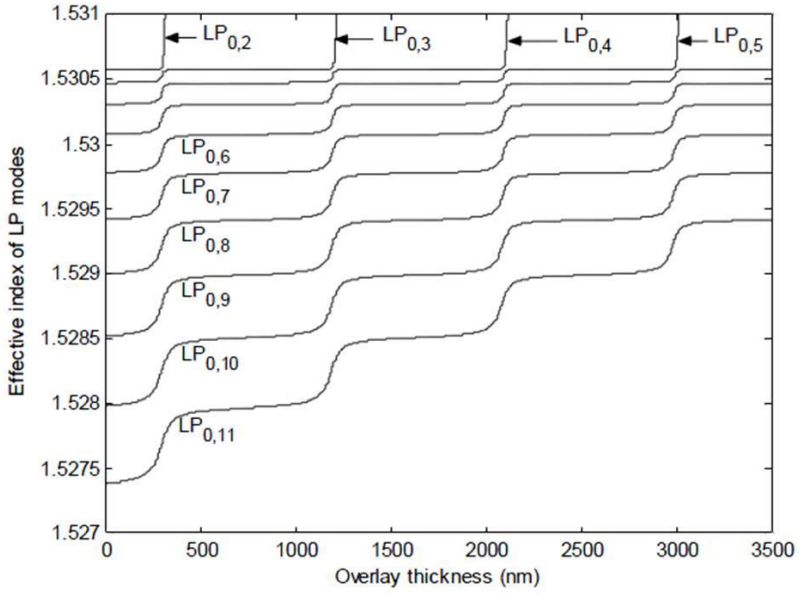

Figure 2-11 showing the reorganisation of the cladding modes from applying a high RI coating calculated by I Del Villar

When coating LPGs the accuracy of the coatings require control on the nanoscale because the optimum coating thickness has a very narrow window of operation. With this in mind three techniques have been most used coating of LPGs; these are the Langmuir-Blodgett (LB) technique [79, 80], Electrostatic self assembly (ESA) [81-83] and Sol-gel coatings [84, 85].

The Langmuir-Blodgett technique relies on forming molecules that have both hydrophobic and hydrophilic tail or head groups, such as soap. The molecules are formed in a solvent and water. The solvent is allowed to evaporate leaving the molecules on the surface of the water. Through the use of a barrier, the surface area is slowly decreased which in turn increases the surface pressure experienced by the molecules. This forces them to interact with each other and align themselves into an ordered array which can be transferred to a solid substrate or optical fibre. This is done through dipping of the optical fibre into the film where the molecules attach layer by layer, according to Figure 2-12, taken from Steve James et al 2006 [74]. The main advantage of this technique is high degree over the controllability of the coating thickness and has been used by several authors for coating optical fibres [86, 87].

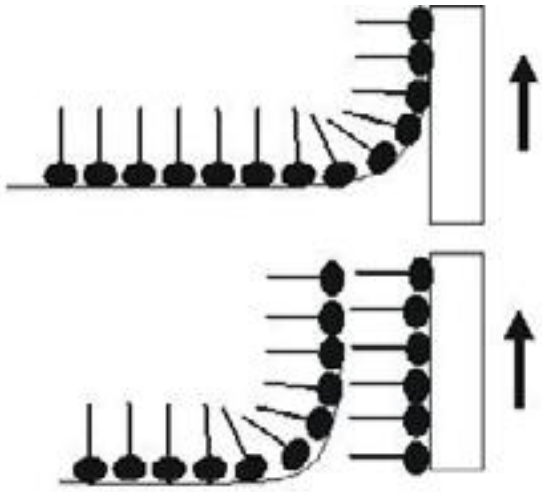

Figure 2-12 showing the hydro phobic/philic parts of an LB film being attached to a substrate.

The second technique is that of electrostatic self assembly and relies on forming the coating layer by dipping the charged optical fibre into alternate layers of cationic and anionic polymers. The coating is formed from the electrostatic bonds between the oppositely charged molecules[88]. The optical fibre is usually immersed in a solution of H_2O_2 and concentrated H_2SO_4 for 30 mins, rinsed and allowed to dry in an oven at 80^oC, which gives rise to the charge on the optical fibre surface[89]. Similar to the LB process, the optical fibre is then dip coated with each immersion of the surface forming another

layer of charged molecules and a thicker coating. The ESA process has been used for coating optical fibres with long period grating inscribed in them and shown to increase their sensitivity[76].

Finally considered is the Sol-gel technique. The Sol-gel usually starts with metal alkoxides, in this case titanium and silicon, water, acid base and alcohol. When all these are put into solution the alkoxides hydrolyse and condensate, leading to particle formation, i.e. sol. A sol is classified as colloidal suspension of solid particles in a liquid. A gel is considered to have formed when a continuous solid skeleton encloses continuous liquid phase. The fibres were dipped into the sol and withdrawn at a constant speed; this allows the sol to coat the fibre surface and the solvent to evaporate when exposed to the air. A densification of the coating can be achieved through heat treatment after deposition. The reason that sol-gel coatings are porous is due to the sol, when the sol form it contains nano-particles and after drying and hear treatment there are gaps between them. The easiest methods of control over the sol-gel coating is quality is to control the speed at which the fibre is withdrawn. With slower withdrawal speeds the sol is allowed to fall off leaving a thinner layer, whereas higher speeds don't allow for this and result in thicker layers. Also if the concentration of particles in sol is lower it leads to thinner coatings, as would be expected. This can lead to similar control over the coating thickness of the Sol-gel process compared to the other techniques. This coupled with the high thermal stability of the coating and the ability to encapsulate species specific indicators[90] has meant the Sol-gel method has been implemented by several authors for multiple sensing applications including bio[91]- and gas sensing[92]. The various coating techniques have been reported to improve the sensitivities of non dual resonances by a factor of up to ten and producing a sensitivity of around 568nm/URI[77, 86]. Research has been carried by, S. Korposh et al, out on coating a LPG that couples to a dual resonance, though no numerical value was reported an increase in sensitivity was observed[93].

2.6.5 Bragg gratings and sampled Bragg gratings

Bragg gratings couple light from the core mode to the counter propagating core mode. As such, they are capable of detecting external stimuli that affect either the effective refractive index or the periodic spacing of the grating period. As a result, Bragg gratings are sensitive to changes in strain and temperature[73]. The wavelength shift of the Bragg wavelength for temperature change can be written as[94].

$$\Delta\lambda_b = \lambda_{res}(\alpha_p + \alpha_n)\Delta T$$

Equation 2-44

And for silica $\alpha_p = 0.55x10^{-6}$ and $\alpha_n = 8.6x10^{-6}$[95].

A further type of grating is the sampled fibre Bragg grating (SFBG) which consists of both a high and low frequency modulation, akin to a fibre grating with both a LPG and FBG period, shown in Figure 2-13. One of the earliest people to inscribe one of these gratings was B. J. Eggleton et al who described the wavelength locations of the transmission peaks using coupled mode theory[95].

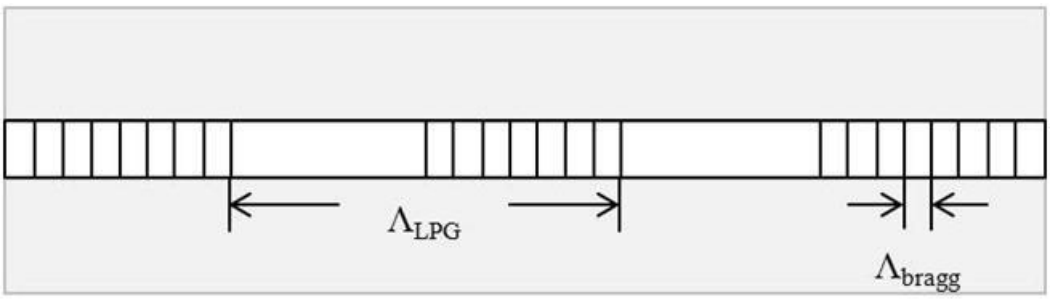

Figure 2-13 Showing the high and low frequency modulation of a SFBG

There are many ways of understanding the underlying properties of the SFBG and one of the best ways is to use SFBGs with Fourier analysis[96]. The low frequency modulation can be considered a convolution of a top hat function with a series of delta functions which results in a series of delta functions with a sinc function imposed on it and this is shown schematically in Figure 2-14.

The high frequency modulation gives the standard Bragg reflection response. Through combining this with the low frequency modulation convolution and since every Fourier component must contribute a reflection peak[95], a series of reflection peaks whose separation is defined by the period of low frequency modulation are produced. This means through control of both periods of the FBG and LPG inscription, the reflectivity characteristics can be tailored for specific wavelength needs.

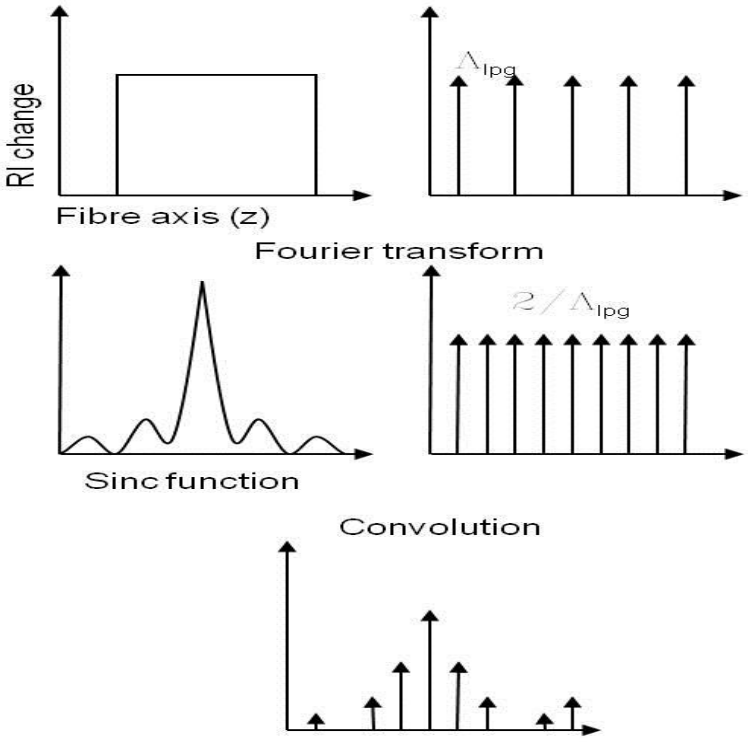

Figure 2-14 showing the low frequency Fourier transform

Assuming an index perturbation similar to that found in[95] and[97],

$$\Delta n(z) = f(z)e^{-j(\frac{2\pi}{M}+\frac{2\pi}{\Lambda})}$$

Equation 2-45

Where δn is the RI change, $M$is the low frequency modulation period and Λ is the high frequency modulation period. Applying Equation 2-45 to the coupled mode equations in section 2.1 a new condition arises where the exponential is maximum and hence coupling to reflections occurs, this is

$$\frac{2\pi m}{M} = 2\pi\left(\frac{2n_{co}}{\lambda_c} - \frac{1}{\Lambda}\right)$$

Equation 2-46

Where n_{co} the RI of the core is, λ_c is the wavelength of the central reflection peak and m is the order of the Fourier reflections. From this it is possible to derive the wavelength spacing between the reflection peaks of an SFBG.

$$\Delta\lambda = \lambda_{res}^2/2n_{co}M$$

Equation 2-47

Typical SFBGs have both an LPG and FBG response. This means they couple to, both, the counter propagating core mode and the co propagating cladding modes. The core modes, similar to the Bragg grating, are unaffected by changes in SRI but are affected by changes in temperature and strain. The cladding mode, like the LPG, is affected by strain, temperature and SRI changes. This has led the SFBG to be used as multi-parameter sensors for strain and temperature [98], temperature and bending [99] and temperature and RI [100]. Where the reported temperature sensitivity of reflected core modes was 12.2 pm/^{o}C and the SRI of the cladding modes was around 45nm/URI, both of which are close to typically expected values for a FBG and LPG.

2.6.6 Etched fibre gratings

HF acid has long been used for etching glass. As such, it has been implemented for removing all or a desired amount of the optical fibre cladding. The advantage of this is that through control of the cladding radius the interaction of the cladding or core mode with SRI can be increased, which increases the sensors sensitivity[101]. For FBGs, the light is bound in the core of the optical fibre and is SRI insensitive. Due to this, the majority (if not all) of the cladding has to be removed to make the FBG sensitive. When this is achieved the etched FBG produces a strong resonance wavelength shift with

increasing SRI [102-105]. However, the wavelength shift produced isn't on the same order of magnitude as an LPG but does have a higher resolution due to the narrow resonance of the Bragg reflection. The enhancement of cladding modes through etching has been investigated using both small angle tilted Bragg gratings [106, 107] gratings and also LPGs [108, 109]. Small angle tilted Bragg grating couple to the lower order cladding modes which, similar to the Bragg grating, requires the majority of the cladding layer to be removed. Though the results achieved are good, this leaves the optical fibre fragile and therefore impractical. Since the LPG couples to higher order cladding modes, compared to the small angle tilted Bragg grating, not as much of the cladding radius has to be removed before an increase in sensitivity is seen. This leaves the etched LPG less fragile than its etched counterparts. The added advantage is that when the cladding is etched there is a reorganisation of the cladding modes[101] which causes a shift is the resonance wavelengths of the LPG. This allows the tuning of the LPG spectrum [110, 111]. This can be used to optimise SRI sensitivity by tuning the resonances of a dual peak [112, 113]. An etched Bragg grating has a reported sensitivity of ~25nm/URI[102] while an etched LPG was~400nm/URI[101]. Though the sensitivity of an etched Bragg grating is lower the resolution is higher. Also, this is the sensitivity achieved for a non dual resonance cladding mode.

2.7 Optical Fibre based surface Plasmon sensors

Optical fibre based surface Plasmon sensors have experienced growing interest in recent years due to their high sensitivity and compact size. To date, all optical fibre surface plasmon sensors are akin to the Kretschmann setup, with light propagating within a prism coupling to the surface plasmon mode of the metal dielectric interface. To do this light has to couple from the core of the optical fibre to the metal dielectric interface. Currently, two ways have been explored for achieving this; firstly, through removing all or part of the

optical fibre cladding which allows the evanescent field to interact with the metal/dielectric interface; secondly, the use of fibre gratings to out couple the light from the core to the cladding layer which in turn couples to the surface plasmon mode. When phase matching occurs this appears as a loss resonance in the transmission spectrum of the sensor. Changing the SRI results in a change in propagation constant of the surface plasmon which alters the phase matching condition and the wavelength at which resonance occurs. This relationship is shown in Equation 2-48 and shows that only when the phase matching condition is equal to zero a resonance occurs. Further to this intensity can be used as a sensing mechanism. From Fresnel reflection theory (stated early) loss can be optimised for the leaky mode and the reflected light to constructively interfere. By moving away from this optimum, through changing SRI, the resonance amplitude changes and gives rise to an alternative sensing mechanism. Optical fibre sensors are limited to evanescent field interactions which, inherently, have their peak SRI sensitivities when the SRI is close the RI of the cladding. SPRs are not dominated by this effect and as such give the possibility of high sensitivities at lower SRIs.

$$k_o \sqrt{\frac{\varepsilon_1 \cdot \varepsilon_2}{\varepsilon_1 + \varepsilon_2}} - k_o . n_{cl}^{eff} = 0$$

Equation 2-48

An alternative approach is to use UV inscribed. This can be done with standard optical fibre or altered optical fibre geometry to enhance and control the surface plasmon resonance sensitivity. Three types of grating have been implemented as grating based surface plasmon sensors including LPGs[114, 115], tilted Bragg gratings[116, 117] and Bragg gratings[118, 119]. The sensitivities produced by grating based device are often lower than their modified optical fibre geometries counterparts, being only of the order 150nm/URI and above. This is a lot lower than the sensor based on changing the optical fibre geometry and can be attributed the requirement of the coupling to the cladding modes

and then the surface plasmon. The exception to this is the work carried out by T. Allsop et who used a partially polished D-shaped optical fibre and a tilted Bragg grating to enhance coupling to the surface plasmon mode[116] and reported a sensitivity of around 3000nm/URI. This sensitivity is comparable to the sensitivities to other sensors who had their optical fibre geometries changed, however due to the inscribed tilted grating the sensor did not require the full removal of the cladding layer. Optical fibre surface plasmon based sensors have shown that they are capable of sensitivities far greater than UV inscribed gratings. However, unlike LPGs and FBGs their behaviour is less predictable with non ideal parameters, such as the metal surface being non uniform. This means that, often, theoretical analysis can only be used as a guide[120] and practical sensor development is needed for full optimization

3 Fabrication and characterisation of refractive index sensitive fibre Bragg gratings

3.1 Long period gratings

3.1.1 Introduction

Long period fibre gratings (LPGs) are periodic induced index modulations upon the core of optical fibre, typically in single mode fibre. They differ from Bragg gratings in two ways: (I) their period is between approximately 100µm and 1mm, which is significantly larger than Bragg gratings; (II) they couple light from the core mode to the co-propagating cladding modes unlike to the contra-propagating modes of a Bragg grating. Where the light is coupled to the cladding modes, in the transmission spectrum LPG attenuation peaks occur. The LPGs have been used as filters[121], but since they are dependent on external stimulus they can be used to detect changes in temperature [37, 122], strain[36], bending[123, 124] and refractive index[42, 72]. The guided cladding modes have an evanescent decay into the surrounding mediums, meaning any change in surrounding medium refractive index (SRI) will change the cladding mode effective index. This in turn affects the phase matching condition, Equation 2-16, and hence the resonant wavelength of the attenuation peak performs a detectable shift in transmission.

3.1.2 Fabrication and typical characteristics

LPGs were inscribed into standard SMF that had been hydrogenated at 80^0C under a pressure of 150 bars for 48 hours. The inscription method was point by point using 244 nm frequency doubled CW argon laser with a power density of ~2.2 kWm^{-2}. LPGs with

various periods were inscribed so as to draw comparison while keeping the grating lengths the same at 2cm. After the inscription the gratings were annealed at 100^0C for 48 hours to expel any excess unreacted hydrogen. The transmission spectra produced can be seen in Figure 3-1; each attenuation peak corresponds to a cladding mode that has been coupled to. As seen from the dispersion curves in Figure 2-8, decreasing the grating period decreases the amount available cladding mode to couple to and results in fewer resonances.

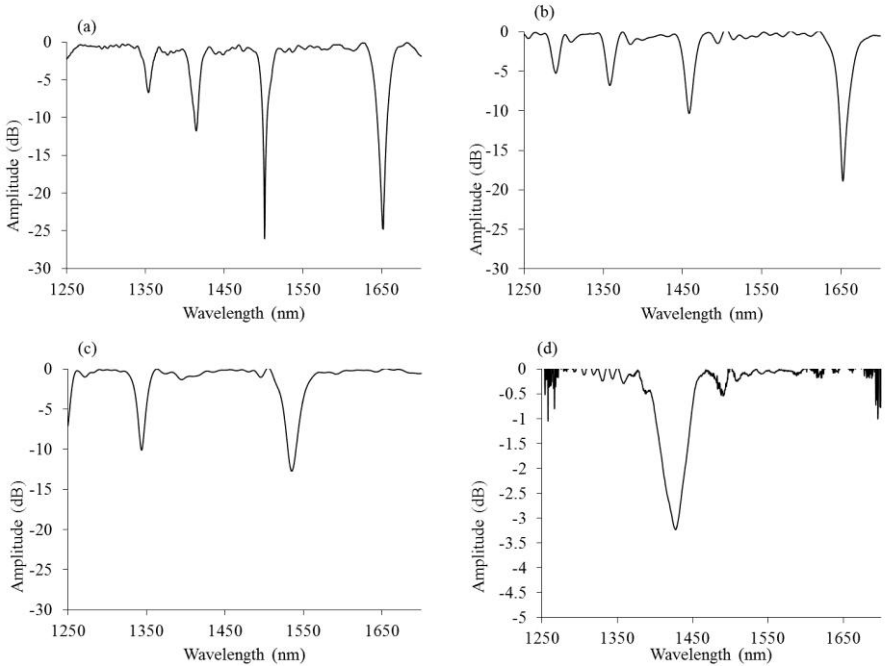

Figure 3-1 showing the transmission spectra for four LPGs with periods (a) 465µm (b) 400µm (c) 322µm and (d) 241µm

As a special case, already mentioned, is the dual resonance LPG where two sets of attenuation peaks exist due to coupling of the same order cladding mode. Figure 3-2 shows the growth of a dual resonance LPG under repeating UV scans. A repeat scan is when the inscription procedure is performed again from the first inscription's starting point. Each scan increases, both, the AC and DC induced index change in the core of the optical fibre, which manifests itself in a wavelength shift and amplitude change of the resonances (This is akin to the slow release of hydrogen from the fibre). This occurs until the peaks from both wavelength sides merge into one as they reach the dispersion turning point where the grating is most sensitive. This method also gives a further way of controlling LPG

characteristics, through repeat scans the desired transmission spectrum can be produced for a given period.

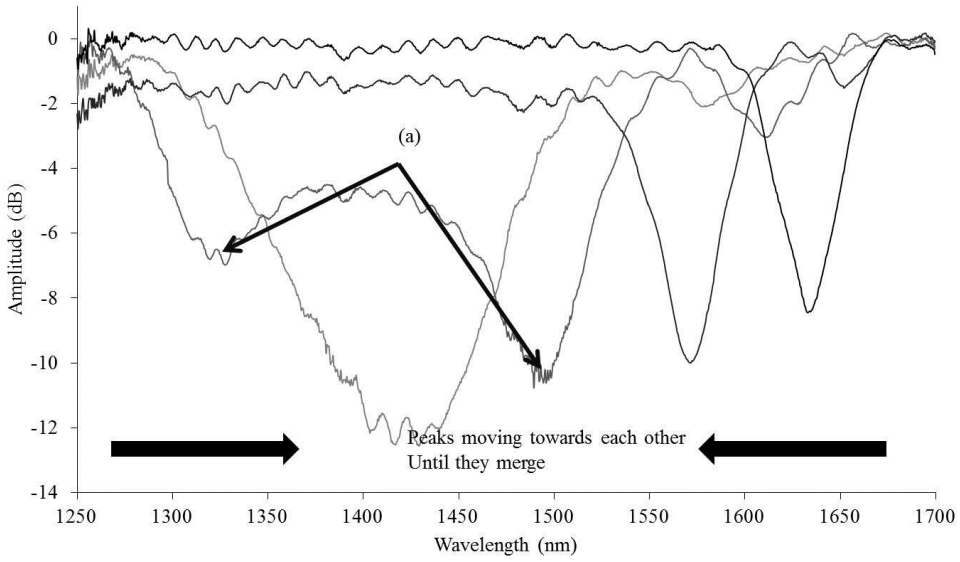

Figure 3-2 showing with repeating scans, the dual resonance peaks moving towards each other and eventually merging to one peak (a)

3.1.3 Refractive index response

To examine the LPG response to SRI sugar solutions of various concentrations were made using pure brown sugar and distilled water, so as to minimise impurities. The relationship between sugar concentration and refractive index is well documented and nearly linear, as shown in Figure 3-3[125].

Figure 3-3 showing the relationship between sugar concentration and refractive index[125]

To perform the SRI response characterisation, the LPG was placed on a metal plate with a 'v' groove and located on an optical bench, which acted like a heat sink minimising any temperature variation effects. The transmission spectra were normalised to remove the variation derived from the light source. The LPG was then covered with the sugar solution and its spectrum was captured. The LPG was cleaned using both distilled water and ethanol until, the attenuation peak shifted back to its position in air. This was to ensure full removal of any contaminants, before exposure to the next concentration.

Figure 3-4 shows the typical response to SRI on a LPG with period 238μm, as expected the wavelength shift and hence sensitivity increases greatly as the SRI approaches the index of the cladding. When the SRI index matches the index of the cladding, not shown here, the cladding is assumed to be infinite meaning no cladding modes are supported and the light is lost through radiation.

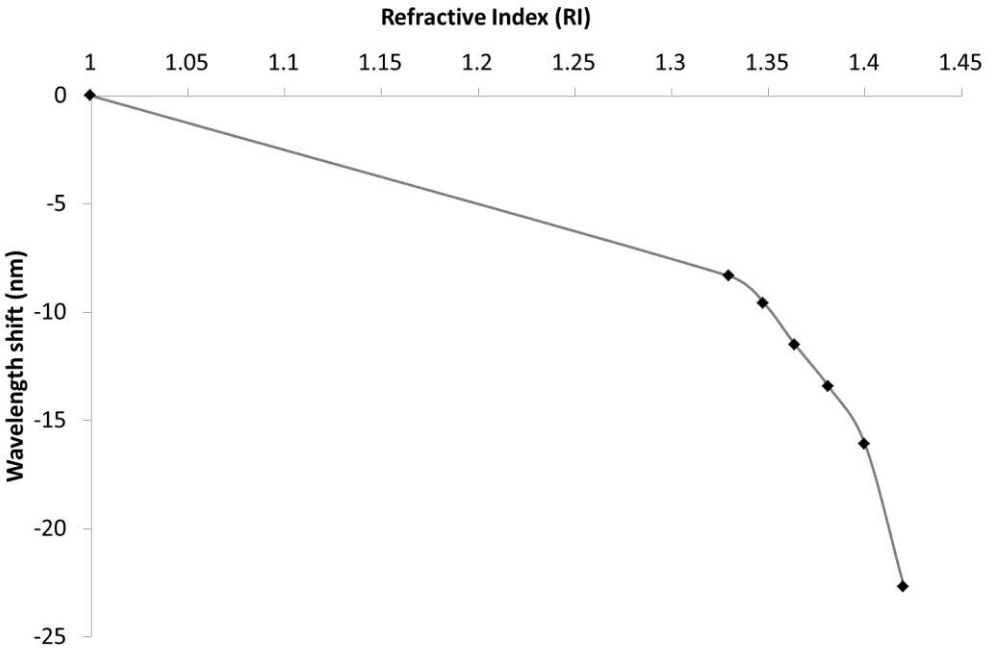

Figure 3-4 showing the refractive index response of the attenuation peak of a 238μm period LPG with the errors being too small to be seen on this scale

Shu et al[49] indicated that different modes should have different sensitivities and this is clearly show practically in Figure 3-5, where for easy comparison the relative shift of each attenuation peak is calculated using air as the reference point. With increasing period, SRI sensitivity increases with higher order cladding modes, which is expected. The most sensitive LPG in this work was found to have a period of 159μm, which had a dual resonance. A more sensitive period may exist, however the inscription method was incapable of producing gratings at periods lower than those reported here. This was because the confinement of the laser beam was not sufficient enough for such small periods, i.e. no periodic perturbation could be produced. What all the modes have in common is the increasing wavelength shift as the external refractive index approaches that of the cladding material. So although LPGs are very capable of detecting SRI changes when in the higher order mode regime, but they are not very sensitive in the SRI range around 1.33-1.38. This could be a disadvantage since many biological solutions interactions occur in this SRI range. Since bio-sensing is a very desirable application methods need to be derived to help overcome this problem. This can be done by careful

selection of grating period so as to maximise sensitivity; cladding etching and coating of the grating with another material of higher value. The last two will be discussed in sections 3.2 and 3.4.

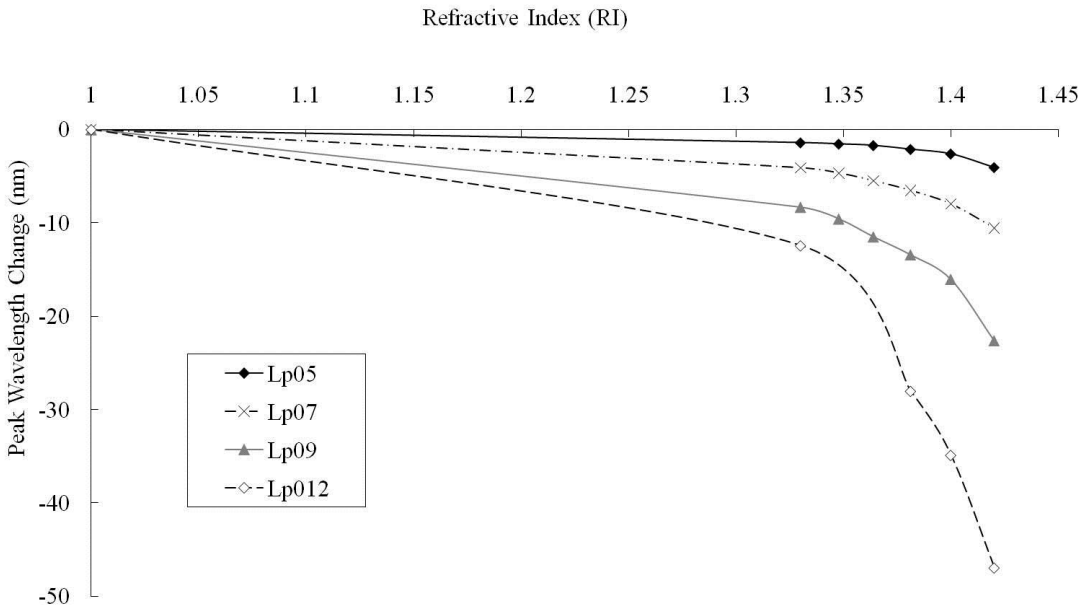

Figure 3-5 showing the SRI induced relative wavelength shifts of LPGs with various periods. The modes have been labelled using the dispersion curves calculated by X. Shu[49].

3.2 Large angle tilted fibre gratings

3.2.1 Introduction

Tilted fibre gratings (TFGs), both FBG and LPG, are simply grating structures that have their index modulation offset with respect to the fibre axis, Figure 3-6 shows an image of a typical large angle TFG. Small angle TFG couple light to the reflected core mode but also to the lower order counter-propagating cladding modes, because of this they are relatively insensitive to SRI change. The phase matching condition of large angle TFG allows the coupling of the core mode to the higher order forward propagating cladding modes and as

such they are much more sensitive to SRI change.

Figure 3-6 is an image of a large angle TFG showing the index perturbation tilted at ~81° and this image is taken from K. Zhou paper[71].

Large angle TFG have similarities with LPGs; both coupled to the co-propagating cladding mode, but the former to higher order and the latter to lower order and both have an SRI response and can be used as sensors[71].

3.2.2 Inscription and spectral property

The large angle TFG, or tilted LPGS, were inscribed into hydrogen loaded standard SMF using a frequency doubled Argon Ion laser at a wavelength of 244nm and a power density at the optical fibre of ~2.2 kWm^{-2}. The standard scanning mask technique was implemented using an amplitude mask from Edmunds Optics that had a period of 6.6µm. It was rotated by 79^{o} externally with respect to the fibre axis and thus, produced an internal index modulation at 81^{o}. Using a broadband light source and a polarisation controller the gratings transmission spectra response for polarised and un-polarised light could be examined, the configuration of which is shown in Figure 3-7. The actual polarisation of the light at the sensor could not be known from the experimental setup. All that was achieved through varying the polarisation was the maximum of one of the resonance doublets for investigation.

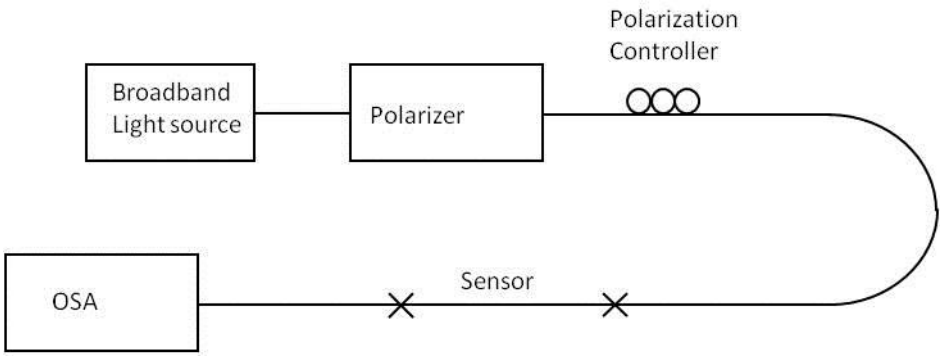

Figure 3-7 Showing the setup used to investigate the TFG properties

Figure 3-8 is an example of a typical large angle tilted Bragg grating spectrum. As can be seen from the figure, the spectrum is made up of resonances that have doublet features. This is seen with gratings coupling to higher order cladding mode[63]. This effect is attributed to the coupling to EH and HE cladding modes. As in LPGs, coupling to lower order modes only couple strongly to pure HE modes, however in higher order modes coupling to EH modes is possible which results in the doublets[63]. With the tilt of the Bragg grating the coupling strength to each single doublet is highly dependent upon the polarisation of light with respect to the grating[63].

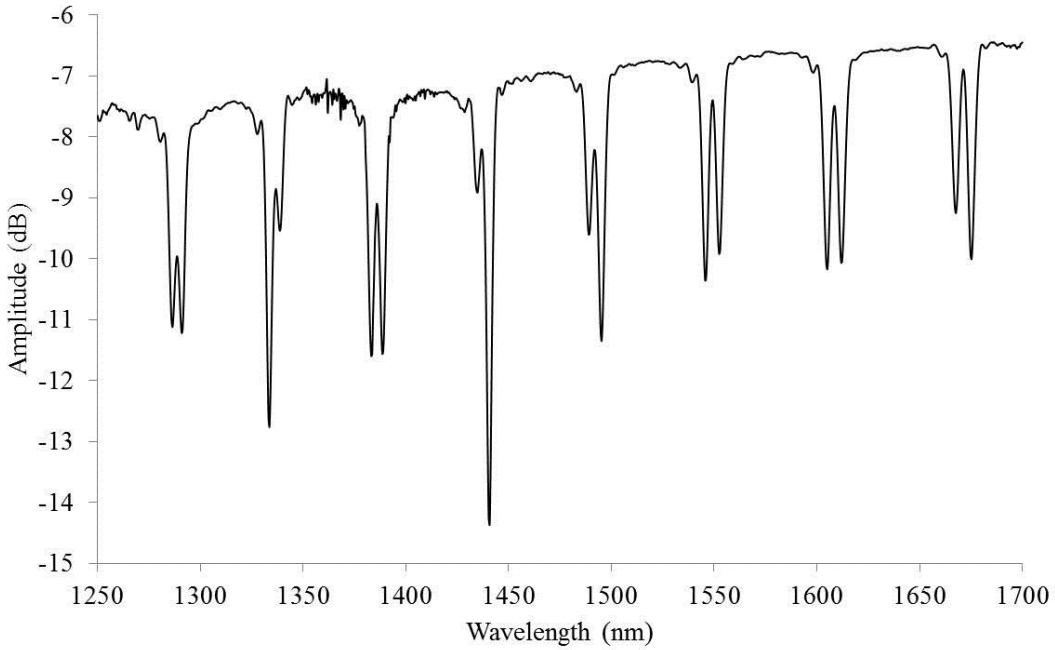

Figure 3-8 showing a typical spectrum for a 81^{o} tilted Bragg grating with the split peaks that has been normalised

.

3.2.3 Surrounding medium refractive index response

The SRI response of large angle TFGs was carried out by using the same ‘v’ groove metal plate, as in Section 3.1. The gratings were immersed in Cargille refractive index liquid, which are an industry standard certified to ±0.0002, ranging from 1.32 to 1.40 RI. After each exposure the transmission spectrum were recorded and then the liquid cleaned off using ethanol followed by distilled water and then allowed to dry. To ensure thorough cleaning the process was ratified by ensuring the spectrum returned to that of the grating in air.

When the 81^{o} TFG is exposed to a medium with higher refractive index, the splits peaks appear to merge, as show in Figure 3-9. By examaning the individual polarisations states some understanding can be extracted. By increasing the SRI the separation of the doublets decreases untill the the completely overlap at a SRI of around 1.4. This suggest that with increasing SRI the difference in effective index of the EH and HE mode decreases. With randomly polarised light the doublet effect dissapear when a higher SRI is applied. This is because the doublets are overlapping and, due to the low resolution of the peaks, there individual responses cannot be distinguished.

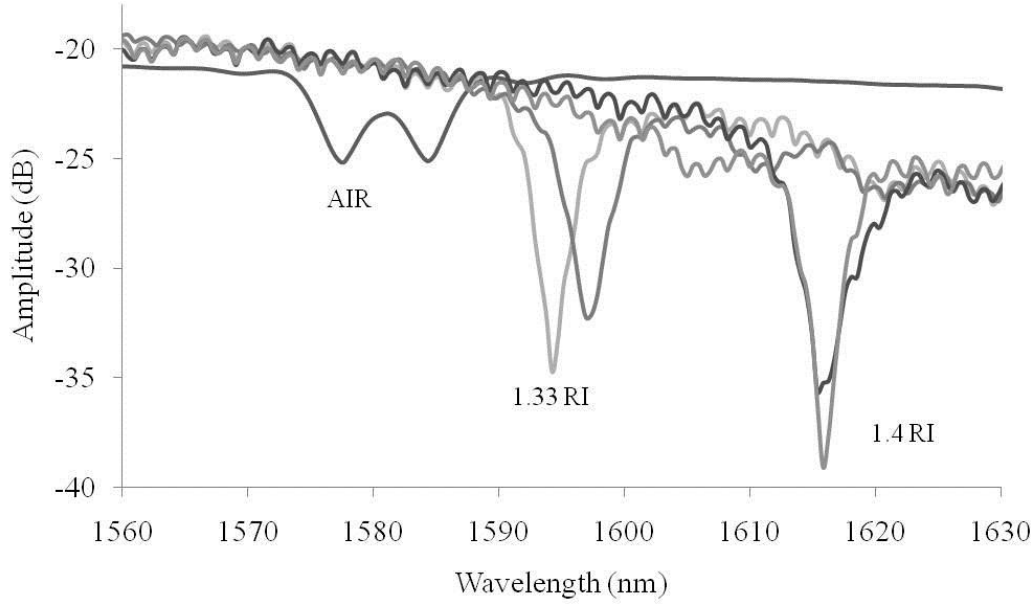

Figure 3-9 showing how the doublet peaks of the 81° TFG change with increasing SRI

The SRI response for the two split polarised states and for un-polarised modes was examined with the results shown in Figure 3-10, the results are normalised with respect to an RI of 1.32 for easy comparison. The doublets are due to coupling to different cladding modes (EH and HE but same azimuthal order) and, hence, have different sensitivities. The polarisation marked as 'A' has a maximum shift of -20.5nm while 'B' has a maximum shift of -17.6nm. Comparing the un-polarised light case with 'A', the most sensitive response, there is no distinguishable difference between them. This means when the doublets form a single peak in a high SRI, there is no sensitivity loss; hence, for best results it is not necessary to used polarised light for large angle TFG.

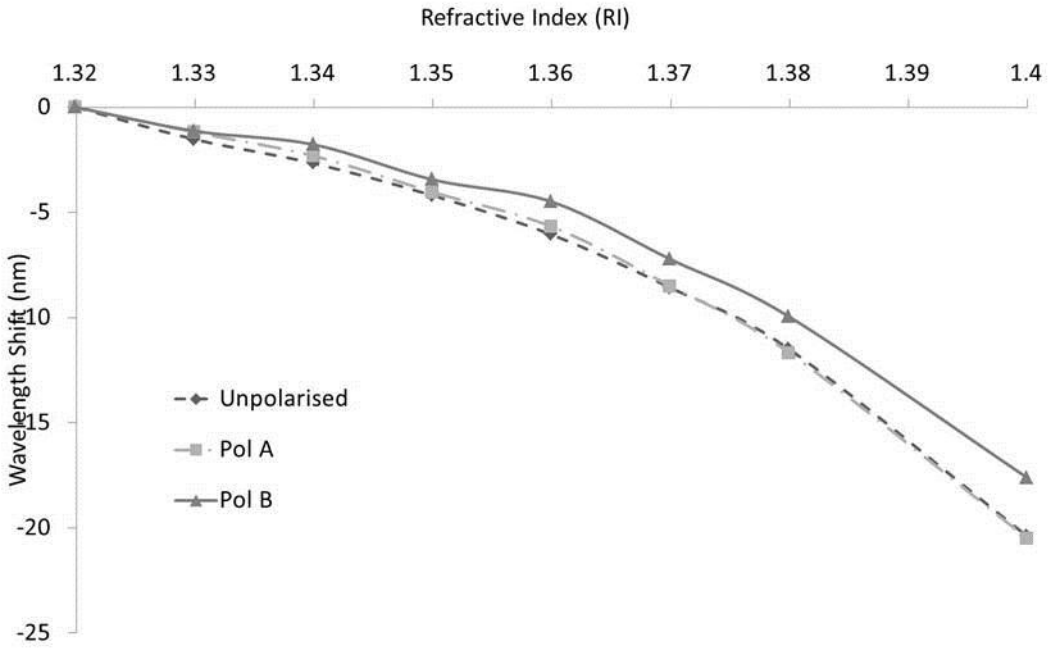

Figure 3-10 showing the SRI of the two polarisations and for unpolarised light

Large angle TFG SRI response is only valid for the SRI range below approximately 1.4, because after this the attenuation peaks start to disappear, first with those on longer wavelength side and then on the shorter wavelengths. The Large TFG couple to the higher order modes thus the effective index of such modes is lower than that of the LPGs, which typically couple to lower order modes. As such, when the SRI approaches the effective index cladding mode, typically 1.45 for LPGs but 1.4 for the large angle TFG, the discrete cladding modes are no longer bound resulting in seemingly infinite cladding and radiation modes, hence the disappearance of the attenuation peaks. The resonances at longer wavelengths disappear at lower SRI than those at lower wavelengths. To explain this the RI for fused silica is taken from the "Handbook of optical constants"[126] and plotted vs. wavelength in Figure 3-11. As you can see with an increase in wavelength there is a decrease in RI. At a wavelength, the difference in effective index between the modes being coupled to is small. However, the modes will follow a similar relationship the RI and wavelength as that showed here. This means, modes at higher wavelength will have lower effective indexes than those at lower wavelengths. Therefore, at longer wavelengths the

cladding seams infinite at lower SRI than at lower wavelengths and no longer sustain cladding modes sooner.

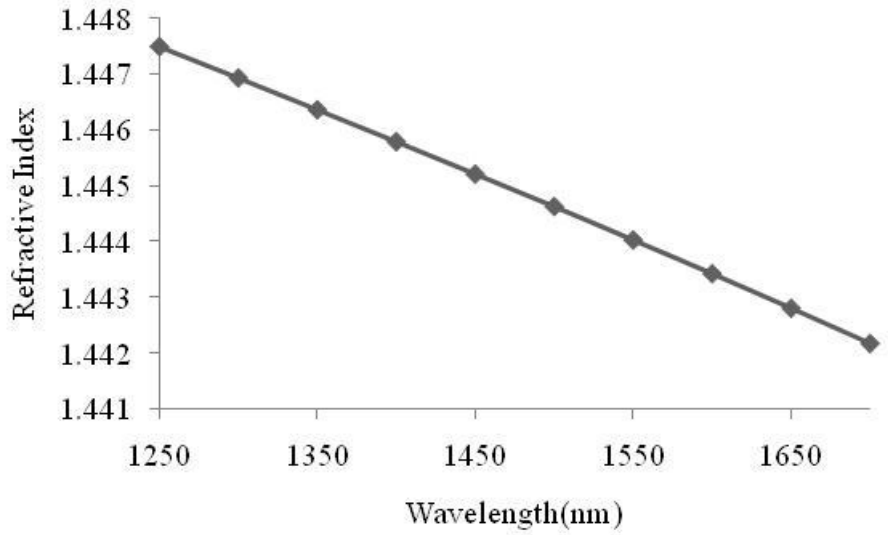

Figure 3-11 Showing the change in RI for fused silica in relation to wavelength

In the wavelength range under examination the 81° TFG couples to multiple high order cladding modes, as shown in Figure 3-9. It is known, from LPG theory, that different modes have different sensitivities[49] and this is the case with the TFG. Three attenuation peaks of the 81° TFG had their wavelength shifts measured for various SRI values and are plotted in Figure 3-12. The mode located at the longer wavelgnth has a greater sensitivity to SRI than those at shorter wavelgnths.

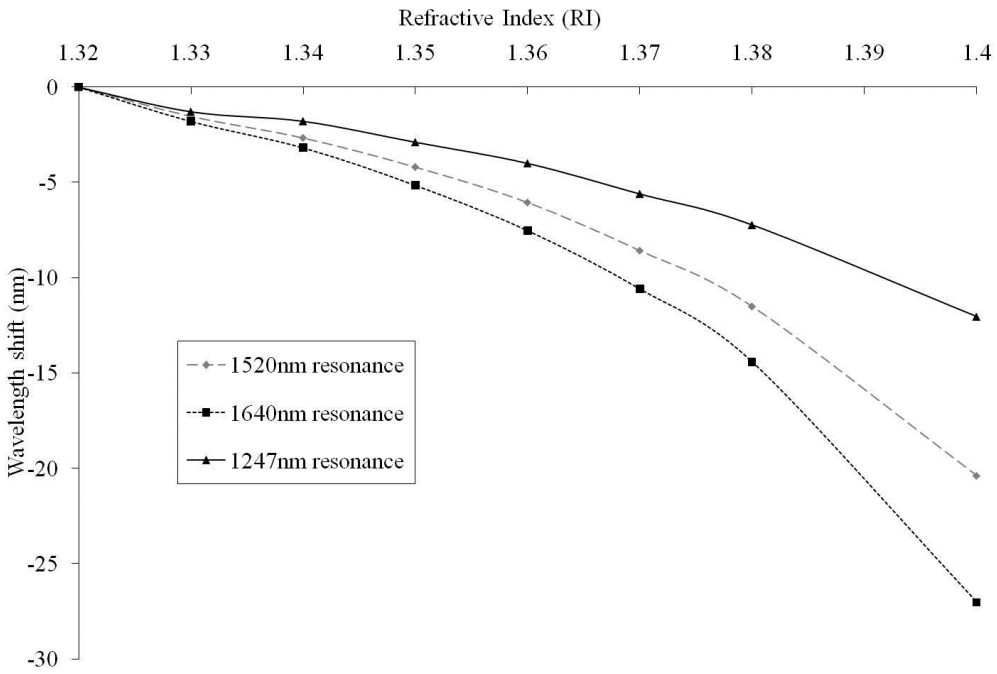

Figure 3-12 comparing the refractive index response of three different modes of a large angle tilted Bragg grating

3.3 Cladding etched large angle tilted fibre gratings

3.3.1 Introduction

Bragg[105, 127], long period[108, 128] and small angle tilted gratings[107] have all previously had their sensitivity SRI by the decreasing of cladding radius, realised either by using D shape fibre[129] or performing cladding etching. The sensitivity increase comes about from two effects: (I) removal of the cladding allows for the control of the grating characteristics, especially LPGs, meaning the careful selection and optimisation of the coupling can take place[112]; (II) the thinning of the cladding allows for a stronger interaction of the evanescent field with surrounding medium and an associated sensitivity increase[101]. To make both small angle and normal Bragg gratings sensitive to SRI changes the cladding surrounding the grating needs to be etched within a few microns of the core, since the modes concerned here are the core and the lower order cladding modes. However as a result of this the fibre does become extremely fragile in the etched region. While LPGs do show high refractive index sensitivity they also have a strong temperature

dependence, which imposes a cross-sensitivity problem. The large angle TFG has a lower thermal sensitivity, compared to the LPG[71], because the grating period is lower and temperature has a weaker effect upon it. Similar to the lower temperature response of FBG to LPG with the large angle TFG being between the two. These disadvantages associated with, small angle tilted, normal Bragg gratings and LPGs may be overcome through relatively small etching of the large angle TFG, as they will offer high SRI sensitivity and a low thermal cross sensitivity intrinsically.

3.3.2 Experimental procedure and etching process

To investigate the possibility of enhancing SRI sensitivity by cladding etching three 81°TFG were immersed into a container of HF acid, of concentration 10% and placed inside a fume cupboard for safety. Using a broadband light source and an OSA, the transmission of one of these three gratings was monitored in-situ, with the spectrum recorded at intervals of 5 min. For comparison, the three 81° TFG were removed from the HF solution at intervals of 90min, 135min and 6 hours. All the etched gratings were cleaned thoroughly before being used for any SRI sensitivity characterisation.

The SRI characterisation followed a similar procedure for the LPGs described in section 3.1.3, with the exception that the SRI range under consideration was between 1.30 and 1.40

3.3.3 Results and discussion

During the etching process the split peaks merged to form single peaks, as one would expect due to the higher refractive index of the HF solution. As soon as the fibre was exposed to the HF acid etching occurred and the peaks began to shift, seen in Figure 3-13.

All attenuation peaks have a blue shift, labelled by the arrow and the wavelength shift of the resonances is expected from theory[101].

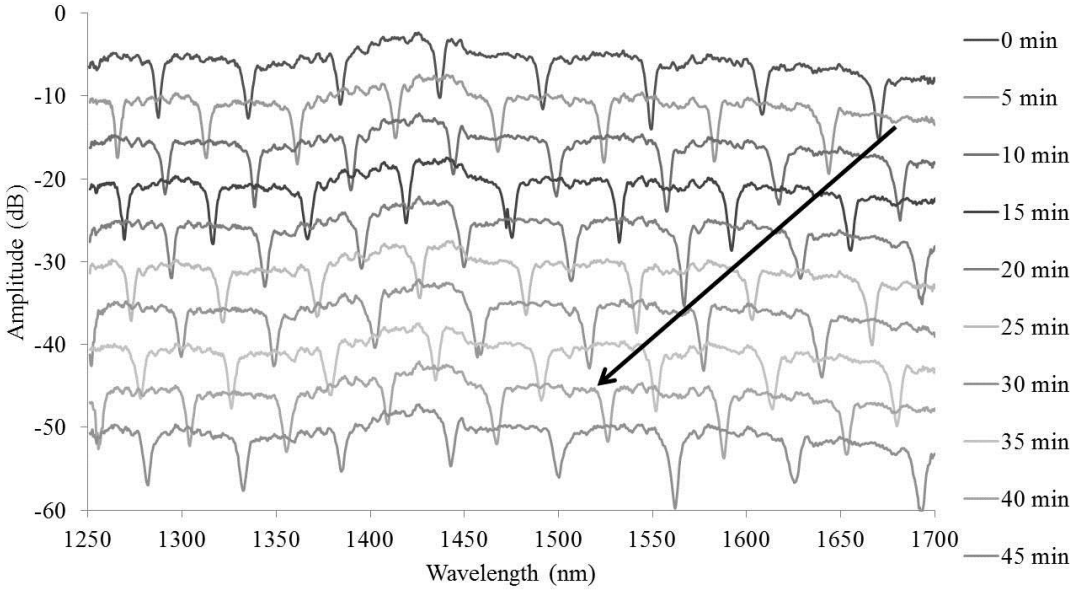

Figure 3-13 showing the wavelength shift of attenuation peaks of an 81° TFG under HF cladding etching

As shown in Figure 3-14, the shift rate is approximately -5nm/min, however, modes situated at longer wavelengths seem to shift slightly quicker than those at shorter ones. Due to this rapid shift of the attenuation peaks, no credible data could be obtained beyond 45 minutes, since all original modes had shifted out of the broadband light sources range. The amount of cladding removed is estimated to be ~0.068μm/min for 10% HF acid[125], which means after 6 hours the cladding diameter is reduced to ~100μm. This cladding thickness is enough to maintain the fibre's robustness, especially compared to a device thickness of only a few microns of an etched Bragg grating.

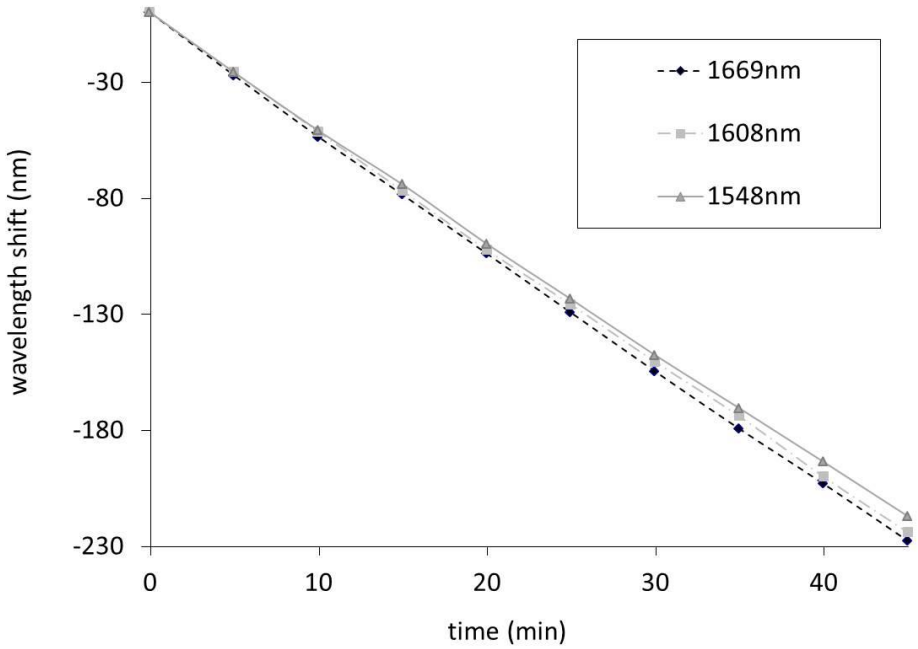

Figure 3-14 showing the wavelength shift rate for three peaks of an 81° TFG under HF acid etching.

The SRI sensitivities for three 81° TFG etched for the three different etching times, are plotted in Figure 3-15, with a non-etched large angle tilted grating for comparison. It can be seen that with increasing etching time and reduced cladding radius the SRI sensitivity increases and the fibre with reduced cladding radius, etched for 6 hours is the most sensitive. The sensitivities achieved are compared to that of a dual resonance LPG with a period 160μm in Figure 3-16. Over the SRI range 1.3-1.36 both the 6 hour etched 81° TFG and the dual resonance LPG exhibit a similar SRI sensitivity. However, from 1.36 to 1.40, the etched grating displays' greater wavelengths shift. In this range the dual resonance gives an average sensitivity of 389.2/URI while the etched large angle TFG has an SRI sensitivity of 506.9nm/URI which is much higher than the former. This means that by employing a relatively easy etching process the large angle TFG could be used for chemical and biological sensing applications.

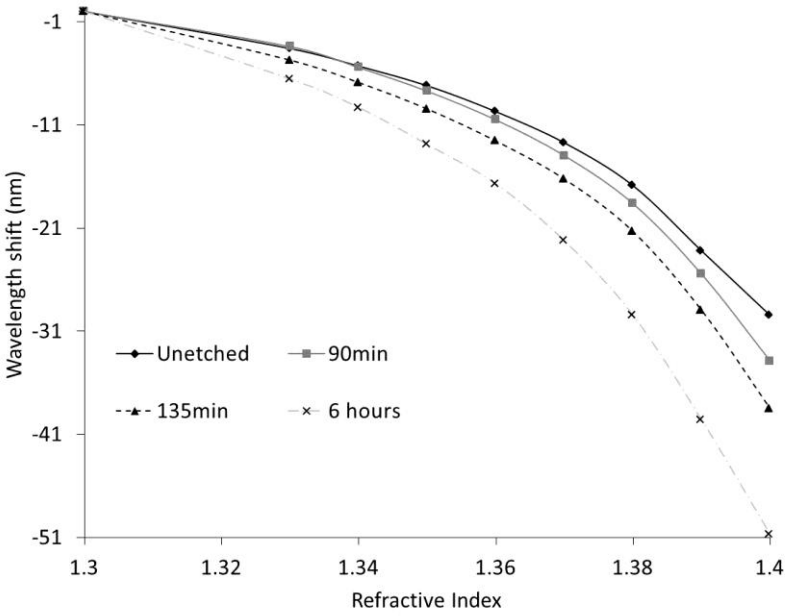

Figure 3-15 showing the RI response for three different etching times and a non-etched grating for comparison

Theory states[101] that the sensitivity of the etched large angle TFG should be related by $Sensitivity = \left(r_{cl}^{unetched}/r_{cl}^{etched}\right)^3$. Using this with the estimated cladding etch rate the increase in sensitivity should be ~x1.95 which correlates well with the experimental results.

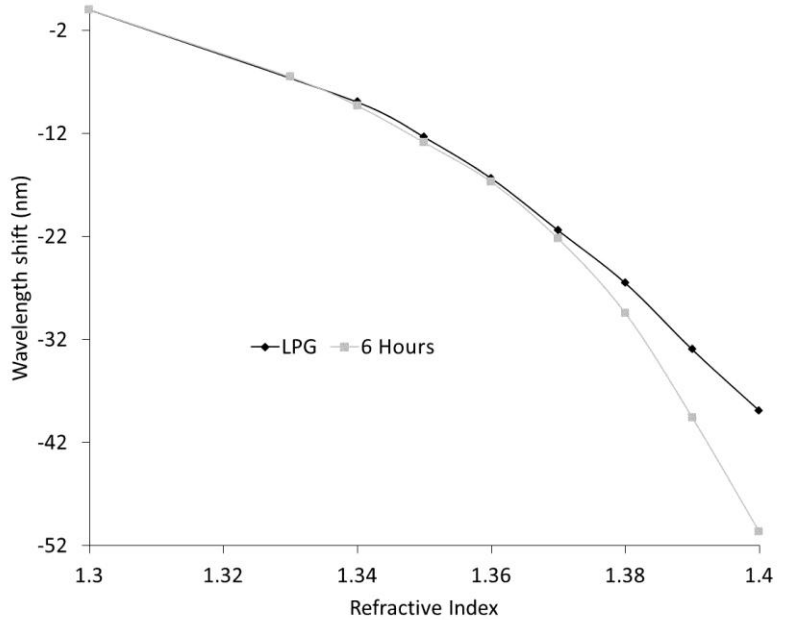

Figure 3-16 comparing the SRI sensitivity of the most sensitive 6 hour etched large angle TFG and a dual resonance LPG

3.4 Sol-gel coated long period gratings and the sensitivity improvement

3.4.1 Introduction

There is increasing demand for sensors to function in chemical and biological areas, such as environmental analysis. Any new sensor must be able to compete with existing methods like immunoassays, chemical test kits and conventional laboratory techniques. A growing field is that of real time in-vivo sensing, which have the criteria that the sensing material should be non-toxic and biocompatible [130-132], all of which are satisfied by sol-gel coatings. Sol-gel coatings have various advantages when considering optical detection of analytes. Biological active agents, such as enzymes, antibodies and cell, can be incorporated into the porous sol-gel coatings allowing for species specific detection and helping to minimise any non-specific interactions at the sensor surface. The non-toxic coating can be applied on an optical fibre's surface [91, 92] with the biological agents while also control of the coatings thickness and refractive index gives the opportunity to increase the sensitivity of the LPG sensors.

3.4.2 Sol-gel coating procedure

The coating of the optical fibres with sol-gel and the analysis of their refractive index and thickness were carried out by collaborators Reeta Viitala and Mikko Salomak at the University of Turku in Finland. Also, the sol-gel method was used to prepare silica and titania films and is the same as that carried out by Reeta et al in "Sol-gel derived coating applied to long-period gratings for enhanced refractive index sensing properties". The precursors used for the silica films were tetraethylorthosilicate (TEOS, $[Si(OC_2H_5)_4]$), ethanol, deionised water, polyethylene glycol molecular weight 2000 (PEG 2000) and HCl or HNO_3 and for titania films tetraisopropyl orthotitanate (TIPT, $[Ti(OC_3H_7)_4]$), ethanol,

deionised water, HNO_3 and PEG 400. The used water to alkoxide mole ratio (R) of the silica sols was 2 and for titania sols 1. The hydrolysis and condensation was done in acidic conditions. The alkoxide concentration in the sol was changed by simply using different amount of ethanol when making up the sol. The other way to control the film thickness is to use different substrate withdrawal speeds. These both methods (alkoxide concentration and withdrawal speed) were used to control the film thickness and the used parameter for silica and titania films are presented in Table 3-1. A dip-coating device was used to prepare the films and the withdrawal speed was controlled with the device. The used withdrawal speed was 20 or 40 mm/min. Eight different sol-gel derived titania and silica coatings were prepared on Si-wafer (Table 3-1.) and four of those (Si01, Ti01, Ti03 and Ti04) were prepared similarly on LPG fibres. Too ensure a clean coating surface both substrate material were washed with ethanol and dried before any dip coating took place. After the dip-coating films were heat-treated at 100 ˚C for 30 min. The thicknesses and refractive index of the coatings, which were deposited on silicon wafer, were measured with ellipsometer. The assumption that similarly prepared coatings on silicon-wafer and on LPG fibre have similar thickness and refractive index.

The RI measurements were performed with a Nanofilm EP3 imaging ellipsometer. The spectral measurement was applied for the sol-gel derived silica and titania coated Si-wafers. The angle of incidence was fixed at 60° and a Xe lamp was used in the spectral range of 370-900 nm. The complete spectral range was used in fitting of the thickness and the refractive index of the coating. The refractive index for the material was determined using the two first terms of the Cauchy dispersion equation ($RI(\lambda)=A+B/\lambda^2$, where λ is wavelength of the light).

Prepared coating	Coating code	Ethanol/ alkoxide	Withdrawal speed [mm/min]
SiO_2	Si01	4	20
	Si02	4	40
	Si03	22	20
	Si04	22	40
TiO_2	Ti01	8	20
	Ti02	8	40
	Ti03	15	40
	Ti04	25	40

Table 3-1 showing the titanium/silicon ethanol to alkoxide mole ratio and withdrawal speed for coating.

3.4.3 Experimental procedure

The LPGs were inscribed using the same procedure as described earlier with the SRI characterisation following the same methodology used for both LPG and the large angle TFG

3.4.4 SRI characterisation and discussion

The effect of RI and thickness of the sol-gel coating was investigated first by coating various near identical LPGs of period 322μm. The key values of the coating are shown in Table 3-2 and were established by coating a silicon wafers using the same condition for easier measurement.

Prepared coatings	Coating code	Coating Thickness		Refractive index
		[nm]	± [nm]	
SiO_2	*Si01*	200.4	0.3	1.44
	Si02	283.1	0.3	1.43
	Si03	53.9	4.1	1.43
	Si04	67.4	2.8	1.42
TiO_2	*Ti01*	147.6	-	1.96
	Ti02	158.9	6.7	1.95
	Ti03	86.8	0.3	1.93
	Ti04	65.4	0.4	1.91

Table 3-2 showing the RI and thickness for various different sol-gel coating

The effects of RI coating was established and plotted in Figure 3-17. All the gratings displayed a blue shift, however the titania coating with, RI 1.96 and thickness 147nm, displayed a larger shift than both the uncoated and the silica coated fibre with, RI 1.44 and thickness 200nm, despite the titania coating having a thinner layer. Furthermore the silica coating produced a larger overall wavelength shift did not increase the grating sensitivity since the relative change between points was left largely unaffected. What is also of interest is that the sensitivity, albeit small in parts, is across the entire RI range under consideration here. Numerically taking the sensitive region as being 1.33 to 1.42 the titania coating had a sensitivity of 419nm/URI whereas the uncoated was only 209nm/URI which is almost doubling the response. The silica having a RI close to that of the cladding didn't really improve the sensitivity, as would be expected since it is the equivalent of increasing the cladding radius.

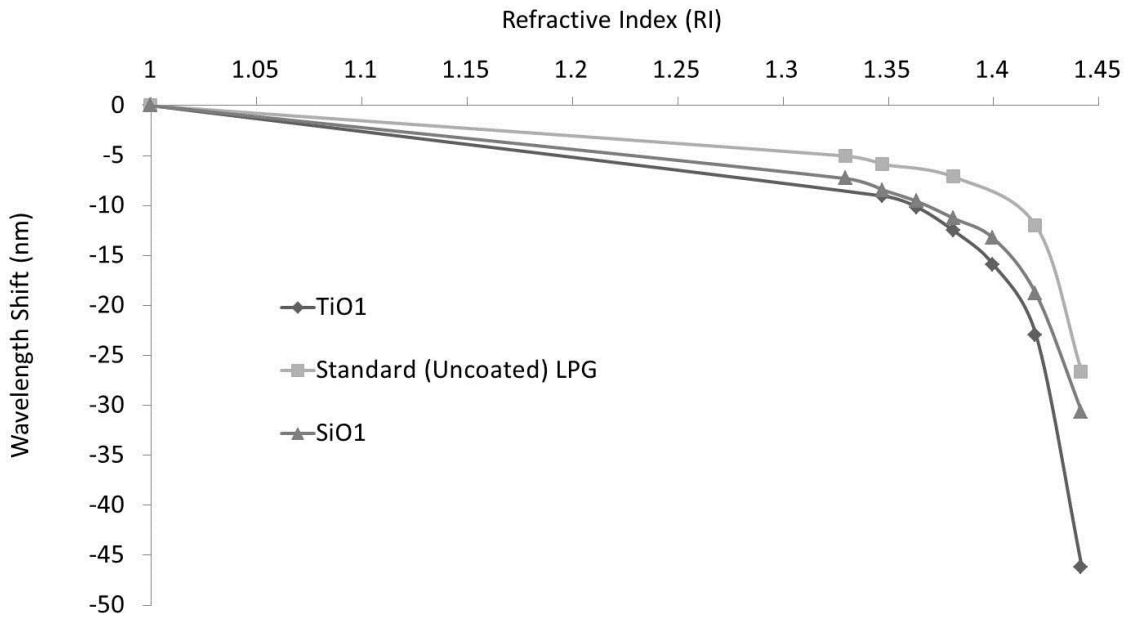

Figure 3-17 showing the SRI response for LPG's with different coating RI values.

This seems to suggest that the sensitivity of the LPG is improved through high refractive index coatings, but what also must be considered is the thickness of these coatings and these results are shown in Figure 3-18. The coating RI values were kept approximately the same for consistency. All the titania coated gratings had greater sensitivity than the uncoated one and, the sensitivity increases with increasing coating thickness. The coated LPGs exhibit the greatest sensitivity when the SRI was approaching the index of the cladding, around 1.44. The estimated SRI sensitivity, in the most sensitive range 1.42-1.44, was found to be 1067nm/URI and 673nm/URI for the thickest coating and the uncoated gratings respectively. Again the sensitivity increase was seen over the entire range examined here, although small this may mean coated LPGs could detect biological substances in solutions.

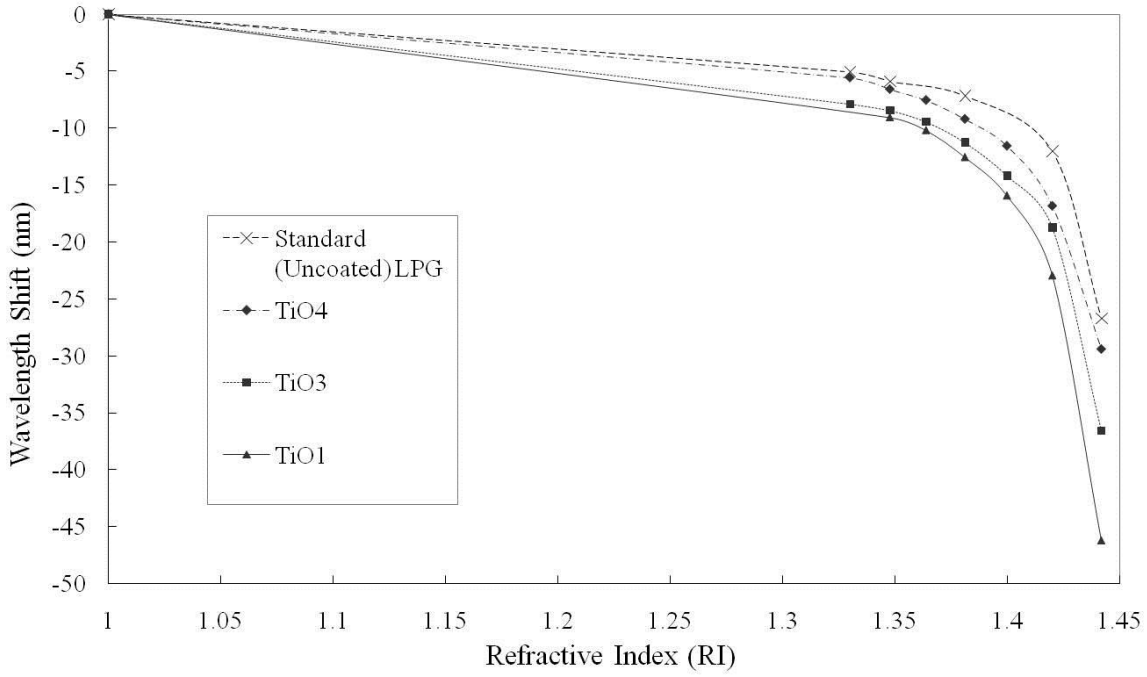

Figure 3-18 showing the SRI response of 3 titania coated LPGs each with a different thickness and an uncoated LPG for comparison

An important factor to be considered in sensor development is the consistency and repeatability of any coated device. Three near identical LPGs were coated using titania and the same dip coating procedure to investigate this and the results are shown in Figure 3-19. The results are very positive with very little variation being seen over the full SRI range used here and error in maximum wavelength shift between the three SRI sensitivity plots of only ±0.5nm.

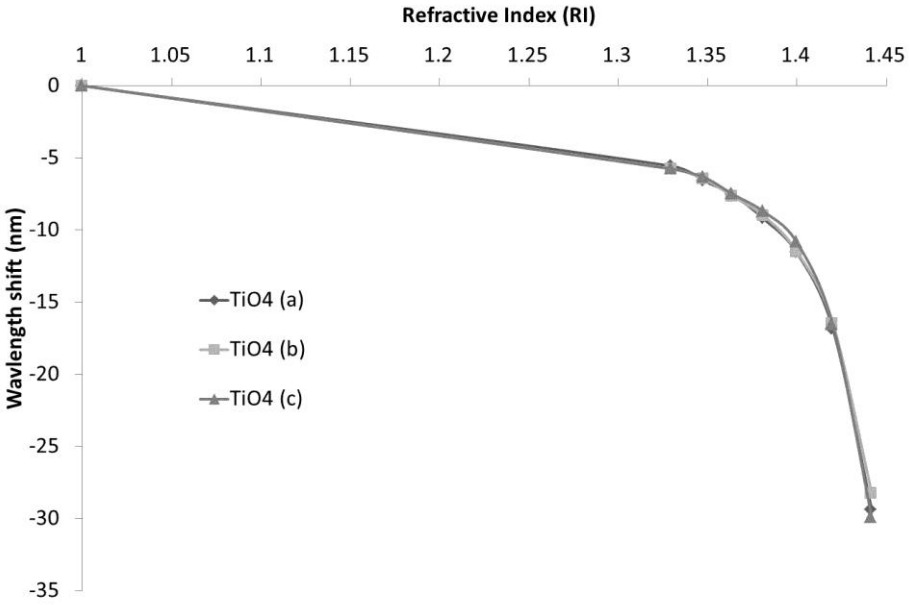

Figure 3-19 showing the SRI response of three near identical LPGs with the same thickness and RI coating.

Although the coated LPGs have displayed a large sensitivity increase, however, even the most sensitive coated LPG discussed here only exhibited a SRI sensitivity similar to a LPG with a relatively short 238µm period, seen in Figure 3-5. To verify if the sensitivity could further be improved LPGs with smaller periods were manufactured, coated and subjected to a sensitivity investigation. Since the titania coatings gave the best increase in sensitivity the silica coatings were not used for this experiment. Figure 3-20 shows the SRI response for three near identical gratings of period 248µm coated with titania coating of thicknesses and RI values listed in in Table 3-3 . Several conclusions can be drawn from Figure 3-20. First, the sensitivity increase is less than that achieved with a coated 322µm period LPG. Since the differences in sensitivity are small to make them more apparent 1.33 SRI is used as the zero value for the attenuation peaks instead of air. Secondly, opposite to a coated 322µm period grating an increase in sensitivity is observed with decreasing coating

thickness, with the highest sensitivity achieved with ~ 100 nm coating of titania.

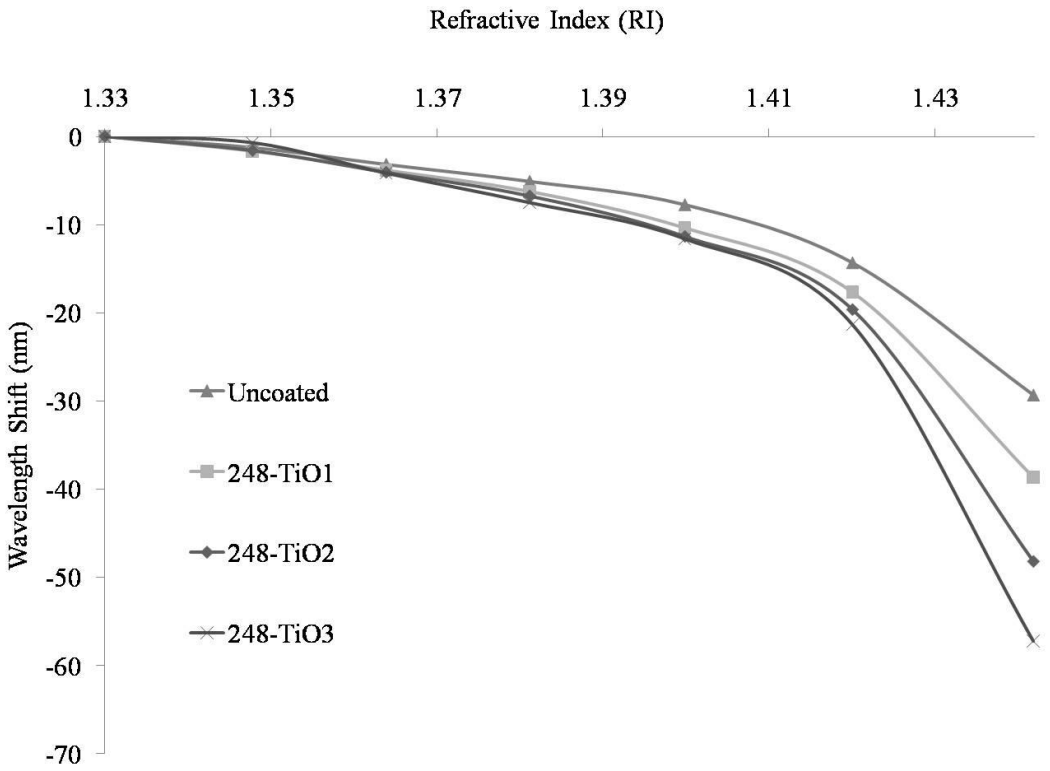

Figure 3-20 showing the SRI response of 3 titania LPGs with different thicknesses and RI values. For comparison an uncoated LPG is also shown

Prepared coatings	Coating code	Coating Thickness		Refractive index
		[nm]	± [nm]	
TiO_2	248-TiO1	400	2	1.86
	248-TIO2	141	1	1.91
	248-TiO3	116	1	1.88

Table 3-3 showing the thickness and the RI values of the coatings used for the 248µm gratings

Investigating a shorter period of 164µm dual resonance LPGs were coated to see if the SRI sensitivity could be further increased. The coating procedure was the same as that used for the 322µm period LPG and the results are shown in Figure 3-21. Looking over the SRI range 1.33 to 1.4201, in Figure 3-21, the sensitivity is increased by almost 2 fold, but this increase is mainly limited to higher SRI values. Similar to the grating period 322µm, but different from 248µm, with increasing coating thickness the SRI sensitivity of the shortest period LPG increases. The maximum sensitivities achieved for each coated period is

shown in Table 3-4. The theory of coated long period grating states that there is an optimum coating thickness for increasing the gratings sensitivity. The work here supports this statement, since different period grating required thinner or thicker coatings to increase SRI sensitivity. However, the sol-gel coating technique is not yet perfected for optical fibre and as such it cannot reach the required control that other techniques currently offer. This means the actual optimum sensitivity thickness cannot be experimentally verified for the sol-gel coated LPGs. Despite this, the sensitivities obtained for the periods 322µm and 248µm are comparable to other coated LPG devices[77], while an numerical sensitivity increase for a dual resonance LPG has been observed and reported here, where previously a numerical value was not reported[93].

Grating period (µm)	RI sensitivity 1.33 to 1.4201 nm/URI
322	419
248	667
164	1458

Table 3-4 Showing the maximum sensitivities for the coated LPGs

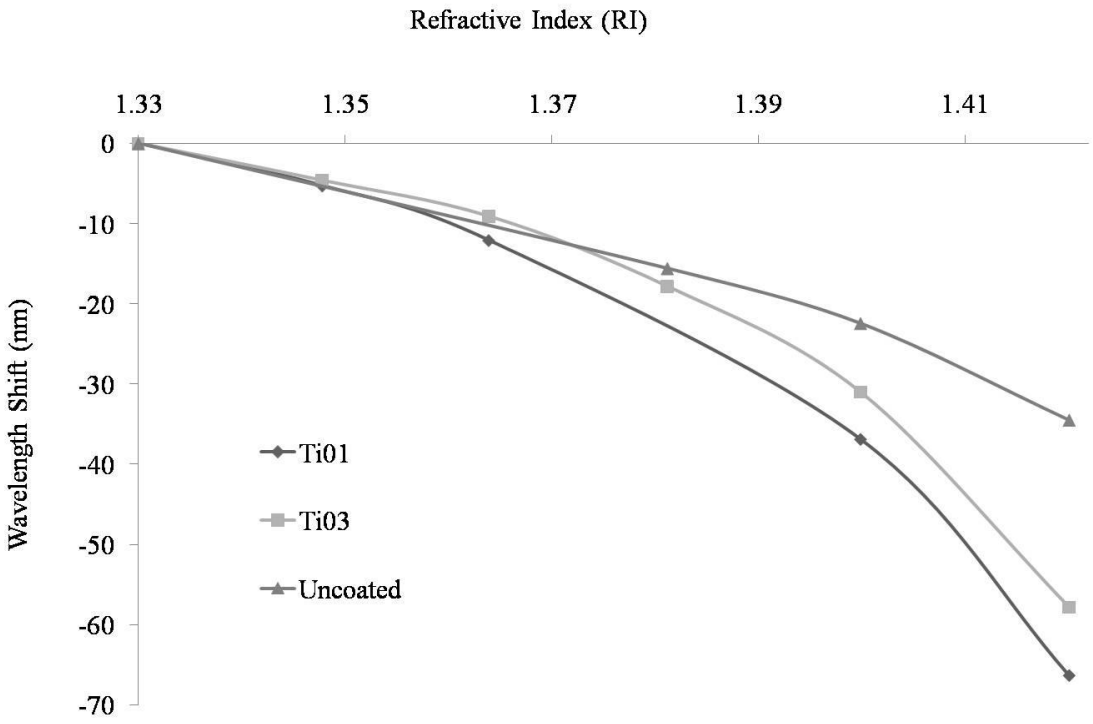

Figure 3-21 showing the sensitivity response of three gratings period 164μm, two coated and one uncoated

3.5 Summary of sensing characteristics of fibre gratings

LPGs have been found to have a characteristics response to changes in surrounding refractive index through the change in wavelength of their attenuation bands, associated with discrete cladding modes. The wavelength shift of the attenuation peaks is dependent on both the relative change in surrounding refractive index and the period of LPGs. This investigation shows that the most sensitive LPGs are the dual resonance types, which have two sets of attenuation peaks associated with the same order cladding mode. Their high sensitivity is due to that the dual resonances are close to the dispersion turning point of the phase match relationship.

Large angle TFGs have been found to exhibit similar properties to that of LPGs, as they also couple light to the forward cladding modes, but at higher orders. However, large angle TFGs are intrinsically polarisation sensitive giving rise to their split peak phenomena. They display similar responses to variation in surrounding refractive index to LPGs,

however with a smaller SRI detection range. The attenuation peaks disappear with SRI values around 1.41, (where discrete modes can no longer be sustained) lower than 1.45, at which the LPG attenuation peaks disappear.

Two methods have been investigated for the improvement of SRI sensitivity for co-propagating cladding mode gratings. Etching of large angle TFG cladding caused wavelength shift of the resonances and an increases in sensitivity. The sensitivity increase from reducing cladding radius matched well with that of the theory. Etching off only a small amount of cladding layer meant the fibre was able to maintain its robustness while achieving a high SRI sensitivity. An etched 81°-TFG has achieved an SRI sensitivity of 506.9nm/URI over the index range 1.36 to 1.40, which is even better than the highly sensitive dual resonance LPG of period 160μm. Cladding coating of LPG with a material of high refractive index, 1.9, using the sol-gel dip method was found to increase their sensitivity. The work supported the theory of there being an optimum coating thickness however, due to poor control over coating thickness the actual optimum could not be found experimentally. Despite this the maximum sensitivities for the sol gel coating LPG were comparable to that in the literature while the coated dual resonance LPG sensitivity increase was observed and reported to be 1458nm/URI, which was better than non dual resonance LPGS (coated and uncoated) and a dual resonance of LPG of the same period uncoated.

4 Femtosecond inscription of optical fibres

4.1 Femtosecond induced long period gratings at various periods

4.1.1 Introduction

As already established, UV inscribed long period gratings (LPGs) have long been implemented for a multiple of sensing parameters. The main method for the inscription procedure is through focusing a UV laser source on to the core of an optical fibre that is germanium doped and hydrogen loaded. This method, although efficient, is limiting since only germanium doped fibre can be utilized, and also time consuming, because the fibre needs hydrogen loading to increase its photosensitivity. There is also the problem of long term stability since even below 100^{o}C there is grating quality degradation[133], though this can be counteracted using thermal annealing. Femtosecond inscription does not require any special fibre pre-treatment relying on a different method for the refractive index change. The induced index change has the possibility of being far more thermally stable over a broader temperature range, compared to UV induced gratings. Also, with the inscription procedure being focused at a location in the core rather than the entire core (as with UV inscription) femtosecond LPGs have a far greater polarisation response and the ability to couple to further sets of cladding modes, compared to the LP_{0m} which the UV inscription technique is bound to. Various periods of LPG were inscribed in the core of SMF and their SRI and polarisation response were investigated.

4.1.2 Inscription characterisation method

The LPGs were inscribed into the core of standard SMF by Dr. Kyriacos Kalli of the Cyprus University of Technology, using a femtosecond laser system with a repetition rate

of 100 kHz and emitting 300fs pulses at a wavelength of 1035nm. A Mitutoyo microscope objective (with a magnification of 50 and a numerical aperture of 0.40) was used because it is less sensitive to any optical fibre curvature. To focus the laser energy, the alignment to the core of the fibre is optimized using the characteristic plasma generated. Implementing a pulse picker, the laser operated at 1 kHz and produced energies of less than 3.5µJ/pulse when exiting the laser. A computer controlled stage and shutter was used, this allowed the individual RI point changed to overlap and produce a continuous RI perturbation. LPGs with period of 320µm, 400µm, 600µm and 960µm were chosen because they gave a wide enough range that a sufficient amount of different cladding modes could be examined.

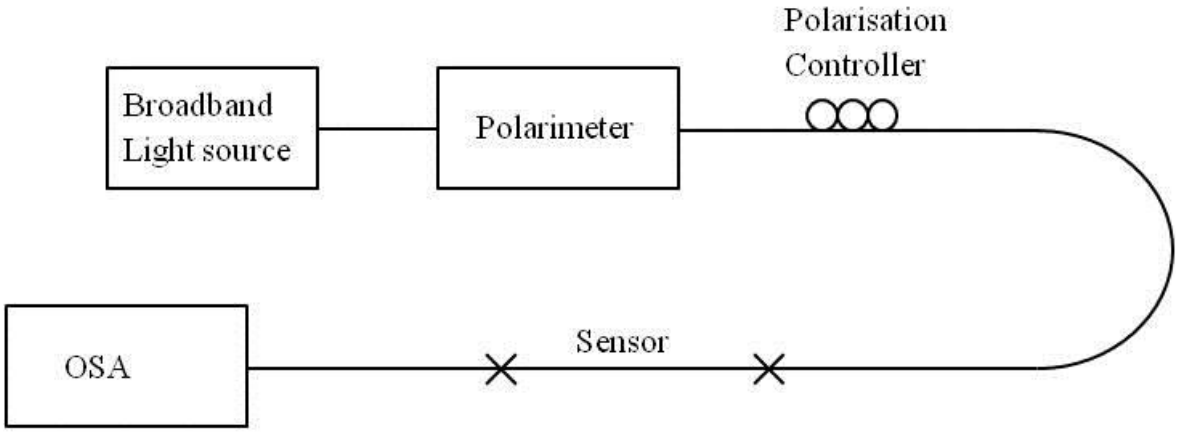

Figure 4-1 showing the setup used to interrogate the femtosecond LPGs

The LPGs were then, in turn, connected to a broadband light source, via a polariser, polarisation controller and then to an OSA, a diagram showing this is displayed in Figure 4-1. Due to the polarisation response of the gratings, all fibre patch cords were fixed securely in position to minimise polarisation drift. The grating part was placed on a metal plate that had a 'v' groove. This acted as both a heat sink and way of ensuring the location/orientation of the grating during interrogation. The polarisation response was optimised for transmission by changing the input polarisation of light and the spectrum was recorded in air. The LPG was then immersed in several certified RI liquids, from Cargille, ranging from 1.33 to 1.444. Once immersed, the transmission spectrum was

recorded and then the fibre was cleaned using ethanol and to ensure thorough cleaning and the spectrum in air was compared to before and after immersing. The process was then repeated to evaluate the response to different RI liquids up to an RI of 1.444.

The polarisation response was investigated by, again, optimizing the transmission spectrum in air. The input polarisation of light was then changed using a computer controlled polarimeter and the polarisation launch of light was changed with increments of 10^{o} ranging from 0^{o} to 180^{o}. The polarisation of the light could not be established at the fibre sensor with the equipment available. As such, the experiments here are merely to characterise the LPGs polarisation response for sensing applications and not to analyse it at each increment, the transmission spectrum was recorded. To analyse the data, the LPG attenuation peaks were tracked and their central wavelengths were calculated using a 2^{nd} order polynomial fitting curve or a centroid fit method (depending on the degree to which the attenuation peak changed shape), as a way of further minimising error. Images were taken of the femtosecond LPGs to assess their location in the optical fibre core. Two images were taken rotating the optical fibre by 90^{o} between captures so as the location could be established in core.

There is an important note, it has been reported for cladding mode coupling the location of the attenuation peaks is dependent upon the grating period. However, it has also been demonstrated that the coupling coefficient is highly dependent upon the location and shape of the refractive index change within in the core of the fibre[63]. The behaviour was attempted to be modelled by Dr. Kyriacos and find this to be the case, with any slight change in location causing a dramatic change in the predicted transmission spectrum. Further to this, the LPGs have a large full half width at maximum compared to cladding resonances of Bragg gratings. As a result, the resonance were found to often overlap which makes it difficult to access which resonances belong to which cladding mode. With both these points in mind, no theoretical model is presented here and no dispersion curves

for the multiple sets of cladding modes. The work here is aimed at reporting the possible sensitivities achievable and not the femtosecond LPGs precise spectral response.

4.1.3 Properties of the femtosecond inscribed LPG of period 320µm

A grating period of 320µm was inscribed into the core of the fibre and the grating structure was then examined under a microscope and the recorded images are shown in Figure 4-2 and Figure 4-3. From Figure 4-2we can see that the index perturbation to be approximately 2µm wide and centrally located in the fibre core. From Figure 4-3 the period was measured and found to be 328µm, close to the design period.

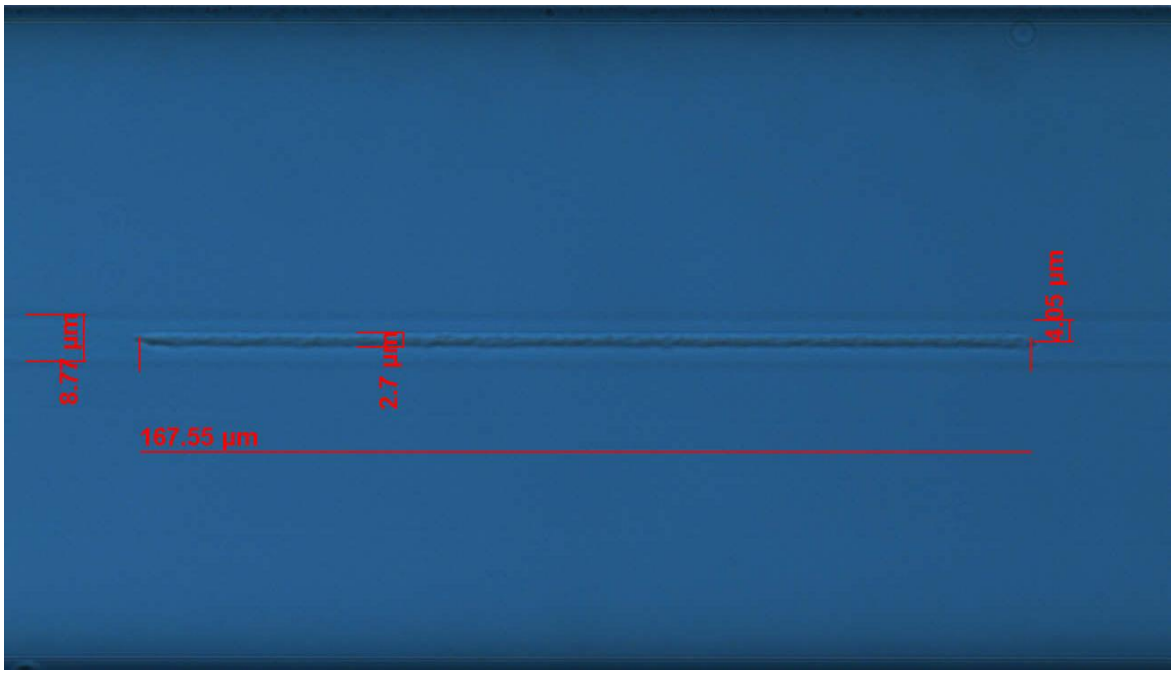

Figure 4-2 showing the femtosecond induced LPG with a period 320µm and the RI change is located in the centre of the core and being approximately 2.7µm wide

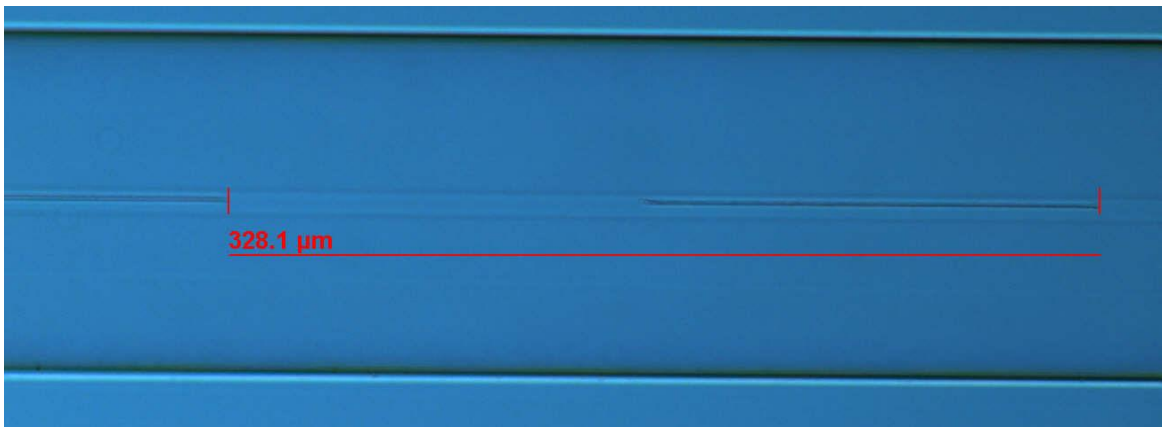

Figure 4-3 showing the femtosecond induced LPG measured period approximately 328µm

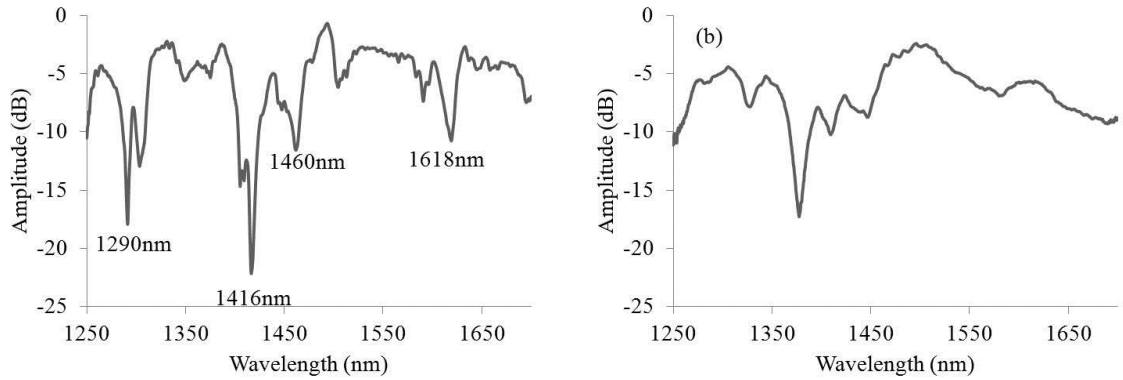

Figure 4-4 showing the transmission spectra of the femtosecond induced LPG of period 320µm in air (a) and in a SRI of 1.444 (b)

Figure 4-4(a) shows the transmission spectra, of the LPG of a period 320µm exhibiting four attenuation peaks at 1290nm, 1416nm, 1460nm and 1618nm. These four peaks were monitored for increasing SRI and the associated wavelength shift for each peak was calculated and is plotted in Figure 4-5. As shown in Figure 4-4(b), all but the peak located at 1290nm in air disappeared at a SRI 1.444, supporting the earlier statement. Each peak shows the characteristic of LPG response, with increasing SRI comes increasing sensitivity. The 1290nm attenuation peak response is less characteristic due to a strong attenuation peak being located very close to it and effecting the response. The interesting point is that most of the attenuation peaks produced a red shift with increasing SRI except the one peak located at 1417nm produced a blue shift. In UV induced LPGs, this behaviour is only seen when the cladding mode dispersion relationship is at a dispersion

turning point, as with increasing SRI the dual peaks move away from each other and this occurs for periods of about 160µm for this wavelength range for UV LPGs. Femtosecond LPGs, as already discussed, are capable of coupling to multiple sets of cladding modes due azimuthal dependence arising from there asymmetry. With most of the attenuation peaks having a red shift with increasing SRI and one having a blue shift, this is further evidence for the multiple cladding mode sets coupling, since this behaviour is only seen in UV LPGs with a period around 160µm[49].

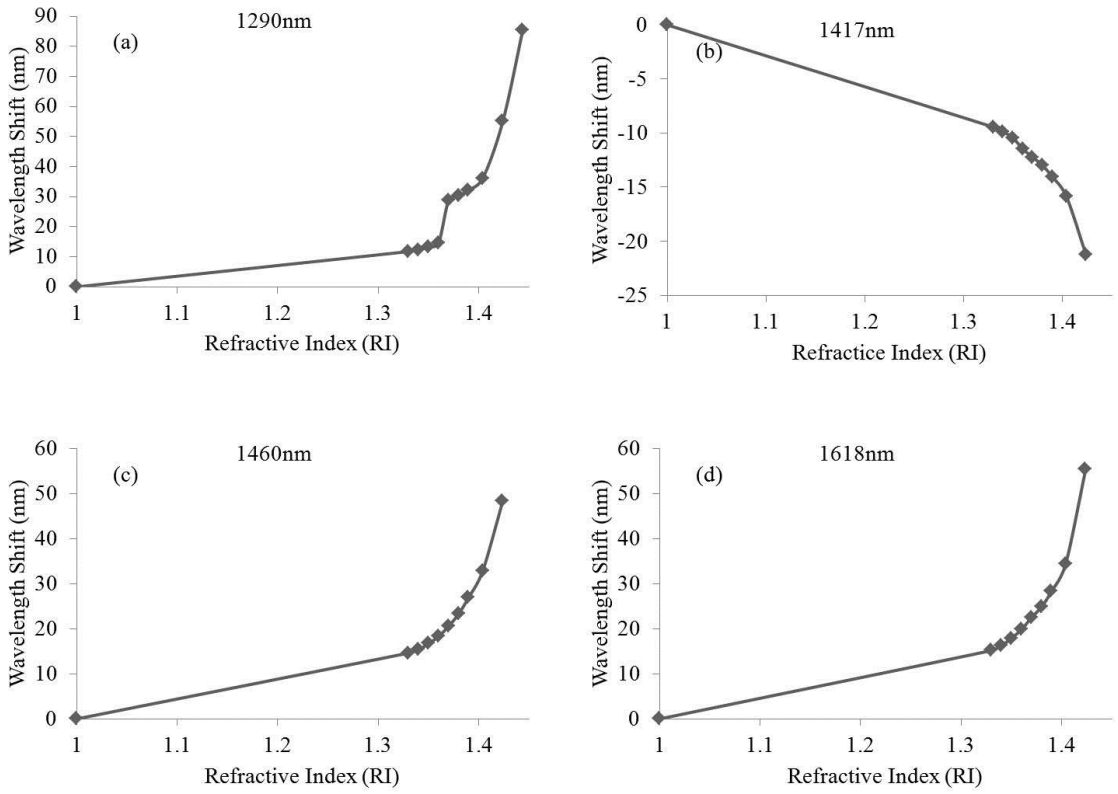

Figure 4-5 showing the SRI response of 4 attenuation peaks for the 320µm period femtosecond inscribed LPG

Through combining the opposite shifts of 1417nm and 1618nm attenuation peaks, the RI sensitivity can be greatly increased beyond the monitoring of a single attenuation peak. The opposing wavelength shift for the two attenuation peaks is plotted in Figure 4-6. Using the values calculated for Figure 4-6, the SRI sensitivity for the individual attenuation peaks and combined for various SRI values is calculated and displayed in Table 4-1. From the table we can see that the maximum sensitivity achieved for the single attenuation peak

is 946.7nm/URI while using the combined shift of the two attenuation peaks it was 1217.4nm/URI, which is almost a 1.3 fold increase in sensitivity. However, using this method the sensitivity increase is seen across the entire SRI range, though it is more prevalent at higher SRI values.

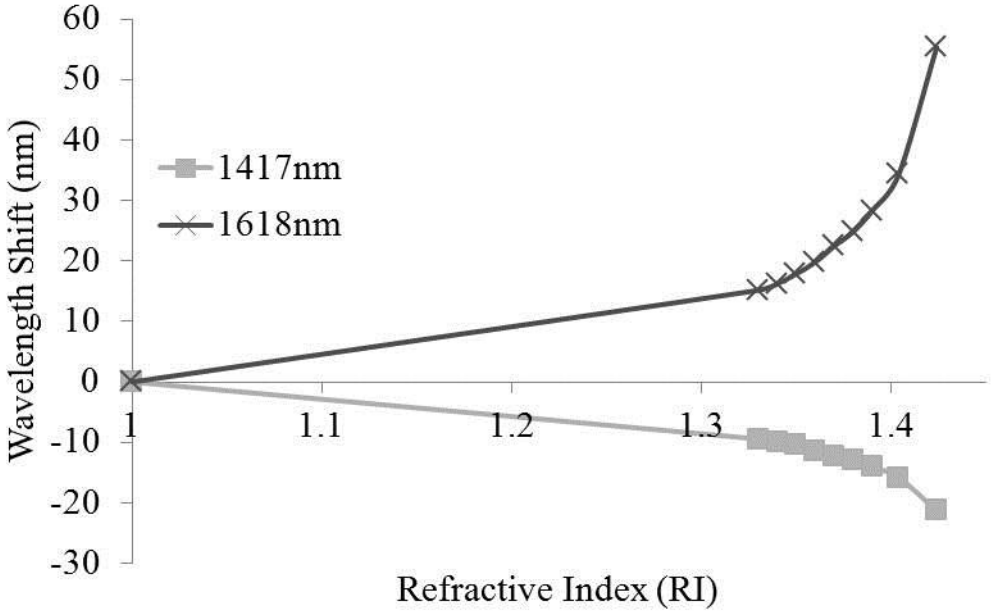

Figure 4-6 showing the peak sensitivity of the 320µm femtosecond induced LPG for two oppositely moving attenuation peaks

	1 to 1.33 nm/URI	1.33 to 1.38 nm/URI	1.38 to 1.424 nm/URI	1.404 to 1.424 nm/URI
Single 1618nm	45.9	369.0	693.4	946.7
Single 1417nm	28.6	71.4	187.5	270.7
Combined	74.5	440.4	880.9	1217.4

Table 4-1 showing the calculated sensitivities for the two most sensitive attenuation peaks over various SRI ranges both individually and combined for the femtosecond inscribed LPG of period 320µm

The polarisation dependency of femtosecond induced LPGs does have the advantage of being able to couple to multiple sets of cladding modes. For sensing applications this can also lead to a disadvantage, because the location and strength of the attenuation peaks can be highly dependent on the input light polarisation. As a result, the power can be split

between each polarisation mode which decreases the resolving power of the sensor. To clarify the uncertainty, the polarisation response for the attenuation peaks located at 1417nm and 1618nm was investigated. These two attenuation peaks were chosen since they gave the best performance as SRI sensors and thus the polarisation effects need to be accounted for. The calculated wavelength shift and amplitude change was calculated and plotted in Figure 4-7. The wavelength shift and amplitude change is due to the shrink and growth of the two competing polarisation responses and results in the apparent shift in wavelength, since the two bands cannot be resolved.

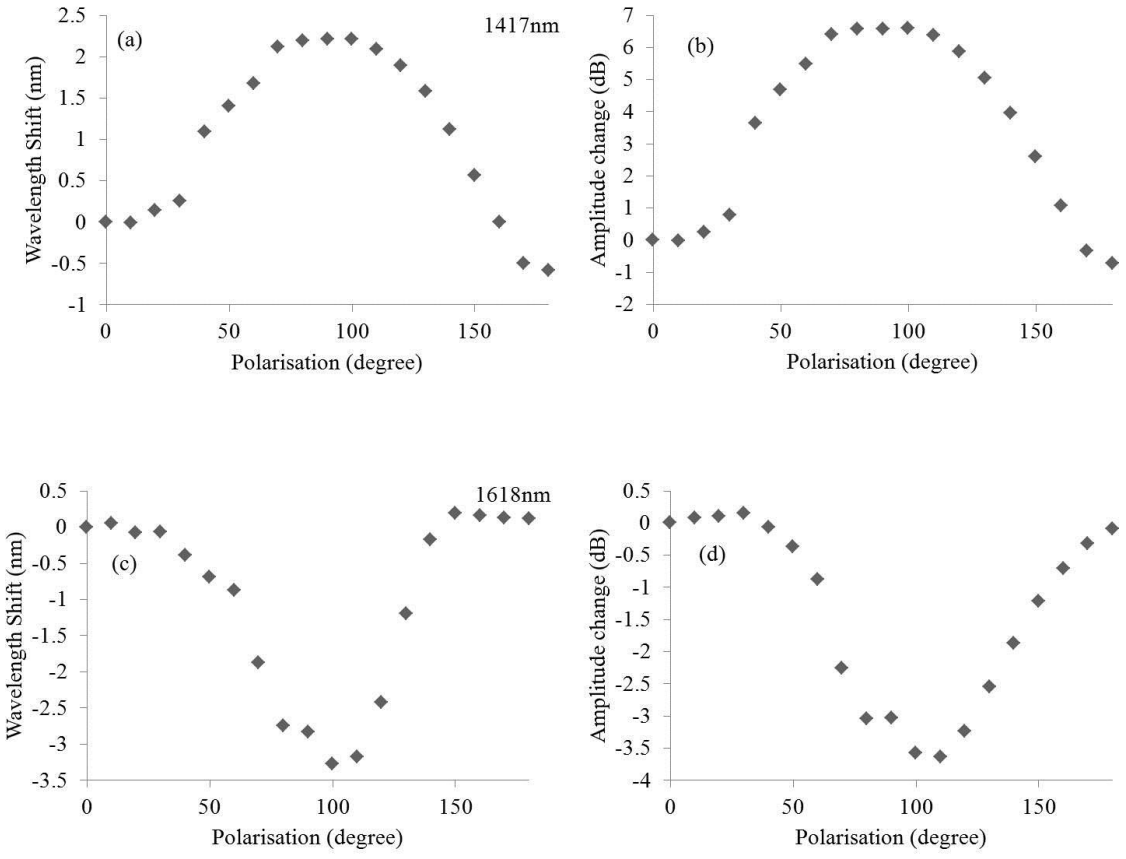

Figure 4-7 showing the polarisation response for the two most sensitive attenuation peaks located at 1417nm and the 1618nm of the femtosecond induced LPG with a period 320µm. The wavelength responses are shown in (a) and (c) and the amplitude responses in (b) and (d) (where positive dB change is a decrease in strength and negative is an increase)

The attenuation peak located at 1417nm had an approximate maximum wavelength variation of 2.8nm and a maximum amplitude variation of 7.3dB and the attenuation peak

located at 1618nm had an approximate maximum wavelength variation of 3.5nm and maximum amplitude variation of 3.8dB, over a polarisation range from 0^o to 180^o. The response curves show the LPG response is sensitive to polarisation, especially in the range from 50^o to 150^o, thus that polarisation effects should be accounted for in sensing but due to the wavelength shifts characterised and with sufficient care, polarisation effects shouldn't effect sensing measurements.

4.1.4 Properties of the femtosecond inscribed LPG of period 400µm

A femtosecond LPG with a period of 400µm was written into SMF optical fibre using a focused beam and the point by point inscription method.

Figure 4-8 showing the femtosecond induced LPG period 400µm showing the RI change to be located on the edge of the core and being approximately 2.5µm wide.

Figure 4-9 showing the femtosecond induced LPG period 400µm showing the measured period to be approximately 408µm

At the examination by changing the input polarisation of light, the transmission spectrum could be optimised for multiple attenuation peaks for this 400µm as well. The transmission spectra for the LPG in air and immersed in a RI liquid 1.444 were recorded and are plotted in Figure 4-10(a) (b), respectively. We can see that, in air there are approximately 2 strong and 3 weak attenuation peaks exhibited, while when the LPG is immersed in RI liquid 1.444, two strong peaks remain with two weak ones. This suggests that the effective indexes of the cladding modes, associated with this, are higher than 1.444. Compared to the femtosecond induced LPG of period 320µm, the LPG of period 400µm is coupling to lower order cladding modes. From coupled mode theory and experience with UV induced LPGs, the longer the period of the LPG the higher the lower the order of modes being coupled to. This is further supported since the all attenuation peaks could be tracked throughout the entire SRI range up to a SRI of 1.444 and did not move out of the wavelength range being examined.

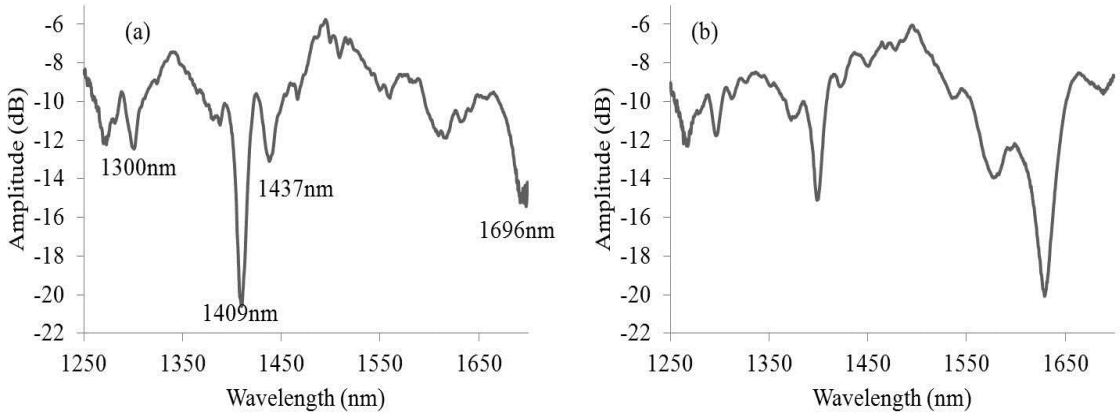

Figure 4-10 showing the transmission spectra of the femtosecond induced LPG of period 400µm in air (a) and in a liquid of SRI 1.444 (b)

Multiple attenuation peaks responses of the 400µm LPG to increasing SRI were monitored and calculated for the four labelled attenuation peaks shown in Figure 4-10(a) and the results are plotted in Figure 4-11. From the figure, there are some differences in SRI response compared to the LPG of period 320µm. Firstly, the spread of sensitivities is very large with the maximum wavelength shift from air to a SRI 1.424 being 69.3nm for the attenuation peak at 1409nm in air while the minimum being 1.7nm. With standard UV induced gratings, coupled modes that produce attenuation peaks in the wavelength range from 1250nm to 1700nm for a fixed period of LPG have sensitivities that are similar to one another; unlike here the femtosecond inscribed ones. This again adds evidence that the femtosecond LPGs are coupling to different sets of cladding modes, explaining the large variation in sensitivities between attenuation peaks. Secondly, the 320µm femtosecond grating produced attenuation peaks that mostly red shifted, with only one single attenuation peak blue shifting, whereas, just in opposite, the 400µm femtosecond LPG produces attenuation peaks that mostly blue shift, with a single attenuation peak red shifting. This may suggest that between these two LPGs there could be a turning point for a set of cladding modes. This further suggests that with refinement of the grating period, the sensitivity could be further increased. However, since the cladding mode coupling is highly dependent on the location of the RI perturbation in the fibre core, the different

period LPGs at different core locations could be coupling to different sets of cladding modes, as clearly shown by the 320µ and 400µm gratings.

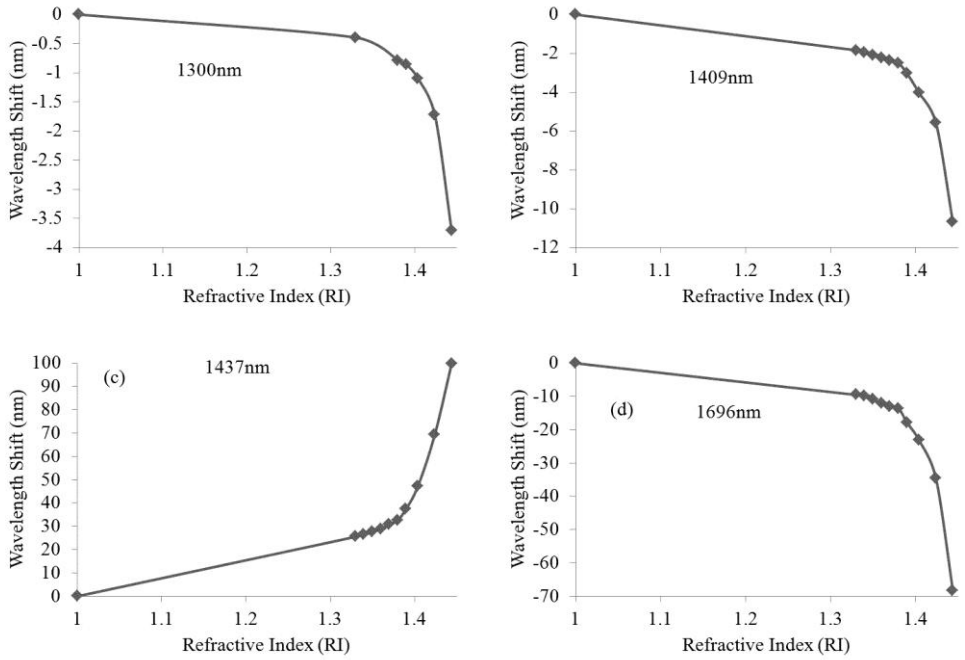

Figure 4-11 showing the SRI response of 4 attenuation peaks for the 400µm period femtosecond inscribed LPG

Since we also see oppositely shifting peaks for the 400µm LPG, the maximum sensitivity can be achieved by combining the opposite shifts of the 1437nm and 1696nm attenuation peak and this is shown in Figure 4-12.

Using the data shown in Figure 4-12, the SRI sensitivity for the individual and combined attenuation peaks for various SRIs regions can be calculated and the results are displayed in Table 4-2. The maximum sensitivity achieved for a single peak is 1106nm/URI for SRI ranging from 1.404 to 1.424. The maximum sensitivity possible through combining the opposite shifts is 1680nm/URI, which is approximately a 1.5 fold increase compared to the sensitivity of the 1696nm attenuation peak. Like all LPGs, the SRI response is nonlinear and the highest sensitivity is in the high SRI range, however using the combined peaks the sensitivity enhancement will be seen across the entire SRI range.

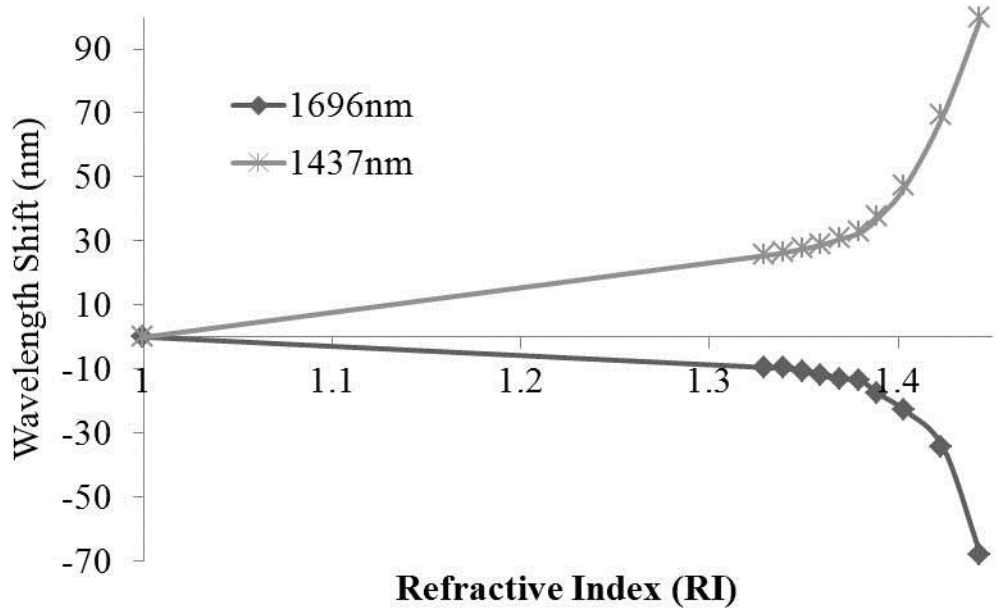

Figure 4-12 showing the peak sensitivity of the 400µm femtosecond induced LPG for two oppositely moving attenuation peaks

	1 to 1.33 nm/URI	1.33 to 1.38 nm/URI	1.38 to 1.424 nm/URI	1.404 to 1.424 nm/URI
Single 1696nm	77.3	142.7	834.4	1106.8
Single 1437nm	28.9	81.0	477.3	573.8
Combined	106.1	223.7	1311.6	1680.5

Table 4-2 showing the calculated sensitivities for the two most sensitive attenuation peaks over various SRI ranges for both individual and combined peaks for the femtosecond inscribed LPG of period 400µm

The polarisation response for the two attenuation peaks located at 1437nm and 1696nm when the grating was in air was calculated using the centroid method. The 1437nm peak produced a maximum wavelength variation of 0.7nm and an amplitude change of 3.6dB over the 180^{o} polarisation range. The wavelength variation is small however the amplitude change is quite large and it was noticed that at one polarisation angle, the peak disappeared completely. The attenuation peak at 1696nm did not vanish and was able to be tracked for the entire 180^{o} polarisation range. The maximum wavelength and amplitude variation were calculated to be 0.8nm and 5.3dB, respectively. As expected, the 1696m attenuation peak

showed a similar response to the 1437nm peak with a relatively small wavelength but a large amplitude variation. Compared to the femtosecond LPG of period 320µm, there is a decrease in polarisation variation which could be linked to either the location of the RI perturbation in the core or the cladding modes being coupled to.

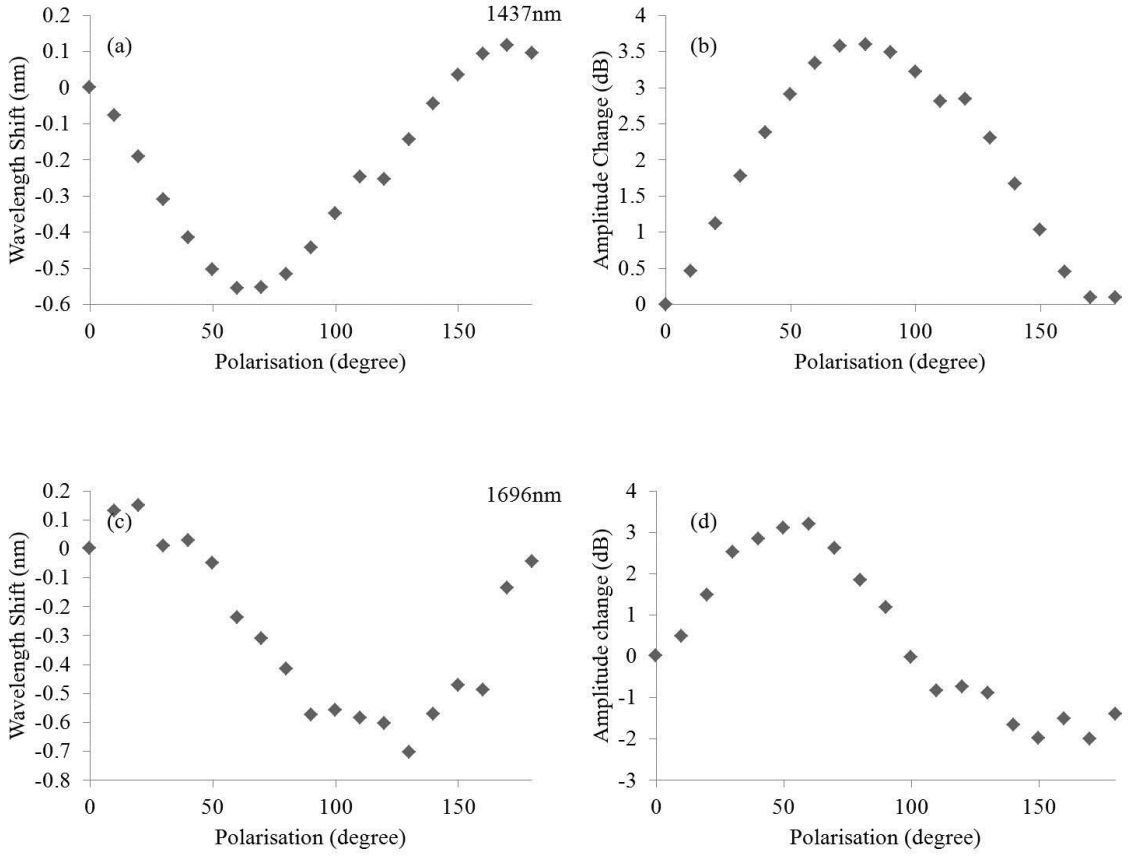

Figure 4-13 showing the polarisation responses for the two most sensitive attenuation peaks located at 1437nm and 1696nm for the femtosecond induced LPG with period 400µm.. The wavelength response is shown in (a) and (c) with the amplitude response represented in (b) and (d)

4.1.5 Properties of the femtosecond inscribed LPG of period 640µm

We further increased the grating period for femtosecond inscribed LPGs to of period 640µm and examined the structure under a microscope. The location of the index perturbation in the core of the fibre was recorded and is shown in Figure 4-14. We can see the grating structure is about 2.9µm wide and is measured to be about 1µm from the core-cladding interface, which indicates the grating is markedly off the core centre. The grating

period was captured and the image can be seen in Figure 4-15; as a result the LPG grating period was measured to be 641µm, close to that of the desired design.

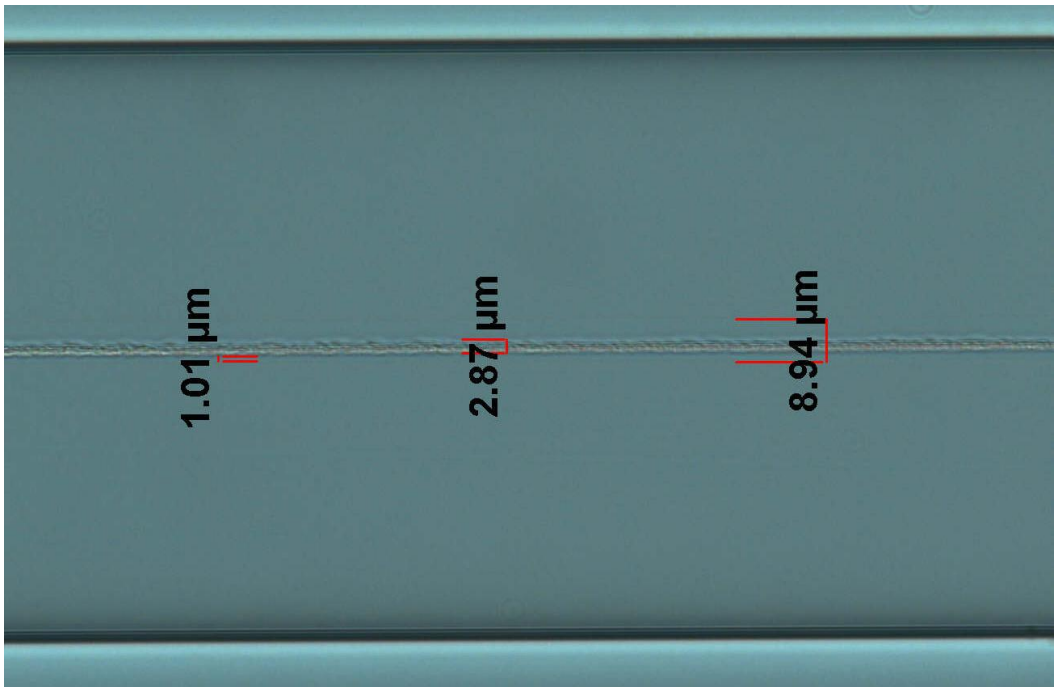

Figure 4-14 showing the femtosecond induced LPG period 640µm with the index change to be located approximately 1µm from the cladding and being approximately 2.9µm wide.

Using a similar procedure, the measured transmission spectra of the 640µm LPG in air and immersed in a SRI 1.444 are displayed in Figure 4-16(a) and (b) respectively. Now there is only one strong peak in air and the peaks remain when the grating is immersed in a liquid with a SRI of 1.444.

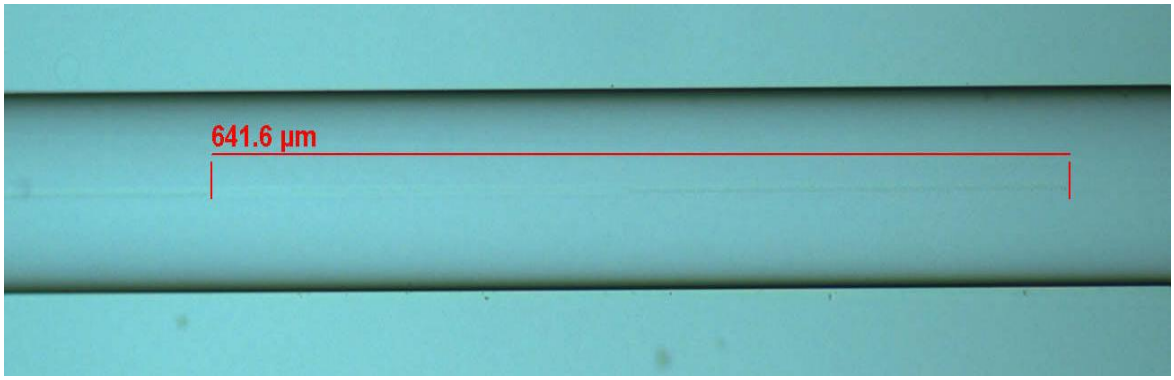

Figure 4-15 showing the femtosecond induced LPG of period 640µm with measured period to be approximately 641µm

This suggests that the femtosecond LPG of period 640µm is only coupling to lower order modes. We further noted that when the SRI response of the LPG was investigated no typical LPG response could be found. To verify this, several gratings were inscribed into SMF with the same period but the same behaviour was observed, which means that this period of femtosecond grating could be coupling to cladding modes far away from the dispersion turning point for multiple sets of cladding modes that are inherently insensitive to SRI. However further investigation should be carried out on the location of the index perturbation in the core and how that effects the cladding modes being able to be couple to for this to be confirmed.

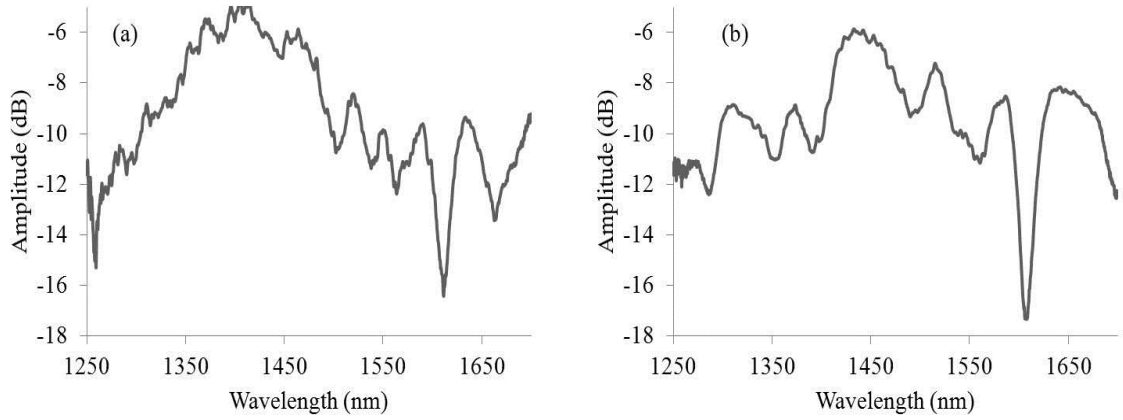

Figure 4-16 showing the transmission spectra of the femtosecond induced LPG of period 640µm in air (a) and in a SRI of 1.444 (b)

4.1.6 Properties of the femtosecond inscribed LPG of period 960µm

The final planned and fabricated grating period was 960µm for the investigation and the microscope images are shown in Figure 4-17 and Figure 4-18. In Figure 4-17 the refractive index perturbation is shown to be approximately 2µm wide and is located at the core cladding interface. The period of the femtosecond LPG is shown in Figure 4-18, due to the large size of the period two images were required to capture the full extent of the

inscription. Using the two images the period for the LPG was measured to be 960.3µm, approximately.

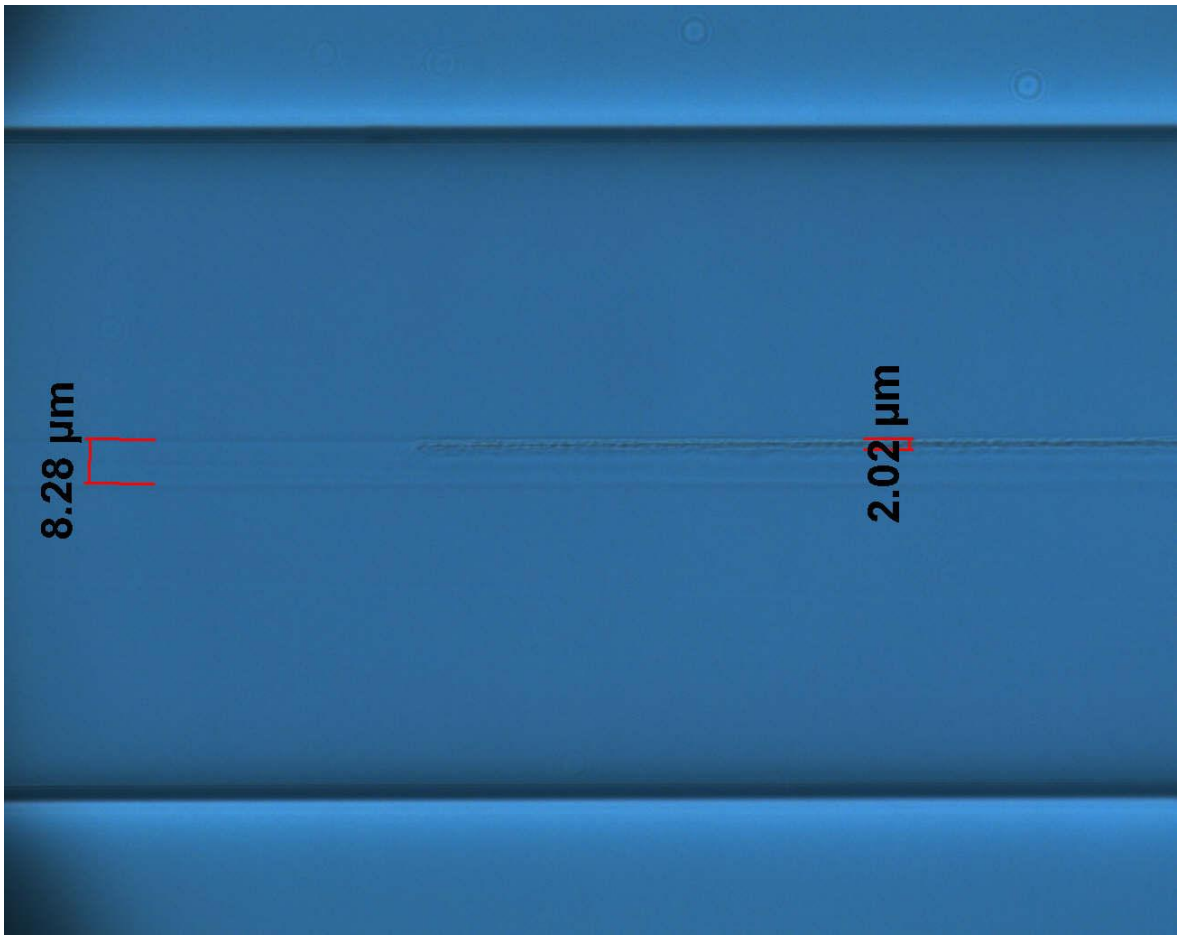

Figure 4-17 showing the femtosecond induced LPG of period 960µm showing the RI change to be located approximately at the core cladding interface and being approximately 2.0µm wide.

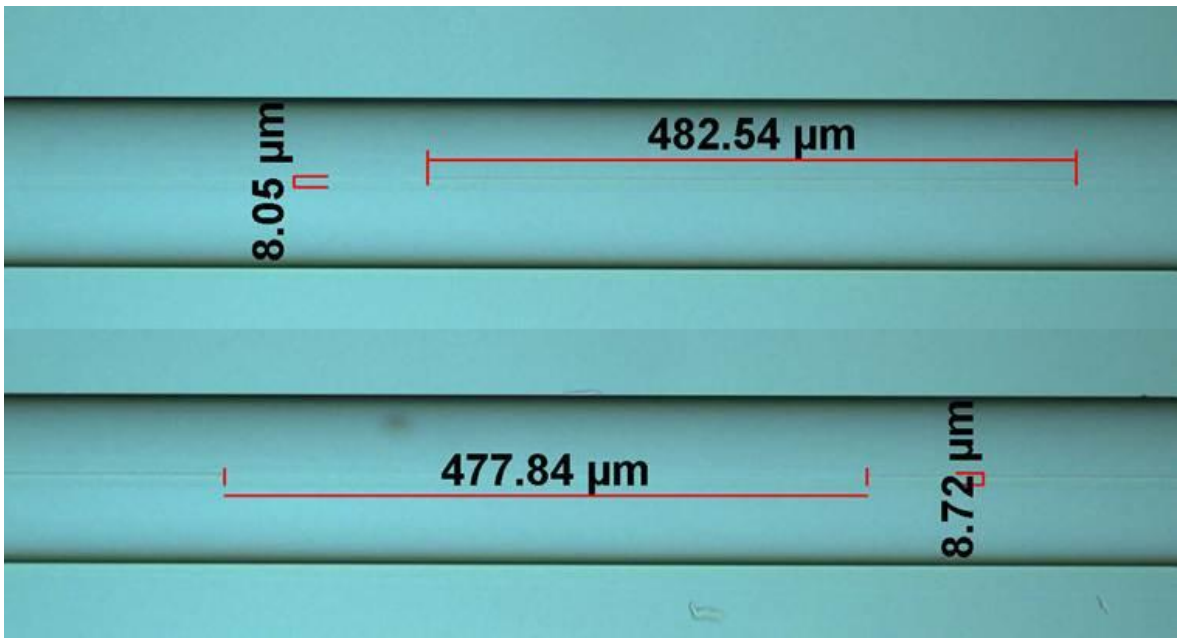

Figure 4-18 the femtosecond induced LPG of period 960µm showing the measured period to be approximately 960.3µm by measuring from two individually captured microscopic images.

In contrast to all other three periods of LPG, we see far more strong attenuation peaks for the 960µm. The transmission spectra in air and in 1.444 were recorded and are shown in Figure 4-19. Taking the transmission spectrum in air and comparing it to the femtosecond LPG of period 320µm, there are more strong attenuation peaks. Using an analogy from a UV inscribed LPG, this behaviour can be explained. For longer periods of LPGs, the dispersion relationships for coupled modes are found to be closer together, resulting in multiple attenuation peaks in the wavelength range 1250nm to 1700nm. The femtosecond LPG of period 960µm is showing this behaviour and explains why there are more attenuation peaks than for the femtosecond LPG of period 320µm. The irregular wavelength locations of the attenuation peaks in Figure 4-19(a) are, again, due to the femtosecond LPG coupling to multiple sets of cladding modes. Comparing Figure 4-19(a) with Figure 4-19(b), all the peaks can be followed as they remain when the SRI is increased to 1.444. This shows that compared to the LPG of period 320µm the femtosecond LPG of period 960µm is coupling to lower order modes.

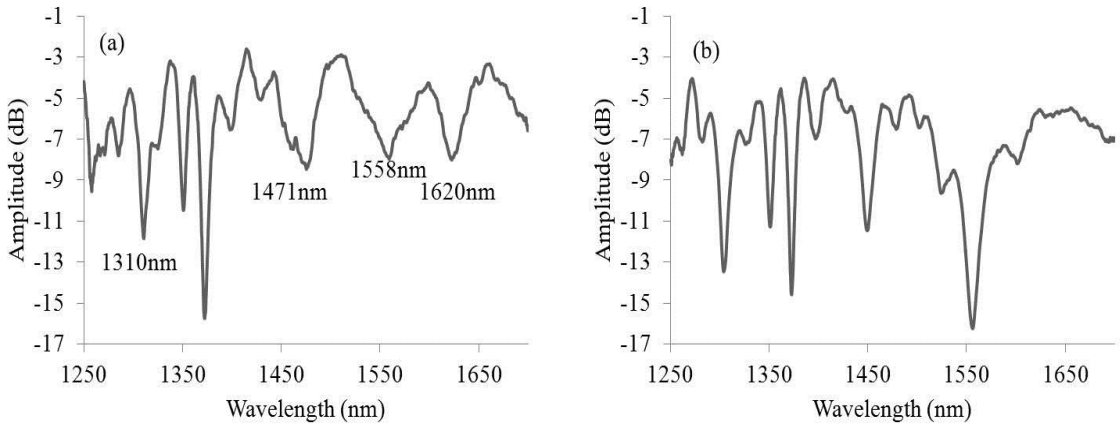

Figure 4-19 showing the transmission spectra of the femtosecond induced LPG of period 960µm in air (a) and in a SRI of 1.444 (b)

Several attention peaks response to SRI changes were investigated and these are labelled in Figure 4-19. The calculated wavelength shifts for the four labelled attenuation peaks are plotted in Figure 4-20. With increasing SRI, the attenuation peaks all experience a blue wavelength shift. This differs from the femtosecond LPGs of periods 320µm and 400µm whose attenuation peaks displayed both red and blue wavelength shifts. This behaviour coupled with the evidence for the attenuation peaks being associated with lower order modes shows that the 960µm is far away from the dispersion turning point in this wavelength range. The sensitivity, overall, is lower than the shorter period femtosecond LPGs, as would be expected with the peak wavelength shift for a SRI of 1.444 being less than 70nm. The sensitivity responses produced are not as smooth as those produced by the other femtosecond LPGs. This behaviour may be due to a combination of two affects: firstly, the sensitivities are smaller than the shorter period femtosecond LPGs meaning any small variation/error has a larger effect of the SRI response; secondly, the refractive index perturbation is located at the core cladding interface, as this could result in a larger polarisation response for the cladding modes being coupled to.

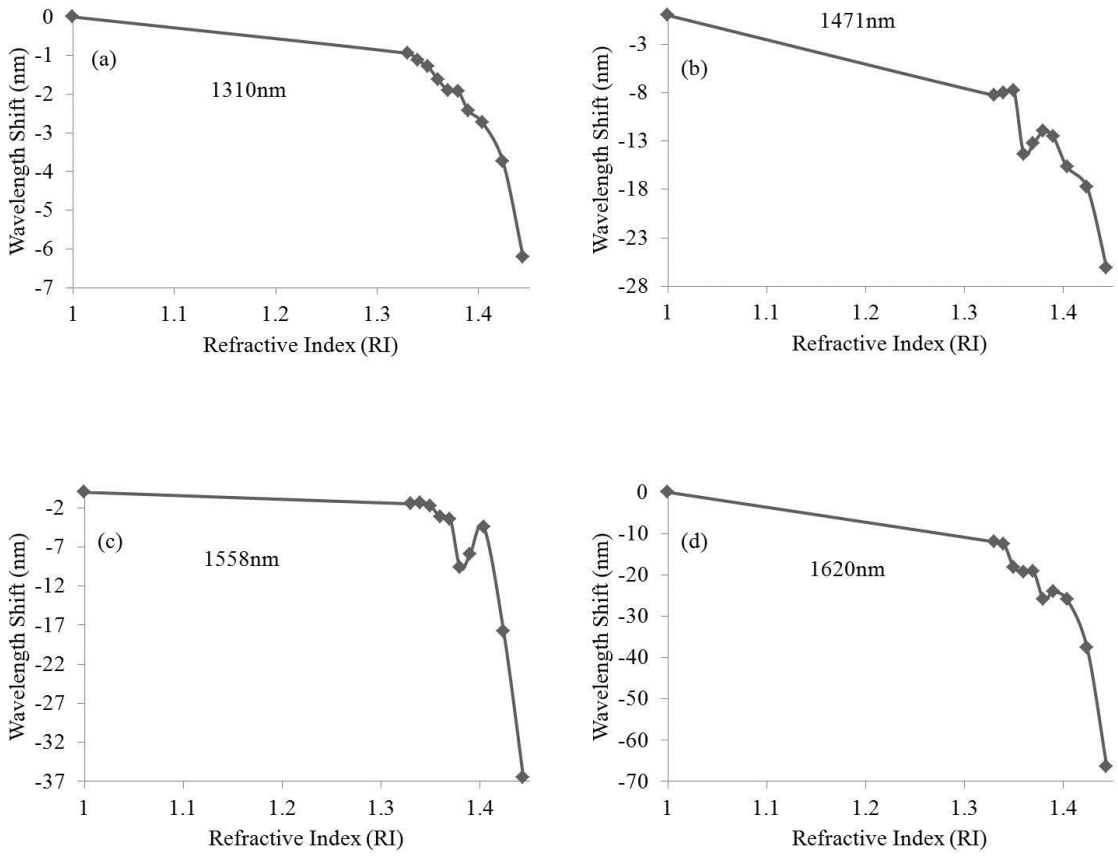

Figure 4-20 showing the SRI response of 4 attenuation peaks for the 960µm period femtosecond inscribed LPG

Since all the attenuation peaks produced by the femtosecond LPG of period 960µm produced a wavelength shift in the same direction, the sensitivity of a single peak can only be reported here. The SRI sensitivity four SRI ranges was calculated for the attenuation peak located at wavelength 1620nm in air and the results are shown in Table 4-3. The peak sensitivity of the femtosecond LPG of period 960µm was 578.5nm/URI which is smaller than that of the shorter period femtosecond LPGs.

	1 to 1.33 nm/URI	1.33 to 1.38 nm/URI	1.38 to 1.424 nm/URI	1.404 to 1.424 nm/URI
Single 1620nm	36.3	278.9	264.3	578.48

Table 4-3 showing the calculated sensitivities for the most sensitive attenuation peak over various SRI ranges for the femtosecond inscribed LPG of period 960µm

A typical polarisation response of one of the attenuation peaks is shown in Figure 4-21, the attenuation peak at 1620nm in air since it gave the highest SRI sensitivity. A centroid method was implemented since the strength and shape of the peak changed when the polarisation changed from 0^o to 180^o. The peak disappeared at one point, meaning a curve fitting could not be applied and, showing the high polarisation sensitivity of the device. The maximum wavelength and amplitude change over the polarisation range was found to be 2.7nm and 5.6dB, respectively. Although these changes are on the same order of magnitude as the shorter periods of LPGs the lower sensitivity explains the less symmetric appearance of the SRI in Figure 4-20.

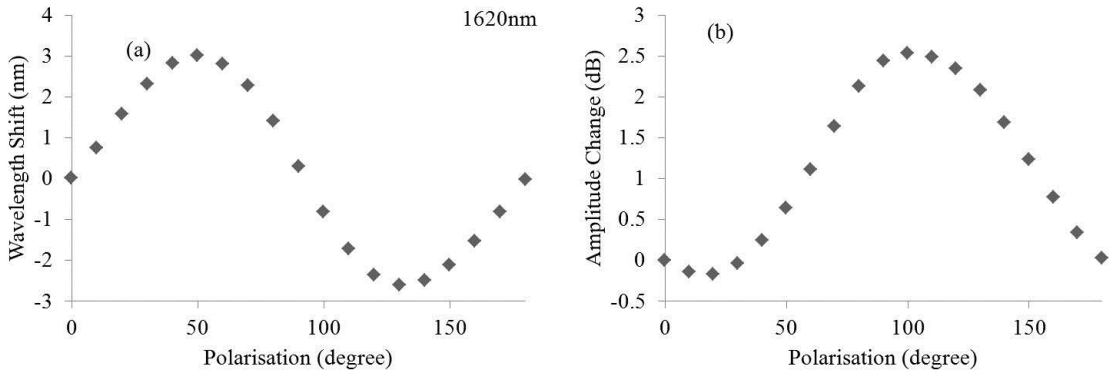

Figure 4-21 showing the polarisation response for the most sensitive attenuation peak for the femtosecond induced LPG period 960µm. The polarisation response for the peak located at 1620nm with the wavelength response is shown in (a) and the amplitude response represented in (b).

4.1.7 Summary and discussion

The distinct behaviour of all of the femtosecond induced LPGs with non-uniform index perturbation within the core of optical fibre has been shown experimentally, which cause the light coupling from the core mode to more sets of cladding modes than a UV induced LPG and has been evident due to the SRI responses of the gratings. The femtosecond inscribed LPGs have also shown the ability to couple to both higher and lower order cladding modes at the same time. This may open up the possibility to use the attenuation

peaks of higher order cladding modes for SRI sensing while using the lower order cladding modes that are SRI insensitive to act as temperature compensators.

A dispersion turning point has been found experimentally for a femtosecond LPG with a period around 400μm, as we see the change in overall wavelength shifts of the attenuation peaks between the two LPG periods 320μm and 400μm. For these two periods of femtosecond LPG, the attenuation peaks produced had both blue and red wavelength shifts in the wavelength range 1250nm to 1700nm. This gives rise to SRI sensitivities far greater than anything achievable through monitoring a single attenuation peak, producing a maximum SRI sensitivity as high as 1680nm/URI.

The femtosecond LPGs were found to have a large polarisation sensitivity which means that for any sensing applications the optical fibres and LPG have to be secured to remove these effects. The polarisation response was most evident for femtosecond LPGs of longer period with lower SRI sensitivities.

4.2 Femtosecond induced sampled FBGs with and without a LPG response

4.2.1 Introduction

Sampled fibre Bragg gratings (SFBGs) are formed by inscribing a superimposed LPG and FBG structure into the core of optical, as the schematic diagram shows in Figure 4-22. Using UV light as the inscription technique, two standard methods to induce a SFBG are: (a) to use a uniform phase mask and shutter, that is controlled using a computer program, to introduce the low frequency LPG element[95, 98] or (b) a two-step process of exposure using two masks, starting with the high frequency FBG inscription using a phase mask and followed by another exposure using an amplitude mask to produce a low frequency LPG

modulation[98]. The superimposed structure has led to transmission spectrum having both a LPG and FBG response which has been implemented for multi-parameter/compensating sensing [100, 134]. An alternative method employing a femtosecond laser to inscribe the FBG element and a CO_2 laser for the low frequency LPG modulation has been demonstrated[135], however this has the distinct disadvantage of requiring two laser processing techniques.

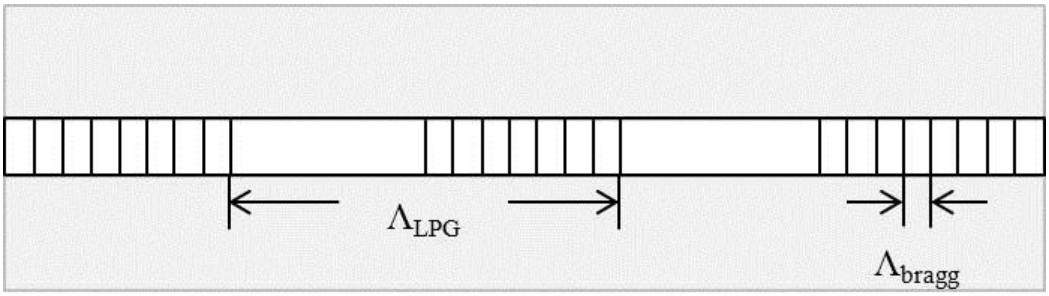

Figure 4-22 showing a schematic of a SFBG structure

One of the uses of SFBG is as a temperature sensor, much like (FBG) it couples the light from the forward to the reflected core mode and as such is dependent on the glass optical fibre characteristics. When the optical fibre with a grating structure is heated, two effects occur that influence the resonant location of reflection[29]. Firstly, a volume increase of the fibre which in turn changes the period of the grating. Secondly, changing the temperature of the fibre causes an effective index change of the mode. Since the spectral location of reflection in both FBG and SFBG is dependent on the core mode effective index any change in this will result in a wavelength shift in the reflection peak. These two factors allow the SF BG to operate as a temperature sensor.

In previous work Kyriacos Kalli et al used femtosecond laser inscription precisely at the optical fibre threshold to produced FBG with low loss insertion and minimum polarisation dependence[136]. Continuing this work and utilizing this femtosecond laser inscription technique a series of SFBG have been produced that have no characteristic LPG response and one that has.

4.2.2 Fabrication and characterisation method

The SFBGs were inscribed by Dr. Kyriacos Kalli's group using a femtosecond laser system with a repetition rate of 100 kHz and emitting 300fs pulses at a wavelength of 1035nm. SMF fibre was chosen for the inscription and with this in mind, a Mitutoyo microscope objective lens (with a magnification of 50 and a numerical aperture of 0.40) was used, because it is less sensitive to any optical fibre curvature. The focus of the laser is aligned to the core of the fibre by optimizing the characteristic plasma generated when focusing onto the fibre core. Implementing a pulse picker, the laser operated at 1 kHz and produced energies of less than 3.5μJ/pulse when exiting the laser. Controlling of the laser repetition rate and the translational stage speed provided accurate control of the high frequency modulation pitch and period. Further to this, a shutter was used to stop and allow the laser beam creating the low frequency modulation. A further LPG inscription was required to achieve the LPG response, since without it the attenuation peaks were not visible in the transmission spectrum. For the LPG inscription the procedure was the same as that in section 4.1.2

Each grating was attached to a tuneable laser light source, ranging from about 1520nm to 1600nm, and a Luna Technology's optical vector analyser. The Luna interrogation equipment was capable of a wavelength resolution as low as 1.6 pm where as the best available OSAs in our laboratory is only as low as 60 pm. Due to the narrow bandwidth of the individual Bragg reflections and the close proximity in wavelength of the multiple reflections in a SFBG structure, the Luna equipment was used for characterisation. For each SFBG, the Luna analyser recorded the multiple measurands including the transmission spectrum, polarisation dependent loss and the reflection spectrum.

Once the device spectrum and polarisation response had been evaluated, the temperature response for each SFBG was investigated. In turn, each SFBG was secured to a 'v' groove

metal plate that was attached to a temperature controlled peltier. The temperature was varied by 5^{o}C increments ranging from 20^{o}C to 80^{o}C and at each temperature the transmission spectrum was recorded. The advantage of using the transmission spectra over the reflection is that the narrow bandwidth of the transmission peak gives better resolution. Once all the data had been collected, a 2nd order polynomial was fitted to the reflection peak for each temperature and the minimum of the transmission was calculated to minimise error.

As is well known, LPGs are good SRI sensors, however they are also temperature sensitive, which can lead to inaccurate results on SRI sensing caused by the temperature cross sensitivity[49]. By inscribing a femtosecond LPG and SFBG parallel to each other in the core, the LPG can act as a SRI senor while the SRI insensitive SFBG acts as a temperature sensor, which can then be used compensate for the temperature cross sensitivity. The advantage of using SFBG rather than a FBG and LPG in series is not due to performance rather that, with the SFBG parallel to the LPG the temperature is the same for both gratings. This allows same location temperature compensation of the SRI sensing element. This is especially useful with liquid level measurements where the liquid being sensed can often be at a different temperature to the surrounding air. With this in mind, a SFBG with a high frequency modulation of 1078nm and a low frequency modulation of 300µm was inscribed into an optical fibre core. In parallel to it an femtosecond LPG of period 300µm was also inscribed into the core.

The location and period of the inscribed SFBG were examined using a microscope and computer software. Due to the weak nature of the index change caused by the femtosecond inscription technique and the large period of the low frequency modulation, an 800nm red light source was used to scatter from light from the gratings and make the grating period more apparent.

4.2.3 Results and discussion

4.2.3.1 SFBG-1 with a high frequency modulation of period 1078nm and a low frequency modulation of period 600µm

The microscope images from the SFBG-1 were recorded and are shown in Figure 4-23(a) and (b). Figure 4-23(a) confirms that the low frequency modulation has a period of ~606µm which is close to the design parameter. Figure 4-23(b) shows that the high frequency modulation is about 1µm which is also close to the design parameter. The figure also shows that the index perturbation is located at the core cladding interface which could result in a high polarisation response, compared to the FBG[136].

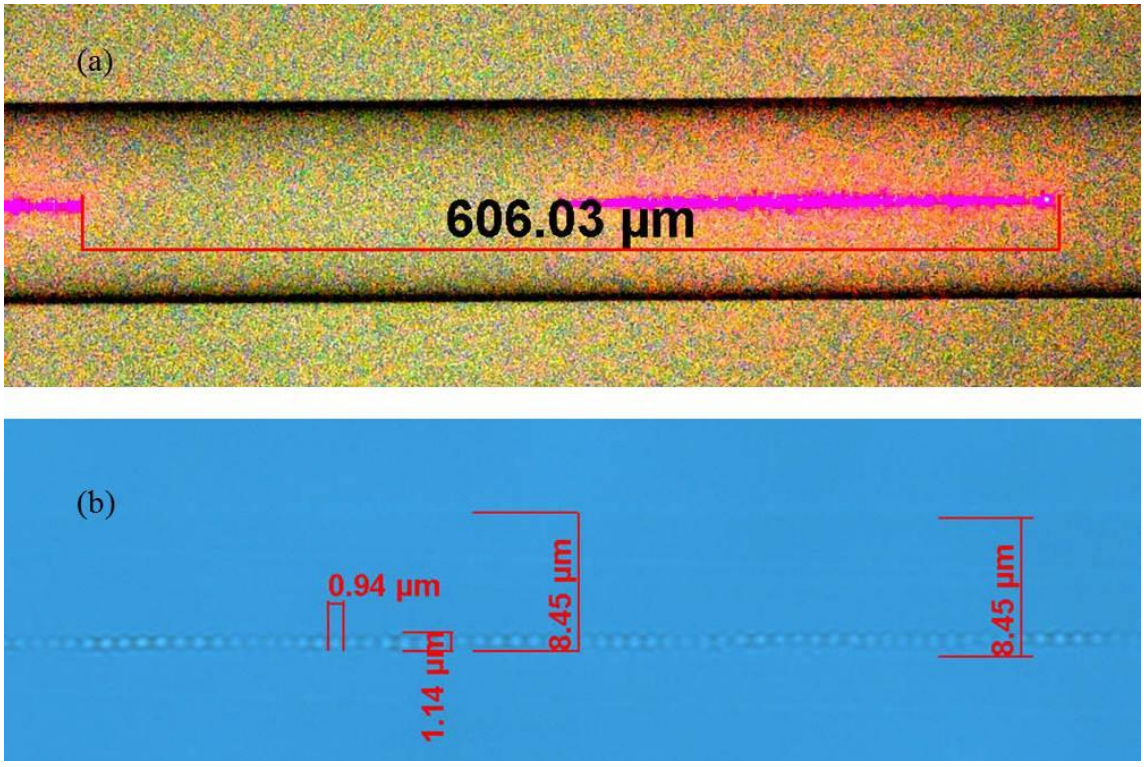

Figure 4-23 showing the microscope images for the low frequency refractive index modulation in (a) and the high frequency modulation in (b) for SFBG-1.

The transmission and reflection spectra for SFBG-1 are shown in Figure 4-24 (a) and (b) respectively. Three reflections due to core modes coupling are marked in Figure 4-24(a) and the wavelength locations of these three modes are at 1559.95nm, 1561.33nm and

1562.72nm. The calculated average spacing between reflections is 1.38nm which compares well to the calculated value of 1.40nm.

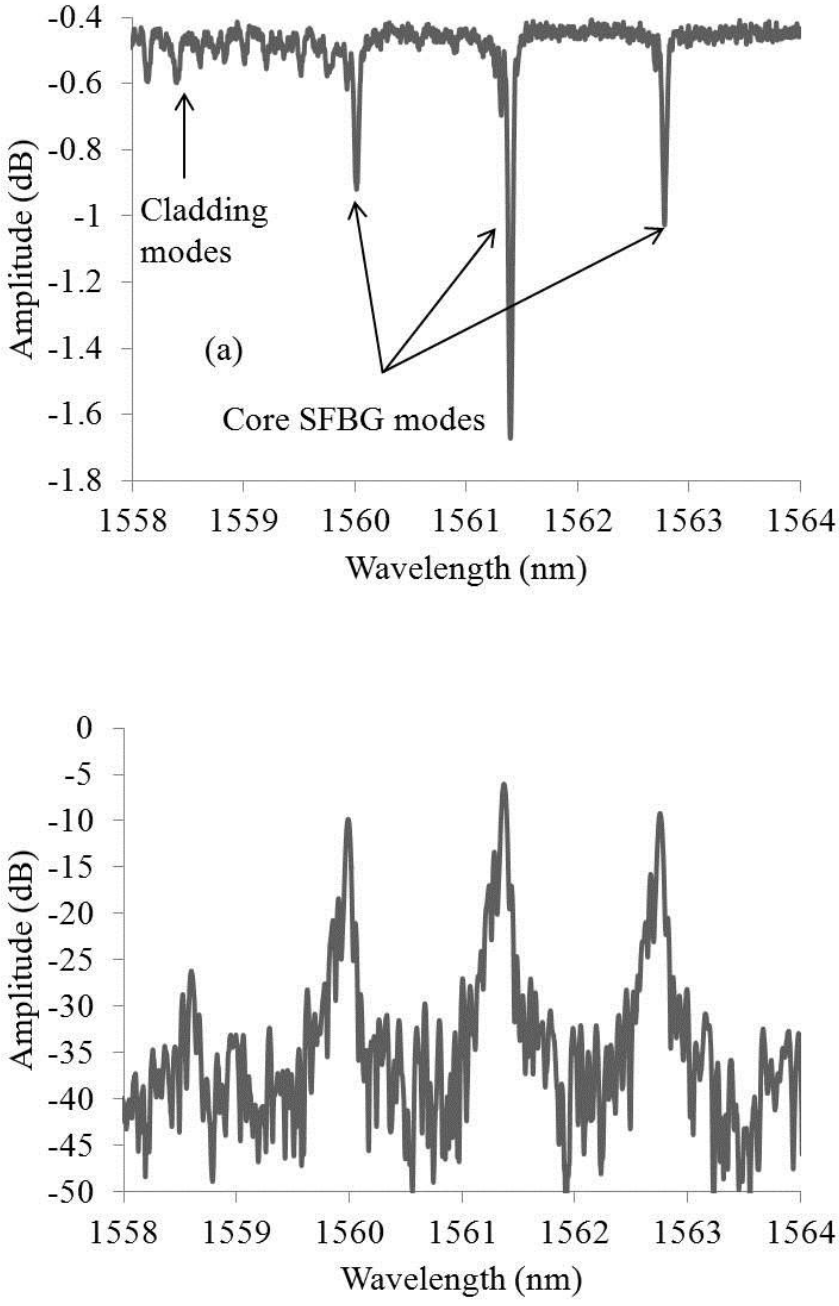

Figure 4-24 showing the SFBG-1 transmission (a) and reflection (b) spectra with the core SFBG and cladding modes identified in (a).

Reflections due to higher Fourier components could not be identified in transmission however low order cladding modes, typical of FBGs, were present and also marked in Figure 4-24(a). The DC insertion loss associated with the inscription of these gratings was quite low as only 0.4dB, making them ideal for optical fibre communication and long

distance sensing applications. Each reflection had a different transmission loss, the central peak located at 1561.33nm had a loss of approximately 1.2dB while the surrounding peaks located at 1559.95nm and 1562nm have transmission losses of ~0.4dB and 0.6dB, respectively. Theory predicts that the side reflection peaks should be weaker due to a sinc envelope function and these experimental results tie in well with the theory. The reflection spectrum in Figure 4-24(b) produces three peaks at the same wavelengths as those found in transmission, as is expected. In reflection, due to the lower background DC level, the higher Fourier components are apparent.

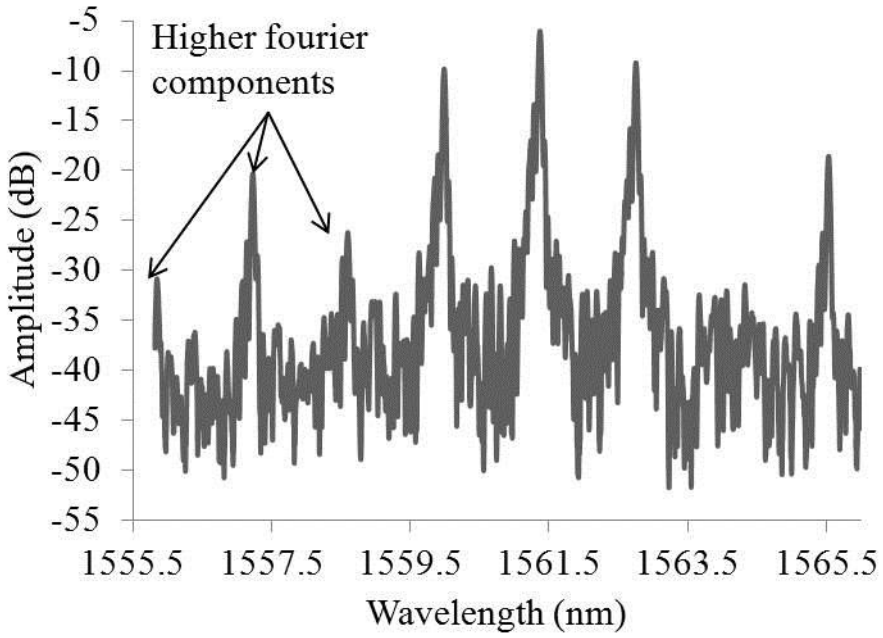

Figure 4-25 showing the reflection spectrum for the SFBG-1 device in the wavelength range from 1555.5nm to 1565.5nm and showing the higher Fourier components.

The higher Fourier components become even more apparent when a wider wavelength range is investigated. The reflection spectrum for a wider wavelength range from 1555.5nm to 1565.5nm is shown in Figure 4-25. From it we can see that the higher Fourier components are evident, as expected from a SFBG structure.

When utilizing femtosecond inscribed fibre gratings, the polarisation effects must always be considered. With this in mind, the polarisation dependant loss was investigated for the

all the SFBG structures and the results are shown in Figure 4-26. As is evident, the strongest reflection peak located at 1561.33nm gives the largest polarisation dependent loss of approximately 0.6dB. Considering the previous work carried out by Dr Kyriacos, this is a high value and can probably be contributed to the non-central location of the index perturbation with in the core of the optical fibre. The weaker reflection peaks show smaller polarisation dependent loss with the higher Fourier components not showing any, this is probably due to the weak nature of these reflection peaks.

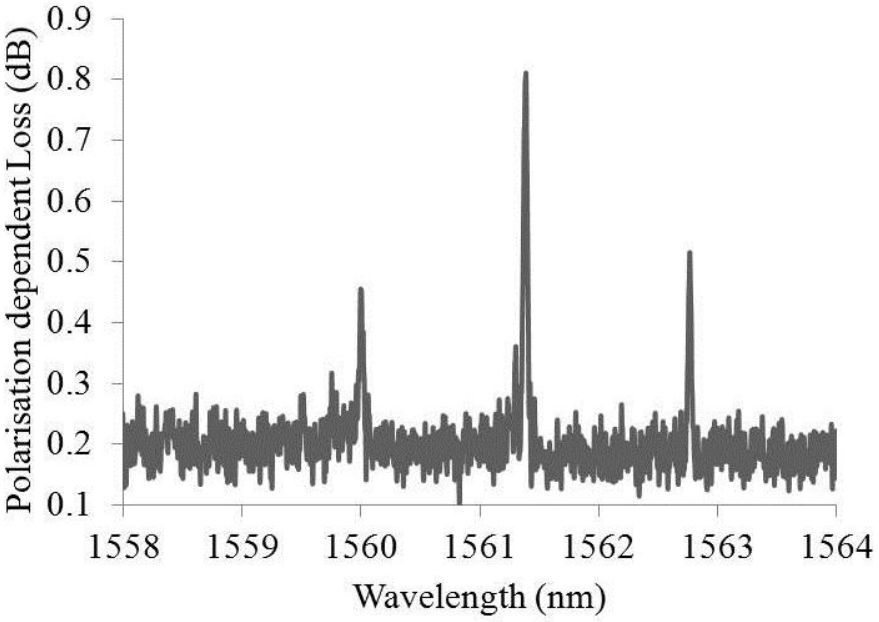

Figure 4-26 showing the polarisation dependent loss of the SFBG-1 device

Finally, the temperature sensitivity of the SFBG-1 was characterised for the three strongest reflection peaks and the results are plotted in Figure 4-27. There is a high degree of consistency in temperature sensitivity between all three reflection peaks, with them all producing a sensitivity of 11.6 pm/^{o}C. This result shows a slight decrease in performance compared to FBGs[73] and other SFBGs[98]. However, the result is of the same order of magnitude. The linear response means that the femtosecond inscribed SFBG-1 could be implemented as a temperature sensor or easily used for compensating for other applications.

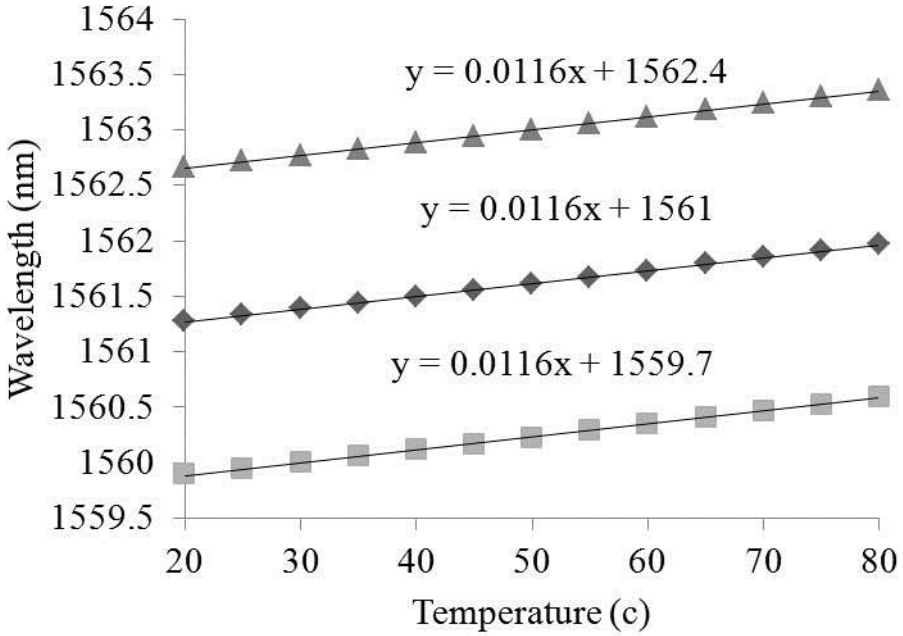

Figure 4-27 showing the temperature response of the three strongest reflection peaks of the SFBG-1 device

4.2.3.2 SFBG-2 with a high frequency modulation of period 1078nm and a low frequency modulation of period 300μm

The microscope images of the second inscribed SFBG with low frequency modulation period 300μm are shown in Figure 4-28. From Figure 4-28(a), the actual period of the low frequency modulation is shown to be ~ 308μm, which is close to the design parameter. Figure 4-28(b) displays the high frequency index modulation with its period being on the same order of magnitude of the design parameter. The index perturbation is located approximately 3μm from the core cladding interface.

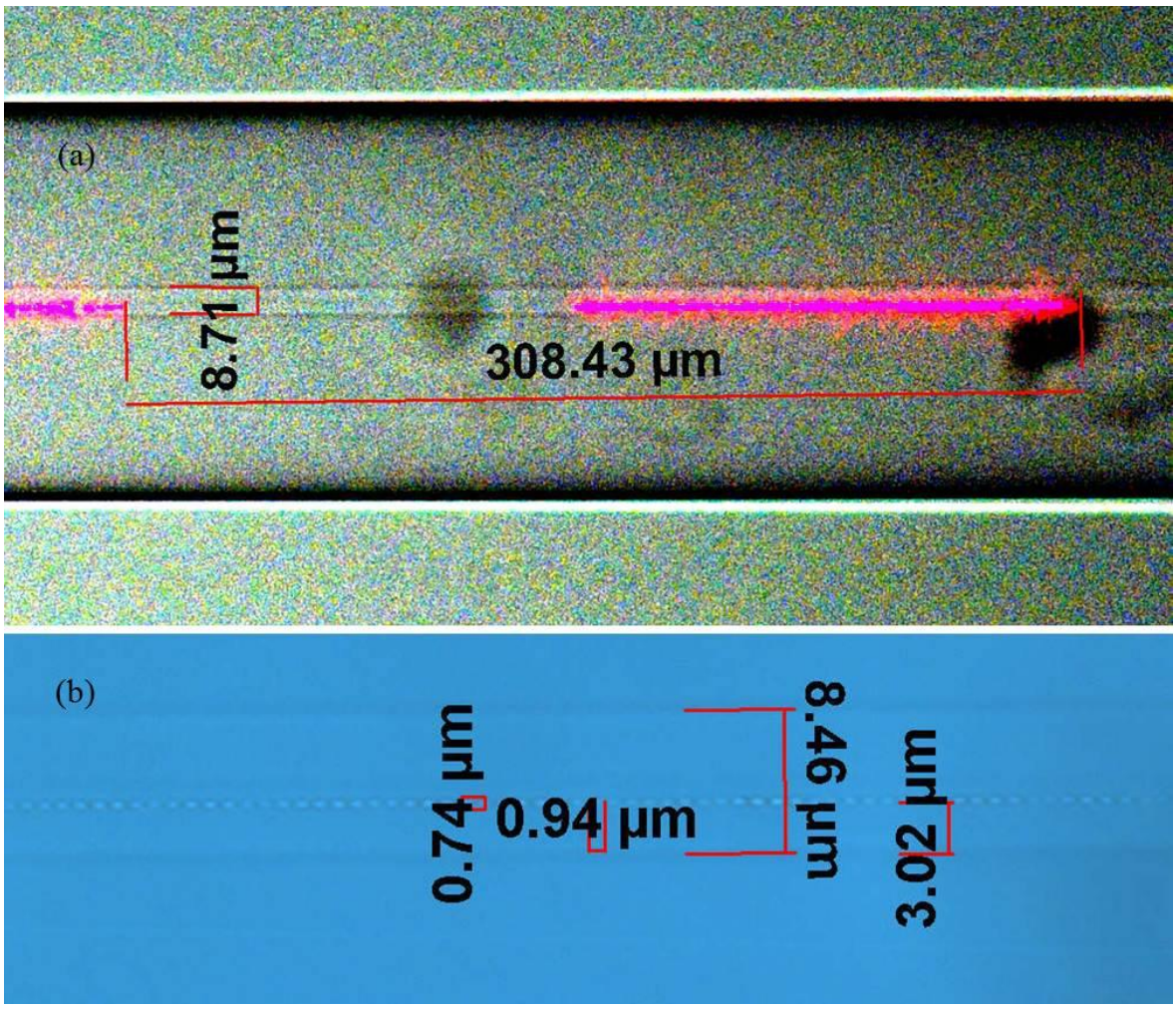

Figure 4-28 showing the microscope images for the low frequency refractive index modulation in (a) and the high frequency modulation in (b) for SFBG-2

The transmission and reflection spectra for SFBG-2 are shown in Figure 4-29(a) and Figure 4-29(b), respectively. Three reflected core modes along with the reflected cladding modes are labelled in Figure 4-29(a). The wavelength locations of the three reflections are found to be at 1558.53nm, 1561.29nm and 1564.07nm. The central reflection, 1561.29nm, is close to that of SFBG-1.This is expected since they both have the same high frequency modulation and it is this that dominates the wavelength location of the central reflection peak.

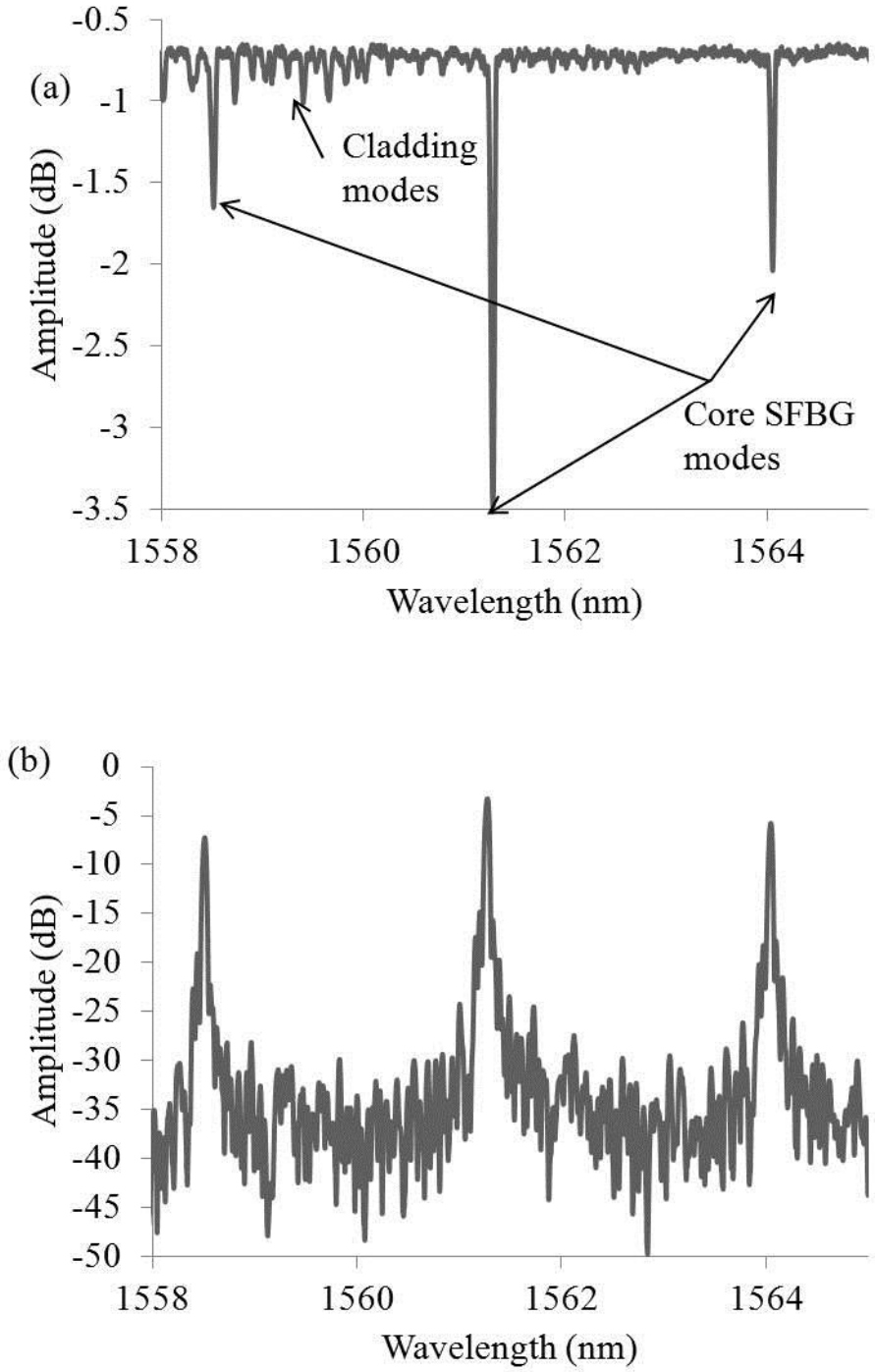

Figure 4-29 showing the SFBG-2 transmission (a) and reflection (b) spectrum , with the core SFBG and cladding modes identified in (a).

Theoritically, the central wavelength location of SFBG-2 should be at a shorter wavelength than SFBG-1, however this can be accounted for by any slight variation in the alingment, temperature or stress induced during the fabrication of the grating. The separation of the reflection peaks was calculated to be 2.77nm which agrees well with the theoretically predicted value of 2.81nm. Therfore the shorter period of the low frequency modulation of

SFBG-2 compared to SFBG-1 results in a wider spacing between reflections. Through changing the low frequency modulation period the spacing and location of the multiple reflection peaks can be controlled. As expected from theory and similar to SFBG-1, the strongest refleciton peak is located centrally at a wavelenth of 1561.29nm and has a transmission loss of ~2.6dB. The weaker side reflection peaks located at 1558.53nm, and 1564.07nm have transmission losses of 0.8dB and 1.2dB, respectively. The reflection peaks of SFBG-2 are noticable stronger than those of SFBG-1, one of the explanations could be the location of the grating in the fibre core. With the index perturbation being more centrally located for SFBG-2 than SFBG-1, the grating has a stronger interaction with the core mode and results in a greated coupling efficiency to the reflected modes. The central location of the grating also explains the larger DC loss from SFBG-2 than SFBG-1. The DC loss from the inscription process is above 0.5dB which is due to more light interacting with the grating in SFBG-2 than in SFBG-1. Though there is an increase in DC loss, it is still quite small and does not effect the quality of the the results and reflection peaks.

Now taking the polarisation response of SFBG-2, the plot of polarisation dependent loss is shown in Figure 4-30. Similar to SFBG-1, the greatest variation is associated with the strongest reflection peak at 1561.29nm and it gave a maximum amplitude change of 1.75dB. Though this can partially be explaind by a greater degree of core mode interaction with the grating, this level of amplitude change is mainly due to polarisation. This may mean that the polarisation repsonse of the SFBG is is highly dependent upon location and shape of the index perturbation. Also, being close to the centre of the core is not adequate for polarisation stability as the shape of the index perturbation is having a strong effect as well as indicating the femtosecond inscribed SFBG structures are inherently more polarisation sensitive than FBGs. This supports some of the current work in the literature[63].

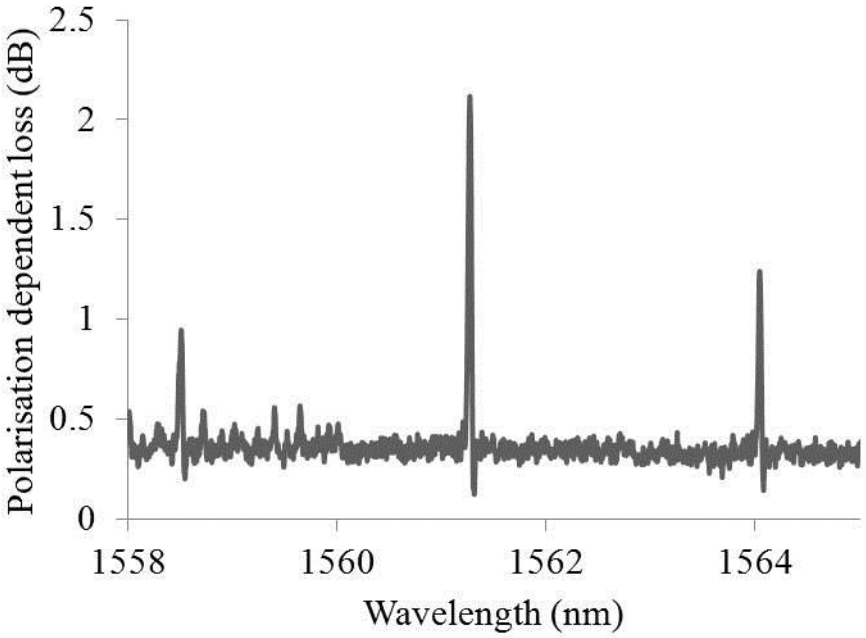

Figure 4-30 Showing the polarisation dependent loss of the SFBG-2 device

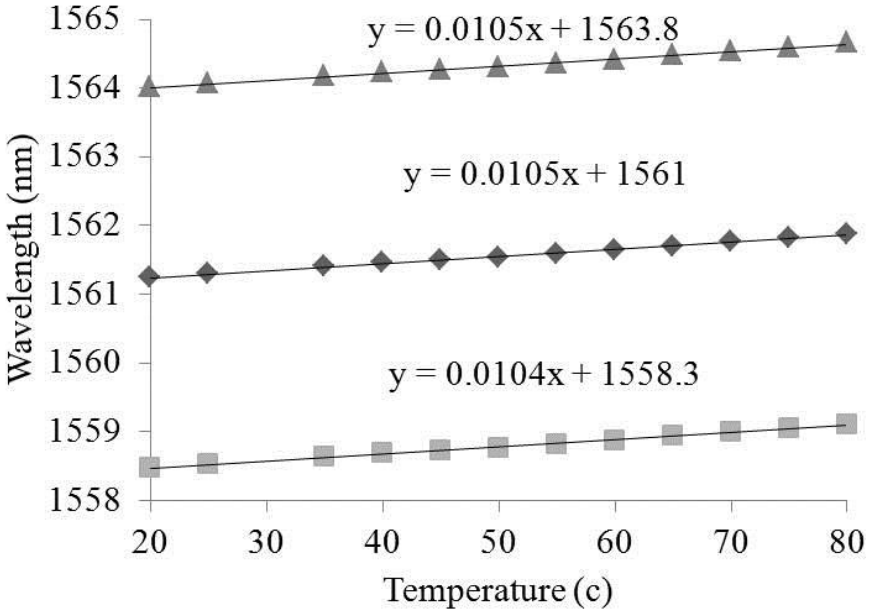

Figure 4-31 showing the temperature response of the three strongest reflection peaks of the SFBG-2 device

The temperature response of the three strongest peaks were evaluated and plotted in Figure 4-31. All three reflection peaks produced a linear response and a good correlation between the sensitivities. The sensitivity of the reflection peaks was calculated to be 11.5 pm/^{o}C, which is similar to the sensitivity of SFBG-1. Again, the linear response means that the

femtosecond SFBG-2 could be implemented as a temperature sensor or easily compensated for in other applications.

4.2.3.3 A SFBG hybrid structure femtosecond laser inscribed with a high frequency modulation of period 1078nm and a low frequency modulation of period 300µm and a LPG of period 300µm in parallel

In the introduction we discussed that a hybrid SFBG/LPG structure may be produced by femtosecond inscription by inscribing these two structures in parallel in the core and here we have fabricated and evaluated such a hybrid structure. The microscope images for this hybrid grating in Figure 4-32(a) show the two distinct regions of the different inscription processes.

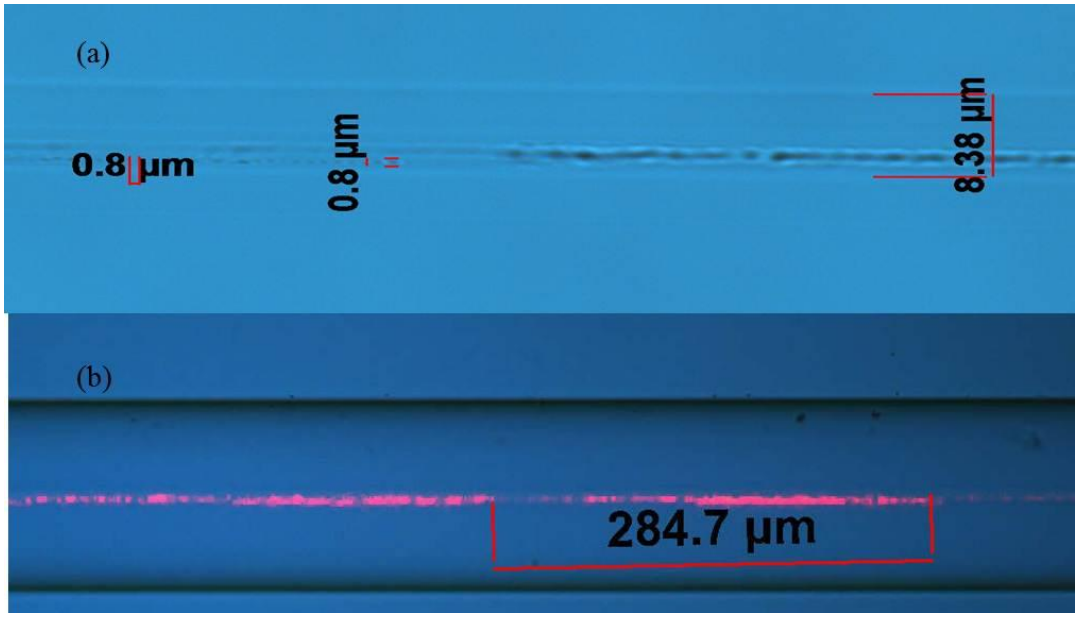

Figure 4-32 showing the microscope images for the low frequency refractive index modulation of the SFBG and the LPG in (a) and the approximate period of either the LPG or the low frequency modulation of the SFBG

The SFBG gives a distinct qausi-circular shape of index perturbations while the LPG shows a line pattern drawn through the core. Both index perturbations are located near the edge of the core near the cladding. The period of the low frequency modulation for the

LPG is harder to evaluate. From Figure 4-32(b), the SFBG and LPG overlap with one another making it hard to distinguish the two structures. However, due to the consistency of the periods of the previous SFBGs the period of both the SFBG and LPG should be close to the design parameters.

The hybrid grating transmission spectrum, which is shown in Figure 4-33(a), had only one strong reflection peak located at 1559.56nm and had a transmission loss of approximately 0.4dB. Peaks were found at both shorter and longer wavelength peaks than the strongest reflection peak, those at shorter wavelength peaks could also be associated with cladding mode coupling. The identity of the reflection peaks can be confirmed through a comparison of the transmission and reflection spectra for the hybrid grating for the wavelength range from 1554nm to 1562nm from Figure 4-33(a) and Figure 4-33(b), respectively. Although the SFBG part of the hybrid grating has the same design parameters as SFBG-1, the spacing between the reflection peaks is no longer uniform, the location of the strongest reflection peak is at a shorter wavelength and the reflection peak strengths vary widely comparing to the SFBG-1 device. This is probably due to the two inscription processes for the SFBG and the LPG. The two inscriptions increase the noise level of the system and 'wash' out the lower strength side reflection peaks; hence they cannot be seen in the transmission spectrum and also explains the relatively weak reflection peak. Further to this, the weakened reflection peak could also be due to the location of the index perturbation at the core/cladding interface, as we have already seen from comparing SFBG-1 and SFBG-2, when the grating is located at the interface the produced reflection peaks are weaker in strength.

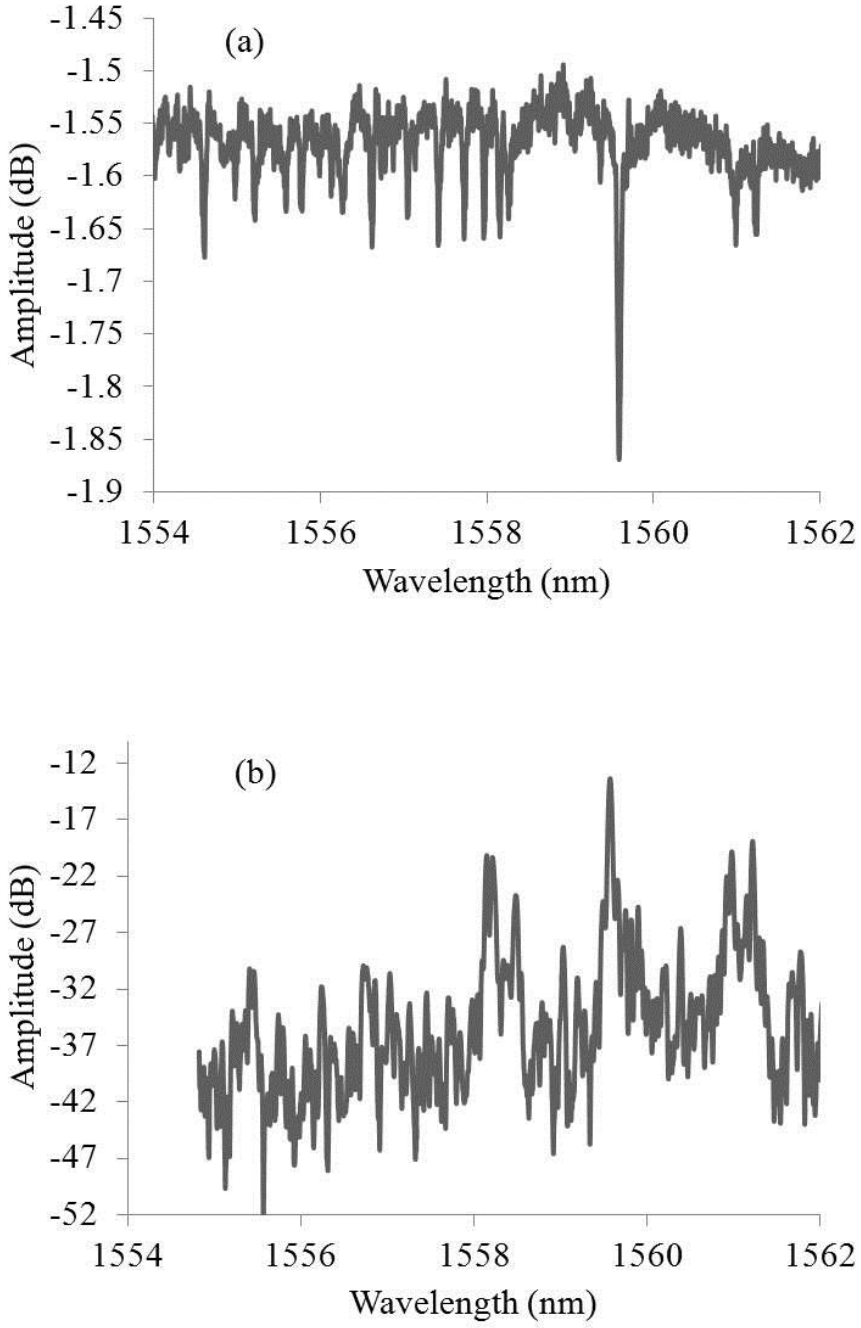

Figure 4-33 showing the hybrid transmission (a) and reflection (b) spectrum for the SFBG response

Figure 4-34 shows the measured polarisation dependent loss of the hybrid grating in a range from 1554nm to 1562nm. The strongest peak located at 1559.56nm had a polarisation dependent loss of approximately 0.25dB, which matches the maximum strength for transmission loss.

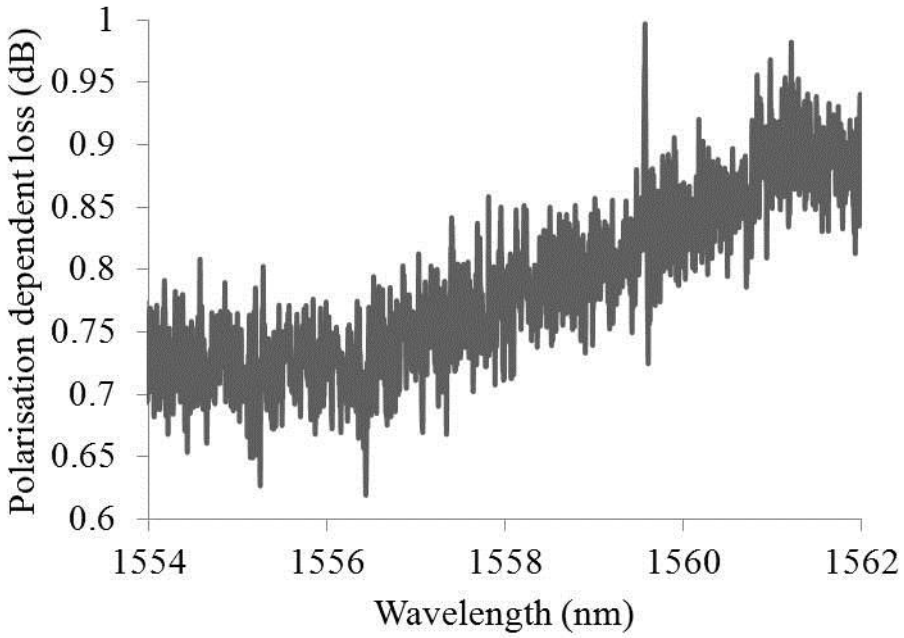

Figure 4-34 showing the polarisation dependent loss of the hybrid device

In all previous devices, the DC polarisation dependent level has remained uniform over this wavelength range. The hybrid device on the other hand, has an increase in polarisation dependent loss with increasing wavelength and this must be due to the LPG inscription.

Looking at a wider wavelength range of 1500nm to 1650nm, the LPG response of the hybrid structure can be seen, as shown in Figure 4-35. Two clear LPG attenuation peaks are produced and are located at wavelength of 1522nm and 1600nm. The 1600nm attenuation peak is located over the wavelength of the strongest reflection peak. Measuring the polarisation dependent loss of the 1600nm attenuation peak by varying the polarisation state of the input light from 0^o to 180^o with 10^o increments, the polarisation response characteristics of the hybrid grating are shown in produces Figure 4-36. Figure 4-36 shows that the maximum change in amplitude for the 1600nm attenuation peak is approximately 3.5dB when changing the polarisation from 0^o to 90^o.

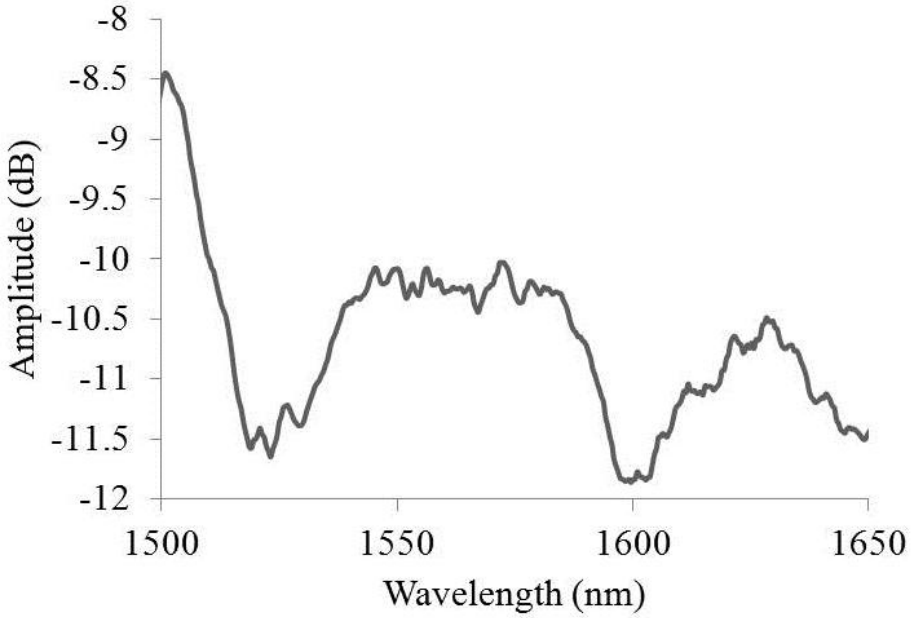

Figure 4-35 showing the LPG induced attenuation peaks in a wider wavelength range for the hybrid structure. Note that due to the low resolution the weak reflection peak, the Bragg reflection cannot be seen in this transmission spectrum

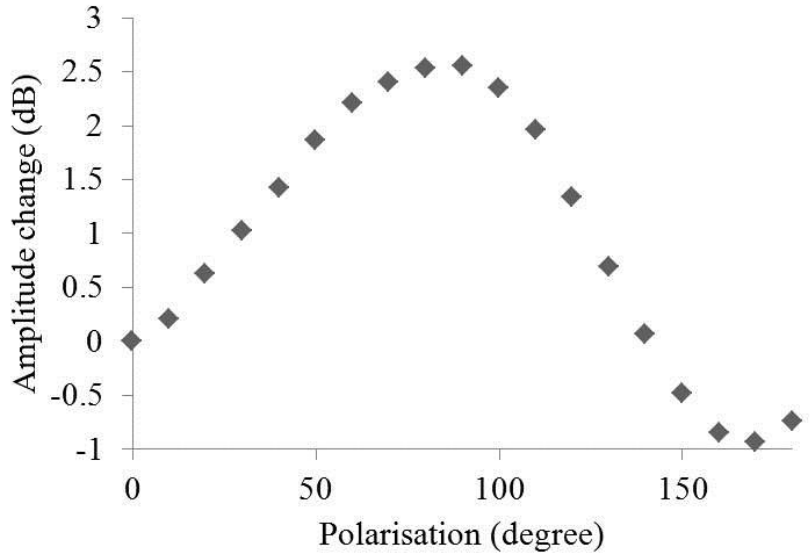

Figure 4-36 Showing the polarisation dependent loss due to variation of the input light polarisation angle for the 1600nm attenuation peak.

The temperature response for the 1559.56 nm reflection peak of the hybrid SFBG/LPG structure was evaluated and the results are shown in Figure 4-37. As with all other SFBGs examined in this work, the relationship between wavelength shift and temperature is linear and produced a sensitivity of 11 pm/^{o}C for the hybrid grating.

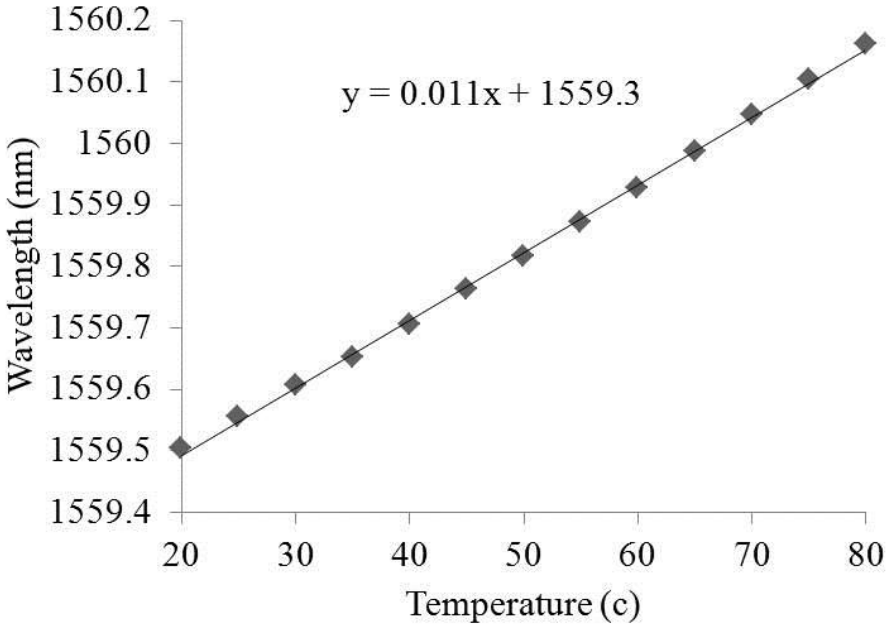

Figure 4-37 showing the calculated temperature response of the three strongest reflection peaks of the SFBG-4 device

The attenuation peak at a wavelength of 1520nm produced then best SRI response and the calculated data are shown in Figure 4-38 along with the SFBG reflection response, which one would expect is unchanging. These two results show the feasibility of the hybrid SFBG/LPG structure do have a dual-function for sensing, as the LPG is sensitive but the SFBG is totally insensitive to SRI, as clearly shown in Figure 4-37 and Figure 4-38. The SRI sensitivity produced is ~5 nm/URI and the temperature sensitivity is 11 pm/^{o}C. The temperature sensitivity is similar to that reported by Xeuwen Shu et al, however in the same publication a sensitivity of ~14 nm/URI to changes in SRI was also reported. The hybrid SFBG temperature response is adequate but the SRI response is three times less than previous work. However, a sensitivity comparable or perhaps better could be achieved using a different period LPG (taking the work carried out in the femtosecond LPG chapters in to consideration) and here the proof of concept has been established.

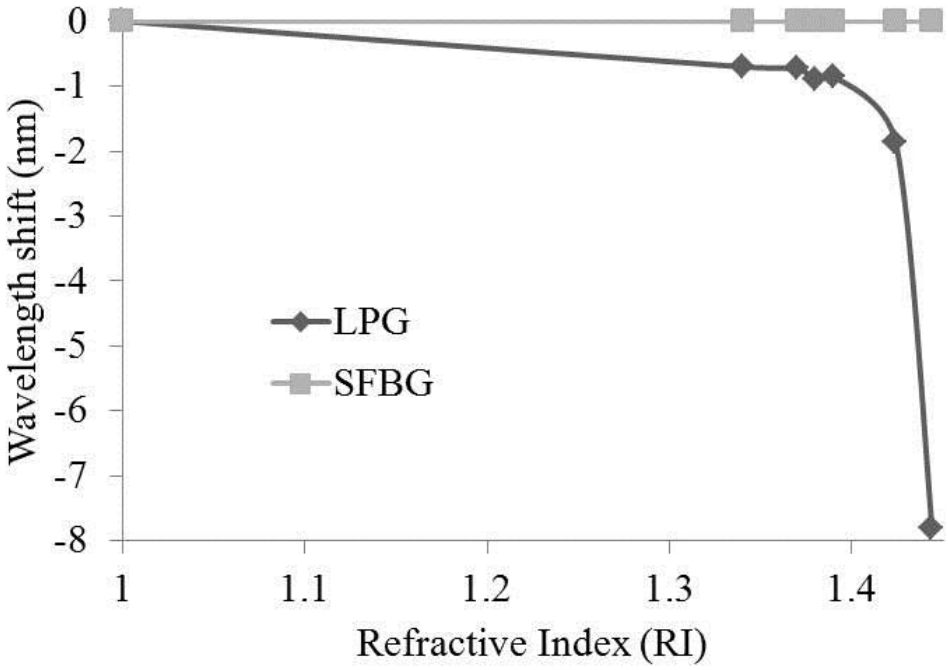

Figure 4-38 showing the hybrid grating response from both the SFBG and the LPG structure.

4.2.4 Summary

Two different SFBGs (SFBG-1 and SFBG-2) have been femtosecond laser inscribed by inducing an index change in the core of an optical fibre that had both one low and one high frequency modulation. For these two devices SFBG-1 and SFBG-2, 3 reflection peaks were produced with the strongest peaks located centrally at the same wavelength since there high frequency modulations were the same and the low frequency modulation index change was akin to a top hat function. Through controlling of the low frequency modulation period, the spacing of the reflection peaks could be increased or decreased and this agreed well with the theoretically predicted values from coupled mode theory. For each SFBG, the polarisation dependent loss was found to be a factor with it being approximately half of the maximum strength of the reflection peaks. Considering previous work of low polarisation dependent FBGS, this could be due to the non-central location of the index perturbation in the core of the optical fibre or an inherent problem with femtosecond SFBGs. The two devices produced linear temperature relationships, with

increasing in temperature the wavelength location of the reflection peak red shifted. The sensitivities produced for SFBG-1 and 2 were calculated to be 11.6 pm/^{o}C and 11.5 pm/^{o}C respectively which were found to be comparable to UV FBG sensors.

The third device was a hybrid structure and was femtosecond inscribed an SFBG in parallel with an LPG in the fibre core and the period of the LPG was chosen the same as the low frequency modulation of the SFBG. The alignment of the SFBG and LPG was slightly out and as such they overlapped and created an increase in the background level of noise. This resulted in only a single reflection peak at a wavelength of 1559.56 nm and had a large DC polarisation dependent loss, which may be contributed to from the LPG element of the device. The LPG element also produced 2 attenuation peaks that were capable of detecting SRI changes (5 nm/URI) and this coupled with the linear temperature sensitivity (11.2 pm/^{o}C) of the SFBG reflection peak produced a dual parameter sensing device. Though the device was not as sensitive as previously reported ones there is scope for increased sensitivity using different periods of LPG inscriptions.

5 Surface Plasmon Resonance RI sensitive Fibre devices

5.1 Introduction

Surface plasmon resonance (SPR) has long been established as a way of detecting small refractive index changes, especially in the biological regime, and optical systems based on SPR have already been developed into commercial bio-sensing systems, such as Biacore who have become leaders in the field. There is also a growing demand for fibre optic sensors since they are cheap, robust and easy to use. To date, the majority of fibre optic sensors have relied on fibre gratings of long period, Bragg and tilted structures. These fibre grating sensors rely on the evanescent field of the cladding modes interaction and as such have a peak sensitivity nearing that of the refractive index of the cladding[137, 138]. This means that they are ideal for sensing relatively high refractive index substance, such as hydrocarbons[55], but less for biological solutions in the aqueous regime. The combination of both surface plasmons and optical fibre seems a natural resolution to overcome both these downsides. Various techniques have been implemented optical fibre surface plasmon sensors using tapered fibre[139], cladding off[140, 141] and D-shaped fibre[116, 142]. The advantage of both the cladding off and tapered fibre method is that you get direct interaction of the surface plasmon with the core mode/modes of the optical fibre. These methods do have some limitations: either you are limited to a single mode where you can only couple to a single surface plasmon and hence limiting the chance of success; or in multimode fibre the various modes can form various surface plasmons but with very little control over and no way to maximise the response, since the energy is spread fairly evenly between the modes. D shape fibre offers a balance as when the fibre is

polished down some of the cladding layer is left. This results in a few moded optical fibre because the remaining cladding is able to support a few cladding modes in the polished region[143]. The 'few modes' means there are multiple chances of coupling to a surface plasmon resonance while still having relatively large amounts of energy in each one, thus maintaining a large dynamic range. Also the induced non-uniformity of the fibre combined with the polarisation response of a surface plasmon means that through varying the polarisation of the input light a certain degree of control can be achieved for the coupling strength. The sensing interaction takes place between the cladding mode and the surface plasmon modes provided by the metal coating. For a thinner cladding layer this occurs naturally due to the core modes' evanescent field leaking into the cladding, however it can be further enhanced, and thus give a larger dynamic range. It has been reported that using tilted Bragg grating coupling and germanium coated optical fibres that have been post UV exposed produces the enhancement in coupling efficiency[144]. These methods and the resultant sensitivity will be discussed in sections 5.2, 5.2.1 and 5.3.1.

5.2 Single metal layer coating on polished D-shaped fibre with a tilted fibre Bragg grating structure in the core

5.2.1 Fabrication and experimental procedure

The SPR fibre sensor was produced using three fabrication steps. Firstly, a 7^{o} internal tilt Bragg grating structure was inscribed into the hydrogenated SMF-28 fibre core using a uniform phase mask with a period of 1.0157μm and a 244nm UV beam from a frequency doubled Argon ion laser using a power density, at the fibre surface, of 2.2 kWm^{-2}. This angle was chosen because in previous work, carried out by Dr T. Allsop, a 7^{o} tilt was found to give the largest coupling strength and dynamic range[116]. The tilt was achieved by mounting the mask on a goniometer and titled to the required angle. When this was done

the optical fibre was labelled so the orientation of the grating could be established for the next step. Secondly, the fibre was polished in the region of the grating to 10µm from the core/cladding interface, with an estimated error of ±1µm, by Fiberlogix Limited. An image of this is shown in Figure 5-1

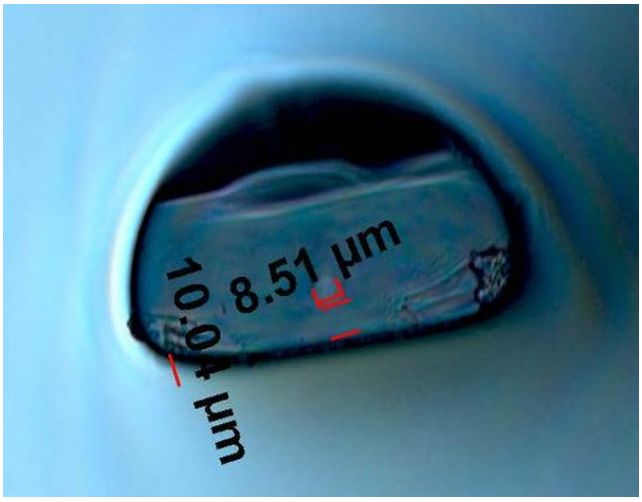

Figure 5-1 showing the lapped D-shape fibre and the ~10µm location of the flat surface from the core

Using the labels from the first step, the fibre was orientated so that when it was polished the fibre axis, gratings vector and the polishing region all lay in the same plane. Thirdly, the flat polished region was then coated with a 35nm layer of gold using a sputter machine. This work was carried out by Dr Ron Neal at the University of Plymouth. The schematic diagram of the tilted fibre Bragg grating (TFBG) based SPR sensor structure is shown in Figure 5-2. It has been reported in previous work that a silver coating of 35nm on a TFBG sensor in D shaped fibre produced SPR coupling and a high SRI sensitivity[143], with this in mind a similar gold coating thickness was chosen. Gold was investigated since it is a standard metal used in many SPR interrogation systems and it was hoped that the dispersion properties would give an enhanced sensitivity, compared to that of the reported silver device[116].

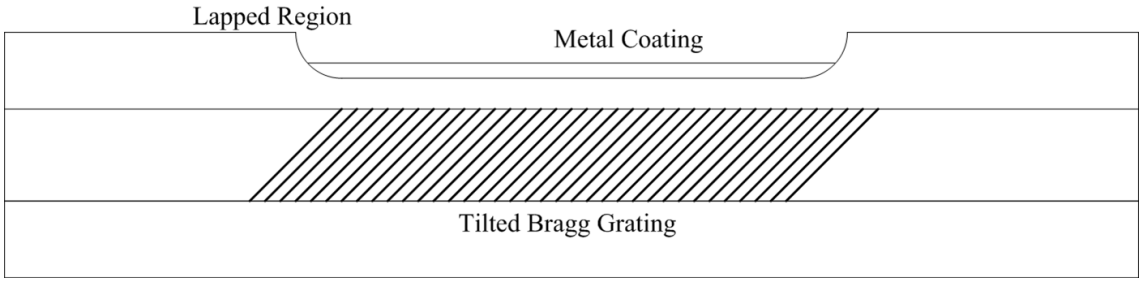

Figure 5-2 showing the schematic of the TFBG based SPR device with single metal coating layer

After the sensor had been fabricated, its polarisation and response to changing SRI was investigated using the setup shown in Figure 5-3. During the characterisation, certain provisions had to take place. The patch cords were all fixed and secured to minimise polarisation drift due to any movement of the optical fibre. To further stabilise experiment, the sensor was placed in a 'v' groove on an aluminium plate, which kept the sensor in position while the aluminium acted as a heat sink, helping to keep temperature variation to a minimum. It is important to note that the polarisation experiments were merely carried out to find out how the sensor operated under changing input light polarisation. The exact polarisation of the light at the sensor could not be deduced from the equipment and as such is not reported here. What is trying to be established is how much effect polarisation plays when concerned with measuring changing SRI.

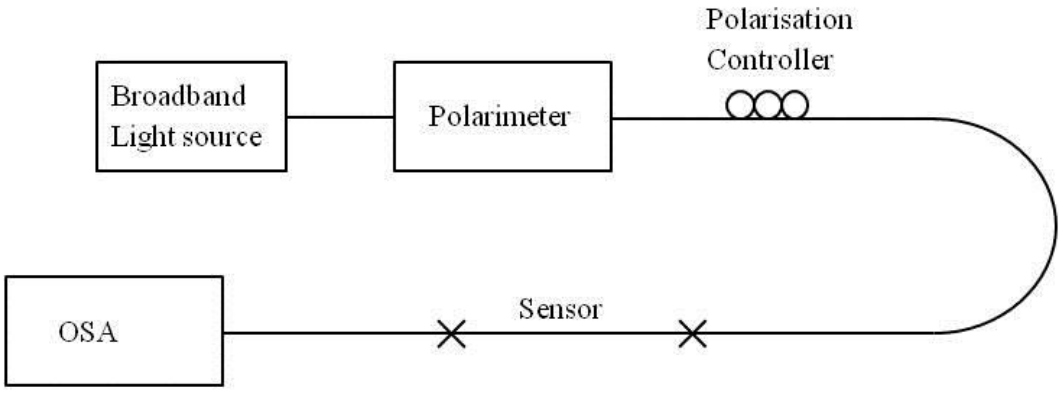

Figure 5-3 showing the experimental setup for the characterisation of the sensor

To establish the RI response of the sensor Cargille Refractive Index liquids were used with an accuracy of ±0.0002URI. The RI response transmission spectrum of the sensor was

normalised and then through control of the polarisation of light, various SPR resonances for the sensor could be established. After selecting a single SPR resonance, its transmission spectrum evolution was recorded for each RI liquid. Without changing the polarisation and touching the sensor fibre, the RI liquid was washed off for each measurement using pure ethanol, as this was found to give the best cleaning results while not damaging the coating surface on the fibre. The sensor was then again covered in another RI liquid and the transmission spectrum recorded and this process was repeated for various RI values ranging from 1, 1.30 to 1.39, as this RI range lies in the biological aqueous regime.

To evaluate the polarisation response of the SPR, the sensor was covered with a refractive index liquid of value 1.36 and its maximum was found. The light was scanned from 0 (being the polarisation of the light at a resonance maximum) to 180^{o} (at which point the resonance should be at maximum again) using the polarisation controller. In the evaluation, the polarisation of light was able to be controlled to 1^{o}.

Since the SPR resonances produced were relatively broad, both the wavelength shift and amplitude change of the resonances were calculated using the centroid method. All the errors were calculated statistically by taking multiple measurements.

5.2.2 Characterisation of refractive index and polarisation response

When immersed in a liquid with a RI of 1.36, the TFBG based SPR sensor was found to exhibit 4 broad resonances within the wavelength range of 1250nm to 1650nm, as shown in Figure 5-4. The polarisation was changed to produce each peak, with each resonance maximum being at a different polarisation angle. The Bragg reflection is not evident in the figure because high loss resonance features override the reflection and also the resolution is not sufficient enough to see it on the wavelength scale used. The four resonances produced are attributed to the coupling of light to the surface plasmon via different

cladding modes. The strongest SPR resonance was located at approximately 1550nm. Despite being able to produce multiple resonances when submerged in a liquid of RI 1.36, there were not any resonances exhibited when the sensor was in air.

Taking the resonance located at approximately 1475nm, the development of the transmission spectrum with increasing surrounding RI is shown in Figure 5-5. The figure shows that with increasing RI, the strength of the SPR resonance decreases and it shifts to the shorter wavelength side. Taking a surrounding liquid with RI 1.3 as the starting point, the calculated numerical shifts and changes for wavelength and amplitude for the resonance at 1475nm are shown in Figure 5-6.

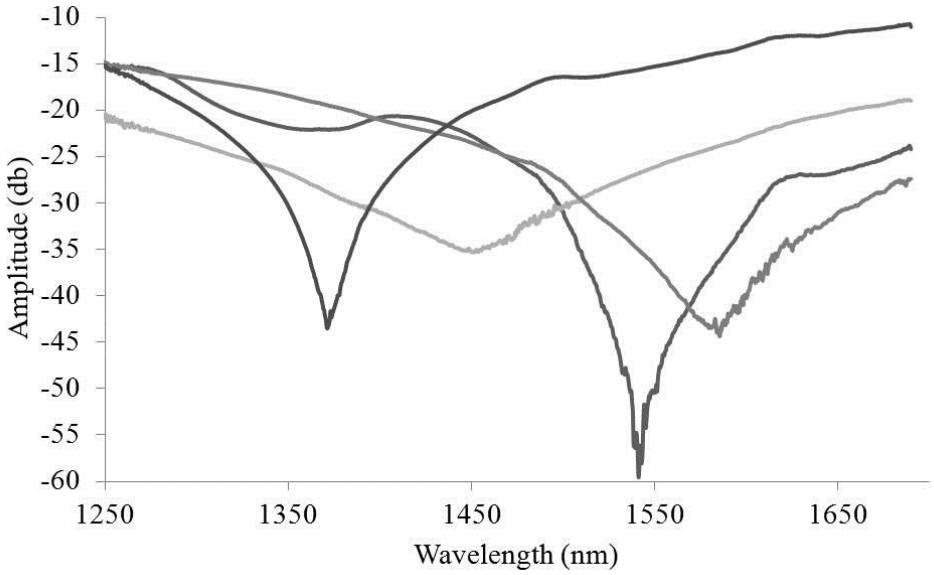

Figure 5-4 showing four SPR resonances produced by the single layer gold coated TFBG based sensor in the D-shaped fibre when submerged in a liquid of RI 1.36

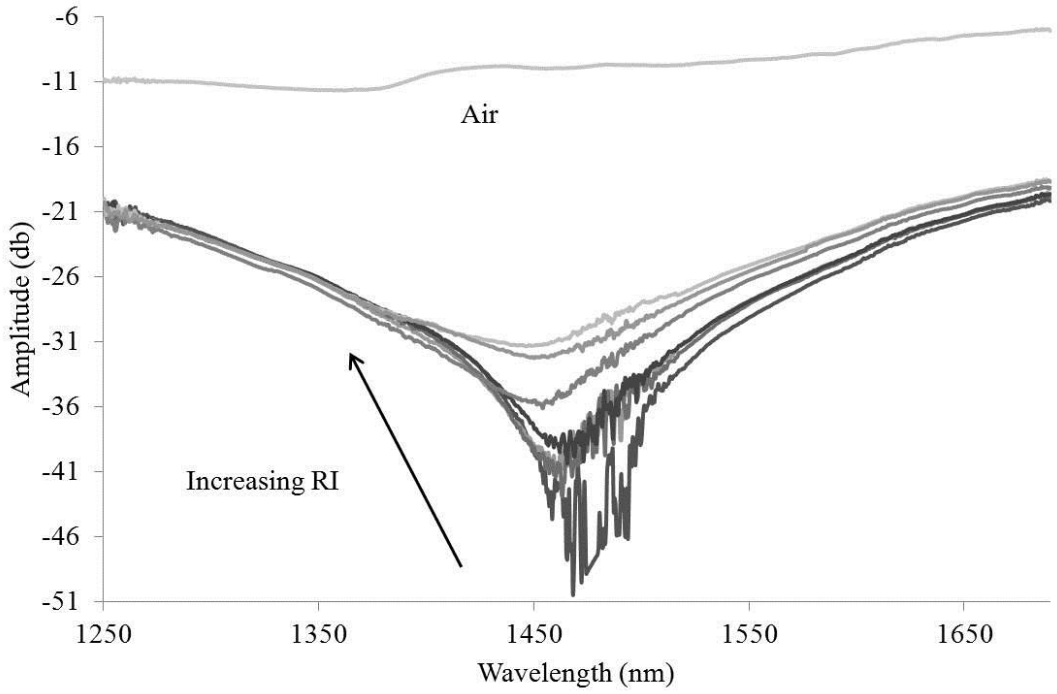

Figure 5-5 showing how the resonance at 1475nm changes with increasing surrounding RI values, and the transmission spectrum in air

Despite this decrease in strength the general trend can still be seen, producing a 2nd order polynomial trend line, with the greater sensitivity being seen in the higher RI region. This is mirrored by the amplitude response, again showing a 2nd order polynomial relationship with better fitting and less error. Note the decrease in error since the centroid method will have averaged out any large effects despite the light source or polarisation variation.

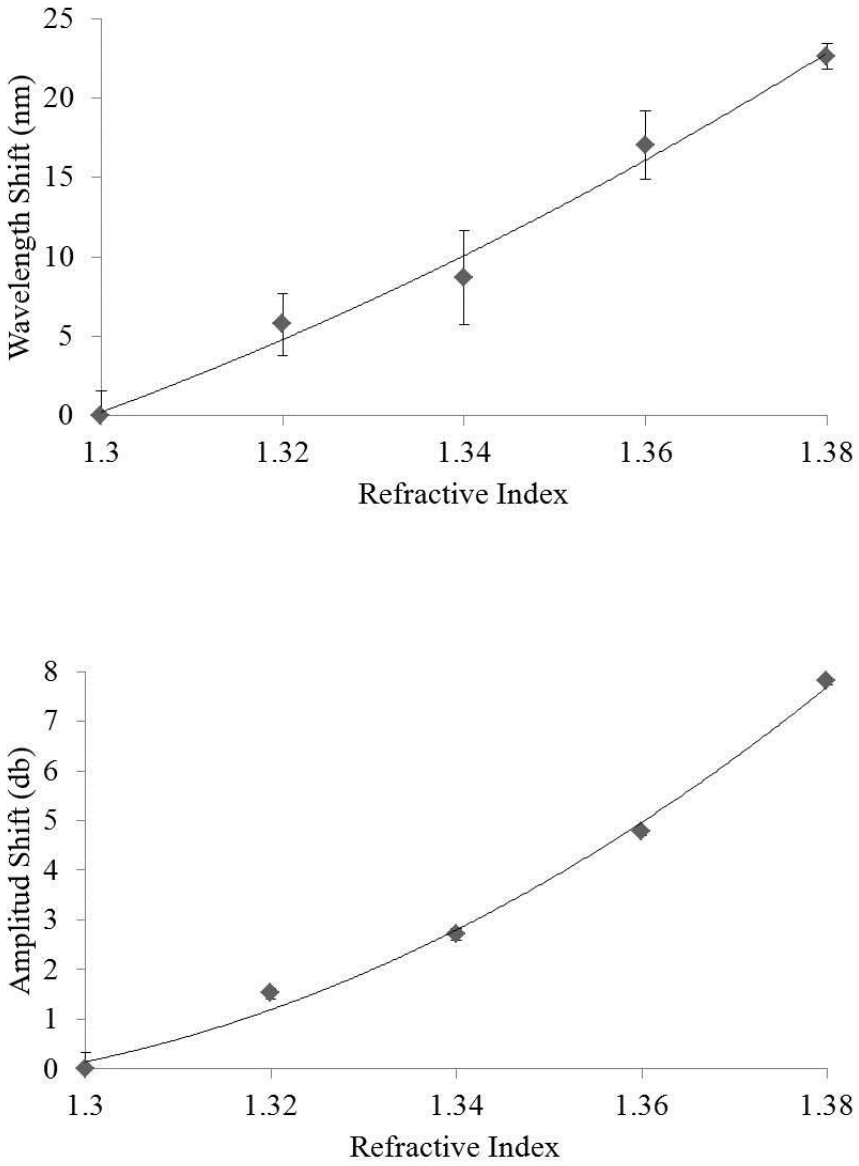

Figure 5-6 showing the RI response for the resonance located at approximately 1475nm for wavelength (top) and amplitude (bottom), using surrounding RI 1.3 as the starting point

Again the amplitude change shows the increasing sensitivity with increasing surrounding RI values and this characteristic is similar to that seen with LPG based RI sensors. Since any cladding mode coupling to the surface plasmon would also be affected by a change in SRI, the cladding mode response would come more into effect, similar to what is shown here. From the figure we may estimate the sensitivities over the range 1.3 to 1.38 to be 262.5nm/URI and 91.5dB/URI for the wavelength shift and amplitude change respectively. Considering the range under examination the results compare better with other typical sensors, such as LPGs.

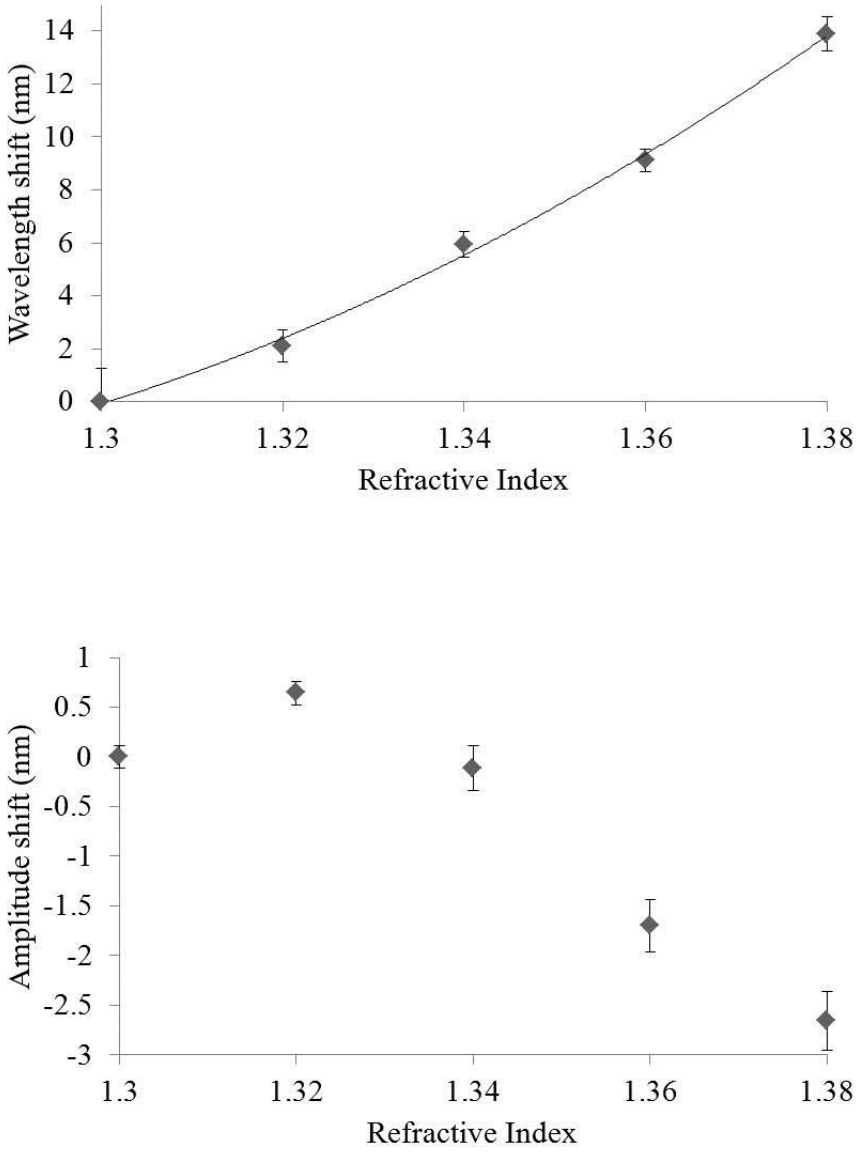

Figure 5-7 showing the RI response for the resonance located at approximately 1550nm for both wavelength (top) and amplitude (bottom), using surrounding RI 1.3 as the zero

Taking the 1550nm resonance, how it changes with input light polarisation was investigated and the results are shown in Figure 5-9. SPRs are only coupled to a single polarisation of light and by altering the polarisation of the input light away from this the intensity of the peak decreases, since there is less available light to couple to the SPR, and this is the dominating factor for the intensity change. The wavelength evolution is due to the coupling of light to other cladding modes which results in a wavelength shift. All this is shown in a typical response taken from the 1350nm resonance in Figure 5-8.

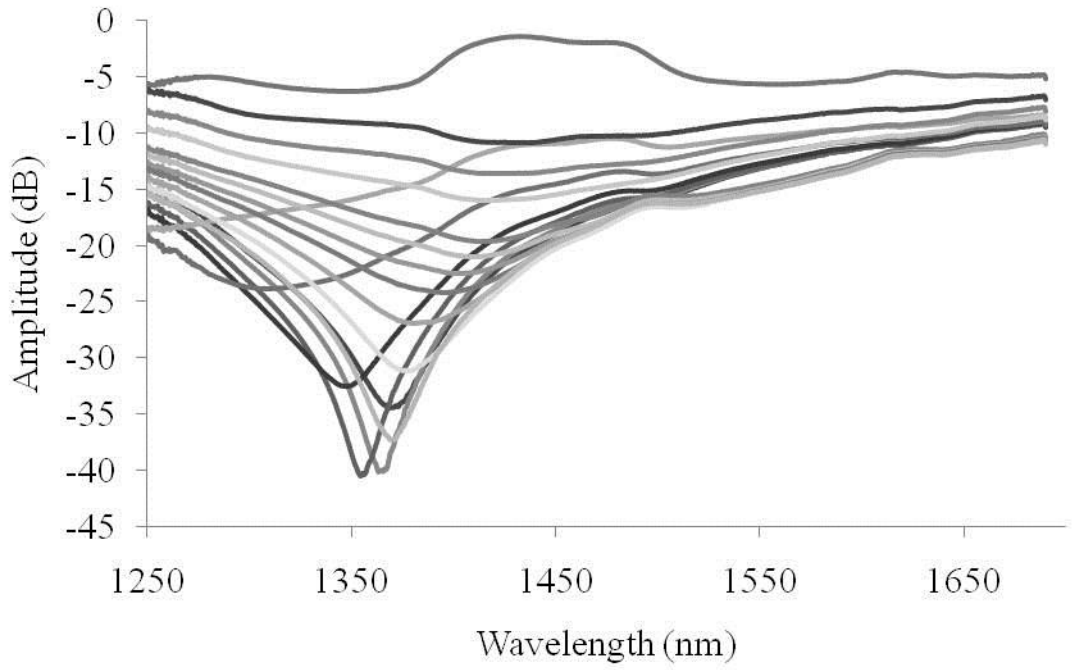

Figure 5-8 Showing the evolution of the 1350nm resonance due to changing polarisation

The change in input light polarisation was carried out using a computer controlled polarimeter which allowed the desired change to be inputted. The change of input light polarisation gives a total of approximately 140nm wavelength shift and 16dB amplitude change.

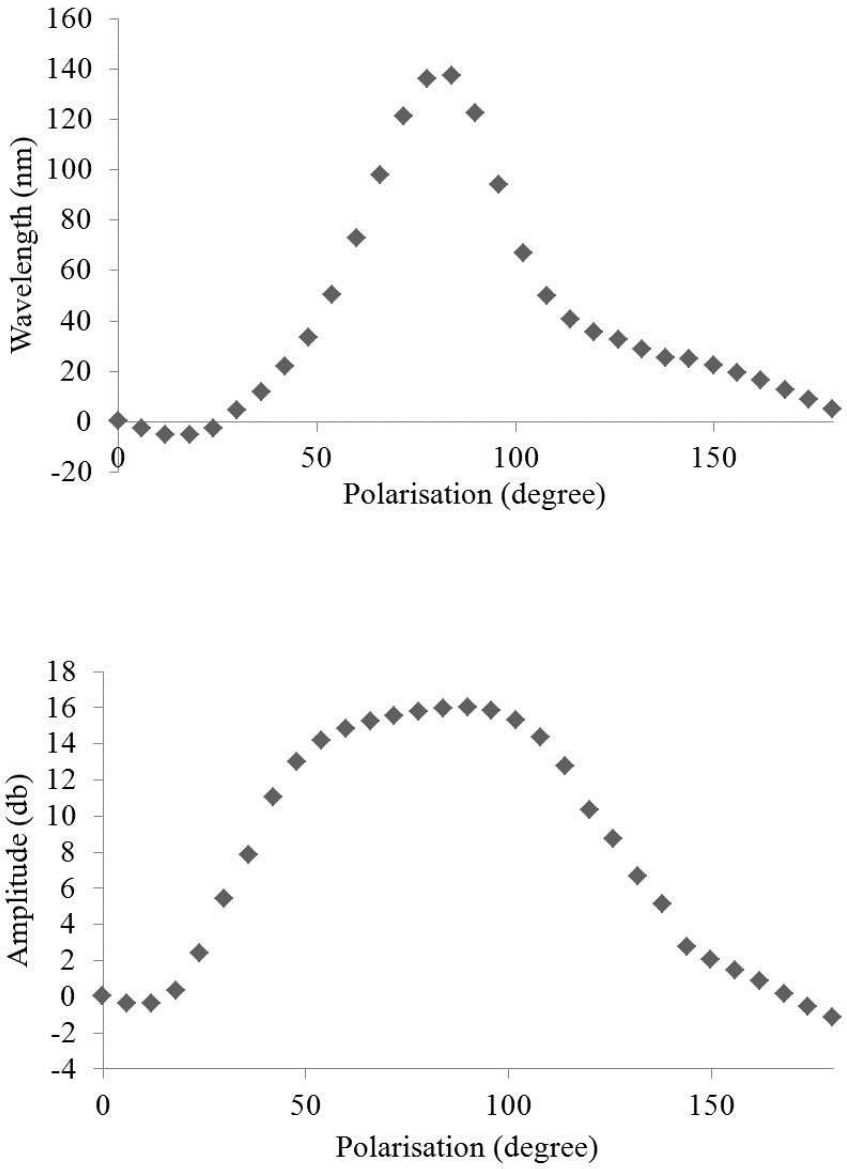

Figure 5-9 showing the polarisation response of the 1550nm resonance for the wavelength and amplitude when changing the polarisation from 0^{o} to 180^{o}

5.2.3 Theory and Discussion

The TFBG has proven itself to be an effective SRI sensor, however, several points need to be discussed to understand what is occurring. These points include how the light of the core is coupling to the SPR, the large dynamic range for SRI sensing range and the broadness of the peaks. Taking each of these points in turn, from the sensor there can be three main ways that light can be coupling from the core to the SPR these are broadband

loss due to a scattering mechanism, coupling from the core mode to SPR directly and finally coupling of from core to cladding to the SPR.

Firstly, the polishing technique was in close proximity to the fibre core and as a result was shown to produce a broadband loss, over the wavelength range 1250 to 1700nm, of around 3dB[143]. However, since several strong discrete SPR resonance were coupled to this is unlikely to be the case since with no TFBG present only weak coupling was observed and low SRI sensitivity for the previous devices investigated by Dr. T. Allsop et al[143]. Secondly, it is possible, for small sufficiently small cladding radius, for Bragg gratings to couple the core mode directly to the SPR mode [118, 119]. G. Nemova et al showed that the phase matching condition governing the SPR wavelength location is[118]:

$$\beta_{co} + \beta_{sp} - \left(\frac{2\pi}{\Lambda}\right) + \kappa_{co-co} = 0$$

Equation 5-1

Examining this phase matching condition, since the fibre used is SMF there is only one core mode and, due to the phase matching condition for SPRs, there is a single SPR mode. As a result there can only be one resonance produced that satisfies this phase matching condition. Since the TFBG SPR device produced multiple resonances the coupling of light from the core mode directly to the SPR cannot be the only mechanism for SPR coupling. Finally, it has been shown that the coupling of light from the core mode the SPR via the cladding modes is possible for the TFBG [145-147]. This allows for coupling of the core mode to multiple sets of cladding modes which increases the possibility of phase matching to the surface plasmon mode[148]. Through a process of elimination, the coupling of light to the SPR via the cladding modes is evident in the TFBG SPR device. Further support to this argument is given by the paper by Dr. T. Allsop et al who calculated the cladding

modes and modelled the theory and produced similar behaviour to that of a TFBG SPR [116].

Secondly, it has been established that the device is coupling to multiple cladding modes and this explains the multiple resonances observed, it can also explain why the TFBG SPR sensor has such a large SRI sensing range. For simplicity, the optical fibre geometry can be considered akin to the Kretschmann configuration for exciting SPRs, which has been found to be adequate for describing TFBG SPR sensors properties[145]. Each cladding mode coupled to can be considered to having a different incident angle to the metal surface. This angle can be calculated using the scattering angle from the effective index of the mode [116, 145].

$$\cos\theta = \frac{n_{cl}^{eff}}{n_{cl}}$$

Equation 5-2

Where the scattering angle, θ, is related to the incident by angle, ϕ, vai $\phi = \theta - 90$. Applying this to the phase matching condition you get the following equation:

$$k_0 \sqrt{\frac{\varepsilon_1 . \varepsilon_2}{\varepsilon_1 + \varepsilon_2}} = k_0 n_{cl} \sin\phi$$

Equation 5-3

Each cladding angle will satisfy the phase matching condition at a different wavelength. Since the difference in effective index between the cladding modes is typically small, which can be seen from the dispersion relationships calculated for an LPG[24], the difference in angle between each cladding mode will also be small. As a result each resonance produced in the transmission spectrum is made up of several cladding mode resonance, which is supported by the wavelength shift of the resonance due to input light polarisation change. Since each resonance is made up of multiple cladding modes, and

hence incident angles, the sensor is able to operate over a wide range of SRIs. At a single certain SRI a single/group of cladding modes will satisfy the phase matching condition. Increasing the SRI by a certain amount means the previous single/group of cladding modes no longer satisfy the phase matching condition, however, since there are multiple interrogation angles another single/group of cladding modes will satisfy the phase matching condition. This also somewhat explains the broad nature of the resonances observed in the transmission spectrum. Further to this, when dealing with such a small coating thickness, the surface roughness will always play a part in both the phase matching condition and the sensitivity of SPR. As such, its effects have been investigated by Maradudin et al found a relationship between surface roughness and the dispersion relationship of SPR modes[149, 150]. They showed that, the roughness of the metal coating leads to the splitting of the SPR dispersion curve. The coating technique was analysed using an atomic force microscope (ATM) and found to have a large variation in surface roughness, with an average variation of 6nm and a maximum height of 58nm. The splitting of the dispersion curve allows for modes to couple to two surface plasmon modes. This, coupled with the previous argument, further explains the broad nature of the resonances observed.

5.3 Multi metal layer coating on tapered D-shape fibre with tilted fibre Bragg grating structure in the core

5.3.1 Fabrication and experimental procedure

The fabrication and analysis process of the multi-layer coated TFBG based SPR sensors were the same as for the single layer coated devices described in section 5.2.1, except this time instead of one layer being coated onto the lapped fibre region there were three layers with an order germanium (48nm), silicon dioxide (48nm) and gold (32nm). The three

layer structure was used as a control to give a direct comparison to the post UV fibre sensor characterised in section 5.4.3. The germanium and silicon dioxide layers had depths on the same order as the metal coating so as not to hinder the out coupling of light. Also with the introduction of the new layers the dispersion relationship of the device is being changed and so will the sensitivity

5.3.2 Characterisation of refractive index and polarisation response

Similar to the single layer coated TFBG based SPR sensors, the multi-layer coated sensor did not produce any resonances when exposed to air, however multiple resonances were produced when the device was submerged in a liquid with a SRI 1.36, as shown in Figure 5-10. All the resonances produced where strong and broad in nature, which are very similar to the gold coated single layer device.

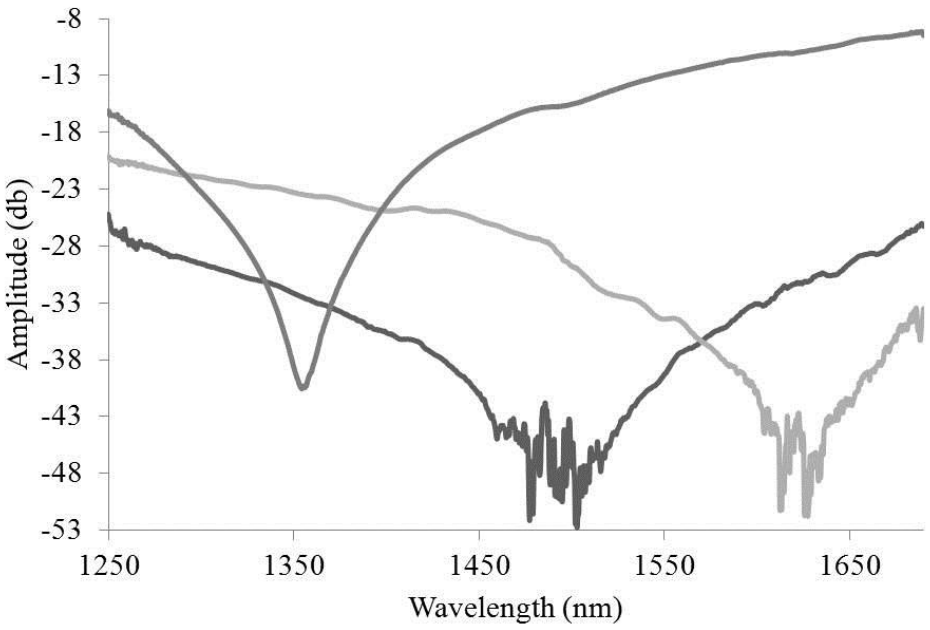

Figure 5-10 showing 3 SPR resonances for the multilayer coated TFBG based SPR sensor submerged with a liquid of RI 1.36

The SRI response of each resonance was similar in nature and as such only the most sensitive one is reported here as a characteristic example. The SRI response for the resonance close to 1450nm is shown in Figure 5-11 and clearly showing no resonance being produced in air. With increasing SRI, the resonance exhibited a red wavelength shift and a decrease in amplitude. The amplitude change is like that seen in section 5.2.2 for the single layer device, which is expected since the resonance was maximised for the starting SRI value. However, the single layer device produced a blue wavelength shift which is opposite to the shift found here. This shows the multi-layer coating is affecting the cladding modes and hence the phase matching condition.

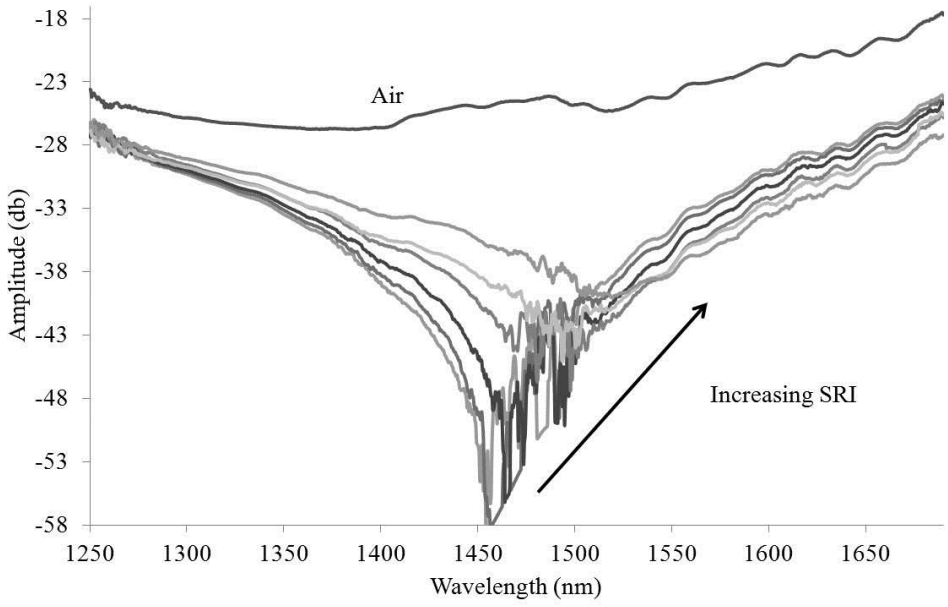

Figure 5-11 showing the spectral evolution of the 1450nm resonance with increasing SRI and there is no resonance when the device is in air. However there is a strong resonance produced with a SRI 1.3

Applying the centroid fitting method, the calculated wavelength shifts and amplitude changes for each SRI for the 1450nm resonance and the results are plotted in Figure 5-12. Both the wavelength and amplitude produced a quadratic relationship. However, the wavelength response increased sensitivity while the amplitude experienced a decrease in sensitivity with increasing SRI. This is due to the two sensitivities being governed by different mechanisms. The wavelength shift is defined by the phase matching condition

between the cladding and the SPR modes. The amplitude (actually the loss) is governed by two factors: the coupling strength between the cladding and SPR modes and the reflections from the multilayer surfaces. Taking the SRI range from 1.3 to 1.38, the average sensitivities for the multilayer coated sensor was calculated to be 426.3nm/URI and 340dB/URI for wavelength and amplitude, respectively, which are much higher than that of 262.5nm/URI and 91.5dB/URI for the single layer device discussed in section 5.2.2. For quantitative comparison, the multi-layer sensor produced approximately a 2 fold increase in wavelength sensitivity and a 3 fold one for amplitude.

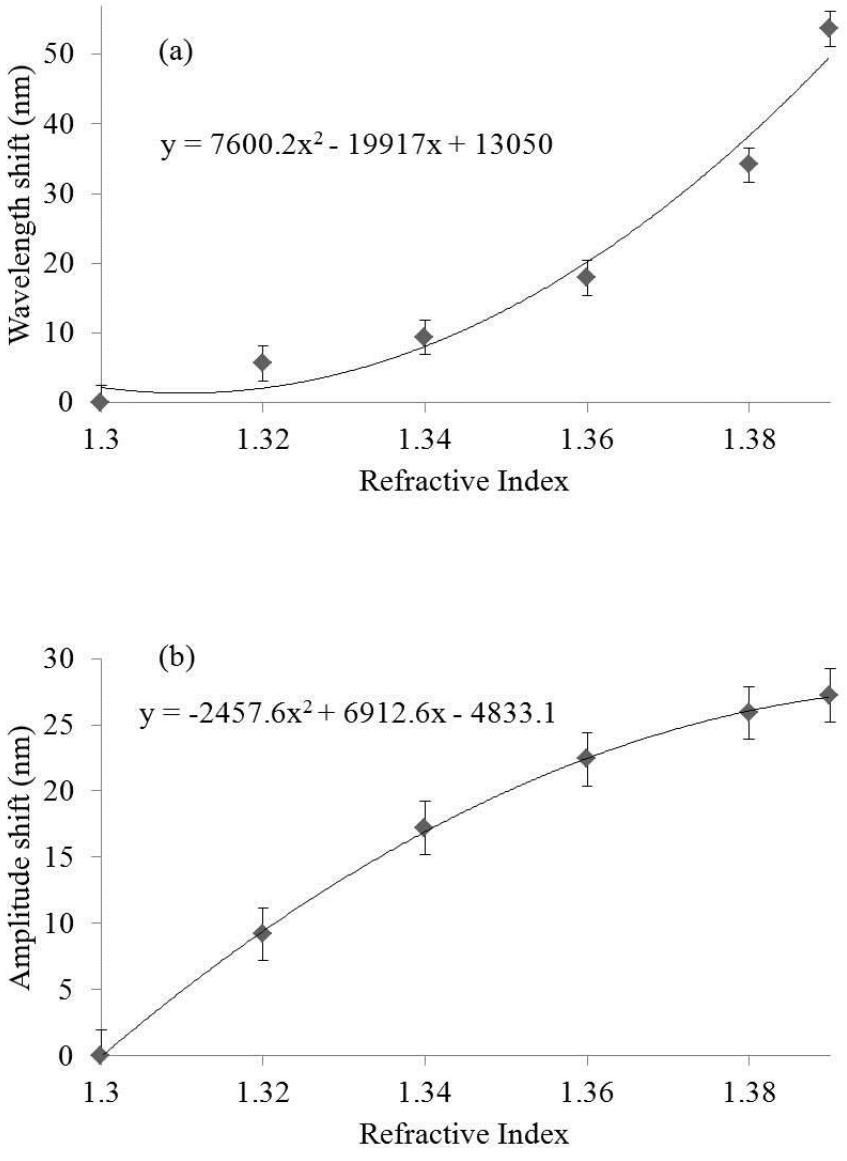

Figure 5-12 showing the RI response for the multilayer coated device's resonance at 1450nm for wavelength (a) and amplitude (b).

The variations of the wavelength and amplitude of the 1450nm resonance due to changing of the input light polarisation are shown in Figure 5-13. Approximately, the maximum wavelength shift is 16.4nm and amplitude change is 20.8dB for polarisation state changing from 0^o to 180^o. These are a lot smaller compared to the single layer device and seems to suggest that, the multiple coating layers are helping to shield against polarisation effect. This could be due to different cladding modes coupling to the surface plasmon resonance or the increased coating thickness could be decreasing the coupling efficiency which would result in a smaller change in polarisation. The smaller polarisation dependence coupled with the increase in sensitivity means the multi-layer coated configuration is a more suitable sensor than the single-layer type with increased sensitivity and decreased polarisation response. The downside to this is the removal of polarisation change as a possible sensing measurand.

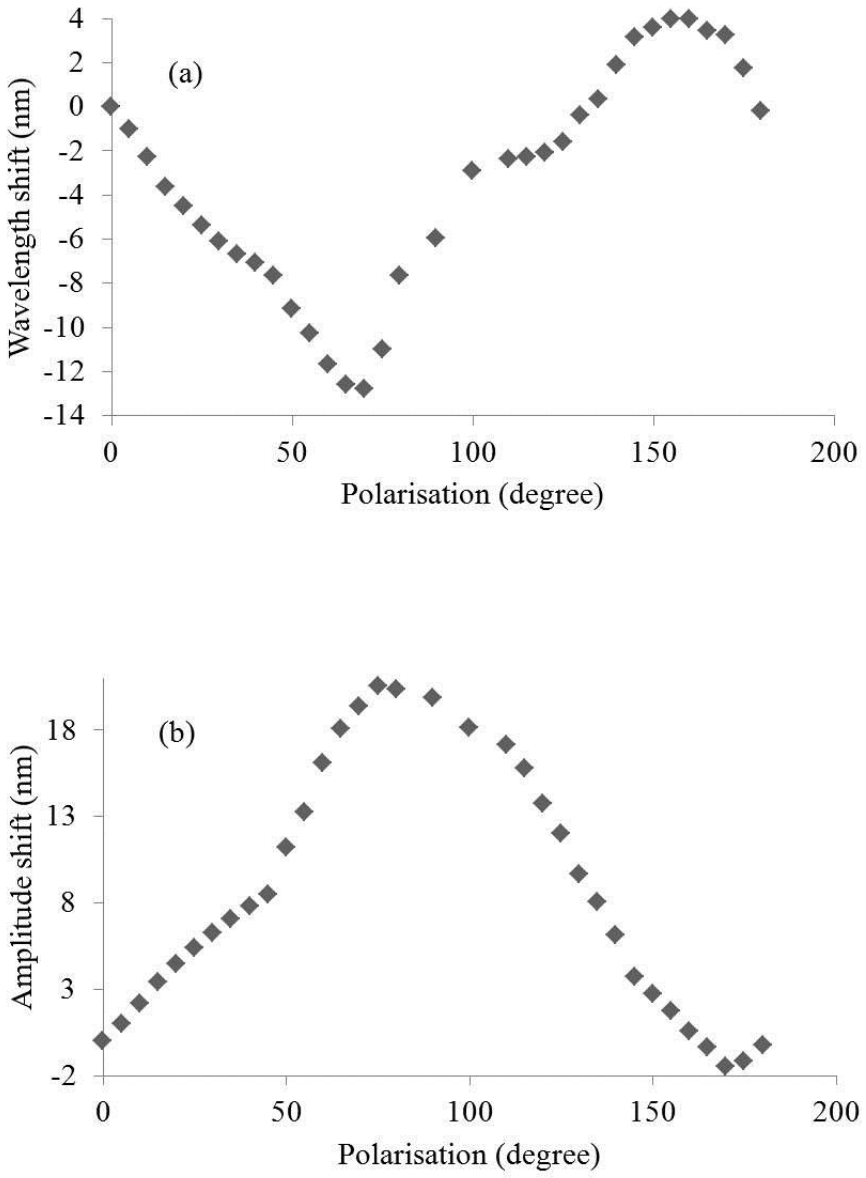

Figure 5-13 showing the Polarisation response of the 1450nm resonance of the multi-layer coated device for wavelength (a) and amplitude (b)

5.3.3 Mechanism and discussion

The sensor was inscribed with a TFBG before the multi-layer coatings were sputtered. With this in mind, the device will have the same coupling mechanism as described in the previous discussion for the single layer device. However, there is a need to establish the difference in sensitivities between the single layer and the multilayer device. The first possibility is that the coating itself inherently increases SPR sensitivities. However, a study

by M. Yao et al[151] investigated the effect of an intermediate dielectric on a multilayer SPR (akin to the sensor here). Their investigation showed that the layer itself had little or no effect on the sensitivity to SRI. This means that the layer itself cannot be enhancing the multilayer devices sensitivity. A reason for the increase in sensitivity could be that the thin but high RI germanium coating is effecting the coupled cladding modes, in a similar way to coated LPGs (refer to the literature review). Equation 5-1 shows the coupling phase matching condition of the core mode to the cladding mode. The phase matching condition is satisfied when the coupled cladding mode is equal to the SPR mode. This means that the sensitivity of the multilayer device is a function of both the SPR propagation constant and the cladding mode effective index. This has been shown to be the case for standard optical fibre[118], side polished optical fibre[152] and further supported by the fact the SPR is dependent upon the dopant levels[153] (relating to the effective index) . It has already been established that the coating of an LPG with high RI coating causes a shifting of the cladding mode which causes the LPG becomes more sensitive to changing SRI[75, 77]. Since the multilayer device is dependent upon cladding mode coupling it is evident that the devices sensitivity would be affected by dielectric coating and thus can explain why the multilayer device has a different sensitivity to that of the single layer. Finally, it could also be a simple case of the multilayer device coupling satisfying the phase matching condition with different, more sensitive cladding modes, than those of the single layer device. Since, it has been shown that different cladding modes coupling to SPRs have different sensitivities[154]. The weighting of each effect requires further investigation

5.4 Optical fibre localised surface plasmon sensor based on surface relief grating structure with multilayer coatings

The third and final structure investigated was a multilayer coated device which was post UV exposed to give a surface relief structure on the metal surface. Through using a

grating structure on the metal surface the sensing mechanism changes to that of a localised surface plasmon resonance (LSPR). This has been shown to be the case by several authors using either grating [155-157] or nano-wires [158-160] and all of which are akin to the structure of the device. The LSPR is investigated since it is known that it is inherently more sensitive than its SPR counterpart [161-163]. This is supported by the work here since the LSPR devices produced the highest RI sensitivity in characterisation but also in application for gas sand biological sensing, which is shown in Section 6.2 and 6.3 respectively

5.4.1 Fabrication and Experimental Procedure

The fabrication process for the third optical fibre SPR sensor structure is similar to the multi-layer TFBG based sensors and the host fibres were also polished to become D-shape. There is no tilted Bragg gratings inscribed into the fibre core before coating takes place. The devices were fabricated to have 3 thin coated layers, including a layer of germanium, silica dioxide and then a metal, a diagram of which can be seen in Figure 5-14. Also, Table 5-1 summarises the coating parameters for the third investigated SPR sensors configuration.

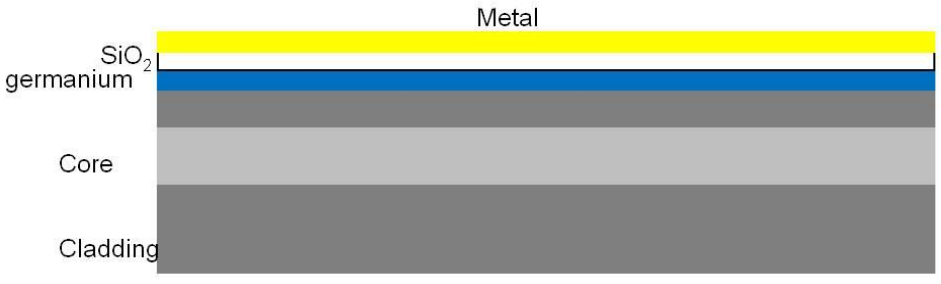

Figure 5-14 showing a schematic of the multilayer structure of the LSPR device

	1st Layer Germanium (nm)	2nd Layer Silica dioxide (nm)	3rd Layer Metal (nm)
Silver	48	48	32
Gold	48	48	32
Platinum	48	48	32

Table 5-1 showing the structure of the multilayer devices and the coating depths

Once the fibre had been coated with the three layers, the flat surface of the fibre was post UV exposed. This was done using a frequency doubled argon ion laser of wavelength 244nm and a phase mask of period 1.018μm. The reasoning behind this procedure and the use of three layer structure are as follows. Firstly from fibre photosensitivity theory, germanium is known to react and change shape under UV exposure, so by exposing the germanium on the fibre surface to a periodic source of UV radiation a surface relief structure is imprinted on the fibre surface[164, 165]. The presence of this structure was confirmed using AFM on the silver coated device and is shown in Figure 5-16. The work carried out by Junji Nishii has also shown this to be the case[166] producing similar images to those seen here. Secondly, Junji Nishii also investigated the reaction of UV exposed thin layers of germanium and silicon dioxide using the sputtering technique and showed a large volume change. Through the coating of the fibre with both germanium and silicon dioxide the post UV processing procedure was enhanced and produced an improved surface relief effect. The reaction of the germanium and silicon dioxide was investigated using X-ray electron spectroscopy (XPS). Through determining the binding energies of the electrons on the surface the composition of the coated fibre surface could be surmised. This was carried out on the silver coated top layer surface relief device and the results are shown in Figure 5-15.

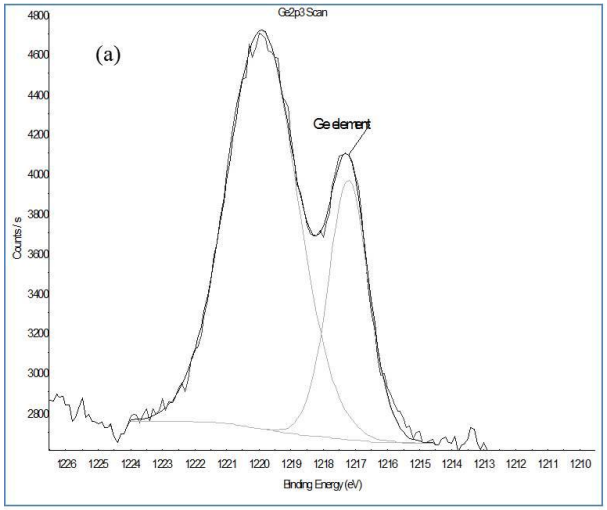

(b)	Analysed data from the XPS	
Substance	Peak binding energy (eV)	Atomic Abundance (%)
O1s	532.6	60.2
SiO_2	102.9	10.4
GeO_2	1219.9	3.9
Ge2p3 elemental	1217.2	3.9
Ag3d oxide	368.1	2.4

Figure 5-15 showing the gathered XPS data showing the presence of GeO2 on the surface of the fibre after exposure in (a), (b) shows the analysed data and the quantity of molecules

Figure 5-15 (a) shows the spectra produced clearly showing the presence of GeO_2 and the analysed data from Figure 5-15 (b) gives its quantity. Since the only materials deposited on the surface were pure germanium and silicon dioxide, the data shown add further evidence for the enhanced surface perturbation caused by UV exposure of both layers. Finally, the final metal layer is intended to act as a LSPR sensor, as such three different metals were used gold, silver (being a standard in SPR sensing) and platinum. Each metal has independent dielectric properties and by using three different metals, different sensing characteristics are produced (see Equation 2-40. The depths of all the material layers were chosen to be similar to previous work since the layers were known to act as a coupling mechanism, after UV exposure, supporting SPRs[167].

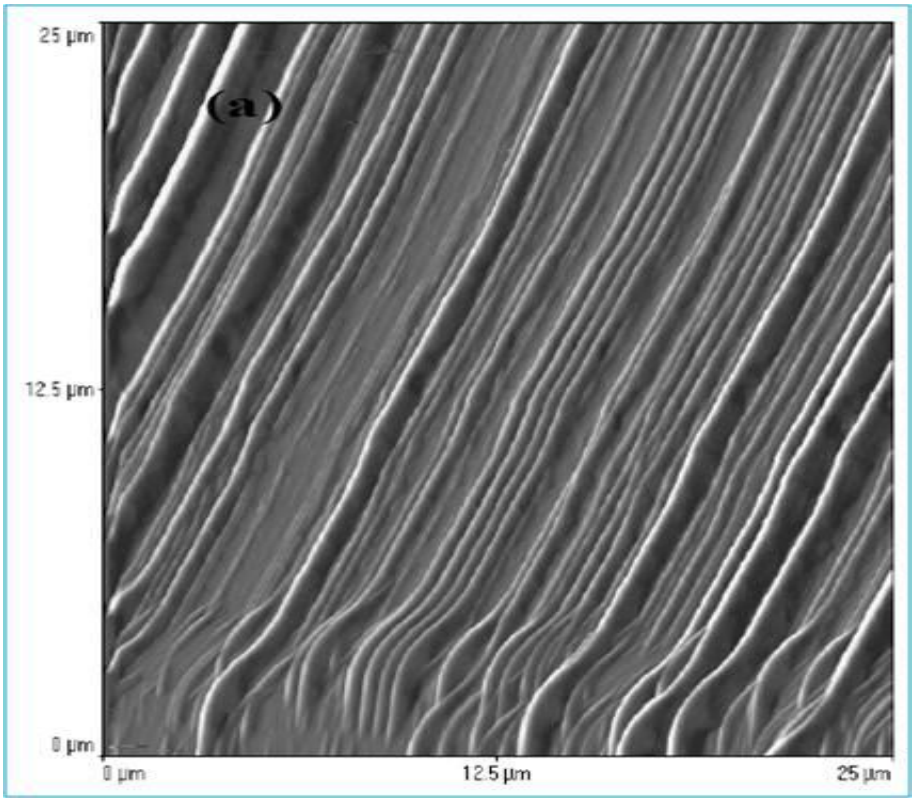

Figure 5-16 showing the surface perturbation of the silver device from post UV exposure

When these surface relief grating based LSPR sensors had been fabricated, their SRI and polarisation responses were investigated using the same technique described previously for the single- and multi-layer coated TFBG based SPR sensors. Each device produced multiple resonances with similar behaviour but much improved sensitivity compared to the fibre core containing TFBG sensors, discussed in the previous section of this chapter. The sensor polarisation properties were also investigated. Similar to previous sensors, it is important to note that the polarisation experiments were merely carried out to find out how the sensor operated under changing input light polarisation. The exact polarisation of the light at the sensor could not be deduced from the equipment and as such is not reported here. These devices were expected to operate as a SRI sensor for very small variations and should be suitable serving as a platform structure for bio/chemical/medical sensing applications.

5.4.2 SRI and polarisation response for the silver coated top layer surface relief based SPR sensor

The device with top layer coated with silver produced two SPR resonances even when it was situated in air, as shown in Figure 5-4, which is in contrast to the previously discussed single- and multi-layer coated TFBG based sensors which have not displayed any resonances in air. This suggests that there is a different mechanism taking place and changing the phase matching condition of the resonances in the surface relief grating based SPR sensor structure.

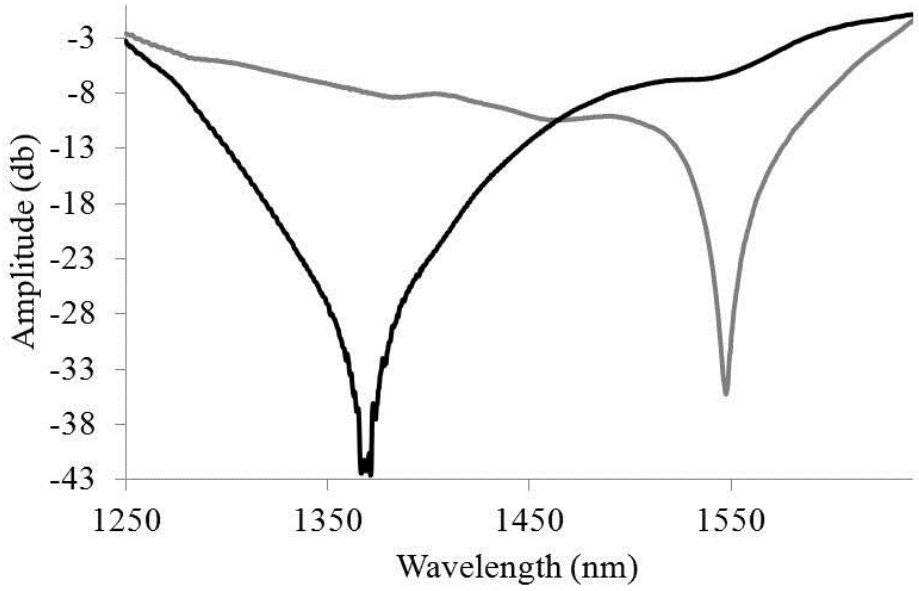

Figure 5-17 showing the multiple resonances produced by the surface relief grating based silver coated top layer device in air

Taking the resonance at 1550nm as the typical case, we have characterised its response with increasing SRI and the spectral evolution showed there is a red wavelength shift accompanied by an increase then a decrease in amplitude of the resonance, shown in Figure 5-18. With the large change in SRI from air to 1.3, it is possible that the resonance produced in air either disappears completely or shifts out beyond the light source range and instead a new resonance arises which satisfies a different phase matching condition with a SRI of 1.3. However, it could also be the same resonance that has simply decreased in

optical strength to a weak resonance. Unfortunately this could not be further investigated since no SRI liquids were available below a RI of 1.3. The shrinking and growth is probably due to the resonance being maximised in air. With the peak maximised an increase in resonance amplitude is expected but this is over a relatively small SRI range. In this experiment the SRI is relatively large and as an increase in resonance size would be expected at some point since the difference between the claddings modes coupling to the resonance would be large, over this SRI range. With this is mind the wavelength shift and amplitude change between air and 1.3 is reported. The observation of a resonance in air was not reported for the SPR devices. As such, the full dynamic range from air to higher SRIs was investigated, this meant the device was not renormalized for higher SRIs.

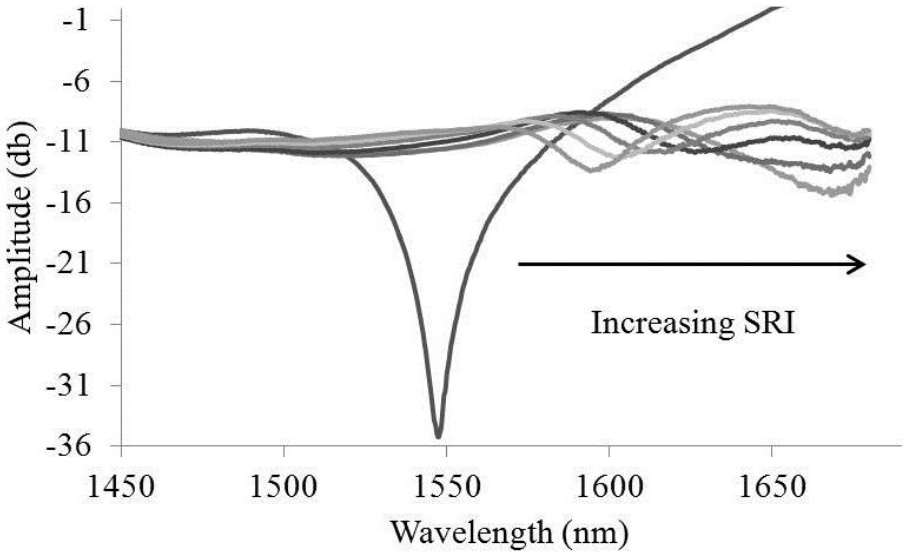

Figure 5-18 showing the spectra evolution of the surface relief grating based SPR sensor with a silver coated top layer. Note, the 1550nm resonance in air and the weaker resonance when submerged in liquid with SRI>1.3

The calculated wavelength shift and amplitude change of the 1550nm and the regenerated resonances are plotted in Figure 5-19. The wavelength response in Figure 5-19(a) may be regarded as two sensitivity regions: for SRI from 1 to 1.3 and from 1.3 to 1.38. Although there is no actual experimental points for the first region, the sensitivity trend is indicative and an average wavelength sensitivity could be as a high as 153.5nm/URI in this region,

which would be sufficient for low RI gas sensing. There is an anomalous result in in the high SRI range which could be due to the broad nature of the resonance at 1.38.

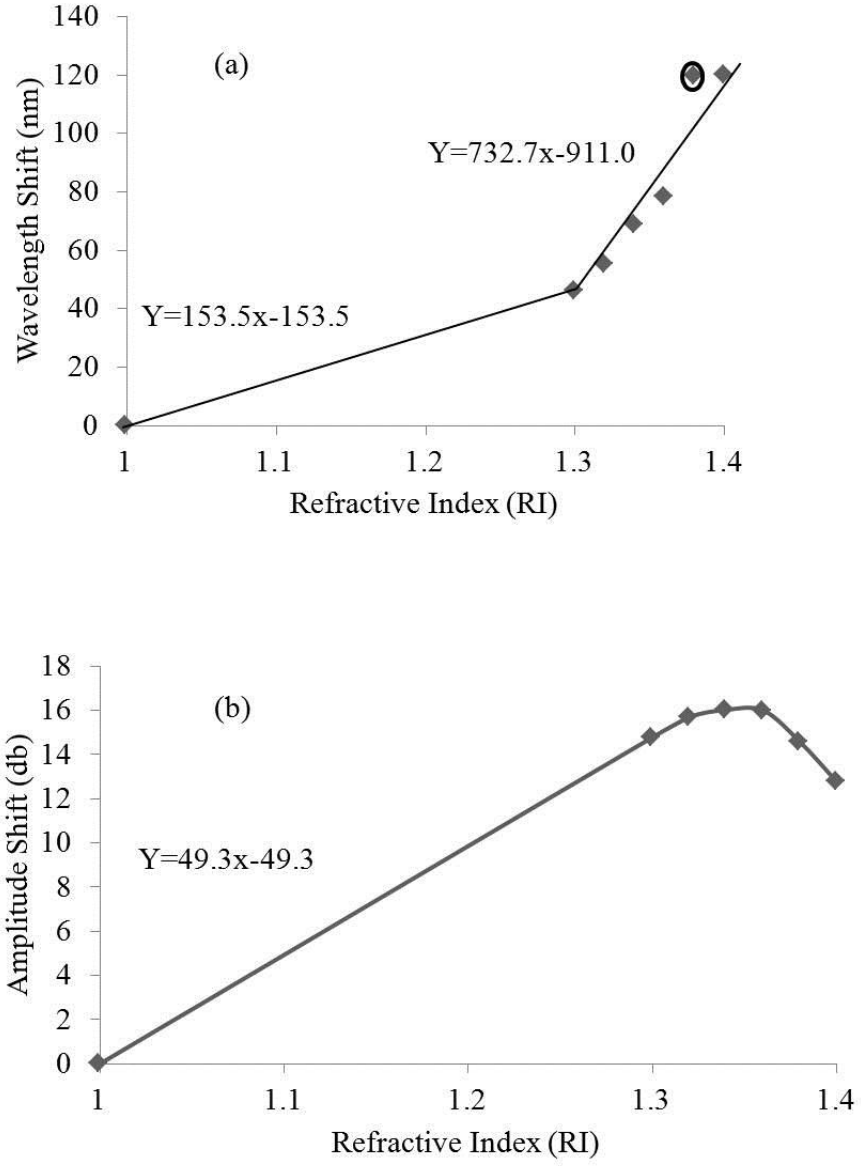

Figure 5-19 showing the RI response for the silver coated top layer device with a resonance at 1548nm for wavelength (a) and amplitude (b). Note, there is an anomalous point circled in (a)

Though the response is not linear and a curve would fit better for ease of comparison between different SRI ranges, two straight lines have been used to calculate the SRI sensitivity and will be used for the other sensors. The sensitivity in the high SRI regime is remarkable high, as it reaches 732.7nm/URI compared to the low regime which produced a sensitivity of 153.5nm/URI. Despite the regenerated resonance being weaker than the

original one in air, the extremely high sensitivity of the surface relief grating based SPR sensor opens up the possibility of very low SRI measurements.

The amplitude change in Figure 5-19(b) shows an increase and followed by a decrease in strength on the regenerated resonance evolving when the SRI changes from 1.3 to 1.38It may be hard to obtain any meaningful data in this high SRI region, the low SRI region may show a linear evolution as the straight line indicates in Figure 5-19(b). As an indication, the change in amplitude from air to 1.3 is 43.3dB/URI. This suggests that the sensor could also operate as a suitable sensor for very low SRI detection and by using amplitude and a low cost photo-detector it would also be cost effective.

Finally, the resonance's wavelength shift and amplitude change due to input light polarisation states by rotating the polarisation state from 0^o to 180^o with an increment of 10^0 was examined and the results are plotted in Figure 5-20. It can be seen that the polarisation has a large effect on both the spectral location and coupling efficiency of the resonance with the wavelength shifting by approximately 50nm and 10dB change in amplitude when the polarisation changes 180^o. The sensor is extremely sensitive to polarisation, it needs to be secured to eliminate polarisation effects when under wavelength or amplitude detection. This is expected as all SPR devices are polarisation sensitive by nature and this is enhanced by the D- shape of the fibre.

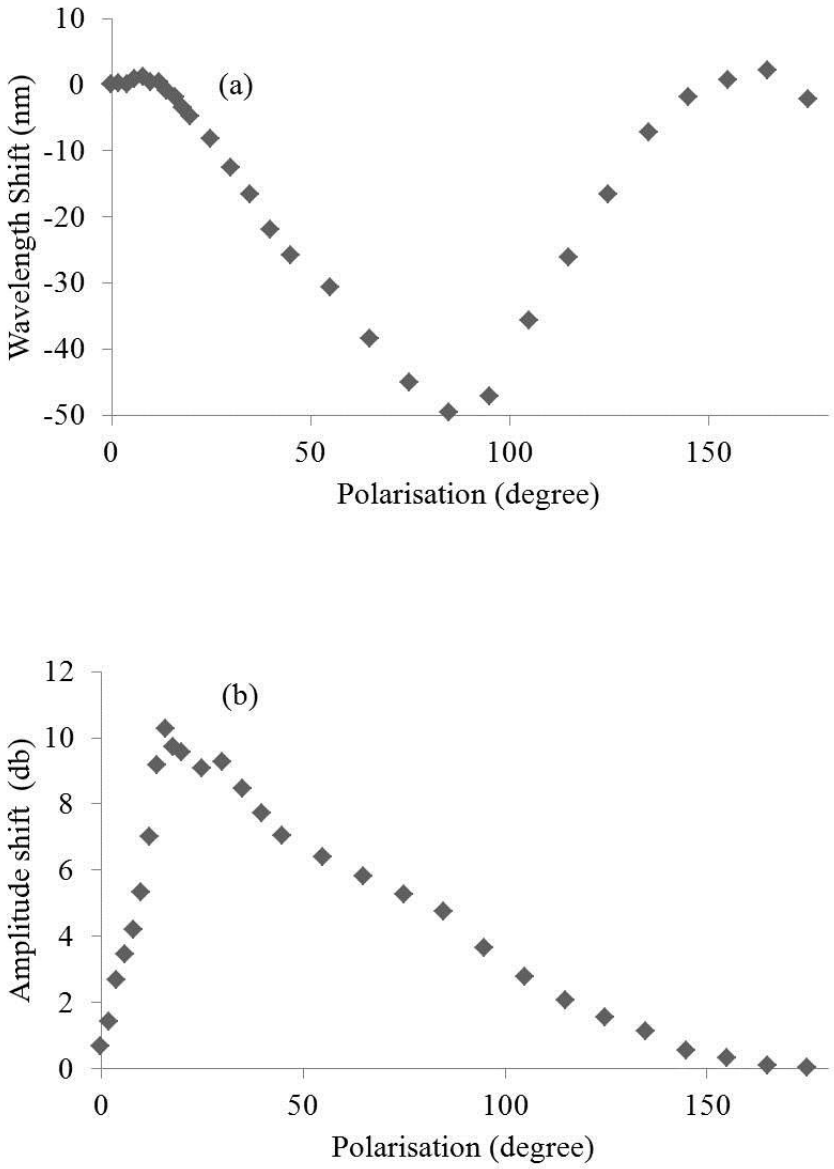

Figure 5-20 showing the Polarisation response of the surface relief grating based sensor with a silver coated top layer for wavelength (a) and amplitude (b)

5.4.3 SRI polarisation for the gold top layer surface relief grating based SPR sensor

The gold coated top layer device was capable of producing 4 distinct SPR resonances when it was submerged in a liquid with SRI 1.36, as shown in Figure 5-21. Unlike the silver, the gold device did not produce any resonances in air. This is slightly unexpected when comparing to the silver but a resonance may have been sustainable in air but was outside of the wavelength range of the light source.

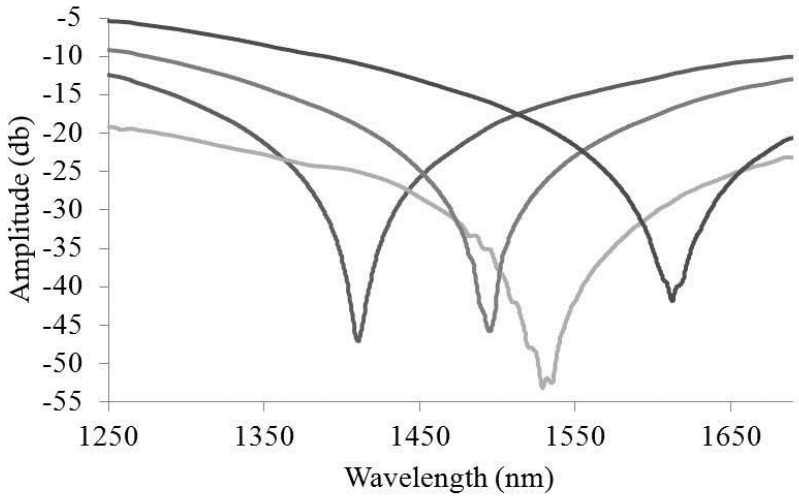

Figure 5-21 showing the multiple resonances produced by the surface relief grating based sensor with gold coated top layer when it was submerged in a liquid with SRI of 1.36

Taking the resonance around 1380nm for an example, the transmission spectral evolution with increasing SRI is shown in Figure 5-22.

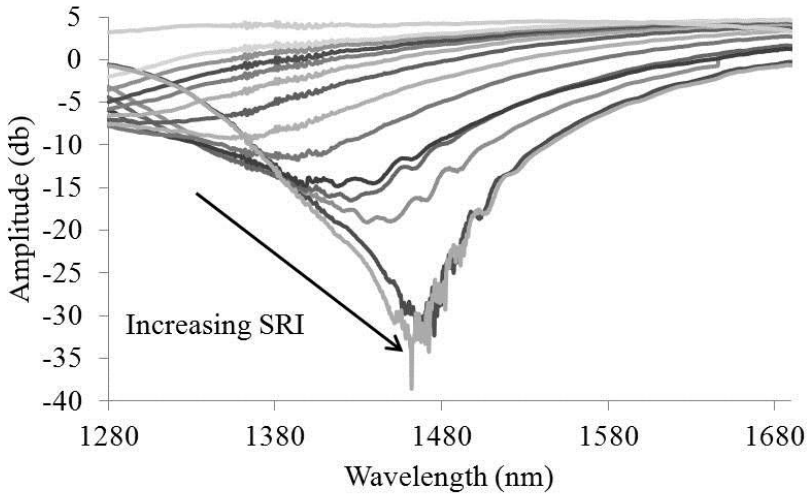

Figure 5-22 showing the spectral evolution of the a gold coated surface relief grating device with increasing SRI, starting with air where there are no resonances

With increasing SRI, we see a red wavelength shift and a decrease in coupling strength of this resonance. Since the wavelength shift is in the same direction as the silver coated device, it would could that the two devices are operating on similar sensing principle.

Calculating the wavelength shift and amplitude change of this device using the centroid method with respect to SRI gives the results plotted in Figure 5-23. Again, the plots are

clearly curved but for comparison two straight lines have been drawn and the errors are too small to be seen on axis scale.

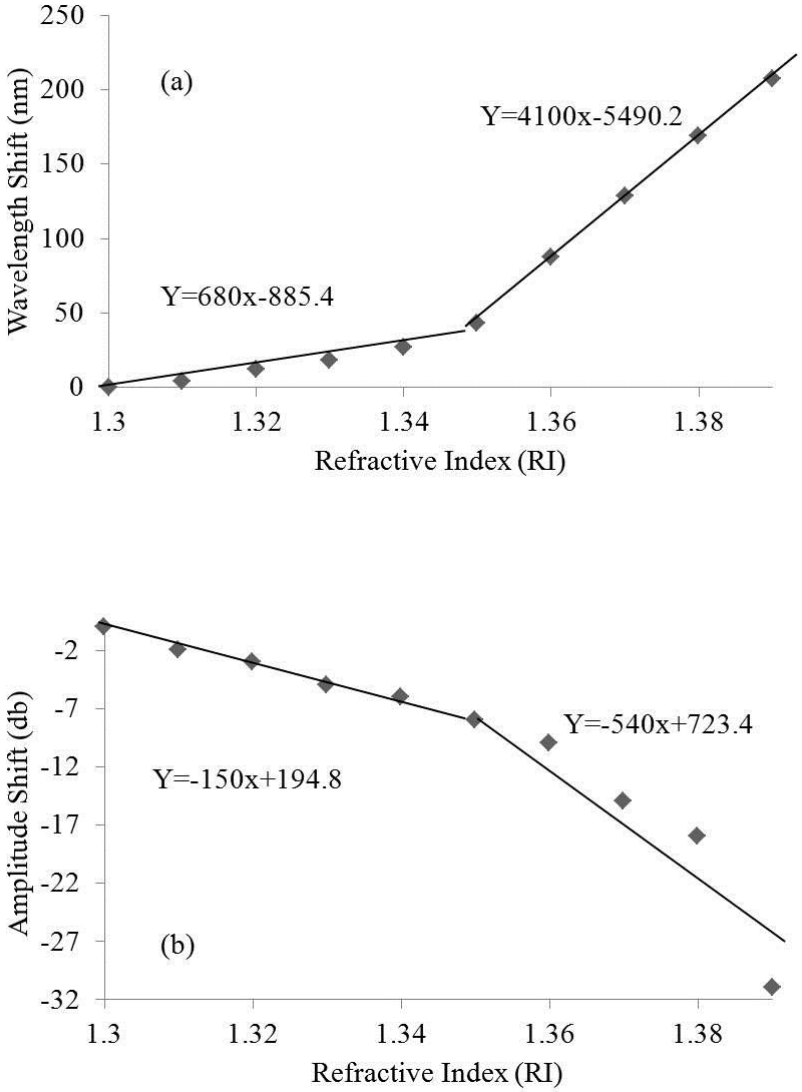

Figure 5-23 showing the SRI response for the gold coated surface relief grating device for wavelength (a) and amplitude (b)

Considering first the wavelength shift plotted in Figure 5-23(a), there are two different regions of sensitivity when the SRI range 1.3 to 1.38. In the lower SRI range from 1.3 to 1.35 the device exhibits a sensitivity of 680nm/URI while in the higher SRI range from 1.35 to 1.39 it has a sensitivity of 4100nm/URI. The latter is almost 6 times the former and is largest SRI sensitivity reported so far. The amplitude change is slightly different, as shown in Figure 5-23(b), the amplitude change produces a curved response. With increasing SRI there is increasing coupling efficiency and hence a decrease in amplitude

caused by a change in balance from the loss caused by the resonance, absorption and the reflection from the multi-layer coating surface. Like the wavelength response, the amplitude change also exhibits extremely high sensitivity, showing a value of 540dB/URI in the SRI range from 1.35 to 1.39and150dB/URI in a lower SRI range from 1.3 to 1.35. Although a linear fit is not the best, it serves as an indication of the slope for comparison purposes.

The gold coated surface relief grating device seems ideally suited to biological aqueous applications with its sensitivity in this SRI range being higher than other methods reported. As always with these SPR sensors, the polarisation response of the device must be examined and the evaluation was carried out the same as was done for the silver coated device. Wavelength shift and amplitude changes due to varying input light polarisation are shown in Figure 5-24(a) and (b) respectively. As we can see from the figure, the magnitude of wavelength shift is approximately 13.2nm, which is smaller than the silver coated device, and the magnitude of amplitude change is 22.0dB, which is on a similar scale to the silver coated device. This means the gold coated device is less polarisation sensitive when compared to the silver device, however polarisation cross sensitivity must still be minimised.

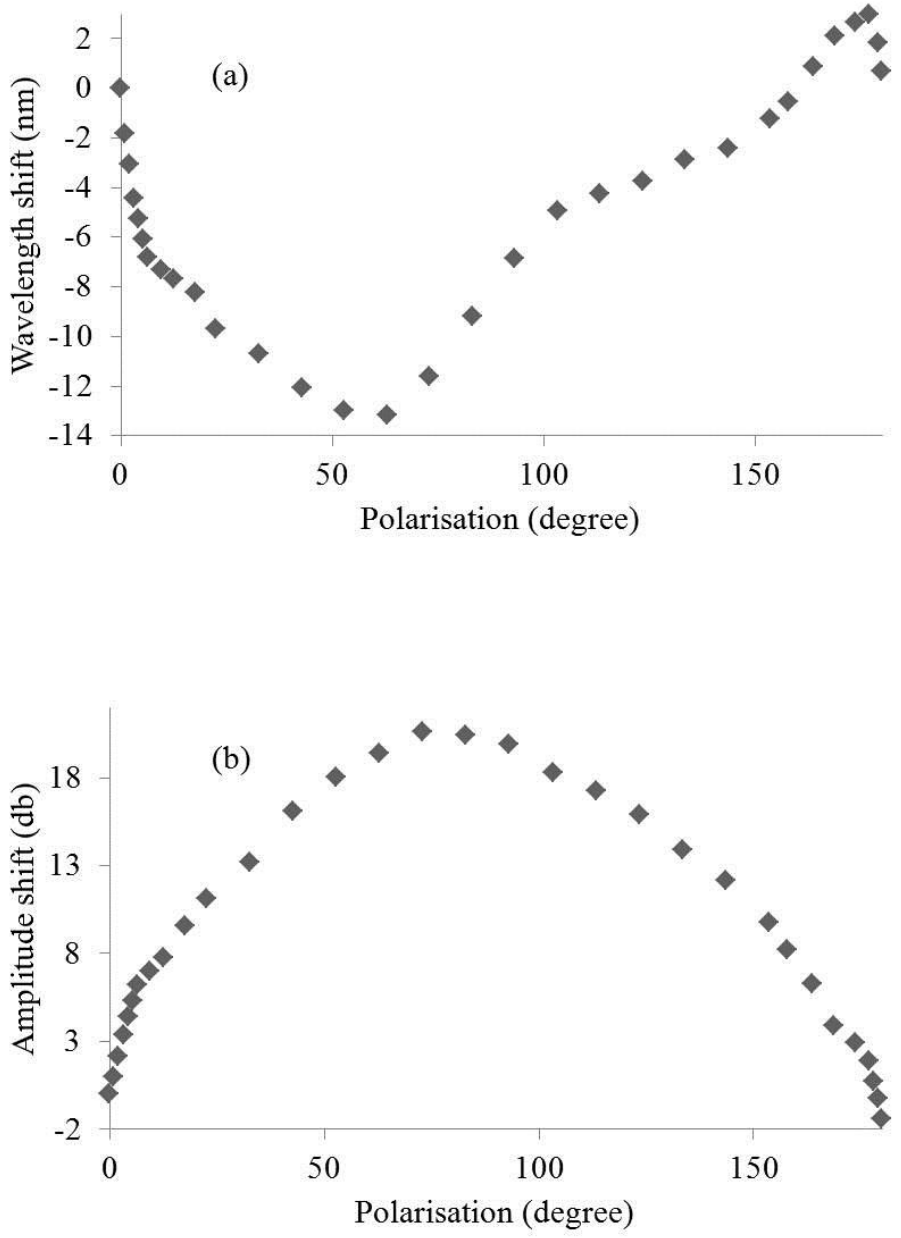

Figure 5-24 showing the polarisation response for the surface relief grating sensor with gold coated top layer for wavelength (a) and amplitude (b)

5.4.4 SRI and polarisation response for the platinum coated top layer surface relief grating based SPR sensor

Finally, the surface relief grating structure with a platinum coated top layer was investigated and found to produce three SPR resonances with a SRI of air, shown in Figure 5-25. Since multiple resonances are occurring in air, the platinum device is behaving similarly to the silver coated device, but exhibiting one more SPR peak in air.

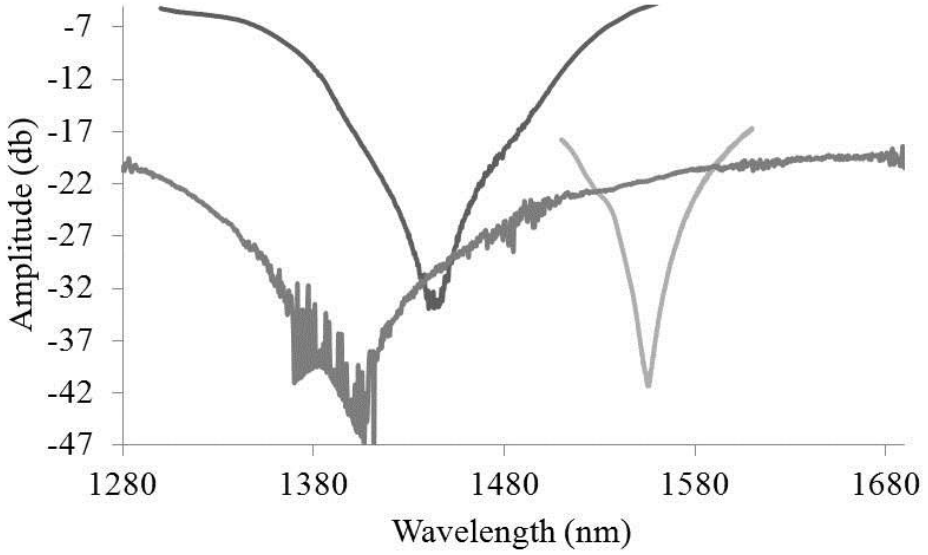

Figure 5-25 showing the three SPR resonances produced by the surface relief grating device with a platinum coated top layer when it is in air

The spectral evolution of the most sensitive peak, at approximately 1380nm, to with increasing SRI is shown in Figure 5-26. Similar to both the silver and gold coated devices, with increasing SRI we see a red shift in resonance wavelength. From Figure 5-26 we can see a very large wavelength shift of about 250nm occurred when the device was transferred from air to liquid. Like the silver device, since a resonance was produced in air its behaviour with increasing SRI was attempted to be followed over a large SRI range. As a result the device were not renormalized with higher SRI The resonance is strong in air and goes to a weaker one when in a higher SRI, similar to the silver coated device. Again, this is because the resonance has been maximised in air through changing polarisation, and any shift in SRI will cause the peak to move away from this maximum. Like the silver coated device, due to the large change in SRI from air to 1.3, it cannot be confirmed if the resonance produced at higher SRI is the same resonance produced in air. . However it could be and as such the sensitivity is reported here as an indication of the low SRI response of the platinum device. Also from Figure 5-26, the amplitude of the resonance is increasing with increasing SRI, although the data may not be accurate as the signal falls to a high noise level due to being very close to the edge of the light source.

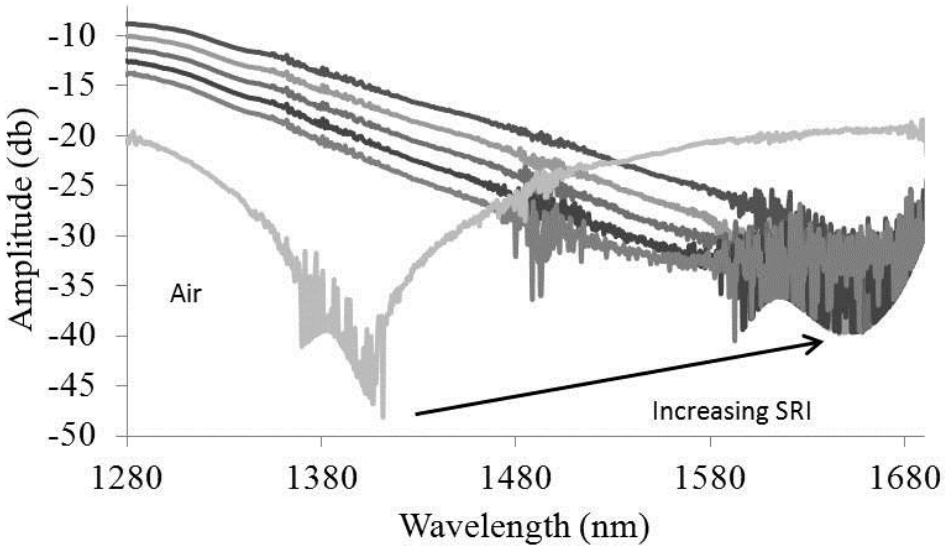

Figure 5-26 showing the Spectra response with increasing SRI with the initial value being air

Using the centroid method, the wavelength shifts and amplitude changes were calculated for increasing SRI and the results are plotted in Figure 5-27. Looking at the wavelength response in Figure 5-27(a), the wavelength response in the SRI range from 1.3 to 1.38 is slightly nonlinear. Although we don't have experimental data for the SRI region from air to 1.3, the straight line would still show the sensitivity trend in this region. For the sake of easy comparison, for the sake of easy comparison the results have been separated into two regions as the linear fitted lines show. This gives a sensitivity of 638nm/URI and 1450nm/URI for the SRI change from 1 to 1.3 and 1.3 to 1.38, respectively. In comparison with the silver and gold coated cases, we this platinum coated device is more sensitive than the silver coated device in both SRI regions, especially the low SRI region, however, it is less sensitive than the gold device in the higher SRI region.

The amplitude response is shown in Figure 5-27(b) and, unlike the wavelength response, shows a decrease in sensitivity with increasing SRI and so the highest sensitivity is at the lower SRI values. The sensitivity was calculated to be 52.1dB/URI and 25.5dB/URI for the SRI regions from 1 to 1.3 and 1.3 to 1.38 respectively. This is a slight improvement

over the silver device in the low SRI regime. However, the results in the low SRI regime must only be considered as a guide because of no actual experimental data to verify.

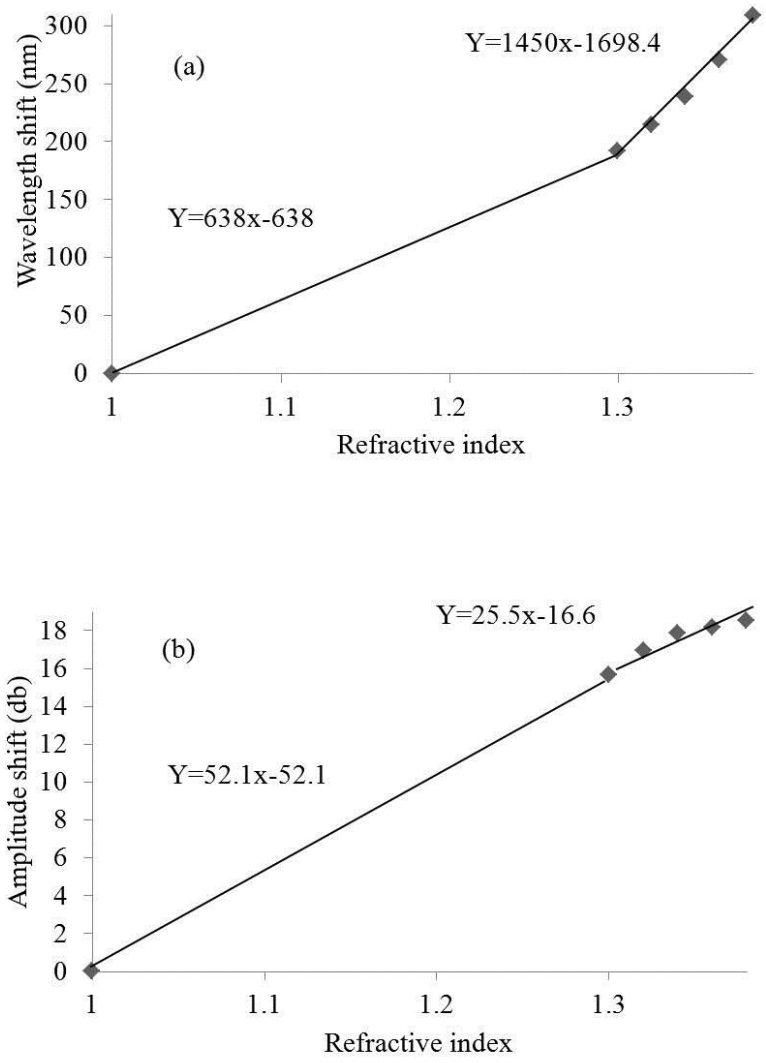

Figure 5-27 showing the SRI response for the platinum coated device for wavelength (a) and amplitude (b).

What is encouraging is, like the gold coated sample, the amplitude response is more consistent in this SRI range. This means that the device with the top layer coated with platinum can be used for SRI sensing using both wavelength and amplitude as an encoded measurement over a large SRI range.

And finally, we also examined the polarisation response to the platinum coated sample by rotating the polarisation state of the input light from 0° to 180° and the results are shown in Figure 5-28. The polarisation responses for both wavelength and amplitude are fairly

regular but more significantly large compared to the silver and gold coated devices. This could be due inconsistencies between the polished fibres but also the surface structure produced from UV exposing germanium through platinum. Both warrant further investigation.

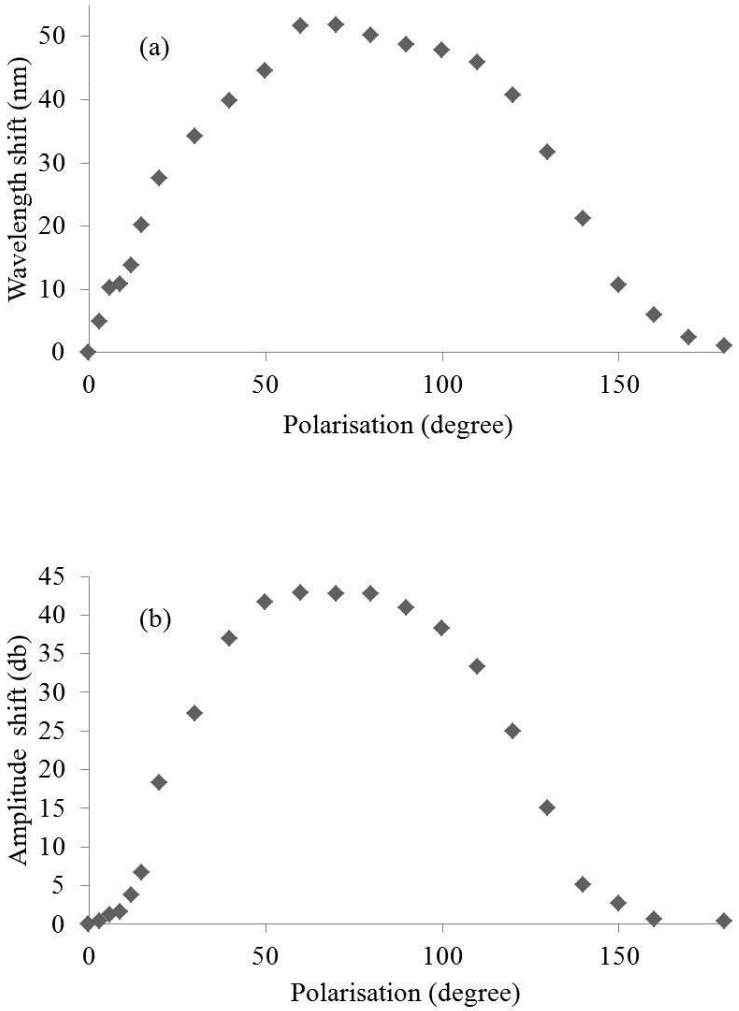

Figure 5-28 showing the polarisation response for platinum coated device for wavelength (a) and amplitude (b).

The platinum coated device has produced a magnitude wavelength shift of 51.8nm and amplitude strength change of 43.3dB, over the change of 180^{o} polarisation state. However, on negative side, it is even more important to keep the device stable for sensing to eliminate the cross-sensitivity effect from polarisation.

5.4.5 Mechanism and discussion

To understand what is occurring for the surface relief grating based sensors with multiple surface layer coatings, three properties need to be explained and understood; these are the function of the coating layers, the mode out-coupling mechanism and the sensing mechanism. Looking at the reasoning behind the layers, the first germanium layer may be considered. Germanium, from fibre optic theory, is known to react with UV light forming Ge/GeO centres; this is explained in section 2.1.1. Through combining of the germanium and the silicon dioxide layers the UV reaction is enhanced. The germanium interacts with the SiO_2 under UV exposure creating a change in volume not seen in bulk material[166]. The exact effect of the SiO_2 and the role it plays is surface compaction needs further investigation. The volume change cause by this process is what is seen in Figure 5-16. The desire behind this surface perturbation is threefold: first, the grating structure on the sensing surface will increase the sensing area available; Second, the discontinuity of the surface will cause the sensing mechanism to change from SPR to localised Surface plasmon resonances (LSPR), which are known to be more sensitive and third, the associated volume change of the Ge layer will cause stress to the fibre core creating a quasi-periodic grating structure to act as an aid for in and out coupling of the fibre core.

Considering the coupling mechanism between the core and SPR mode, there are three possible reasons for it: first, a UV induced grating located in the core of the fibre; second, a compaction and associated strain effect from the UV exposure of the germanium and silicon dioxide layer which would transfer themselves through to the core of the fibre causing a semi periodic stress field over the fibre core which would be either capable of coupling to the cladding modes or radiation modes or both; thirdly, broadband scattering loss due to the low quality of the polishing technique used to create the D-shape fibre (known causing 3dB loss previously discussed in section 5.2.3) which couples to the radiation modes.

We may further examine these three possible coupling mechanisms. Since the fibre was not hydrogen loaded the photosensitivity in the core would be extremely low. Also, the fibre was exposed to UV light on the flat coated surface meaning much of the light would be absorbed by the multi-layer structure (especially considering the skin depths of the metal). Both these facts would make any UV induced grating in the core highly unlikely. To help confirm this, the reflection spectrum of the device was investigated. If a Bragg grating structure existed a reflection in the spectrum would occur. In all devices no peak in reflection was seen, showing that if a grating structure was induced it would be very weak and unlikely to contribute to the strong coupling the surface relief device portray. To confirm the non-existence of a UV induced grating in the core the platinum device was annealed up to 450^{o}C over a period of time, well above the temperature at which the grating should be bleached out and the results of which are shown in Figure 5-29 with (a) being the DC amplitude change and (b) being the change in resonance strength. Looking at the data, the first thing to note is that the resonance of the platinum top layer device is still strong even at 450^{o}C. This proves that the coupling mechanism cannot be a UV induced Bragg grating in the centre of the fibre core.

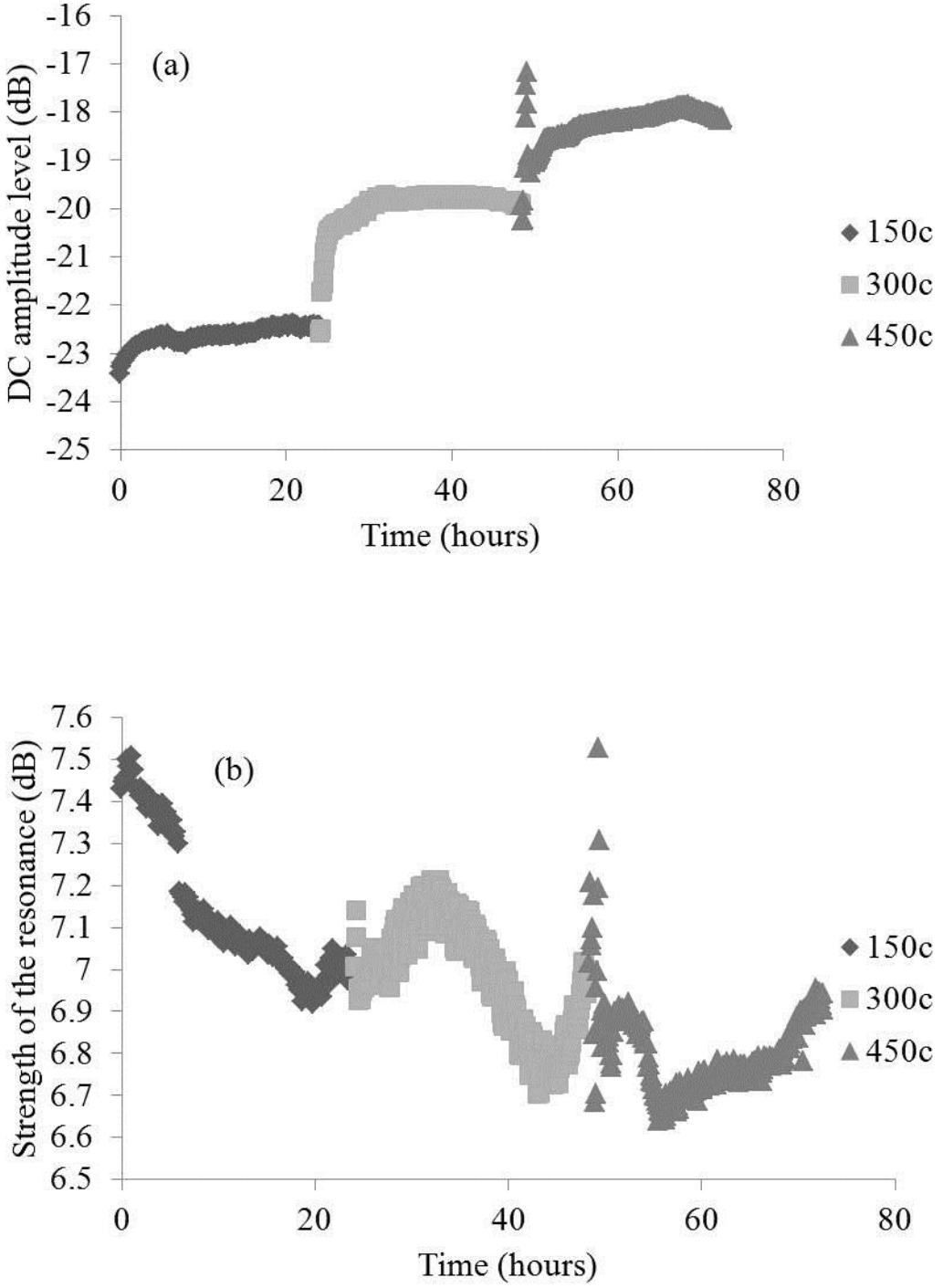

Figure 5-29 showing the calculated response of the platinum coated top layer device over time with increasing surrounding temperature with (a) being the DC change and (b) being the change in resonance strength.

Thus, the other two coupling mechanisms are dominant. The broadband loss due to the polishing of the fibre undoubtedly plays a role in the coupling of light from the fibre core. However, since the resonances are not observed before UV exposure it is unlikely to be the dominant cause. The stress induced field due to the surface compaction of the germanium and silicon dioxide layer clearly alter the fibre structure since it produces clear resonance

not seen before UV exposure. The stress induced by this method on a smooth fibre would be minimal; this therefore leads me to believe that a combination of scattering losses, which are caused by cracks in the polishing surface due to the poor quality of the technique, combine with the UV germanium compaction process causing semi periodic larger stress fracture that permeate to the core cladding interface of the fibre are the cause of the out coupling. The exact contribution of each process and whether this combined effect is coupling to bound cladding modes or radiation modes is still open to debate and needs further investigation.

Finally, the sensing mechanism is different from the tilted Bragg grating based surface plasmon sensors discussed in the first part of this chapter, as the surface relief grating based sensors with silver and platinum coated top layers were capable of producing multiple resonances air. As already discussed, the phase matching condition between the surface plasmon modes supported in the metal layers and the cladding modes makes this highly unlikely to be met. However, the LSPR modes are not confined by this phase matching condition but instead need just an electromagnetic field around a metal surrounded by a dielectric to function. This means that it is possible for cladding modes of even low orders to produce LSPRs. Typical LSPRs are far more sensitive than SPRs in nature, which would explain the larger sensitivity of the surface relief grating sensors than that based on titled Bragg gratings in the core, especially the surface relief grating structure with gold coated top layer which is far too big to be considered a surface area effect alone. The change in mechanism from SPR to LSPR can be explained by the surface relief grating feature. The surface roughness due to the sputtering technique is relatively large, being on the scale of ±10nm. This combined with the thin layer of material leads to island states capable of sustaining LSPR. However, because the layer is a continuous medium these effects are minimal with the SPR effect dominating. Through the introduction of the surface relief grating structure, the surface is no longer able to sustain SPR and the

continuous medium effect is negated, thus leaving the LSPR to dominate. The resistance of the metal surface was measured using a multi-meter attached to micro scale wires. The wires were placed at several regions of the sensor surface and the resistance measured, meaning if any region carried current there would be a high probability of detecting it. Resistance of the silver top layer device was found to be infinite, meaning the metal sensing layer is not continuous and cannot support SPRs leaving only LSPR to act as the sensing mechanism. Similar work has been carried out, but in a more uniform way, by using nanowires on the same scale as the surface perturbation which give similar results and explanation to the work here[160, 168-170]. Also, LSPRs have smaller spatial extensions into the analyte compared with SPRs. Evidence of this occurring for the gold coated top layer device is shown in section 6.3, adding further support to LSPR as the sensing mechanism for surface relief grating based sensors.

5.5 Summary and Comparison

Three different types of sensors were manufactured and their response to varying input light polarisation and changing SRI was characterised. The gold single layer and multi-layer tilted coated sensors operate on a SPR sensing mechanism. Through the use of a post UV exposure process a surface perturbation were imprinted on top of the metal coatings. The surface relief created an increase in sensitivity and supported resonances in a SRI of air. This strongly suggests that this type of sensor utilizes LSPR as the sensing mechanism. The surface relief sensor had three different top layer metal coatings, consisting of platinum, gold and silver. All the different sensors produced different sensitivities over a large SRI range. The wavelength response for all the devices can be seen in Figure 5-30

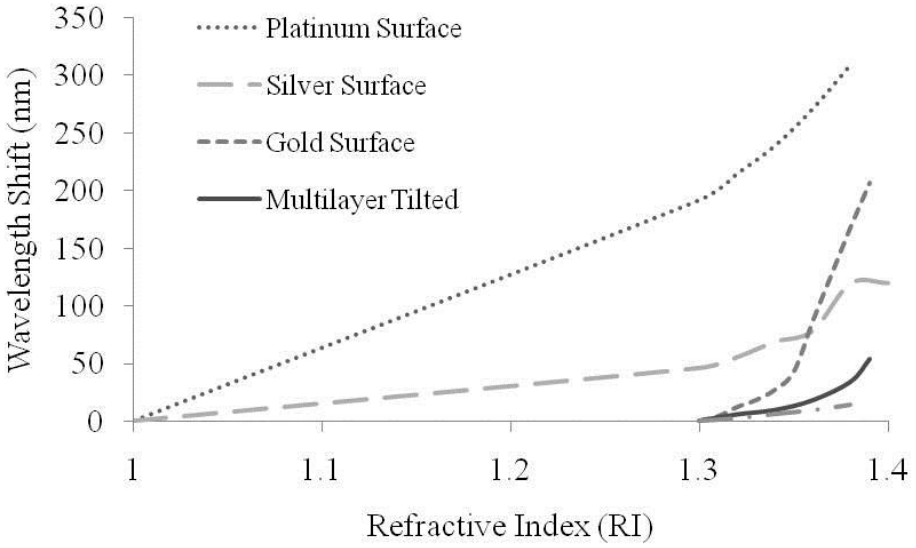

Figure 5-30 showing the wavelength shift due to varying SRI for all the sensors for comparison

To find the applications best suited for each sensor the SRI of all the devices are plotted in Table 5-2 and are split into two SRI the low range, being 1 to 1.3 RI, and the high, being 1.3 to 1.38. All the gold devices are only sensitive in the high RI range with the largest sensitivity being due to the surface relief gold device.

	Wavelength Sensitivity (nm/URI)		**Amplitude Sensitivity (db/URI)**	
Sensor Type	**1 to 1.3 SRI**	**1.3 to 1.38 SRI**	**1 to 1.3 SRI**	**1.3 to 1.38 SRI**
Single layer Gold	-	262.5	-	91.5
Multilayer Gold	-	426.3	-	340
Surface Relief Gold	-	2112.5	-	225
Surface Relief Silver	153.5	732.7	43.3	-
Surface Relief Platinum	638	1450	52.1	25.5

Table 5-2 showing the numerical SRI sensitivities for all the sensors in two SRI ranges

Bio-logical reactions occur in aqueous solutions that have a RI value in this range. As such, the gold devices would make ideal biological sensors and this has been investigated in section 6.3. Both the platinum and silver Surface relief sensors produced resonances in air while also showing a comparable high sensitivity in the low RI range. Despite showing a higher sensitivity in the higher RI range, this property of resonances in air opens up the

possibility of gas sensing using SRI change, something unfeasible with traditional optical sensors such as LPGs, and has been investigated in Section 6.2.

6 Surface Plasmon Sensor Applications

6.1 Introduction

Applications for Surface Plasmon Sensors are many and varied, but perhaps the two most in demand fields are that of gas sensing, for safety and environmental concerns, and biological systems, for drug testing, in-vivo monitoring and again environmental contamination. As such the sensors characterised in section 5.4 are investigated for applications in both these fields. This chapter will detail the analysis and response for the LSPR sensors for gas and thrombin detection.

6.2 Gas Sensing

6.2.1 Introduction

Fibre optic sensors at current mainly use two sensing techniques for gas detection. First is spectroscopy, where the gas molecule under detection has an absorption in the light spectrum creating a loss peak encoded with the gas property. The amplitude or wavelength of the absorption loss peak can be detected using methods such as cavity ring down or photonic crystal fibre. There are limitations when using these methods since the molecules under detection need to have a strong absorption peak in the desired wavelength range. This limits the wavelength range and the amounts of detectable analytes. The second gas detection technique is through the functionalising of the fibre surface with a specific coating whose spectral response changes when exposed to a specific gas. Such sensors include LPGs and FBGs and are commonly coated with Palladium for the detection of Hydrogen[171]. Although this technique is relatively easy to implement the downside again is that is only works for one analyte at a time and the sensor is reliant on one coating

for one gas detection. However, species specific coating detection technique have proven very accurate with reported detection limits of 0.22 ppm[172], 300 ppm[173] and 231 ppm[174]. In general, the RI change associated with different gasses is very small for which the methods already mentioned here are incapable of detecting. However, this is not the case for the metal coated fibre with a surface relief grating structure. Such structure form LSPR capable of detecting the small RI change in the gas regime and are not limited to the detection of a single gas. Furthermore, the multiple resonance peaks produced by these sensors give a greater scope for tenability and versatility in sensing gas in the wavelength domain.

6.2.2 Experimental Procedure

Two LSPR fibres sensor samples of different coatings were investigated since they both exhibited resonance in air meaning they could be used to detect changes in SRI in the gas RI regime. Both types of sensors were first coated with germanium (48nm) and silica (48nm), followed by a metal layer, either silver (32nm) or platinum (38nm), and then had been UV exposed via a phase mask of period 1.018μm to generate a surface relief structure. Figure 6-1shows the gas chamber with detection system used to evaluate the gas sensing functionality of the two fabricated LSPR fibre sensors. Since the LSPR is extremely sensitive to the polarisation, a polariser and polarisation controller are used to control the polarisation state of the light lunched to the fibre sensor

The four gases under examination were methane, ethane, propane and butane. The refractive indexes of these gases can be found in "CRC handbook of Chemistry and Physic" 89th edition, Taylor and Francis Group[175]. Each gas was flushed through the system to completely fill the chamber and this was carried out 3 times by opening and closing the valves to maximise the amount of analyte gas and ensure no amount of air or previous test gas was left inside the chamber. Then, by changing the polarisation

controller, a maximum SPR resonance can be seen on the OSA. The transmission spectrum was allowed to settle for around 500 second after this it was then recorded 4 times with intervals of 30 seconds, which meant the stability of the system could be analysed. When the results had been collected, the same procedure was performed for the next gas and the order of investigation for the gases was selected to go lightest to heaviest. The flow rate was monitored since the magnitude change was under investigation here, the flow rate was considered in a further experiment. Due to the broad nature of the LSPR spectral peak, the centroid method was employed to calculate both the wavelength shift and amplitude change for the silver device. The platinum device's peak was more defined and symmetrical, so the wavelength shift and amplitude change were calculated by curve fitting a binomial line whose minimum centred on the minimum of the resonance and from the fitted equation the true minimum was found.

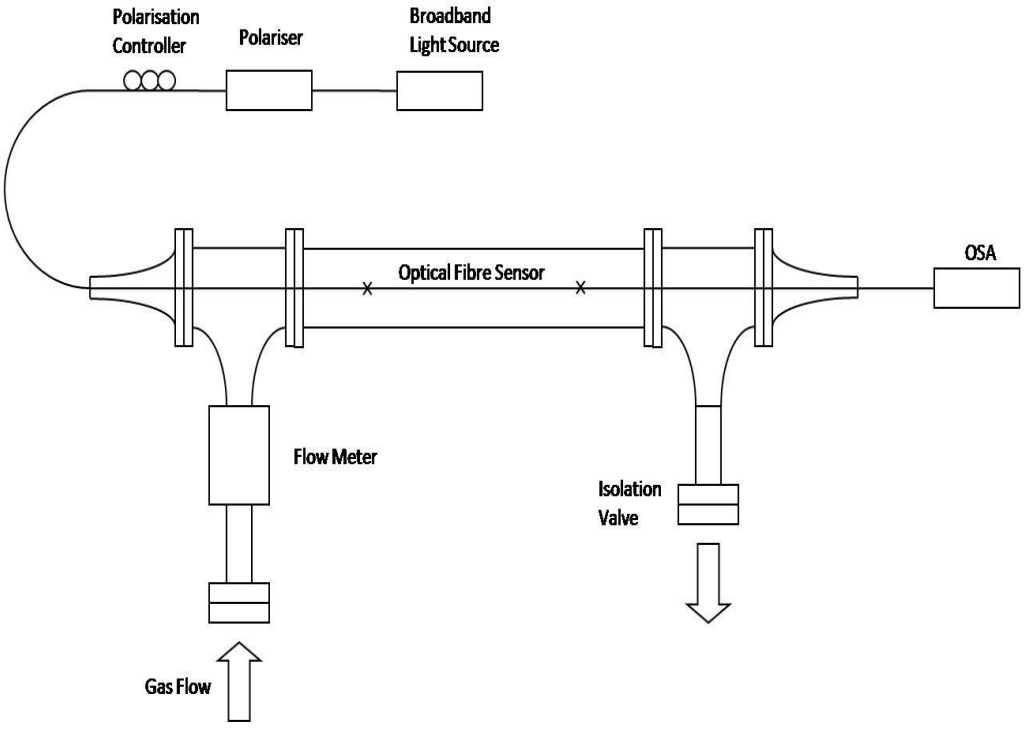

Figure 6-1 the experimental setup for investigating the gas response for LSPR devices

The temperature response of the silver coated device was examined by placing the sensor in a peltier and secured in place removing any polarisation drift caused by movement. The LSPR was measured for a temperature range from 22 to 27^0C going up in increments of one degree and at each measurement the peltier and device were allowed to stabilise before the transmission spectrum was recorded.

The platinum device has a resonance around 1550nm in wavelength and as such the time response of the device could be investigated using a DFB laser at 1550nm (replacing the broadband light source) and a photo-detector, which converted optical power into volts on an oscilloscope (replacing the OSA). The device was tuned to achieve the minimum in optical power, assuming this was due to the resonance. The gas under investigation was allowed to flow through the gas chamber, being controlled using a valve and the rate monitored using the flow meter. While the gas was entering the chamber the output was continually recorded every 2 seconds, which was as fast as the electronics would allow. By doing this, the different flow rates of a gas could be calculated, always necessary when dealing with a fluid, but it also showed that the sensor could be implemented cheaply, compared to a wavelength response, despite the peak of the resonance being located slightly out of the DFB lasers wavelength range.

6.2.3 Results and Discussion

The Transmission spectrum of the silver coated LSPR device changed when it was surrounded by different gases, as shown in Figure 6-2. It is obvious from this that the changing SRI of the different gases is causing a red shift in resonance and an increase in amplitude. To clearly see the wavelength shift and amplitude change, the calculated values are plotted for evolving over time separately in Figure 6-3, where the time taken for the transmission spectrum to stabilise is not displayed.

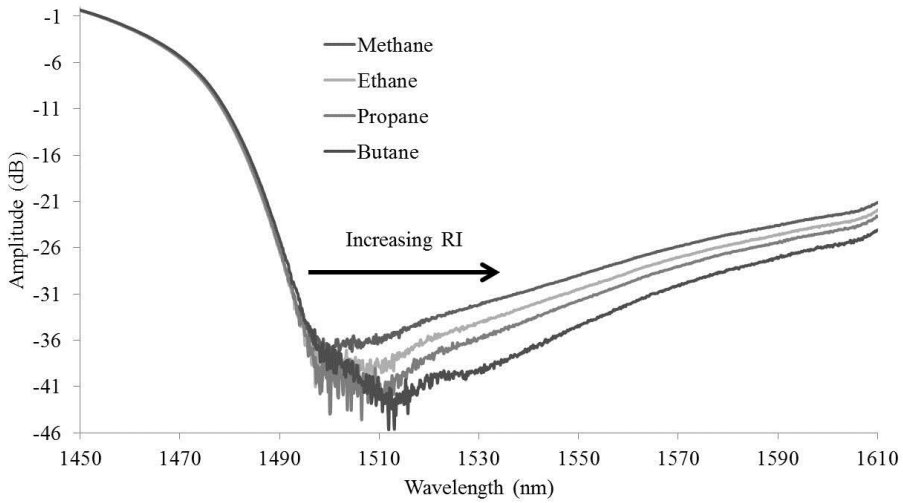

Figure 6-2 showing how the transmission spectrum changes with exposure to different gases for the silver coated device

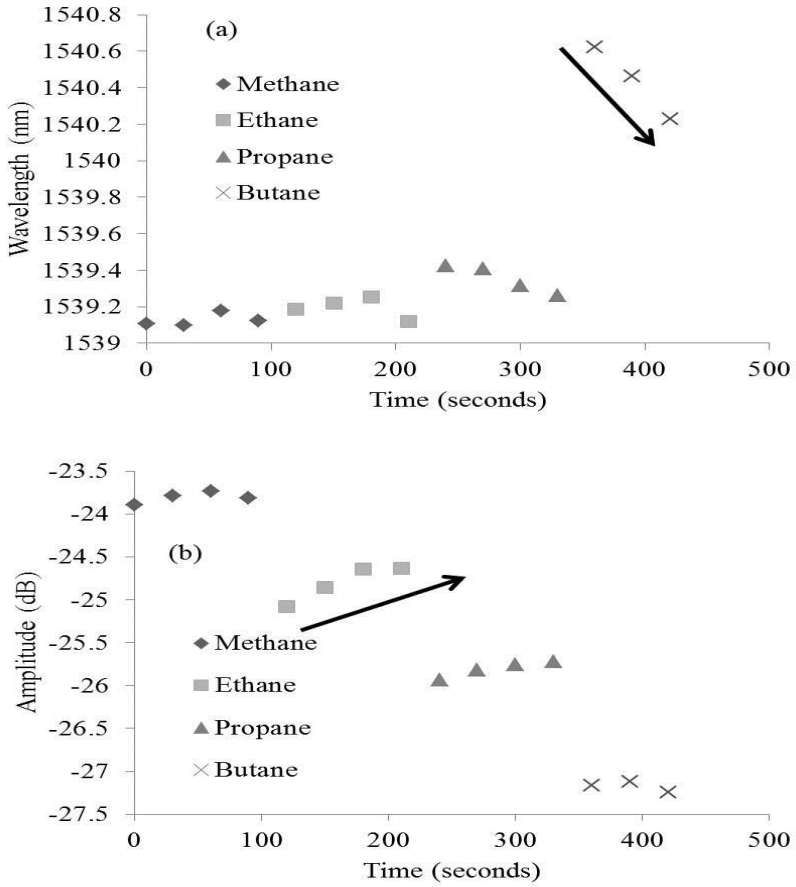

Figure 6-3 the centroid calculation of the wavelength (top) and amplitude (bottom) of the silver sample resonance for the 4 different gases. (The error bars due to the instability are too small to be seen on this scale)

From Figure 6-3 (a), the silver coated LSPR sample shows a general trend of increasing wavelength with increasing gas RI, i.e. the heaviest gas (Butane) has the largest shift. However, the wavelength response is not that clear with only the trend being apparent and

not the step index changes between the different gases. The wavelength shifts are very small and closely distributed with only the heaviest gas Butane showing a larger shift of about 1nm, however with more marked drift. The amplitude change is significantly better, as shown in Figure 6-3(b). The LSPR amplitude increases with gas RI with the largest amplitude change associated with the gas Butane. Again, the amplitude drifts slightly with respect to time for each gas. Two causes of the spectrum drift could be temperature and polarisation. As will be seen later, the temperature device was not very temperature sensitive. The drift could be accounted by the change in temperature of the gases coming into equilibrium with the room. Although the optical fibre fixed at both ends, a large section of the fibre was freely hanged in the gas. This allowed it to resonant with only a small perturbation (for example someone entering the room) and could further add to the drift due to polarisation effects.

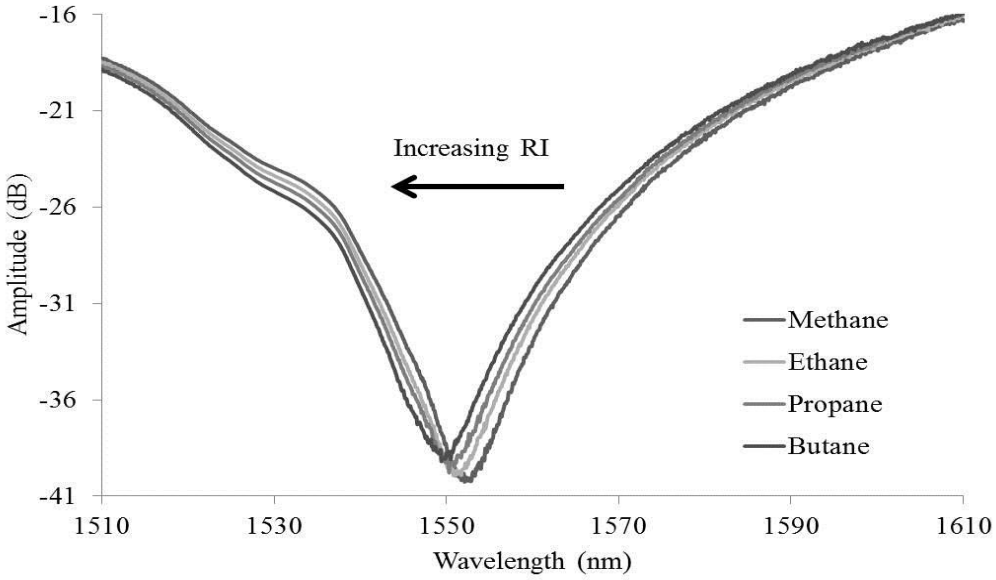

Figure 6-4 showing how the transmission spectrum changes with exposure to different gases for the platinum coated device

A similar experiment was performed using the platinum coated LSPR sensor and the detected resonance profiles for the four gases are shown in Figure 6-4. Compared to the spectra of the silver coated sample in Figure 6-2, the resonance peaks here are more refined and resembles a LPG response, though broader and stronger.

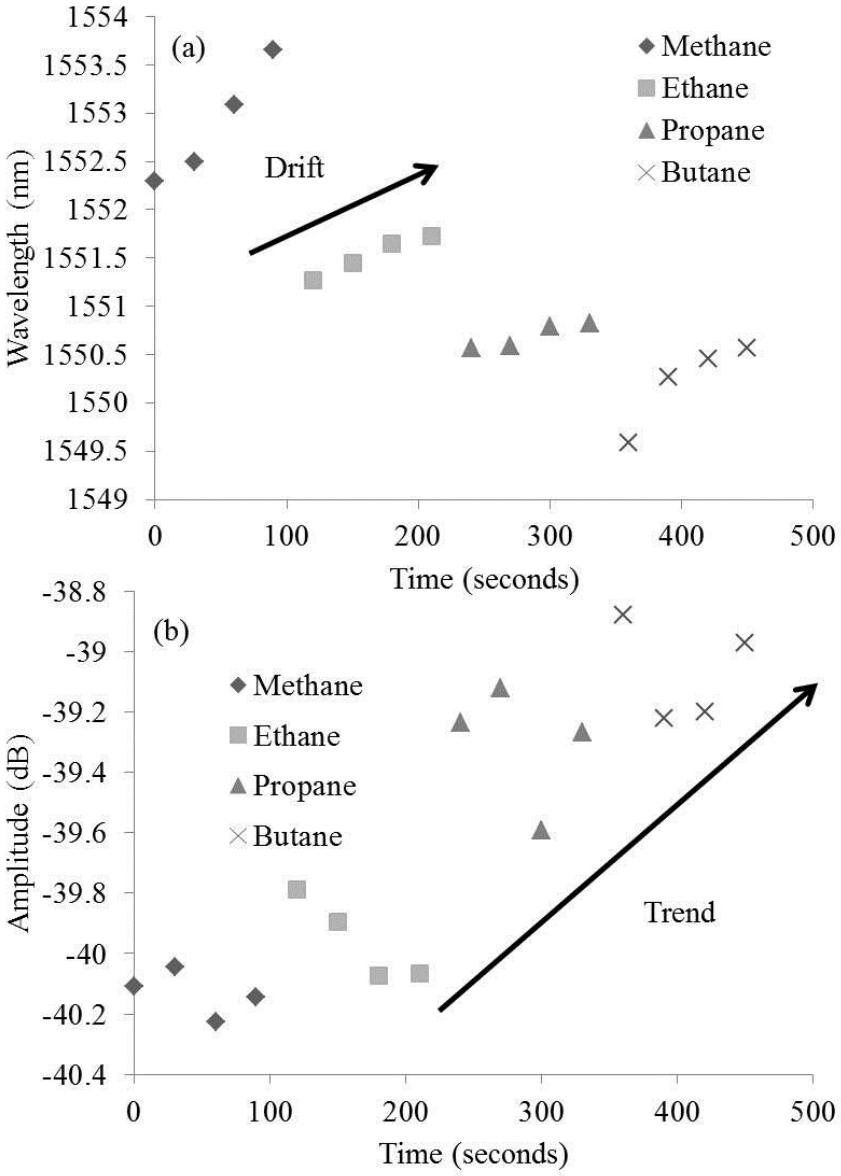

Figure 6-5 showing the wavelength (a) and amplitude resonance response for 4 gases of the platinum coated device. (The error bars due to the instability are too small to be seen on this scale)

Another difference that can be seen from the platinum coated LSPR sensor is the direction of the resonance shift due to changing gas. The silver LSPR sample shows a red shift while the platinum LSPR gives a blue shift with increasing RI of the gas. Similar to Figure 6-3, the time evolving trends of the wavelength and amplitude for the platinum coated sample are plotted in Figure 6-5 (a) and (b), respectively. In contrast to the silver coated sample, the time evolving behaviour is much more orderly. There is a clear trend that of resonance blue shift with increasing RI of gas and there is also a clear distinction between each gas. Within the results there is also a time evolving trend for each gas, the resonance shift

towards the longer wavelengths gradually. The slow drift behaviour of the silver coated sample is more likely due to the oscillation of the fibre, but the quasi regular drift from the platinum coated sample is less easy to explain and could probably be caused by the oscillation of the fibre combining with an inherent change in the system. The amplitude change shown in Figure 6-5 (b) indicates a time evolving linear trend showing decreasing amplitude with increasing gas RI. The distinction between the individual gases is less clear for the platinum coated sample than that of the silver coated with the random drift being more pronounced for each gas.

In order to see more clearly the comparative picture of the gas detection for both the silver and platinum LSPR sensors, the average values for the wavelength shift and amplitude change are plotted against RI for the four gases in Figure 6-6 (a) and (b). All the responses produced a near linear trend with the platinum coated sample producing better overall wavelength response and the silver sample a better amplitude sensitivity. The sensitivities of both samples in terms of both wavelength shift and amplitude change were established based on a linear fit with the results shown in Table 6-1. As discussed in section 3.5, the peak sensitivity achieved by a coated LPG was 1458nm/URI in the RI range from 1.40 to 1.42. The silver and platinum devices have produced a sensitivity that is similar or greater than this, but what is most remarkable is it being in the RI range 1 to 1.00258 where the LPGs are totally insensitive.

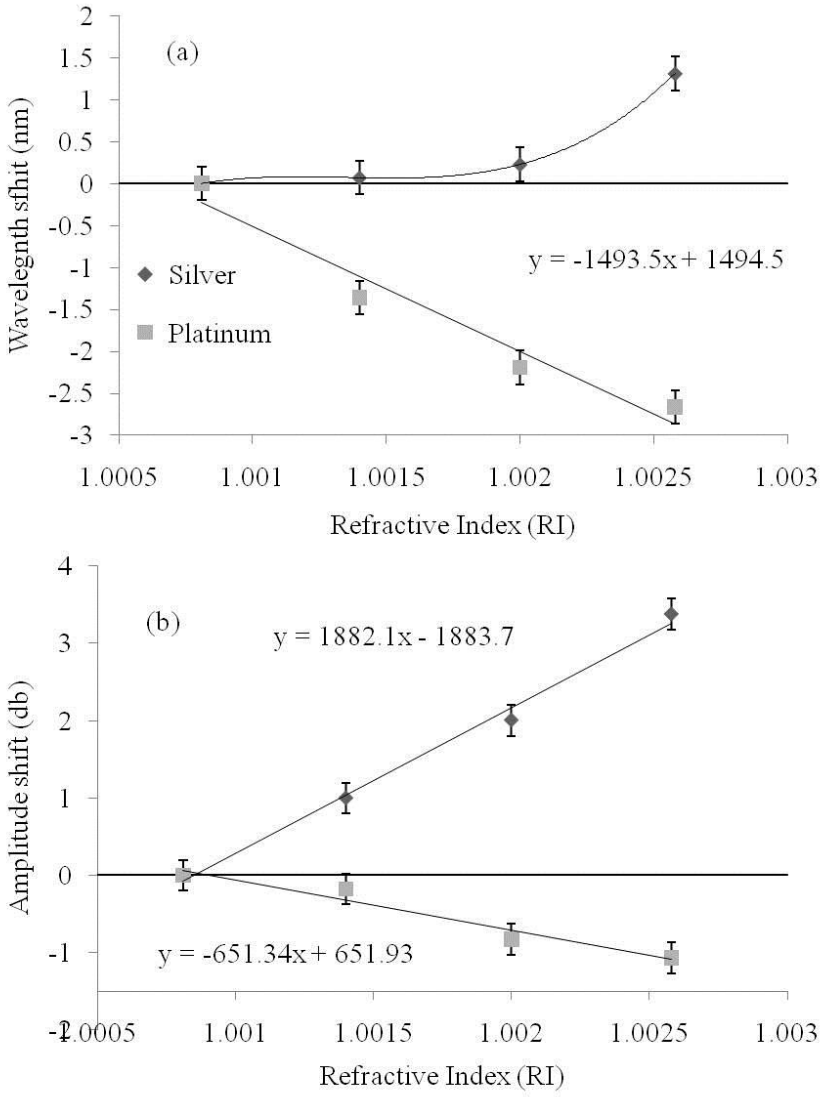

Figure 6-6 showing the calculated values for the wavelength (top) and amplitude shift (bottom) for the different gases and there corresponding RI values

	Amplitude sensitivity dB/URI	Wavelength Sensitivity nm/URI
Platinum	651.3	1493.5
Silver	1882.1	690.5

Table 6-1 showing the relative sensitivities of both silver and platinum coated samples for wavelength and amplitude detection.

Although the devices have shown to be adequate as gas sensors, when dealing with such small variations in RI the temperature response of the devices have to be taken into consideration. As such the temperature response of the silver coated device was investigated in air and the results are plotted in Figure 6-7. The platinum coated device has

not been subjected to the temperature response evaluation; however it is expected to show a similar response to the silver coated device. For a more high resolution sensing application, it may need to be characterised independently.

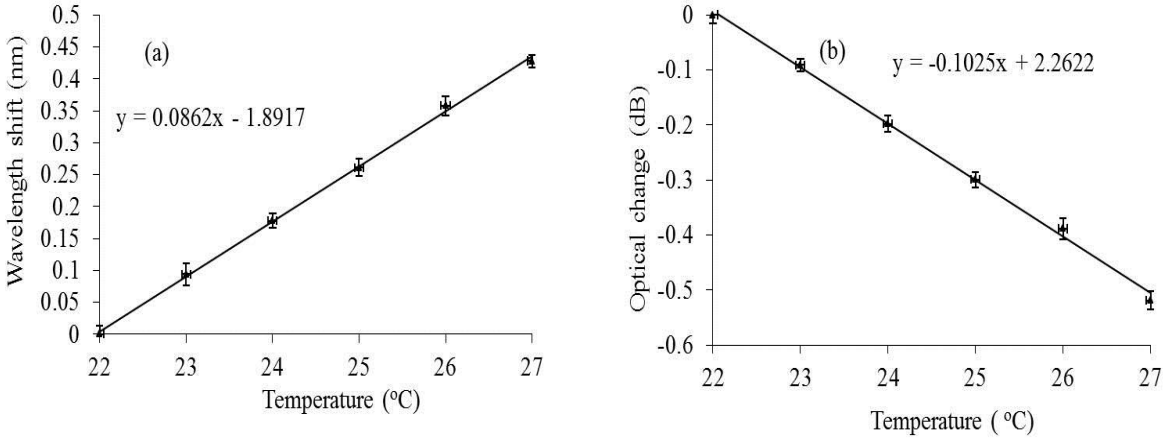

Figure 6-7 showing the wavelength (a) and amplitude (b) change against temperature for the silver coated device

The temperature affect on the silver coated sensor sample was evaluated for a room temperature range from 22 to 27 ^{0}C and the wavelength shift and amplitude change are plotted against temperature as shown in Figure 6-7 (a) and (b), respectively. Deriving from the gradients of the graphs in Figure 6-7, we can obtain the wavelength and amplitude sensitivity of (0.086nm±0.010)/^{0}C and (0.10dB±0.01)/^{0}C, respectively. The room temperature fluctuation caused changes are much smaller than the gas induced changes in wavelength and amplitude, so it may be omitted for more general applications.

Gases by their very nature are fluidic and as such move freely, so when developing a gas sensor flow rates have to be taken into account. Figure 6-8 shows the change in output from a photodetector when the platinum coated device was probed using a DFB laser. The gradual change from air to Ethane to Butane can be seen, with the largest change associated with Butane.

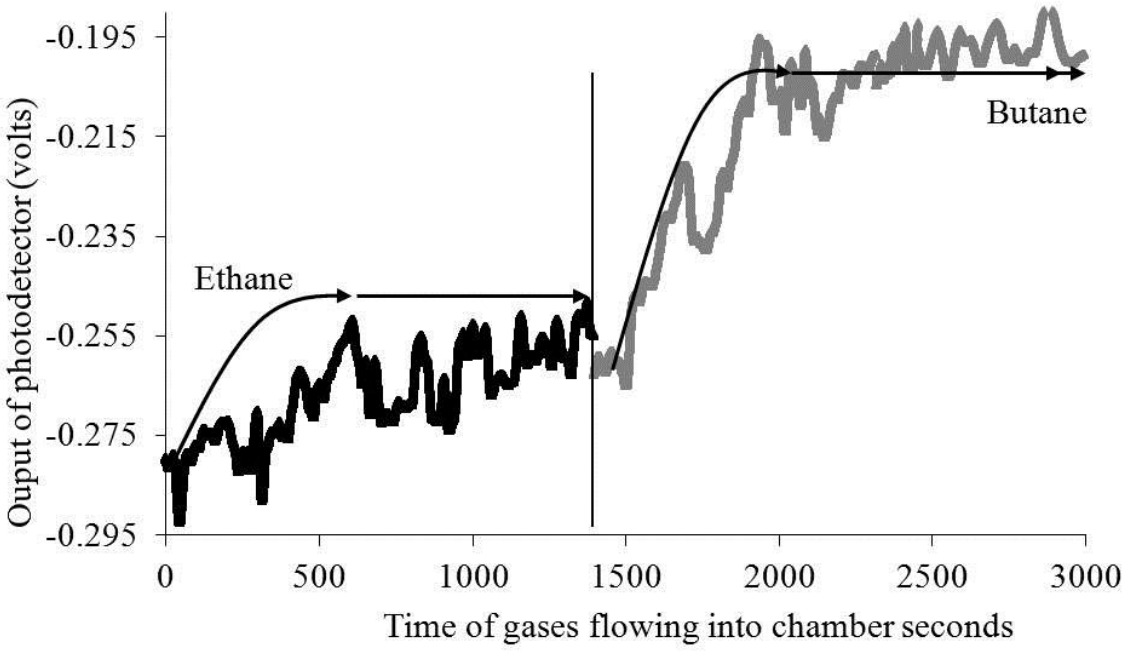

Figure 6-8 showing the change in output from the photo-detector for both Ethane and Butane with flow rates of 0.5 litres/second for the platinum coated device

With continuous gas flow, there is a point where the gas under consideration will push out the entire previous gas. This means the chamber will be filled with only one type of gas under consideration. This point is clearly shown in Figure 6-8 where the voltaic change stops and the signal variation is only due to noise. For different flow rates the time it takes to reach this equilibrium point will be different, with quicker flow rates taking less time. This is confirmed in Figure 6-9 showing 4 different flow rates for Butane gas. Butane was chosen since it gave the largest shift and easily distinguishable from the noise flow rates as high as 4 litres/second for Butane gas. Also shown in is the drift at around a time of 2000 sec which is probably due to polarisation changes, previously discussed. Using this setup and accounting for the noise the minimum concentration of Butane detectable is ~2% which equates to ~1881 ppm by volume. This value is an order of magnitude larger than the majority of the literature [172, 174]. This shows the sensor will require a species specific element to improve its sensitivity. The high SRI sensitivity combined with a species specific element to increase analyte concentration at the sensor surface may be able to produce sensitivities on the same order of magnitude if not better.

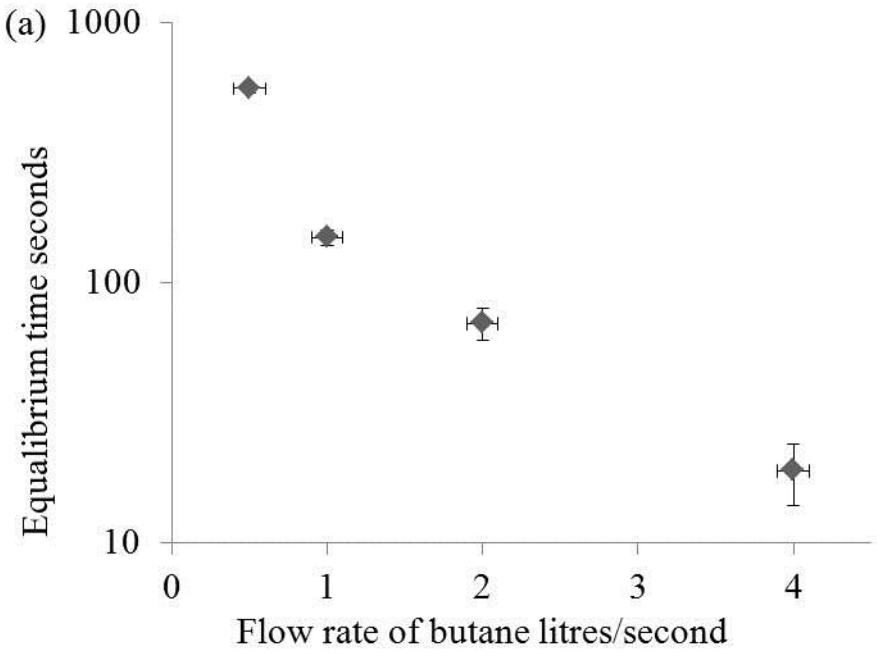

Figure 6-9 showing measured time for the platinum device it took for different flow rates or Butane to reach equilibrium inside the gas chamber

6.2.4 Summary of Gas sensing

Two LSPR fibre sensors with top coating of either silver or platinum were evaluated for application in gas sensing. The two types of sensors have shown capability to detect four different gases (methane, ethane, propane and butane) with different RI values by monitoring the changes either in wavelength or in amplitude of the SRP resonance. In comparison, the silver coated sensor performed better for amplitude detection while the platinum coated sample better for wavelength detection. The calculated maximum peak sensitivities were 1882.1dB/URI and 1493.5nm/URI for silver and platinum coated sensors, respectively, which are remarkably high for RI sensing in this exceptionally low RI range.

As the metal coated SPR fibre sensors are supposed to be used in room temperature environment, we have evaluated the temperature effect by heating the silver coated sensor from 22°C to 27°C and found the temperature fluctuation induced changes are so small

compared with the gas RI induced signal. Assuming a temperature fluctuation of ±0.5^{o}C and taking the platinum device as an example, this equates to only ~3% of the wavelength shift observed.

The flow rate of the gas examined and how that affected the sensor were also investigated. The gradual change between air, ethane and butane as the gases flowed into the chamber over time could be seen until an equilibrium time was reached. This equilibrium time can be measured and used to distinguish between different flow rates with the peak flow measured being 4litres/second. A detection limit of ~1881 ppm by volume is also reported which is an order of magnitude greater than the literature and shows that a species specific coating is required to increase the devices sensitivity.

6.3 Thrombin aptamer sensor

6.3.1 Introduction

In the field of biotechnology, two areas of growing interest are aptamers and optical sensors. Antibodies have been well established in industry as a standard for environmental, food and clinical analysis; however they do have some draw backs when dealing with multi-analytes or complex samples. As such aptamers have been explored as alternatives and have been investigated for applications as diagnostic assays[176] and biosensors[177, 178]. An application of aptamers is the detection quantification of human thrombin, which plays an important role in the coagulation of blood in the body. Several tests already exist that use spectrophotometers and fluorescent substrates [179], however these are bulky and take the concentration of thrombin throughout the whole body rather in the blood clotting area.

Fibre optics sensors using the evanescent field offer an alternative with the added advantage of in-vitro sensing possibilities. Through the use of SPR detection the sensitivity of the fibre optic sensors can be greatly increased, especially in the biological refractive index range. By coating the metal surface of a SPR sensor with aptamers it will create a species specific sensor with the ability to detect thrombin through a RI index change. The sensing RI change will be caused by either the attaching thrombin or the associated change in shape of the aptamer and thrombin combination. Three different sensor types were investigated with only one having the required sensitivity and this sensor has been subjected to buffer solutions with thrombin detection going as low as 10fM but with the potential of detecting even lower concentrations.

6.3.2 Experimental Preparation

The LSPR sensor was made from standard SMF-28 which was lapped down to within 10µm of the core. The lapped region was then coated with multiple layers consisting of germanium (48nm), silicon dioxide (48nm) and gold (38nm). Once the coating had been applied the sensing region was expose UV with a phase mask of 1.018µm. This created a surface perturbation on the gold coating causing the LSPR effect. The UV inscription and the LSPR effect from such a structure and are described in section 5.3.3 and will not be discussed here further.

To make the sensor species specific, an aptamer layer was attached to the sensing surface and this work was carried out by M. Mascini at the D Dipartimento di Chimica, Università di Firenze. The aptamer used was 5'- SH(CH2)6-GGT TGG TGT GGT TGG-3' and was attached to the metal surface using a thiol mediated linkage. aptamers are single strands of DNA, double strands of DNA form the helical shape that we are common with but this is not the case for the single strand aptamers. With the aptamers being only a single strand of DNA means there have unused charged bonds. With no other strands of DNA to interact

with the aptamer interacts with its own molecules and causes it to create a unique shape. This unique shape combined with the intermolecular charge gives rise to the aptamers species specific binding properties, similar to enzymes molecules.

The aptamer coated LSPR sensors were then placed in a ‘v’ groove made in metal plate which kept the sensor straight and in position. The sensing region was covered with a buffer solution which consisted of 50mM Tris 140mM NaCl 1mM $MgCl_2$, having pH 7.4. With the sensor in solution the transmission spectrum was first normalised, removing any variation inherent from the light source, and then maximized. The resonance maximization took place in buffer solution since its RI value would be closest to that of the thrombin solutions and gave the best sensitivity. The thrombin solutions were made by first making a large quantity at a high concentration and then diluting this solution down to the required smaller amounts of lower concentrations. This was the most accurate method to make the low concentration solutions and the procedure was carried out by Dr. Dave Negal, from the Aston school of life sciences, who was our collaborator. Using his expertise meant the solution concentration could be assured while removing any possibility of cross contamination of the solutions both before and during the experiment. The experiment was split into two parts. First, a 50mM HCl solution was used to strip the thrombin from the aptamer in conjunction with a light source ranging from 1220 to 1700nm. Secondly, a 2M NaCl stripping solution was implemented with a light source ranging from 900 to 1600nm. The gold coated top layer surface relief device had already shown to produce multiple resonances. As a result, two light sources were used to interrogate the sensor, so as many resonances could be examined. Through doing this, the chances of a finding the most sensitive resonance was increased.

6.3.3 LSPR sensor for aptamer/thrombin detection binding and stripping- Experiment I: Using 5mM HCl solution and light source with a range from 1220nm to 1700nm

The sensor was covered using a pipette with 1ml of the different concentrations of thrombin solutions, ordered as 1nM, 10nM, 100nM and 1mM. By initially using the lower concentrations the sensor would have its maximum sensitivity for the lowest concentration, since no thrombin would have been left on the sensor surface from a previous experiment. Also, if the stripping solution was unsuccessful the higher concentration of thrombin solutions would still give a response.

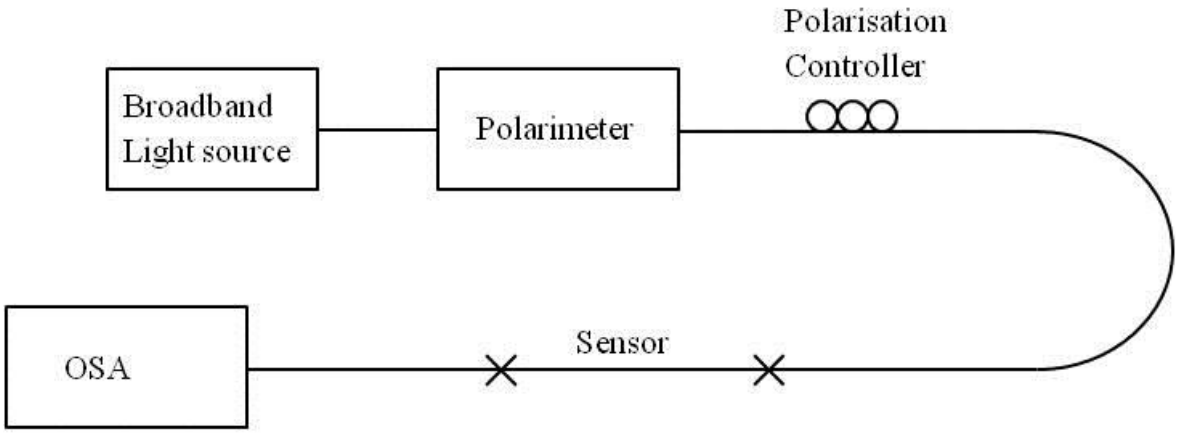

Figure 6-10 showing the experimental setup for the aptamers experiment

Before the sensor was covered with any solution the OSA was set to record the transmission spectrum. The advantages of this were twofold, if the reaction occurred quickly any shift would not be missed and also it gave an obvious point in data analysis of when the solution was applied. The recording of the spectra in experiment lasted 20 minutes which allowed for the full thrombin/aptamer binding to take place. The thrombin solution was then removed from the surface of sensor using a pipette. The 5mM HCl stripping solution was applied, again using a pipette, and left for 5 min. After 5 min the stripping solution was removed from the fibre surface and a fresh quantity of stripping

solution was applied and left for a further 5 min. By applying the stripping solution twice any reacted stripping molecules were removed and the concentration of the solution was maintained. This gave the maximum chance for the removal of the thrombin from the aptamer. Again, using a pipette the second stripping solution was removed and the fibre was washed twice using the buffer solution. This washed away any removed thrombin or unused stripping solution and was checked by seeing if the spectrum had moved back to the original starting position. A higher concentration of thrombin solution was then applied to the sensor, with the whole process repeating itself for all concentrations of thrombin solution.

Before the aptamer coated sensors were exposed to any thrombin the transmission spectrum was recorded and examined. The sensor before the aptamer coating produced 4 resonances with a surrounding RI of 1.36, as shown in Figure 6-11(a). It was believed that the multiple resonances in the wavelength range would give the maximum probability of a response after the aptamer coating had been applied. However, after the coating only the edge of a single resonance could be found Figure 6-11(b). The edge was located at 1220nm, which coincided with the limit of the light source available at that time in the laboratory. However by monitoring the change of this resonance edge, the aptamer sensing function was still able to be examined.

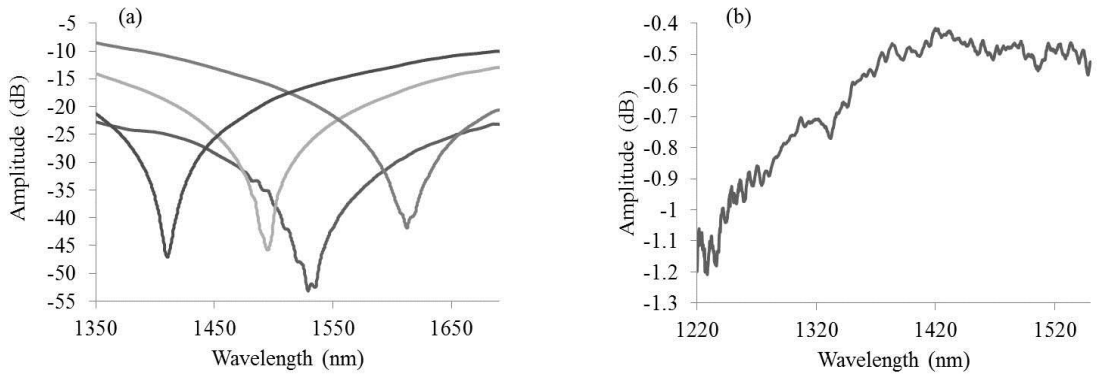

Figure 6-11 showing the transmission spectral response for the multilayer gold surface relief grating before (a) and after (b) aptamer Coating

LPG and SPR sensors have spatial extensions much larger than sensors utilizing LSPR. This means their electric fields extend past the sensing region (i.e. the aptamer coating) and into the buffer solution. Any change in RI from thrombin attaching to the aptamer would be decreased for LPG and SPR sensors because of this effect. LSPR sensors, having a much smaller spatial extension, primarily see the aptamer and the full effect of thrombin attachment. The large shift in resonance, before and after aptamer coating, suggest that the spatial extension of the sensors electric field is very small and adds further evidence that this sensor is using LSPR as the sensing mechanism.

Due to the broad nature and the changing shape of the LSPR peak, a centroid method has been found to give the best results and as such has been implemented here to evaluate the thrombin binding effect.

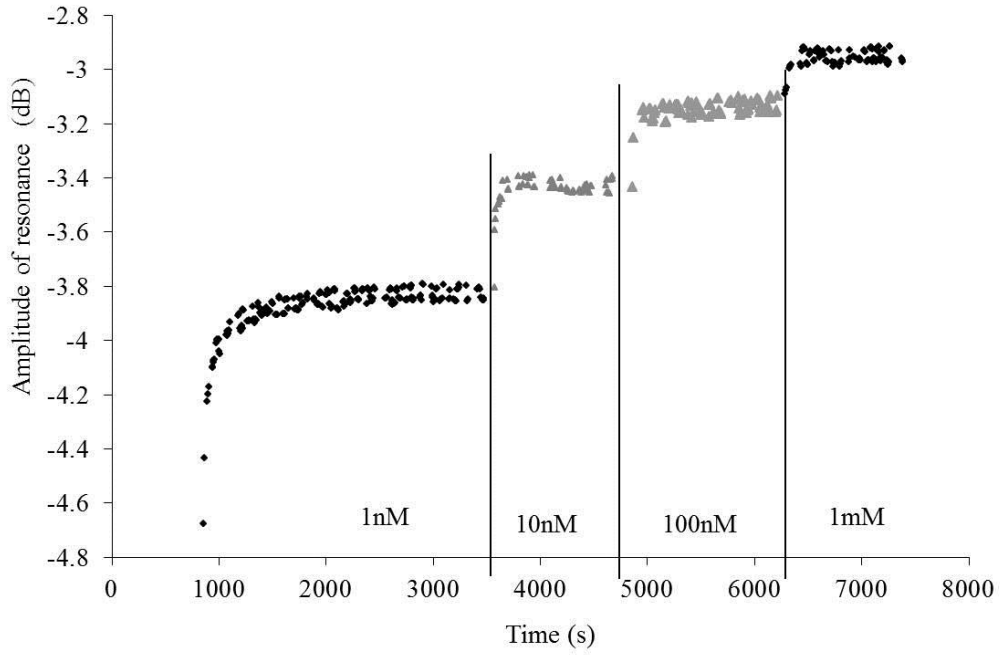

Figure 6-12 showing the change in optical power of the resonance for the aptamer coated LSPR sensor

Looking at the amplitude response, the change due to the binding of the thrombin to the aptamer is obvious especially with the 1nM thrombin solution. As the thrombin binds to the aptamer the optical power rapidly changes, decreasing until equilibrium is reached, where the power change stabilises. This response is similar in characteristic to commercial

SPR bio-sensors and shows the high sensitivity of the fabricated device. With the higher concentration of thrombin solutions it is apparent that the stripping solution of 50mM HCl is failing to remove the thrombin from the aptamer. This is shown in Figure 6-12 where each concentration of thrombin solution continues on from where the previous concentration left off. The starting amplitude for each concentration is approximately the final amplitude of the previous which is because the amplitude reported is absolute and not relative. It also corresponds to the HCL solution failing to strip off any of the thrombin. Despite this, since higher concentrations were used, the equilibrium between the aptamer and thrombin is different for each solution, with higher concentration solutions 'forcing' more thrombin onto the surface of the sensor. This means the maximum change for each concentration could be measured, even if the full transition may not be possible. What is encouraging is that each concentration still shows the characteristic response of a Surface Plasmon Biosensor. The 1nM solution induced amplitude change of about 1dB which is above the level of noise and shows promise for the sensing working at lower concentrations.

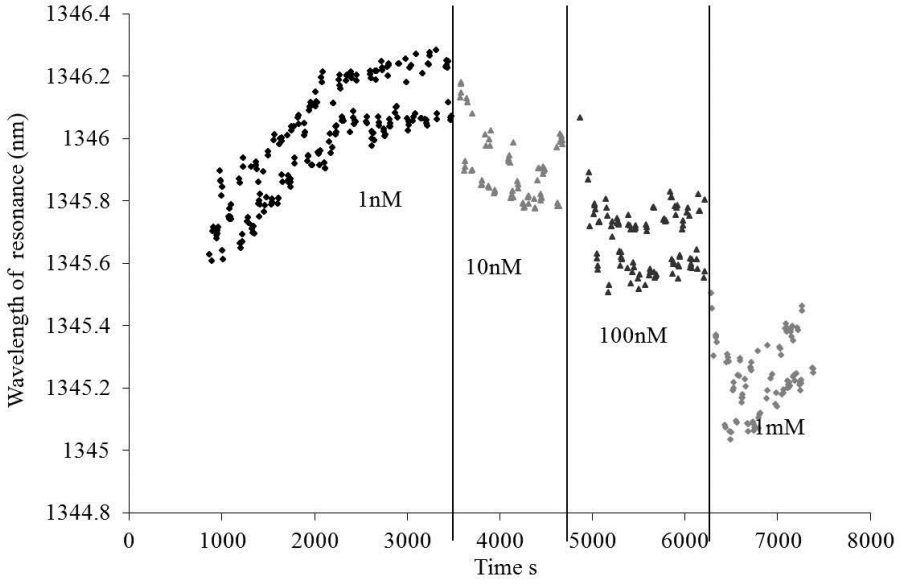

Figure 6-13 showing the change in wavelength of the resonance for the aptamer coated LSPR sensor

Taking the same data but analysing it for wavelength response gives the results shown in Figure 6-13. Straight away it is obvious that the wavelength response is not as good as the amplitude response. This issue is caused by the resonance being located out of the range of the broadband light source. Only a small section of the resonance could be analysed, meaning the resolution for the change in wavelength is greatly decreased since the peak of the resonance was unavailable. This affected both the amplitude and wavelength response, with the greater limitation on the wavelength. Thus, with a light source with an output extending to the shorter wavelength range, the sensitivity of the system can be improved and this will be discussed later in a different experiment. The experimental setup was incapable of measuring the transitional steps of the thrombin/aptamer interaction. However, it was capable of showing the step changes between concentrations and the overall trend with increasing concentrations giving a decrease in resonance wavelength.

Using the 1nM concentration solution as a zero point, since it is the only concentration unaffected by previous experiments, and plotting the relative maximum change between different concentrations for both the amplitude and wavelength an idea of the sensitivity limit of this setup can be evaluated and this is shown in Figure 6-14. However, the linear relationship shown is merely an indicator. The true response at lower concentrations is not known since the limiting factor of detection (the aptamers or the sensor) is yet to be established and requires further investigation.

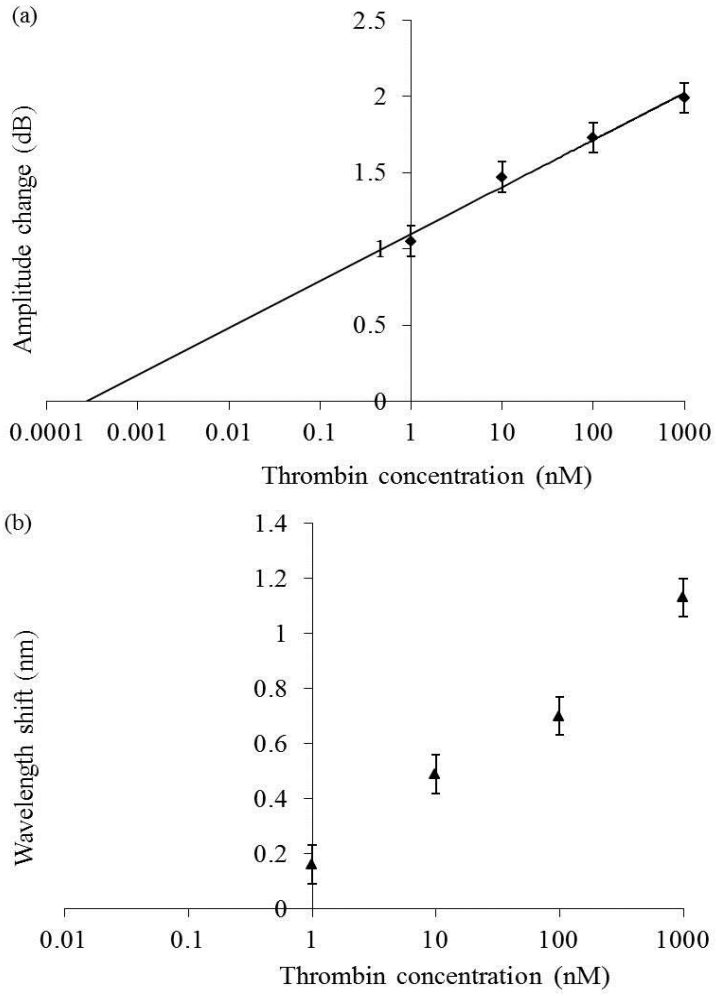

Figure 6-14 comparison in change in amplitude (a) and wavelength (b) of the resonance for different concentration of aptamer solutions using 1nM as the zero point

As expected, the wavelength response shows that with this setup the sensor is near its detection limit, hence no extrapolation needs to be plotted. The amplitude is quite different showing a linear fit, which seams consistent with the results gathered. A conservative estimate of being able to distinguish transitional steps of around 0.2 dB gives the detection limit possible as low as 1fM. Since the stripping solution was no effective and light source was not suitable to view the change in full range, the experiment was repeated using a different light source and NaCl as the stripping solution, which is discussed in the following section.

6.3.4 LSPR sensor for aptamer/thrombin binding and stripping- Experiment II: using a 2M NaCl solution and a light source with a range from 900nm to 1600nm

The experiment was repeated using the same setup as described in section 6.3.2, however the light source used had a much broader range from 900 to 1600nm and a much higher concentration solution of 2M NaCl was used for thrombin stripping. The HCl acid was of a much lower concentration because it was believed that anything higher may have damaged the metal layer. This low concentration was obviously insufficient, lacking the overall bulk charge needed to effect the intermolecular interactions of the aptamer. The NaCl, being just a salt solution should not damage the metal layer and as such the higher concentration was used. The experiment was repeated 4 weeks later but the sensors were kept refrigerated and stored in buffer solution. Despite this long delay the aptamers on the sensor surface were still found to be functional, meaning the sensors are durable when kept in the correct conditions. The original Agilent light source, with a range of 1220-1700nm, was replaced by a tuneable fianium laser which was capable of outputting light down to 900 nm. The transmission spectrum of this laser was inherently less smooth and hence noisier when normalised. However due to its wide range and high power output overall the light source gave a better performance. The transmission spectrum of the LSPR sensor excited by this new light source is shown in Figure 6-15, despite the noisy appearance the resonance is clearly visible at approximately 1250nm and amplitude of 40dB. This is closer to the resonance strength of the original pre aptamer sensor, compared to only1dB using the previous light source, shown in Figure 6-11(b). The resonance is located at 1250nm which is at a slightly longer wavelength than in the previous experiment. This is probably due to a slight change in the orientation of the fibre causing a different polarisation response.

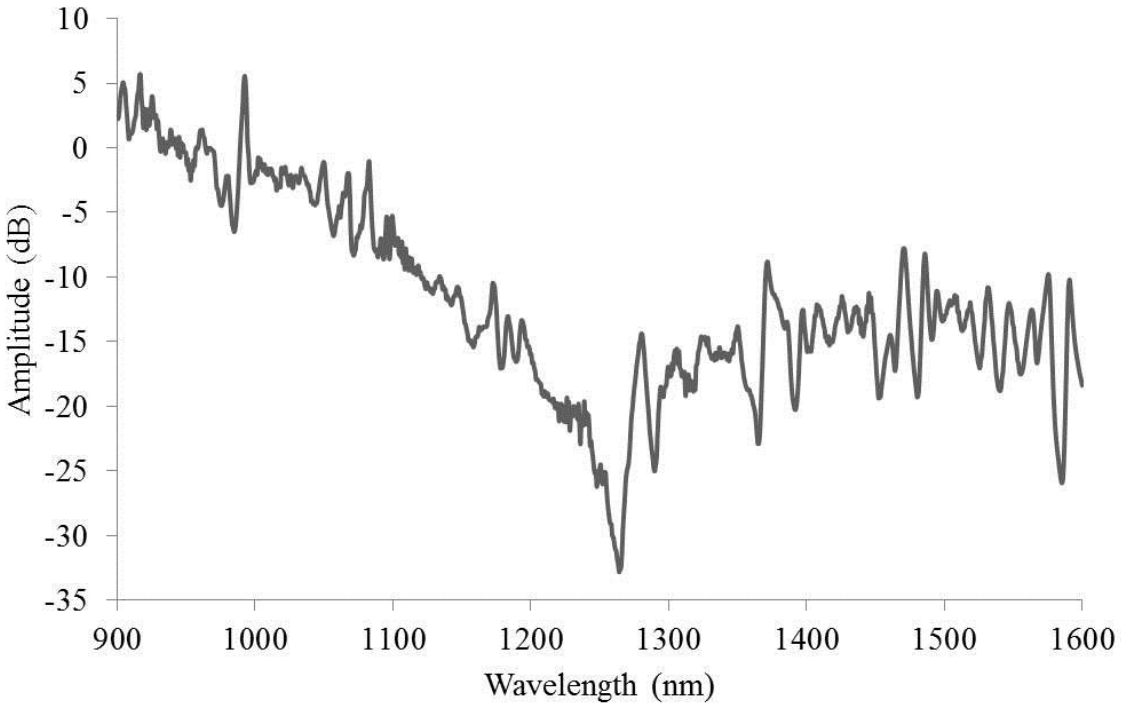

Figure 6-15 showing the full transmission spectrum for the sensor going as low as 900nm

To ensure the thrombin was being removed by the NaCl stripping solution, the spectral evolution of the process was recorded for viewing any changes, as shown in Figure 6-16. The circled regions represent the strength and location of the resonance before the stripping solution was applied using a pipette. This means no confusion could take place between the application of the solutions and the stripping process. From Figure 6-16 it can be seen that the process takes a while to start but once reached, it is fairly rapid taking place in only a few seconds before an equilibrium state is achieved.

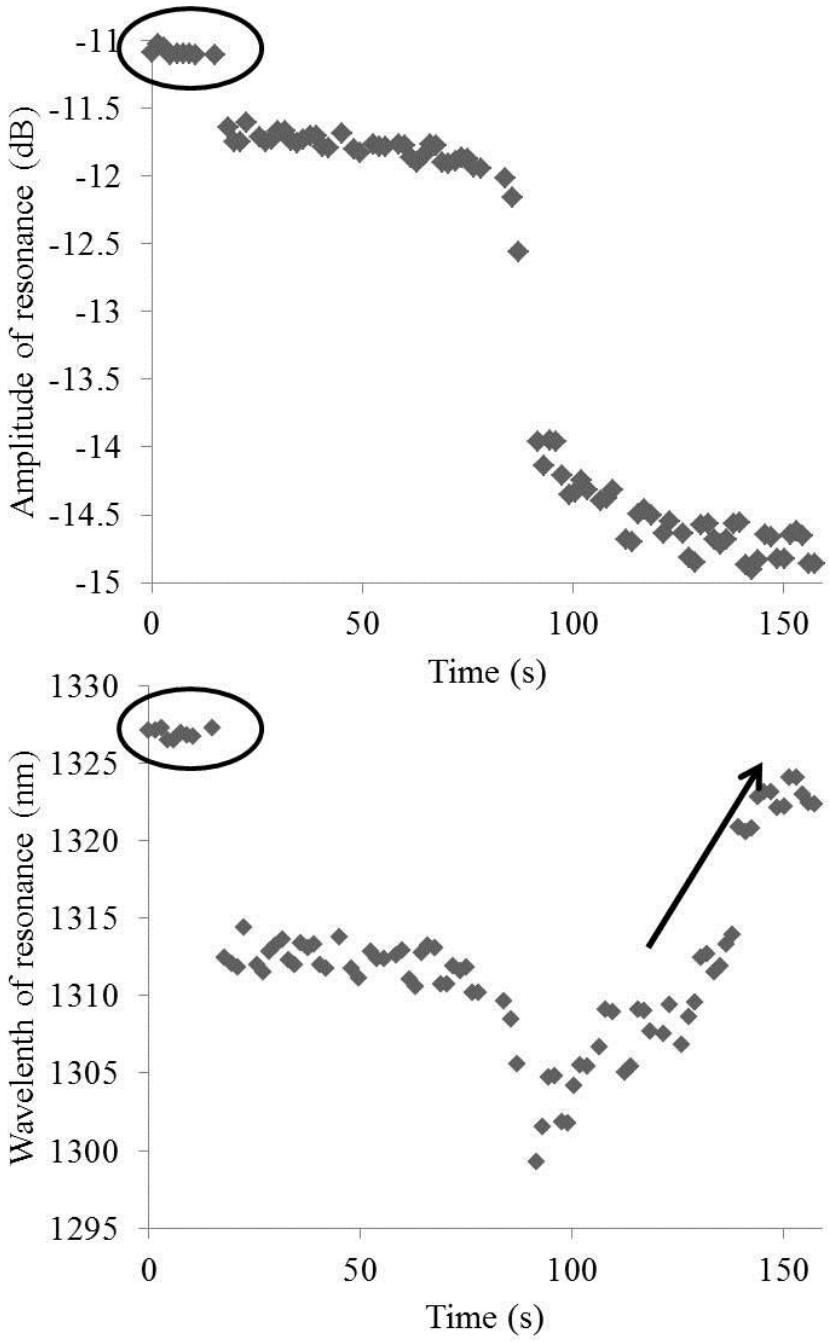

Figure 6-16 showing the response of the sensor to the NaCl stripping solution for both the amplitude (top) and the wavelength (bottom) of the resonance

The thrombin stripping by the NaCl solution created a decrease in amplitude with increasing time. This is the opposite of the binding experiment, so clearly shows the stripping solution is removing the thrombin from the aptamer. The wavelength response matches the trend displayed by the amplitude with appropriate shifts coinciding with the same time scale as the amplitude response. The transitional steps of the process are now evident, where they were not shown in the experiment using HCl as the stripping solution.

There is a drift for the wavelength, shown by the arrow in Figure 6-16, but not for the amplitude and this is probably due to the noise of the source. The overall amplitude change was about 4 dB and this large change can be explained by the increase in sensitivity of the system due to using a much better light source. Also, in the previous experiment, a high quantity of thrombin had been attached on the surface of the fibre meaning a large amount of thrombin was removed.

After the thrombin had been stripped from the surface of the LSPR sensor, a thrombin solution of 10fM was used to cover the sensor. This was chosen since it should have been below the detection limit and used to establish the sensitivity limits of the sensor experimentally. However, this was found not to be the case, as shown in Figure 6-17. The amplitude change still gave a step change of approximately 0.7dB while also maintaining the sensor's ability to show the transitional steps. There is more noise in the system, but despite this the characteristic curve of a binding molecule response is still obtained, (i.e. initial rapid response to an equilibrium level where saturation of the aptamer has occurred). Now the full spectral feature of the resonance is available for analysis the wavelength response mirrors that of the amplitude. The characteristic curve is again obtained, showing the transitional steps, while the step wavelength change is approximately 10nm. The noise for the wavelength was ±2nm, which means if a less noisy light source was available the resolution and hence sensitivity could be greatly improved. The noise for the amplitude was ±0.08dB and using assuming a minimum distinguishable amplitude change of about 0.4dB means the sensor had not yet reached its limit of detection and has further scope for investigation.

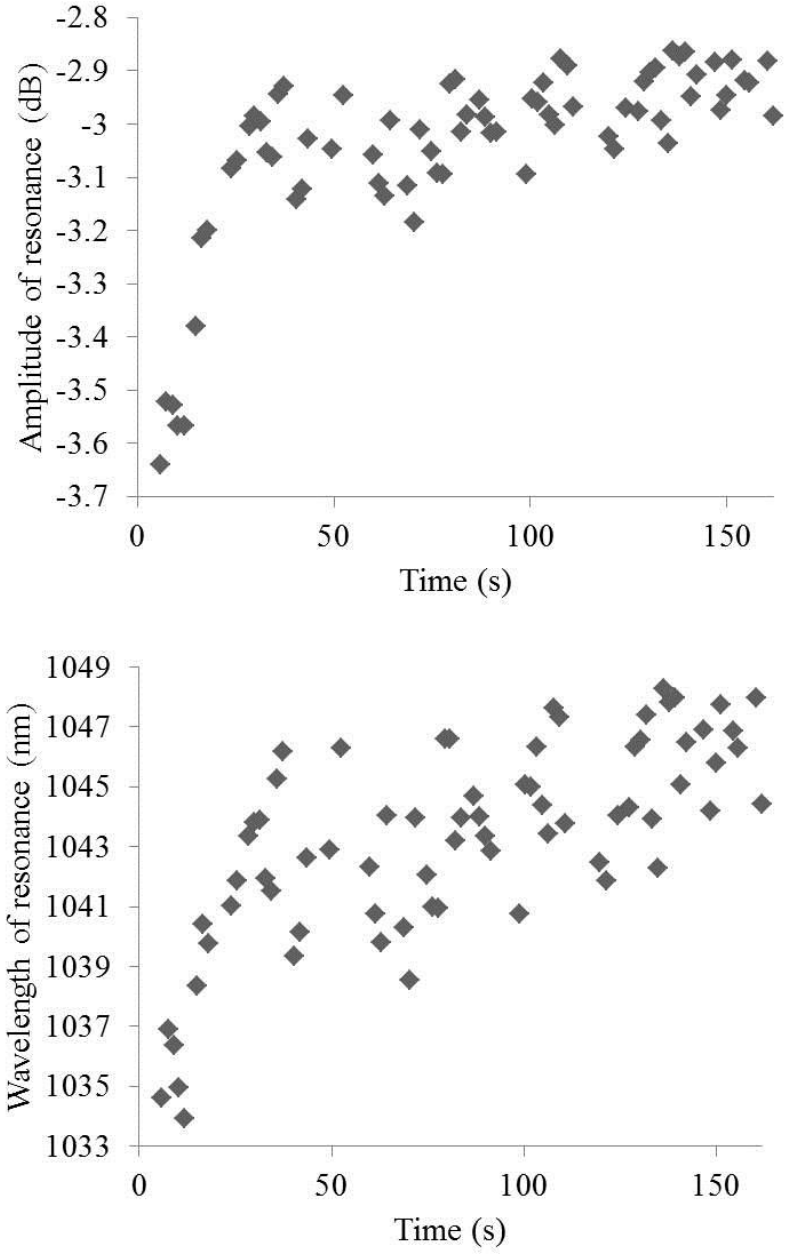

Figure 6-17 showing the sensors response for a 10fM solution of thrombin for amplitude (top) and wavelength (bottom)

Unfortunately, during the cleaning process of the sensor, the fibre was broken and the binding and stripping experiments with different concentrations could not be investigated. However, some further conclusions could still be drawn. It is reported that localised surface plasmons have a higher response than standard surface plasmon resonances. The single layer Gold Bragg grating, whose sensing function is based on standard SPR effect and described in a previous section, was also coated with aptamers and investigated for thrombin detection. This device was unable to yield results for even higher concentrations

of thrombin. Coupled with the large change in transmission response after aptamer coating, this adds further evidence that the surface relief sensor operates using LSPR and not the standard SPR.

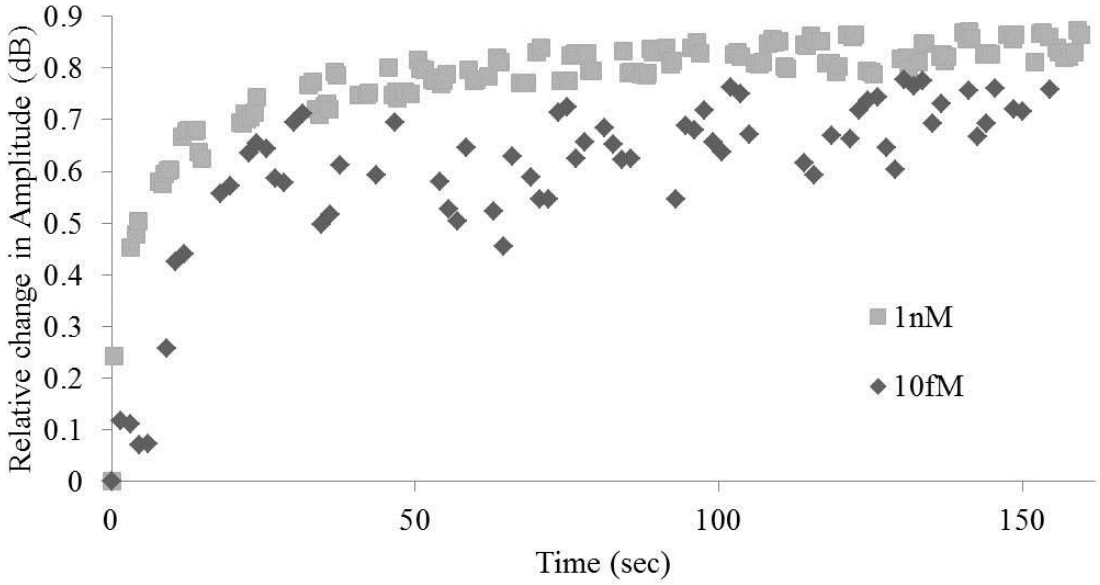

Figure 6-18 showing the amplitude response between the two concentrations of 1nM (a) and 10fM (b) with HCl and NaCl as the stripping buffer respectively.

Comparing the two amplitude results of the 1nM thrombin solution from Experiment I and the 10fM from Experiment II and plotting them results in Figure 6-18. Although the sensitivities for each experimental setup are different some conclusions can still be drawn. The responses are similar meaning that with a less noisy light source the detection limit could possibly 3 orders of magnitude lower 0.00001nM. Despite the sensitivity difference, the lower concentration of thrombin takes longer to reach equilibrium and the amplitude steady state is lower than the 1nM thrombin solution, which is to be expected

It is typical for binding experiments to calculate the binding association and disassociation constants. This will give a numerical value on how well the aptamer coating is performing. One of the ways to calculate this is to use Pseudo First order kinetics. This is different from standard association binding experiments, which are calculated using the measured the disassociation constant, which was beyond the initial scope of the experiment. Despite

this, the pseudo first order kinetic approximation is quite adequate for producing a comparable numerical value.

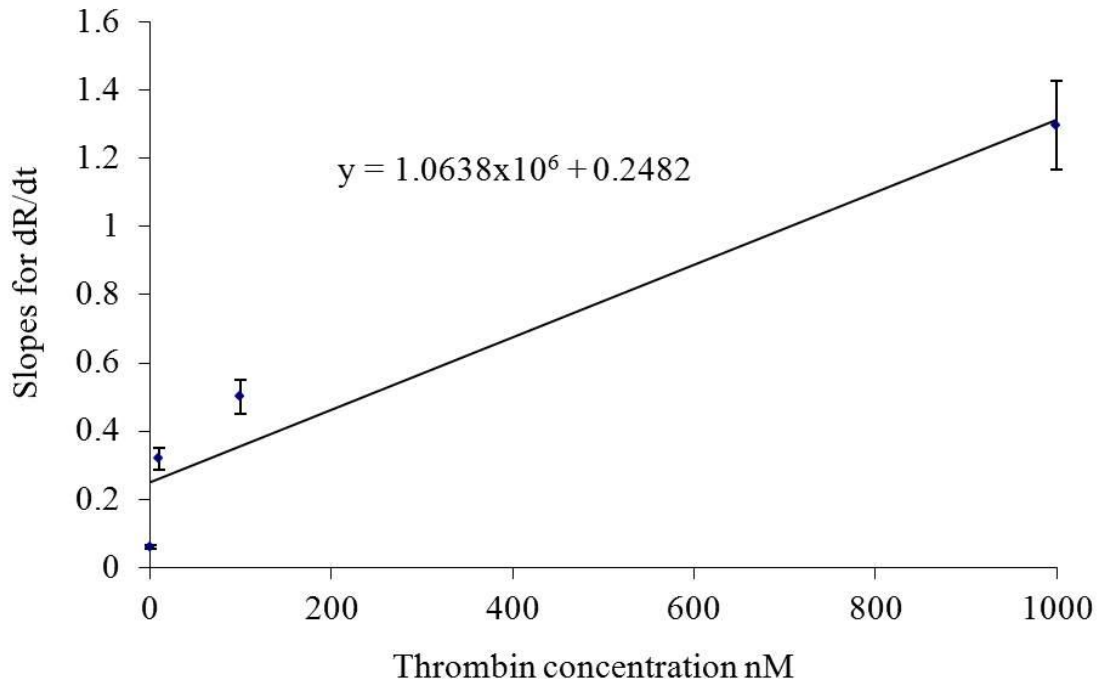

Figure 6-19 showing the calculation of the association and disassociation constants from the thrombin /aptamer binding amplitude data

Calculating the rate until equilibrium has been achieved for each concentration and plotting them gives the results in Figure 6-19, where the gradient of the plot gives the association constant and the intercept to the y-axis gives the disassociation constant and these values are in summarised in Table 6-2 with other bio-sensing methods for comparison. The system here compares well with the BiaCore literature as giving similar results within an order of magnitude. There is obviously a large variation between techniques, the electrical impedance technique for example, and all will depend upon the aptamer coating quality and sensor response. However, taking the sensor produced in this work, it has a comparable large Association constant, showing the supporting the strong selectivity and binding strength of the aptamer. This assists the optical fibre sensor in having such a good performance and low detection limit.

Technique	Association Constant, $M^{-1}s^{-1}$	Disassociation constant, s^{-1}	Equilibrium Constant, M	Limit of Detection	Reference
Multilayer SPR Aptamer	$1.0638x10^{6}$	0.2482 s^{-1}	$4.29x10^{6}$	10fM	This work
Biacore SPR	$2.90x10^{5}$	$1.80x10^{-3}$	-	-	S. Davies application note 305, 1994
Florescence	-	-	$3.14x10^{8}$	0.14nM	W. Wang et al, analytical Biochemistry, 373, 213-219, 2008
Electrical Impedance	$6.7x10^{-3}$	$1x10^{-4}$	-	0.03nM	3X. Li, et al Biosensors and Bioelectronics, 23, 1624-1630, 2008

Table 6-2 showing the calculated association and disassociation constants for this work and comparison to other techniques

6.3.5 Summary of aptamer Sensing

Three different types of sensor were investigated for the detection of different thrombin concentrations using an aptamer coating. The multilayer type coated with, layers germanium (48nm), silicon dioxide (48nm) and gold (38nm), that had been post UV exposed to create a surface relief grating structures, was the only sensor found to have the required sensitivity. Coupled with the large shift of the resonance wavelength before and after aptamer coating, this fibre sensor has provided further evidence supporting the localised surface plasmon theory as the sensing mechanism

Two different stripping solutions were investigated for the removing of thrombin from the aptamer. To avoid damage to the metal surface layer, a weak 50mM HCl solution was used first and found to be inadequate. A second solution of 2M NaCl was capable of stripping the thrombin and with it being a salt solution no damage was found to be caused to the metal surface despite the high concentration.

The sensor was able to detect a wide range of thrombin concentrations, going as high as 1mM and as low as 10fM. The sensor was shown to be capable of giving analogous responses for both amplitude and wavelength, which could be used to show the different equilibrium rates for different concentrations. The association and disassociation rates were calculated to be $1.0638\times10^{6}Ms^{-1}$ and $0.2482s^{-1}$ respectively, showing the high selectivity and strength of the binding process of the thrombin to aptamer. This supports the existing work stating that aptamer could be a suitable alternative to enzymes. It also helps to explain the low detection limit of the sensor.

7 Conclusions

The response of LPGs of various periods has been investigated and through monitoring the wavelength shifts of the attenuation peaks, their response to increasing SRI has been characterised. From this, we found that the relative wavelength shift of the LPG attenuation peak is dependent on both the grating period and the SRI. In this work, the most SRI sensitive LPG in the wavelength range of 1250 nm to 1700 nm has been found to be the LPG of period 160 μm and it is a dual resonance LPG. Dual resonances of LPG are due to the core mode coupling to a cladding mode very close to the dispersion turning point, thus producing two attenuation peaks associated with a single mode. With both attenuation peaks situated around the dispersion turning point, the LPGs are highly sensitive to any SRI changes and it is this make the LPG of 160 μm period showing the highest sensitivity among all investigated LPGs in this work.

The large angle TFG was found to behave similarly to an LPG with coupling light from the core mode to the co-propagating cladding modes. Several differences are also apparent for the large angle TFG. Firstly, the large angle TFG couples to higher order cladding modes with the transmission attenuation peaks disappearing with an SRI of ~1.41 much below the cladding index while the LPG attenuation peaks disappear at an SRI of ~1.45 close to the cladding index. The large angle TFG modes disappear at lower SRI than those of an LPG clearly shows that the modes are being coupled to have lower effective indexes and are higher order modes. Secondly, due to the tilt and resultant non-uniform nature of the induced index perturbation within the core of the fibre, large angle TFG is intrinsically polarisation sensitive and gives rise to split peaks.

To increase the sensitivity of the co-propagating cladding mode coupling of grating devices, two methods were implemented. Firstly, the large angle TFG devices had their

claddings etched using HF acid and the sensitivity increase from reducing cladding radius matched well with that of the theory. The peak sensitivity of an 81^{o} TFG was 506.9 nm/URI over the RI range 1.36 to 1.40, which was an improvement over even the dual resonance LPG of period 160 μm. Secondly, LPGs of various periods were coated using a dipping method combined with a sol-gel porous coating. Through doing this, the cladding regions of the LPGs were coated with a high RI material of TiO_2. By doing this, the effective indexes of the cladding modes were increased which in turn increased the sensitivity of the coated LPG, compared to the uncoated LPGs. The work supported the theory of there being an optimum coating thickness however, due to poor control over coating thickness the actual optimum could not be found experimentally. Despite this the maximum sensitivities for the sol gel coating LPG were comparable to that in the literature while the coated dual resonance LPG sensitivity increase was observed and reported to be 1458nm/URI, which was better than non dual resonance LPGS (coated and uncoated) and a dual resonance of LPG of the same period uncoated.

LPGs induced using a femtosecond laser inscription technique were investigated and found to produce non uniform index perturbation within the core of SMF fibre. This non-uniformity allows the femtosecond LPG to couple to multiple sets of cladding modes with different azimuthal orders compared to the one cladding mode azimuthal set normally with UV induced gratings. This led to more attenuation peaks in transmission spectrum of the femtosecond grating, compared to the UV gratings. The femtosecond LPGs were also found to be capable of coupling to both higher and lower order cladding modes simultaneously for a fixed period. The non-uniformity of the index perturbation also resulted in a polarisation response for the femtosecond LPGs which was most evident for LPGs with longer periods, due to their lower sensitivity.

Through comparison of the SRI sensitivities of the femtosecond LPGs with various periods, there is evidence to suggest that a dispersion turning point exists for a set of

cladding modes had been found experimentally between two LPGs of periods 320 μm and 400 μm. It was observed that these two femtosecond LPGs both blue and red wavelength shifts of the attenuation peaks for increasing SRI. Through monitoring the relative opposite shifts of two attenuation peaks, a far greater SRI sensitivity could be produced, compared to monitoring a single attenuation peak. Utilising this method, the maximum sensitivity was produced by a femtosecond LPG of period 400 μm with a value as high as 1680 nm/URI.

Two SFBGs were produced using femtosecond laser inscription that had different low frequency modulation periods. Both SFBG produced three reflection peaks with the strongest being centrally located between the three peaks. We have shown that through controlling of the low frequency modulation period, the spacing of the three reflection peaks can be either increased or decreased and the reflection peaks spacing agrees well with the predicted theory from the coupled mode equations. The SFBGs were shown to be highly polarisation dependent and this was deduced to be either from the non-central location of the index perturbation within the core of the fibre or the shape of the index change which is inherent problem associated with SFBG. The two devices produced a linear temperature response, with increasing temperature the central wavelength location of reflection peak red shifted. The sensitivities produced were 11.6 pm/^{o}C and 11.5 pm/^{o}C for the SFBG-1 and SFBG-2 devices, respectively, which was comparable to similar devices in the literature.

A hybrid device consisting of both an SFBG and an LPG element was formed using a two-step femtosecond inscription process. This process created a device which had both SFBG reflection peaks and LPG attenuation peaks. The increased noise from the dual inscription 'swamped out' the other reflection peaks, leaving only the strongest central peak. Utilising the hybrid characteristics of this device, both the temperature response of the reflection peaks and the SRI response of the attenuation peaks were characterised. The LPG element

also produced 2 attenuation peaks that were capable of detecting SRI changes (5 nm/URI) and this coupled with the linear temperature sensitivity (11.2 pm/^{o}C) of the SFBG reflection peak produced a dual parameter sensing device. Though the device was not as sensitive as previously reported ones there is scope for increased sensitivity using different periods of LPG inscriptions.

Three different SPR devices were fabricated and their responses to SRI were characterised. Both the single and multilayer coated TFG sensors operate on a sensing mechanism utilising SPR and the mechanism for the out-coupling of light was discussed. The third type of device utilised a post UV exposing procedure which created a surface relief structure on the sensor. The UV post exposing aided the out coupling of light from the core to the metal layer and the possible explanations for this were discussed. It also formed a discontinuous surface which could no longer support SPRs and as a result, it changed the sensing mechanism to LSPR. Three different metals were implemented for the top LSPR sensing layer. Each LSPR was found to have far greater SRI sensitivity than the coated TFG structures while also the silver and platinum metals were found to produce resonances in air. The gold surface relief device was found to have the highest sensitivity producing a 2112.5 nm/URI response in an SRI range of 1.3 to 1.38.

Due to both the silver and platinum surface relief devices producing resonances in air, their ability to operate as gas sensors was investigated. Both devices were found capable of detecting the minute SRI changes associated with different gasses with the peak sensitivities produced being 1882.1 dB/URI and 1493.5 nm/URI for silver and platinum, which are remarkable high for the SRI range under investigation. However, this only translated to a limit of detection of ~1881 ppm. This is a lot higher than other gas sensors reported and shows the need for a species specific element to increase the concentration at the surface of the sensor. The temperature response for the silver coated sensor was investigated and shown to produce smaller wavelength and amplitude shifts than those due

to the different gasses. The feasibility of the platinum coated device to act as a cheap gas flow sensor was investigated using a DFB laser and a fast response power meter. The change between different gasses could be observed while also the different equilibrium times of different flow rates could be calculated.

Due to the extremely high sensitivity of the gold coated surface relief sensor, it was immobilised with a thrombin sensitive aptamer and implemented as a biological thrombin sensor. Two stripping solutions were used and a 2 M NaCl solution was found to give the best results. The sensor was able to detect a wide range of Thrombin solutions ranging from 1mM to as low as 10 fM, though this is not the limit of detection for the sensor. Both the amplitude and wavelength shifts gave analogous responses and utilising this, the association and dissociation constants could be calculated. The association and disassociation rates were calculated to be 1.0638×10^{6} Ms^{-1} and 0.2482 s^{-1} respectively, showing the high selectivity and strength of the binding process of the thrombin to aptamer.

8 Future work

Many of the advances reported in this thesis are initial pieces of work and as such there is some scope for further development and understanding of the various devices. Potential work detailed below may be carried out in future.

The Sol-gel coating by its very nature is porous and this gives rise to two main areas of future work. Firstly, when attempting to conduct a non-specific biological binding experiment, it was noted that there was a wavelength shift associated with the water from the solution being absorbed into the porous sol-gel coating, through osmosis. As a result, the most sensitive coated LPG sensors may be investigated for humidity response. A large wavelength shift of the attenuation peak was observed for a humidity of 90%. Through control of the coating parameter and hence the porous properties of the coating, the Sol-gel coated LPG sensor has the possibility of operating as a humidity sensor. Secondly, through incorporating an enzyme, aptamer of other specific binding substance into the Sol-gel mix, the sensitivity to biological compounds may be further increased and as such it deserves some investigation. Even if the sensitivity of the LPG coated sensor is found to be insufficient, coating an SPR of femtosecond LPG sensor with a species specific Sol-gel coating may yield desirable results.

The femtosecond LPG and SFBG have yielded exciting results, however one of the major drawbacks is the polarisation sensitivity of both devices. A more thorough investigation through modelling and a systematic examination of the laser power and index perturbation within the optical fibre core should be completed. This will allow the correct selection of period and location for the highest sensitivity with the lowest polarisation response for both types of devices and possible stronger reflection peaks for the SFBG. Further techniques for the inscription of SFBGs should be investigated to see if an apodisation

could be introduced. Through the introduction of an apodisation, the sinc function defining the reflection peaks strengths could be removed and allowing for all reflection peaks to have similar strengths. This would be very desirable for multiplexing and also possible future applications in photonic computing.

One of the main hindrances of the both the SPR and LSPR work was that the experiments were run for the first time. As such, there is further work to undertake to fully understand what is occurring. Firstly, a detailed investigation of the coupling mechanism needs to be looked at using a comparison experimentally between low polish quality lapped D-shaped fibre and a more high quality polished D-shaped fibre. This would allow us to assess the role of the micro fractures of the lapping technique in the coupling mechanism. Also, an examination of the D-shape fibre surface before coating and after UV exposure, with the coating removed, would allow us to see to some extent that the semi-periodic UV germanium exposure plays in light coupling.

Once the coupling mechanism has been investigated, the properties of the LSPR need to be modelled. One of the common methods of LSPR modelling in the literature is rigorous coupled mode analysis and this would allow for the coatings to be optimised and more repeatable on an industry scale. The modelling is made difficult through the semi-periodic nature of the UV exposure, if a femtosecond laser was used to periodically ablate section of the metal sensing surface, a more modelling friendly and repeatable structure could be produced. Also, by embedding the D-shape fibre SPR sensors in a glass substrate, the polarisation sensitivity would be minimised and the robustness of each device greatly increased.

Finally, the aptamer experiment yielded some of the best results contained in this work, however, with the advances made in this thesis, the results could yet be improved upon. Through the use a smoother and more powerful light source in the desired wavelength

range, the minimum concentration detectable could be further increased with a better resolution. Also, with proper modelling, the sensor could be designed to produce a resonance located at about 1550 nm. This would allow the use of a cheap DFB laser and open up the possibility for a cheap and robust thrombin sensor, and this would be similar to the gas flow test investigated for other LSPR sensors.

9 References

[1] K. D. Simmons, S. LaRochelle, V. Mizrahi, G. I. Stegeman, and D. L. Griscom, "Correlation of defect centers with a wavelength-dependent photosensitive response in germania-doped silica optical fibers," *Opt. Lett.*, vol. 16, pp. 141-143, 1991.

[2] H. Kawazoe, "Effect of modes of glass-formation on structure of intrinsic or photon induced defects centered on III, IV or V cations in oxide glasses," *Journal of Non-Crystalline Solids*, vol. 71, pp. 231-243, 1985.

[3] T. Tsai, x, Ein, D. L. Griscom, E. J. Friebele, and J. W. Fleming, "Radiation induced defect centers in high purity GeO<inf>2</inf> glass," *Journal of Applied Physics*, vol. 62, pp. 2264-2268, 1987.

[4] R. Kashyap, J. R. Armitage, R. Wyatt, S. T. Davey, and D. L. Williams, "All-fibre narrowband reflection gratings at 1500 nm," *Electronics Letters*, vol. 26, pp. 730-732, 1990.

[5] K. S. Chiang, M. G. Sceats, and D. Wong, "Ultraviolet photolytic-induced changes in optical fibers: the thermal expansion coefficient," *Opt. Lett.*, vol. 18, pp. 965-967, 1993.

[6] B. Poumellec and et al., "The UV-induced refractive index grating in Ge: ##IMG## [http://ej.iop.org/images/0022-3727/29/7/019/toc_img1.gif] preforms: additional CW experiments and the macroscopic origin of the change in index," *Journal of Physics D: Applied Physics*, vol. 29, p. 1842, 1996.

[7] P. J. Lemaire, R. M. Atkins, V. Mizrahi, and W. A. Reed, "High pressure H₂ loading as a technique for achieving ultrahigh UV photosensitivity and thermal sensitivity in GeO₂ doped optical fibres," *Electronics Letters*, vol. 29, pp. 1191-1193, 1993.

[8] G. Bai-Ou and et al., "Growth characteristics of long-period gratings in hydrogen-loaded fibre during and after 193 nm UV inscription," *Measurement Science and Technology*, vol. 12, p. 818, 2001.

[9] R. R. Gattass and E. Mazur, "Femtosecond laser micromachining in transparent materials," *Nat Photon*, vol. 2, pp. 219-225, 2008.

[10] T. Brabec and F. Krausz, "Intense few-cycle laser fields: Frontiers of nonlinear optics," *Reviews of Modern Physics*, vol. 72, p. 545, 2000.

[11] C. B. Schaffer and et al., "Laser-induced breakdown and damage in bulk transparent materials induced by tightly focused femtosecond laser pulses," *Measurement Science and Technology*, vol. 12, p. 1784, 2001.

[12] C. Schaffer, N. Nishimura, E. Glezer, A. Kim, and E. Mazur, "Dynamics of femtosecond laser-induced breakdown in water from femtoseconds to microseconds," *Opt. Express*, vol. 10, pp. 196-203, 2002.

[13] M. Sakakura and M. Terazima, "Initial temporal and spatial changes of the refractive index induced by focused femtosecond pulsed laser irradiation inside a glass," *Physical Review B,* vol. 71, p. 024113, 2005.

[14] S. K. Sundaram and E. Mazur, "Inducing and probing non-thermal transitions in semiconductors using femtosecond laser pulses," *Nat Mater,* vol. 1, pp. 217-224, 2002.

[15] J. B. Ashcom, R. R. Gattass, C. B. Schaffer, and E. Mazur, "Numerical aperture dependence of damage and supercontinuum generation from femtosecond laser pulses in bulk fused silica," *J. Opt. Soc. Am. B,* vol. 23, pp. 2317-2322, 2006.

[16] E. N. Glezer and E. Mazur, "Ultrafast-laser driven micro-explosions in transparent materials," *Applied Physics Letters,* vol. 71, pp. 882-884, 1997.

[17] B. Malo, K. O. Hill, F. Bilodeau, D. C. Johnson, and J. Albert, "Point-by-point fabrication of micro-Bragg gratings in photosensitive fibre using single excimer pulse refractive index modification techniques," *Electronics Letters,* vol. 29, pp. 1668-1669, 1993.

[18] D. Z. Anderson, V. Mizrahi, T. Erdogan, and A. E. White, "Production of in-fibre gratings using a diffractive optical element," *Electronics Letters,* vol. 29, pp. 566-568, 1993.

[19] K. O. Hill, B. Malo, F. Bilodeau, D. C. Johnson, and J. Albert, "Bragg gratings fabricated in monomode photosensitive optical fiber by UV exposure through a phase mask," *Applied Physics Letters,* vol. 62, pp. 1035-1037, 1993.

[20] S. L. Mihailov, R. B. Walker, T. J. Stocki, and D. C. Johnson, "Fabrication of tilted fibre-grating polarisation-dependent loss equaliser," *Electronics Letters,* vol. 37, pp. 284-286, 2001.

[21] M. Jalie, *The Principles of Ophthalmic Lenses*, 4th ed. London: The Association of British Dispensing Opticians, 1992.

[22] J. Alonso and E. Bernabeu, "A method for the measurement of the refractive index of dielectric cylinders," *Pure and Applied Optics: Journal of the European Optical Society Part A,* vol. 6, p. 147, 1997.

[23] A. Yariv and P. Yeh, *Optical electronics in modern communications*. Oxford: Oxford University Press, 2007.

[24] T. Erdogan, "Cladding-mode resonances in short- and long-period fiber grating filters," *J. Opt. Soc. Am. A,* vol. 14, pp. 1760-1773, 1997.

[25] D. Marcuse, *Theory of Dielectric Optical Waveguides*. London: Academic Press Limited, 1974.

[26] Y. Liu, "Advanced fibre gratings and their applications," Doctor of Philosophy, Photonics, Aston University, Birmingham, 2001.

[27] T. Erdogan and J. E. Sipe, "Tilted fiber phase gratings," *J. Opt. Soc. Am. A,* vol. 13, pp. 296-313, 1996.

[28] K. S. Lee and T. Erdogan, "Fiber mode conversion with tilted gratings in an optical fiber," *J. Opt. Soc. Am. A,* vol. 18, pp. 1176-1185, 2001.

[29] A. Othanos and K. Kalli, Fiber Bragg Gratings-fundamentals and applications in telecommunications and sensing: Artech House Inc, 1999.

[30] G. Laffont and P. Ferdinand, "Tilted short-period fibre-Bragg-grating-induced coupling to cladding modes for accurate refractometry," *Measurement Science and Technology,* vol. 12, p. 765, 2001.

[31] S. A. Maier, *Plasmonics: Fundamentals and Applications*. New York: Springer, 2007.

[32] H. Raether, Surface Plasmons: on Smooth and Rough Surfaces and on Gratings. London: Springer-Varlas, 1988.

[33] E. Kretschmann, "Die Bestimmung optischer Konstanten von Metallen durch Anregung von Oberflächenplasmaschwingungen," *Zeitschrift für Physik A Hadrons and Nuclei,* vol. 241, pp. 313-324, 1971.

[34] J. D. Jackson, *Classical Electrodynamics*: Wiley, 1998.

[35] G. Mie, "Beitr\"{a}ge zur Optik tr\"{u}ber Medien, speziell kolloidaler Metall\"{o}sungen," *Annalen der Physik,* vol. 330, pp. 377-445, 1908.

[36] H. J. Patrick, G. M. Williams, A. D. Kersey, J. R. Pedrazzani, and A. M. Vengsarkar, "Hybrid fiber Bragg grating/long period fiber grating sensor for strain/temperature discrimination," *Photonics Technology Letters, IEEE,* vol. 8, pp. 1223-1225, 1996.

[37] V. Bhatia and A. M. Vengsarkar, "Optical fiber long-period grating sensors," *Opt. Lett.,* vol. 21, pp. 692-694, 1996.

[38] Y. Liu, L. Zhang, and I. Bennion, "Fibre optic load sensors with high transverse strain sensitivity based on long-period gratings in B/Ge co-doped fibre," *Electronics Letters,* vol. 35, pp. 661-663, 1999.

[39] L. Zhang, Y. Liu, L. Everall, J. A. R. Williams, and I. Bennion, "Design and realization of long-period grating devices in conventional and high birefringence fibers and their novel applications as fiber-optic load sensors," *Selected Topics in Quantum Electronics, IEEE Journal of,* vol. 5, pp. 1373-1378, 1999.

[40] Y. Liu, J. A. R. Williams, and I. Bennion, "Optical bend sensor based on measurement of resonance mode splitting of long-period fiber grating," *Photonics Technology Letters, IEEE,* vol. 12, pp. 531-533, 2000.

[41] H. J. Patrick, C. Chang, and S. T. Vohra, "Long period fibre gratings for structural bend sensing," *Electronics Letters,* vol. 34, pp. 1773-1775, 1998.

[42] H. J. Patrick, A. D. Kersey, and F. Bucholtz, "Analysis of the response of long period fiber gratings to external index of refraction," *Lightwave Technology, Journal of,* vol. 16, pp. 1606-1612, 1998.

[43] B. H. Lee, Y. Liu, S. B. Lee, S. S. Choi, and J. N. Jang, "Displacements of the resonant peaks of a long-period fiber grating induced by a change of ambient refractive index," *Opt. Lett.,* vol. 22, pp. 1769-1771, 1997.

[44] S. Thomas Lee, R. Dinesh Kumar, P. Suresh Kumar, P. Radhakrishnan, C. P. G. Vallabhan, and V. P. N. Nampoori, "Long period gratings in multimode optical fibers: application in chemical sensing," *Optics Communications*, vol. 224, pp. 237-241, 2003.

[45] W. J. Stephen and P. T. Ralph, "Optical fibre long-period grating sensors: characteristics and application," *Measurement Science and Technology*, vol. 14, p. R49, 2003.

[46] D. Gloge, "Weakly Guiding Fibers," *Appl. Opt.*, vol. 10, pp. 2252-2258, 1971.

[47] M. J. Adams, *An Introduction to Optical Waveguide*: John Wiley and Sons Inc, 1981.

[48] G. A. Agrawal, *Fiber-Optic Communication system*, Third edition ed. New York: Wiley-Interscience, 2002.

[49] X. Shu, L. Zhang, and I. Bennion, "Sensitivity Characteristics of Long-Period Fiber Gratings," *J. Lightwave Technol.*, vol. 20, p. 255, 2002.

[50] R. Hou and et al., "Modelling of long-period fibre grating response to refractive index higher than that of cladding," *Measurement Science and Technology*, vol. 12, p. 1709, 2001.

[51] K. Sarfraz and et al., "Enhanced sensitivity fibre optic long period grating temperature sensor," *Measurement Science and Technology*, vol. 13, p. 792, 2002.

[52] O. Duhem, J.-F. o. Henninot, M. Warenghem, and M. Douay, "Demonstration of Long-Period-Grating Efficient Couplings with an External Medium of a Refractive Index Higher than that of Silica," *Appl. Opt.*, vol. 37, pp. 7223-7228, 1998.

[53] H. J. Patrick, C. G. Askins, R. W. McElhanon, and E. J. Friebele, "Amplitude mask patterned on an excimer laser mirror for high intensity writing of long period fibre gratings," *Electronics Letters*, vol. 33, pp. 1167-1168, 1997.

[54] X. Shu and D. Huang, "Highly sensitive chemical sensor based on the measurement of the separation of dual resonant peaks in a 100-[mu]m-period fiber grating," *Optics Communications*, vol. 171, pp. 65-69, 1999.

[55] T. Allsop, L. Zhang, and I. Bennion, "Detection of organic aromatic compounds in paraffin by a long-period fiber grating optical sensor with optimized sensitivity," *Optics Communications*, vol. 191, pp. 181-190, 2001.

[56] S. Khaliq, S. W. James, and R. P. Tatam, "Fiber-optic liquid-level sensor using a long-period grating," *Opt. Lett.*, vol. 26, pp. 1224-1226, 2001.

[57] S. Grice, W. Zhang, K. Sugden, and I. Bennion, "Liquid level sensor utilising a long period fiber grating," 2009, p. 72120C.

[58] R. Falciai, A. G. Mignani, and A. Vannini, "Long period gratings as solution concentration sensors," *Sensors and Actuators B: Chemical*, vol. 74, pp. 74-77, 2001.

[59] Y. Kondo, K. Nouchi, T. Mitsuyu, M. Watanabe, P. G. Kazansky, and K. Hirao, "Fabrication of long-period fiber gratings by focused irradiation of infrared femtosecond laser pulses," *Opt. Lett.*, vol. 24, pp. 646-648, 1999.

[60] F. Hindle, E. Fertein, C. Przygodzki, F. Durr, L. Paccou, R. Bocquet, P. Niay, H. G. Limberger, and M. Douay, "Inscription of long-period gratings in pure silica and Germano-silicate fiber cores by femtosecond laser irradiation," *Photonics Technology Letters, IEEE,* vol. 16, pp. 1861-1863, 2004.

[61] N. N. David, "Long-period gratings in a standard telecom fibre fabricated by high-intensity femtosecond UV and near-UV laser pulses," *Measurement Science and Technology,* vol. 17, p. 960, 2006.

[62] A. W. Snyder and W. R. Young, "Modes of optical waveguides," *J. Opt. Soc. Am.,* vol. 68, pp. 297-309, 1978.

[63] J. Thomas, N. Jovanovic, R. G. Becker, G. D. Marshall, M. J. Withford, A. Tünnermann, S. Nolte, and M. J. Steel, "Cladding mode coupling in highly localized fiber Bragg gratings: modal properties and transmission spectra," *Opt. Express,* vol. 19, pp. 325-341, 2011.

[64] T. Allsop, M. Dubov, A. Martinez, F. Floreani, I. Khrushchev, D. J. Webb, and I. Bennion, "Bending characteristics of fiber long-period gratings with cladding index modified by femtosecond laser," *Lightwave Technology, Journal of,* vol. 24, pp. 3147-3154, 2006.

[65] A. I. Kalachev, V. Pureur, and D. N. Nikogosyan, "Investigation of long-period fiber gratings induced by high-intensity femtosecond UV laser pulses," *Optics Communications,* vol. 246, pp. 107-115, 2005.

[66] Y. Yu, S. Ruan, H. Yang, C. Du, and J. Zheng, "Temperature sensor using a long period fiber grating fabricated by 800 nm femtosecond laser pulses," Dalian, China, 2010, pp. 76550Q-6.

[67] K. S. Lee and T. Erdogan, "Fiber Mode Coupling in Transmissive and Reflective Tilted Fiber Gratings," *Appl. Opt.,* vol. 39, pp. 1394-1404, 2000.

[68] C. Chen, L. Xiong, A. Jafari, and J. Albert, "Differential sensitivity characteristics of tilted fiber Bragg grating sensors," Boston, MA, USA, 2005, pp. 60040B-10.

[69] S. Lu, O. Xu, S. Feng, and S. Jian, "Analysis of radiation-mode coupling in reflective and transmissive tilted fiber Bragg gratings," *J. Opt. Soc. Am. A,* vol. 26, pp. 91-98, 2009.

[70] K. Zhou, G. Simpson, X. Chen, L. Zhang, and I. Bennion, "High extinction ratio in-fiber polarizers based on 45° tilted fiber Bragg gratings," *Opt. Lett.,* vol. 30, pp. 1285-1287, 2005.

[71] K. Zhou, L. Zhang, X. Chen, and I. Bennion, "Optic sensors of high refractive-index responsivity and low thermal cross sensitivity that use fiber Bragg gratings of >80° tilted structures," *Opt. Lett.,* vol. 31, pp. 1193-1195, 2006.

[72] V. Bhatia, "Applications of long-period gratings to single and multi-parameter sensing," *Opt. Express,* vol. 4, pp. 457-466, 1999.

[73] A. D. Kersey, M. A. Davis, H. J. Patrick, M. LeBlanc, K. P. Koo, C. G. Askins, M. A. Putnam, and E. J. Friebele, "Fiber grating sensors," *Lightwave Technology, Journal of,* vol. 15, pp. 1442-1463, 1997.

[74] W. J. Stephen and P. T. Ralph, "Fibre optic sensors with nano-structured coatings," *Journal of Optics A: Pure and Applied Optics,* vol. 8, p. S430, 2006.

[75] I. Del Villar, I. Matías, F. Arregui, and P. Lalanne, "Optimization of sensitivity in Long Period Fiber Gratings with overlay deposition," *Opt. Express,* vol. 13, pp. 56-69, 2005.

[76] I. Del Villar, M. Achaerandio, I. R. Matías, and F. J. Arregui, "Deposition of overlays by electrostatic self-assembly in long-period fiber gratings," *Opt. Lett.,* vol. 30, pp. 720-722, 2005.

[77] A. Cusano, A. Iadicicco, P. Pilla, L. Contessa, S. Campopiano, A. Cutolo, and M. Giordano, "Cladding mode reorganization in high-refractive-index-coated long-period gratings: effects on the refractive-index sensitivity," *Opt. Lett.,* vol. 30, pp. 2536-2538, 2005.

[78] C. S. Cheung, S. M. Topliss, S. W. James, and R. P. Tatam, "Response of fiber-optic long-period gratings operating near the phase-matching turning point to the deposition of nanostructured coatings," *J. Opt. Soc. Am. B,* vol. 25, pp. 897-902, 2008.

[79] I. R. Peterson, "Langmuir-Blodgett films," *Journal of Physics D: Applied Physics,* vol. 23, p. 379, 1990.

[80] M. C. Petty, *Langmuir-Blodgett Films*. Cambridge: Cambridge University press, 1996.

[81] Y. Liu, A. Wang, and R. O. Claus, "Layer-by-layer electrostatic self-assembly of nanoscale Fe[sub 3]O[sub 4] particles and polyimide precursor on silicon and silica surfaces," *Applied Physics Letters,* vol. 71, pp. 2265-2267, 1997.

[82] Y. Liu, Y. Wang, and R. O. Claus, "Layer-by-layer ionic self-assembly of Au colloids into multilayer thin-films with bulk metal conductivity," *Chemical Physics Letters,* vol. 298, pp. 315-319, 1998.

[83] K. M. Lenahan, Y.-X. Wang, Y. Liu, R. O. Claus, J. R. Heflin, D. Marciu, and C. Figura, "Novel Polymer Dyes for Nonlinear Optical Applications Using Ionic Self-Assembled Monolayer Technology," *Advanced Materials,* vol. 10, pp. 853-855, 1998.

[84] C. J. Brinker and G. W. Scherer, Sol-Gel Science: The Physics and Chemistry of Sol-Gel Processing: Academic Press, 1990.

[85] L. L. Hench and J. K. West, "The sol-gel process," *Chemical Reviews,* vol. 90, pp. 33-72, 1990.

[86] I. M. Ishaq, A. Quintela, S. W. James, G. J. Ashwell, J. M. Lopez-Higuera, and R. P. Tatam, "Modification of the refractive index response of long period gratings using thin film overlays," *Sensors and Actuators B: Chemical,* vol. 107, pp. 738-741, 2005.

[87] N. D. Rees, S. W. James, R. P. Tatam, and G. J. Ashwell, "Optical fiber long-period gratings with Langmuir?Blodgett thin-film overlays," *Opt. Lett.,* vol. 27, pp. 686-688, 2002.

[88] G. Decher, J. D. Hong, and J. Schmitt, "Buildup of ultrathin multilayer films by a self-assembly process: III. Consecutively alternating adsorption of anionic and cationic polyelectrolytes on charged surfaces," *Thin Solid Films,* vol. 210-211, pp. 831-835, 1992.

[89] A. Rosidian, Y. Liu, and R. O. Claus, "Ionic Self-Assembly of Ultrahard ZrO2/Polymer Nanocomposite Thin Films," *Advanced Materials,* vol. 10, pp. 1087-1091, 1998.

[90] S. A. Grant, J. H. Satcher, and K. Bettencourt, "Development of sol-gel-based fiber optic nitrogen dioxide gas sensors," *Sensors and Actuators B: Chemical,* vol. 69, pp. 132-137, 2000.

[91] S. A. Grant and R. S. Glass, "Sol-gel-based biosensor for use in stroke treatment," *Biomedical Engineering, IEEE Transactions on,* vol. 46, pp. 1207-1211, 1999.

[92] Z. Gu, Y. Xu, and K. Gao, "Optical fiber long-period grating with solgel coating for gas sensor," *Opt. Lett.,* vol. 31, pp. 2405-2407, 2006.

[93] S. Korposh, S. W. James, S.-W. Lee, S. Topliss, S. C. Cheung, W. J. Batty, and R. P. Tatam, "Fiber optic long period grating sensors with a nanoassembled mesoporous film of SiO2 nanoparticles," *Opt. Express,* vol. 18, pp. 13227-13238, 2010.

[94] G. Meltz and W. W. Morey, "Bragg grating formation and germanosilicate fiber photosensitivity," Quebec City, Canada, 1991, pp. 185-199.

[95] B. J. Eggleton, P. A. Krug, L. Poladian, and F. Ouellette, "Long periodic superstructure Bragg gratings in optical fibres," *Electronics Letters,* vol. 30, pp. 1620-1622, 1994.

[96] X. Liu, "Design of superstructure fiber Bragg gratings with a Fourier analysis technique and its applications to multiple ultranarrow transmission gratings," *Optical Engineering,* vol. 47, pp. 115001-7, 2008.

[97] L. Hongpu, S. Yunlong, L. Yao, and J. E. Rothenberg, "Phased-only sampled fiber Bragg gratings for high-channel-count chromatic dispersion compensation," *Lightwave Technology, Journal of,* vol. 21, pp. 2074-2083, 2003.

[98] G. Bai-Ou, T. Hwa-Yaw, T. Xiao-Ming, and D. Xiao-Yi, "Simultaneous strain and temperature measurement using a superstructure fiber Bragg grating," *Photonics Technology Letters, IEEE,* vol. 12, pp. 675-677, 2000.

[99] B. A. L. Gwandu, X. Shu, Y. Liu, W. Zhang, L. Zhang, and I. Bennion, "Simultaneous and independent sensing of arbitrary temperature and bending using sampled fibre Bragg grating," *Electronics Letters,* vol. 37, pp. 946-948, 2001.

[100] X. Shu, B. A. L. Gwandu, Y. Liu, L. Zhang, and I. Bennion, "Sampled fiber Bragg grating for simultaneous refractive-index and temperature measurement," *Opt. Lett.,* vol. 26, pp. 774-776, 2001.

[101] K. S. Chiang, Y. Liu, M. N. Ng, and X. Dong, "Analysis of etched long-period fibre grating and its response to external refractive index," *Electronics Letters,* vol. 36, pp. 966-967, 2000.

[102] A. Iadicicco, A. Cusano, A. Cutolo, R. Bernini, and M. Giordano, "Thinned fiber Bragg gratings as high sensitivity refractive index sensor," *Photonics Technology Letters, IEEE,* vol. 16, pp. 1149-1151, 2004.

[103] A. Iadicicco, S. Campopiano, A. Cutolo, M. Giordano, and A. Cusano, "Refractive index sensor based on microstructured fiber Bragg grating," *Photonics Technology Letters, IEEE,* vol. 17, pp. 1250-1252, 2005.

[104] W. Liang, Y. Huang, Y. Xu, R. K. Lee, and A. Yariv, "Highly sensitive fiber Bragg grating refractive index sensors," *Applied Physics Letters,* vol. 86, p. 151122, 2005.

[105] N. Chen, B. Yun, and Y. Cui, "Cladding mode resonances of etch-eroded fiber Bragg grating for ambient refractive index sensing," *Applied Physics Letters,* vol. 88, pp. 133902-133902-3, 2006.

[106] C. Caucheteur, K. Chah, F. Lhomme, M. Debliquy, D. Lahem, M. Blondel, and P. Megret, "Enhancement of cladding modes couplings in tilted Bragg gratings owing to cladding etching," in *Fibres and Optical Passive Components, 2005. Proceedings of 2005 IEEE/LEOS Workshop on*, 2005, pp. 234-239.

[107] C. Chen and et al., "The sensitivity characteristics of tilted fibre Bragg grating sensors with different cladding thicknesses," *Measurement Science and Technology,* vol. 18, p. 3117, 2007.

[108] A. Iadicicco, S. Campopiano, M. Giordano, and A. Cusano, "Spectral behavior in thinned long period gratings: effects of fiber diameter on refractive index sensitivity," *Appl. Opt.,* vol. 46, pp. 6945-6952, 2007.

[109] A. Martinez-Rios, D. Monzon-Hernandez, and I. Torres-Gomez, "Highly sensitive cladding-etched arc-induced long-period fiber gratings for refractive index sensing," *Optics Communications,* vol. 283, pp. 958-962, 2010.

[110] S. A. Vasiliev, E. M. Dianov, D. Varelas, H. G. Limberger, and R. P. Salathé, "Postfabrication resonance peak positioning of long-period cladding-mode-coupled gratings," *Opt. Lett.,* vol. 21, pp. 1830-1832, 1996.

[111] K. Zhou, H. Liu, and X. Hu, "Tuning the resonant wavelength of long period fiber gratings by etching the fiber's cladding," *Optics Communications,* vol. 197, pp. 295-299, 2001.

[112] X. Chen, K. Zhou, L. Zhang, and I. Bennion, "Dual-peak long-period fiber gratings with enhanced refractive index sensitivity by finely tailored mode dispersion that uses the light cladding etching technique," *Appl. Opt.,* vol. 46, pp. 451-455, 2007.

[113] C. Xianfeng, H. Marcus, Z. Kaiming, D. Edward, Z. Lin, H. Anna, and B. Ian, "Long-Period Fibre Grating Based Biosensor for Detection of DNA Hybridisation," 2007, p. BTuE4.

[114] J.-L. Tang, S.-F. Cheng, W.-T. Hsu, T.-Y. Chiang, and L.-K. Chau, "Fiber-optic biochemical sensing with a colloidal gold-modified long period fiber grating," *Sensors and Actuators B: Chemical,* vol. 119, pp. 105-109, 2006.

[115] G. Nemova and R. Kashyap, "Theoretical model of a planar integrated refractive index sensor based on surface plasmon-polariton excitation with a long period grating," *J. Opt. Soc. Am. B,* vol. 24, pp. 2696-2701, 2007.

[116] T. Allsop, R. Neal, S. Rehman, D. J. Webb, D. Mapps, and I. Bennion, "Characterization of infrared surface plasmon resonances generated from a fiber-optical sensor utilizing tilted Bragg gratings," *J. Opt. Soc. Am. B,* vol. 25, pp. 481-490, 2008.

[117] Y. Y. Shevchenko, A. Ianoul, C. Chen, and J. Albert, "Realization of surface plasmon resonance sensor in standard optical fibers," Ottawa, Ontario, Canada, 2007, pp. 67961Z-12.

[118] G. Nemova and R. Kashyap, "Fiber-Bragg-grating-assisted surface plasmon-polariton sensor," *Opt. Lett.,* vol. 31, pp. 2118-2120, 2006.

[119] G. Nemova and R. Kashyap, "Novel fiber Bragg grating assisted plasmon-polariton for bio-medical refractive-index sensors," *Journal of Materials Science: Materials in Electronics,* vol. 18, pp. 327-330, 2007.

[120] B. Lee, S. Roh, and J. Park, "Current status of micro- and nano-structured optical fiber sensors," *Optical Fiber Technology,* vol. 15, pp. 209-221, 2009.

[121] A. M. Vengsarkar, P. J. Lemaire, J. B. Judkins, V. Bhatia, T. Erdogan, and J. E. Sipe, "Long-period fiber gratings as band-rejection filters," *Lightwave Technology, Journal of,* vol. 14, pp. 58-65, 1996.

[122] M. N. Ng and K. S. Chiang, "Thermal effects on the transmission spectra of long-period fiber gratings," *Optics Communications,* vol. 208, pp. 321-327, 2002.

[123] H. J. Patrick, "Self-aligning bipolar bend transducer based on long period grating written in eccentric core fibre," *Electronics Letters,* vol. 36, pp. 1763-1764, 2000.

[124] T. Allsop, A. Gillooly, V. Mezentsev, T. Earthgrowl-Gould, R. Neal, D. J. Webb, and I. Bennion, "Bending and orientational characteristics of long period gratings written in D-shaped optical fiber [directional bend sensors]," *Instrumentation and Measurement, IEEE Transactions on,* vol. 53, pp. 130-135, 2004.

[125] Z. Kaiming and et al., "Implementation of optical chemsensors based on HF-etched fibre Bragg grating structures," *Measurement Science and Technology,* vol. 17, p. 1140, 2006.

[126] E. D. Palik, *Handbook of optical constants of solids*. San Diego: Academic Press, 1998.

[127] W. Liang, Y. Huang, Y. Xu, R. K. Lee, and A. Yariv, "Highly sensitive fiber Bragg grating refractive index sensors," *Applied Physics Letters,* vol. 86, pp. 151122-151122-3, 2005.

[128] S. Kim, Y. Jeong, S. Kim, J. Kwon, N. Park, and B. Lee, "Control of the Characteristics of a Long-Period Grating by Cladding Etching," *Appl. Opt.,* vol. 39, pp. 2038-2042, 2000.

[129] K. Zhou, X. Chen, L. Zhang, and I. Bennion, "High-sensitivity optical chemsensor based on etched D-fibre Bragg gratings," *Electronics Letters,* vol. 40, pp. 232-234, 2004.

[130] B. I. Bluestein, I. M. Walczak, and S.-Y. Chen, "Fiber optic evanescent wave immunosensors for medical diagnostics," *Trends in Biotechnology,* vol. 8, pp. 161-168, 1990.

[131] M. Mehrvar, C. Bis, J. M. Scharer, M. M. Young, and J. H. Luong, "Fiber-Optic Biosensors-Trends and Advances," *Analytical Sciences,* vol. 16, pp. 677-692, 2000.

[132] P. T. Kissinger, "Biosensors--a perspective," *Biosensors and Bioelectronics,* vol. 20, pp. 2512-2516, 2005.

[133] S. R. Baker, H. N. Rourke, V. Baker, and D. Goodchild, "Thermal decay of fiber Bragg gratings written in boron and germanium codoped silica fiber," *Lightwave Technology, Journal of,* vol. 15, pp. 1470-1477, 1997.

[134] B. A. L. Gwandu, X. W. Shu, Y. Liu, W. Zhang, L. Zhang, and I. Bennion, "Simultaneous measurement of strain and curvature using superstructure fibre Bragg gratings," *Sensors and Actuators A: Physical,* vol. 96, pp. 133-139, 2002.

[135] X. Fang, X. Y. He, C. R. Liao, M. Yang, D. N. Wang, and Y. Wang, "A new method for sampled fiber Bragg grating fabrication by use of both femtosecond laser and CO2 laser," *Opt. Express,* vol. 18, pp. 2646-2654, 2010.

[136] K. Kyriacos, A. Tom, K. Charalambos, D. Edd, W. David, and Z. Lin, "Femtosecond Laser Inscription of Fiber Bragg Gratings with Low Insertion Loss and Minor Polarization Dependence," 2010, p. BMA3.

[137] S. A. Vasiliev and O. I. Medvedkov, "Long-period refractive index fiber gratings: properties, applications, and fabrication techniques," Moscow, Russia, 2000, pp. 212-223.

[138] R. P. Espindola, R. S. Windeler, A. A. Abramov, B. J. Eggleton, T. A. Strasser, and D. J. DiGiovanni, "External refractive index insensitive air-clad long period fibre grating," *Electronics Letters,* vol. 35, pp. 327-328, 1999.

[139] R. K. Verma, A. K. Sharma, and B. D. Gupta, "Surface plasmon resonance based tapered fiber optic sensor with different taper profiles," *Optics Communications,* vol. 281, pp. 1486-1491, 2008.

[140] A. K. Sharma and B. D. Gupta, "Fibre-optic sensor based on surface plasmon resonance with Ag–Au alloy nanoparticle films," *Nanotechnology,* vol. 17, p. 124, 2006.

[141] M. Kanso, S. Cuenot, and G. Louarn, "Sensitivity of Optical Fiber Sensor Based on Surface Plasmon Resonance: Modeling and Experiments," *Plasmonics,* vol. 3, pp. 49-57, 2008.

[142] S.-F. Wang, M.-H. Chiu, J.-C. Hsu, R.-S. Chang, and F.-T. Wang, "Theoretical analysis and experimental evaluation of D-type optical fiber sensor with a thin gold film," *Optics Communications,* vol. 253, pp. 283-289, 2005.

[143] T. Allsop, R. Neal, S. Rehman, D. J. Webb, D. Mapps, and I. Bennion, "Generation of infrared surface plasmon resonances with high refractive index sensitivity utilizing tilted fiber Bragg gratings," *Appl. Opt.,* vol. 46, pp. 5456-5460, 2007.

[144] T. Allsop and et al., "Low refractive index gas sensing using a surface plasmon resonance fibre device," *Measurement Science and Technology,* vol. 21, p. 094029, 2010.

[145] Y. Y. Shevchenko and J. Albert, "Plasmon resonances in gold-coated tilted fiber Bragg gratings," *Opt. Lett.,* vol. 32, pp. 211-213, 2007.

[146] B. pa?ková and J. í. Homola, "Theoretical analysis of a fiber optic surface plasmon resonance sensor utilizing a Bragg grating," *Opt. Express,* vol. 17, pp. 23254-23264, 2009.

[147] C. Caucheteur, Y. Shevchenko, L.-Y. Shao, M. Wuilpart, and J. Albert, "High resolution interrogation of tilted fiber grating SPR sensors from polarization properties measurement," *Opt. Express,* vol. 19, pp. 1656-1664, 2011.

[148] Y.-J. He, Y.-L. Lo, and J.-F. Huang, "Optical-fiber surface-plasmon-resonance sensor employing long-period fiber gratings in multiplexing," *J. Opt. Soc. Am. B,* vol. 23, pp. 801-811, 2006.

[149] A. A. Maradudin and W. Zierau, "Effects of surface roughness on the surface-polariton dispersion relation," *Physical Review B,* vol. 14, p. 484, 1976.

[150] T. S. Rahman and A. A. Maradudin, "Surface-plasmon dispersion relation in the presence of surface roughness," *Physical Review B,* vol. 21, p. 2137, 1980.

[151] M. Yao, O.-K. Tan, S.-C. Tjin, and J. C. Wolfe, "Effects of intermediate dielectric films on multilayer surface plasmon resonance behavior," *Acta Biomaterialia,* vol. 4, pp. 2016-2027, 2008.

[152] S. M. Tripathi, A. Kumar, E. Marin, and J. P. Meunier, "Side-Polished Optical Fiber Grating-Based Refractive Index Sensors Utilizing the Pure Surface Plasmon Polariton," *Lightwave Technology, Journal of,* vol. 26, pp. 1980-1985, 2008.

[153] R. Jha and G. Badenes, "Effect of fiber core dopant concentration on the performance of surface plasmon resonance-based fiber optic sensor," *Sensors and Actuators A: Physical,* vol. 150, pp. 212-217, 2009.

[154] S. Mani Tripathi, E. Marin, A. Kumar, and J.-P. Meunier, "Refractive index sensing characteristics of dual resonance long period gratings in bare and metal-coated D-shaped fibers," *Appl. Opt.,* vol. 48, pp. G53-G58, 2009.

[155] K. H. Yoon, M. L. Shuler, and S. J. Kim, "Design optimization of nano-grating surface plasmon resonance sensors," *Opt. Express,* vol. 14, pp. 4842-4849, 2006.

[156] F. J. Garcia-Vidal, J. Sanchez-Dehesa, A. Dechelette, E. Bustarret, T. Lopez-Rios, T. Fournier, and B. Pannetier, "Localized surface plasmons in lamellar metallic gratings," *Lightwave Technology, Journal of,* vol. 17, pp. 2191-2195, 1999.

[157] K. Atsushi and et al., "Femtosecond microscopy of localized and propagating surface plasmons in silver gratings," *Journal of Physics B: Atomic, Molecular and Optical Physics,* vol. 40, p. S259, 2007.

[158] D. Kim, "Effect of resonant localized plasmon coupling on the sensitivity enhancement of nanowire-based surface plasmon resonance biosensors," *J. Opt. Soc. Am. A,* vol. 23, pp. 2307-2314, 2006.

[159] K. M. Byun, S. J. Kim, and D. Kim, "Profile effect on the feasibility of extinction-based localized surface plasmon resonance biosensors with metallic nanowires," *Appl. Opt.,* vol. 45, pp. 3382-3389, 2006.

[160] K. Kim, S. J. Yoon, and D. Kim, "Nanowire-based enhancement of localized surface plasmon resonance for highly sensitive detection: a theoretical study," *Opt. Express,* vol. 14, pp. 12419-12431, 2006.

[161] L. A. Lyon, D. J. Peña, and M. J. Natan, "Surface Plasmon Resonance of Au Colloid-Modified Au Films: Particle Size Dependence," *The Journal of Physical Chemistry B,* vol. 103, pp. 5826-5831, 1999.

[162] L. He, M. D. Musick, S. R. Nicewarner, F. G. Salinas, S. J. Benkovic, M. J. Natan, and C. D. Keating, "Colloidal Au-Enhanced Surface Plasmon Resonance for Ultrasensitive Detection of DNA Hybridization," *Journal of the American Chemical Society,* vol. 122, pp. 9071-9077, 2000.

[163] T. Okamoto, I. Yamaguchi, and T. Kobayashi, "Local plasmon sensor with gold colloid monolayers deposited upon glass substrates," *Opt. Lett.,* vol. 25, pp. 372-374, 2000.

[164] J. F. Young, J. E. Sipe, and H. M. van Driel, "Regimes of laser-induced periodic surface structure on germanium: radiation remnants and surface plasmons," *Opt. Lett.,* vol. 8, pp. 431-433, 1983.

[165] J. F. Young, J. E. Sipe, and H. M. van Driel, "Laser-induced periodic surface structure. III. Fluence regimes, the role of feedback, and details of the induced topography in germanium," *Physical Review B,* vol. 30, p. 2001, 1984.

[166] J. Nishii, "Permanent index changes in Ge-SiO2 glasses by excimer laser irradiation," *Materials Science and Engineering B,* vol. 54, pp. 1-10, 1998.

[167] T. Allsop, R. Neal, C. Mou, P. Brown, S. Saied, S. Rehman, K. Kalli, D. J. Webb, J. Sullivan, D. Mapps, and I. Bennion, "Exploitation of multilayer coatings for infrared surface plasmon resonance fiber sensors," *Appl. Opt.,* vol. 48, pp. 276-286, 2009.

[168] L. Malic, B. Cui, M. Tabrizian, and T. Veres, "Nanoimprinted plastic substrates for enhanced surface plasmon resonance imaging detection," *Opt. Express,* vol. 17, pp. 20386-20392, 2009.

[169] K. Byun, S. Kim, and D. Kim, "Design study of highly sensitive nanowire-enhanced surface plasmon resonance biosensors using rigorous coupled wave analysis," *Opt. Express,* vol. 13, pp. 3737-3742, 2005.

[170] K. M. Byun, S. J. Yoon, D. Kim, and S. J. Kim, "Sensitivity analysis of a nanowire-based surface plasmon resonance biosensor in the presence of surface roughness," *J. Opt. Soc. Am. A,* vol. 24, pp. 522-529, 2007.

[171] T. Chuen-Lin, C. Hong-Wei, L. Wen-Fung, and L. Yung-Sen, "Side-polished fiber Bragg gratings coated with thin palladium film for hydrogen sensing device," in *Lasers and Electro-Optics, 2006 and 2006 Quantum Electronics and Laser Science Conference. CLEO/QELS 2006. Conference on,* 2006, pp. 1-2.

[172] J. Zhang, X. Tang, J. Dong, T. Wei, and H. Xiao, "Zeolite thin film-coated long period fiber grating sensor for measuring trace chemical," *Opt. Express,* vol. 16, pp. 8317-8323, 2008.

[173] J. Barnes, M. Dreher, K. Plett, R. S. Brown, C. M. Crudden, and H.-P. Loock, "Chemical sensor based on a long-period fibre grating modified by a functionalized polydimethylsiloxane coating," *Analyst,* vol. 133, pp. 1541-1549, 2008.

[174] S. M. Topliss, S. W. James, F. Davis, S. P. J. Higson, and R. P. Tatam, "Optical fibre long period grating based selective vapour sensing of volatile organic compounds," *Sensors and Actuators B: Chemical,* vol. 143, pp. 629-634, 2010.

[175] D. R. Lide, *CRC Handbook of Chemistry and Physics*: Taylor Francis Group, 2009.

[176] S. D. Jayasena, "Aptamers: An Emerging Class of Molecules That Rival Antibodies in Diagnostics," *Clin Chem,* vol. 45, pp. 1628-1650, September 1, 1999 1999.

[177] C. O'Sullivan, "Aptasensors - the future of biosensing?," *Analytical and Bioanalytical Chemistry,* vol. 372, pp. 44-48, 2002.

[178] S. Tombelli, M. Minunni, and M. Mascini, "Analytical applications of aptamers," *Biosensors and Bioelectronics,* vol. 20, pp. 2424-2434, 2005.

[179] M. K. Ramjee, "The Use of Fluorogenic Substrates to Monitor Thrombin Generation for the Analysis of Plasma and Whole Blood Coagulation," *Analytical Biochemistry,* vol. 277, pp. 11-18, 2000.

Publication list

Allsop, T. and et al. (2010). "Low refractive index gas sensing using a surface plasmon resonance fibre device." Measurement Science and Technology **21**(9): 094029.

Allsop, T., D. Nagel, et al. (2010). Aptamer-based surface plasmon fibre sensor for thrombin detection, Brussels, Belgium, SPIE.

Allsop, T., R. Neal, et al. (2009). Gas sensing using a surface plasmon resonance fibre device, SPIE.

Allsop, T., R. Neal, et al. (2009). The exploitation of thin film coatings for fibre sensors for the application of chemical sensing, Orlando, FL, USA, SPIE.

Davies, E., Z. Lin, et al. (2008). Refractive index sensing properties of long-period fibre grating with sol-gel derived coatings. Sensors, 2008 IEEE.

Davies, E., P. Saffari, et al. (2009). Refractive index sensitivity enhancement of 81[degree] tilted Bragg gratings by cladding etching, SPIE.

Davies, E. M. and et al. (2009). "Sol–gel derived coating applied to long-period gratings for enhanced refractive index sensing properties." Journal of Optics A: Pure and Applied Optics **11**(1): 015501.

Mou, C., K. Zhou, et al. (2009). Fibre laser using a microchannel based loss tuning element for refractive index sensing, Edinburgh, United Kingdom, SPIE.